Fatigue and Rutting Performance of Hybrid Recycled Plastic Asphalt Concrete

BY

Muhammad Abubakar Dalhat

A Dissertation Presented to the

DEANSHIP OF GRADUATE STUDIES

KING FAHD UNIVERSITY OF PETROLEUM & MINERALS

DHAHRAN, SAUDI ARABIA

In Partial Fulfillment of the

Requirements for the Degree of

DOCTOR OF PHILOSOPHY

In

CIVIL ENGINEERING

March 2017

KING FAHD UNIVERSITY OF PETROLEUM & MINERALS

DHAHRAN- 31261, SAUDI ARABIA

DEANSHIP OF GRADUATE STUDIES

This thesis, written by Muhammad Abubakar Dalhat under the direction of his thesis advisor and approved by his thesis committee, has been presented and accepted by the Dean of Graduate Studies, in partial fulfillment of the requirements for the degree of **DOCTOR OF PHILOSOPHY IN CIVIL ENGINEERING.**

Dr. Hamad I. Al Abdul Wahhab
(Advisor)

Dr. Salah U. Al-Dulaijan
Department Chairman

Dr. Ibnelwaleed A. Hussein
(Member)

Dr. Salam A. Zummo
Dean of Graduate Studies

Dr. Husain J. Al-Gahtani
(Member)

4/6/17
Date

Dr. Shamsad Ahmad
(Member)

Dr. Rezqallah H. Malkawi
(Member)

© Muhammad Abubakar Dalhat

2017

DEDICATED TO MY PARENT

ACKNOWLEDGMENTS

In the name of Allah, the Beneficent, the most Merciful. All praises and thanks are due to Allah, the Lord of the world for the successful completion of this research work. May His peace be upon the last messenger, Prophet Muhammad, his family and companions.

Acknowledgement is due to the King Fahd University of Petroleum and Minerals for providing me with study scholarship and the research facilities that make this work possible.

My gratitude and acknowledgment are due to Dr. Hamad I. Al-Abdul Wahhab, my thesis Advisor, for his constant support, encouragement and inspiration. The vital support provided by Dr. Ibnelwaleed A. Hussein (committee member) is greatly appreciated. I am also very grateful to my other committee members for their guidance and continuous support in all the phases of this work, Dr. Rezqallah Hasan Malkawi, Dr. Husain Jubran Al-Gahtani and Dr. Shamshad Ahmad, your contribution is highly appreciated.

I want to particularly acknowledge the tremendous assistance I received from Mr. Mirza Ghouse Baig and Engr. Khalil Al-Adham from Civil and Environmental Engineering Department, Engr. Imran Syed and Engr. Umar Hussein all from the departmental laboratories. Similarly, I would like to extend my regards to the Nigerian community in KFUPM, my colleagues in the department and all my friends for providing me with wonderful company.

My sincere appreciation goes to my parents, my wife, brothers, sisters, my entire family for their love, encouragement, patience and prayers.

Finally, I pray to Almighty Allah to reward all those who contributed, either directly or indirectly, towards the success of this work.

TABLE OF CONTENTS

LIST OF TABLES

LIST OF FIGURES

LIST OF ABBREVIATIONS

AC	Asphalt Concrete
AAHSTO	American Association of State Highway and Transportation Officials
AMPT	Asphalt Mix Performance Tester
EVA	Ethylene Vinyl Acetate
FM	Francken Model
FM_FN	Francken Model Flow Number
FN	Flow Number
FN:N	Flow Number to Test Duration Ratio
FTIR	Fourier transform infrared spectroscopy
CRB	Crumb Rubber
DR	Degradation Index
DR(G^*)	Complex Modulus Degradation Index
DR(δ)	Phase Angle Degradation Index
DSC	Differential Scanning Calorimetry
G^*	Complex Modulus
KSA	Kingdom of Saudi Arabia
MPW	Mixed Plastic Waste
MSW	Municipal Solid Waste
ME-PDG	Mechanistic Empirical Pavement Design Guide
PG	Performance Grade
PG^+	Performance Grade Plus
PMB	Polymer Modified Asphalt
PP	Polypropylene
HDPE	High Density Polyethylene

LAST	Laboratory Asphalt Stability Test
LDPE	Low Density Polyethylene
MFM	Modified Fracken Model
MFM-1	Modified Fracken Model 1
MFM-2	Modified Fracken Model 2
MFM-1_FN	Modified Francken Model 1 Flow Number
MFM-2_FN	Modified Francken Model 2 Flow Number
PET	Polyethylene Terephthalate
PS	Poly Styrene
PVC	Polyvinyl Chloride
PB	Polybilt
PW	Plastic Waste
PDC	Permanent Deformation Curve
RAP	Recycled Aggregate Pavement
RPW	Recycled Plastic Waste
RTFO	Rolling Thin Film Oven
RLDPE	Recycled Low Density Polyethylene
RHDPE	Recycled High Density Polyethylene
RPP	Recycled Polypropylene
RPET	Recycled Polyethylene Terephthalate
PCC	Portland Cement Concrete
RPS	Recycled Polystyrene
RPVC	Recycled Polyvinyl Chloride
SBS	Styrene Butadiene Styrene
SEM	Scanning Electron Microscopy

SHRP	Strategic Highway Research Program
SMA	Stone Mastic Asphalt
SR	Separation Index
$SR(G^*)$	Complex Modulus Separation Index
$SR(\delta)$	Phase angle Separation Index
UPGT	Upper Performance Grade Temperature

ABSTRACT

Full Name : Muhammad Abubakar Dalhat

Thesis Title : Fatigue and Rutting Performance of Hybrid Recycled Plastic Asphalt Concrete
Major Field : Civil Engineering
Date of Degree : 2017

Huge amount of globally generated non-biodegradable plastic wastes, constitute a major environmental nuisance. The annual Recycled Plastic waste (RPW) generation from Kingdom of Saudi Arabia (KSA) exceeds 1,400,000 tones. Extreme KSA climate necessitates expensive polymer modification of the local available asphalt binder. The potential of RPW in enhancing the performance and reducing the cost of asphalt concrete (AC) has been explored. Dynamic storage stability, high temperature performance, non recoverable creep compliance (J_{nr}), and recovery of recycled high and low density polyethylene (RHDPE & RLDPE), and recycled polypropylene (RPP) modified asphalt binders in combination with styrene-butadiene-styrene (SBS) and polybilt (PB) were presented in this study. The purely RPW modified binders lack of elastic recovery was successfully improved by incorporating minor proportion of elastomeric virgin polymer (SBS). Even though the RPWs modified binders lack sufficient strain recovering ability, RLDPE and RHDPE could be utilized along with an elastomeric SBS to achieve a higher recovery and strain resistance, than that which could be achieved if same amount of SBS alone is employed. Some of the RPP modified asphalt binder (content above 2%) were found to be unstable. A RPW size ranging between No. 8 and No. 40 was found to be the best for AC modification via aggregate substitution. An optimum RPW aggregate substitute of 9.5% by mass was established. All the ACs containing RPW-aggregate showed higher dynamic modulus than the conventional crumb rubber modified binder mix, at lower loading frequency. None of the hybrid RWP-aggregate mixture flowed within the standardized flow number (FN) test period. The presence of the RPW aggregate in the fresh+RPW mix has more than doubled the fresh AC fatigue life. Adopting recycling alternative of polymer modification in KSA alone could eliminate up to 500,000 million metric tons of carbon emission and 500 tons of non-methane volatile organic compounds every year. The 20 years simulation results of the RPW modified AC life under heavy traffic has shown an overall excellent performance of the RPW modified binder AC mixture. The simulation results further confirms inferences made from laboratory test results that most of the hybrid-RPW ACs are superior to the CRB_76 AC for higher loading time scenario.

ARABIC ABSTRACT

الاسم الكامل: محمد أبو بكر طلحت

عنوان الرسالة: أداء الإجهاد والتخدد للخلطات الإسفلتية قبل وبعد استخدام الألياف السيلولوزية المعاد تدويره

الملخص: دراسة معملية

تاريخ الرسالة: 2017

تعد الكثير من المواد البلاستيكية غير قابلة للتحلل حيث تم القاؤها في المياه والتربة مما يسبب مشكلة صحية وضرر بيئي كبير. حيث تم انتاج ما يقارب من مليون وأربعمائة ألف (1.400.000) طن من البلاستيك المعاد تدويره في المملكة العربية السعودية. في حين أن الظروف المناخية القاسية في المملكة تفرض طرق استخدام كثيرة وأنواع مختلفة من حيث خصائص السفلتة مما يستلزم البحث عن خلطات إسفلتية قادرة على تحمل هذه الظروف. حيث تناولت هذه الدراسة الكشف عن أداء الرصف السفلتي المحتوي على ألياف المواد البلاستيكية المعاد تدويرها. حيث شملت الدراسة كل من ثبات التخزين الحيوي ومؤشرات الأداء عند الحرارة العالية ومعامل المطاوعة لجزء غير المستردد بالإضافة الى نسب قرارات رداد المرونة وتلك استخدام المواد البلاستيكية المعاد تدويرها والتي شملت على البولي إيثيلين عالي الكثافة، والبولي إيثيلين قليل الكثافة، والبولي بروبلين مضافة الى البولمر المرصوف مثل البيتومين والمطاط الصناعي. وتوصي النتائج الأولية لهذه الدراسة إلى أن خصائص استعادة المرونة لربط البيتومين عند استخدام المواد البلاستيكية المعاد تدويرها المضافة الى كيس البولي إيثيلين من المطاط الصناعي. وعلى الرغم عدم تلاؤم هذه المواد البلاستيكية خصائص ارتداد المرونة إلا أن متبقي في هذه الدراسة أن دمج هذه المواد مع المطاط الصناعي قد تحسن من هذه الخاصية بشكل أفضل سواء للمطاط فقط. وتبين من فحص الربط الأسفلتي المحسن باستخدام البولي بروبلين المعاد تدويره بنسب أعلى من 7% أنه غير مستقر، ونتج من هذه الفحوصات أن استخدام البلاستيك المعاد تدويره بمقاس استنتاجه من خلال مقاس 8 ورقم 10 هو الحل الأمثل في خلطات السفلتية عن طريق استبدال جزء من الحصى الناعم بهذه المواد بمحتوى يصل الى 5.9% من الوزن. بوضع فحص الخلطات السفلتية التي تحتوي على البلاستيك المعاد تدويره باستخدام ترددات منخفضة، أشارت النتائج الى قيم أعلى من المعامل الحيوي مقارنة بالخلطات التي تحتوي على المطاط المعاد تدويره، كما تبين من النتائج انه لا يوجد إشارة الى التفوق خلال اختبار رقم التفوق. إن وجود البلاستيك المعاد تدويره كجزء من الحصى في الخلطات السفلتية يزيد من المقاومة تراضي التشوه على قاومة الجدال كثر من المضاعف. كما أن استخدام المواد المعاد تدويرها كمواد مضافة في الخلطات السفلتية في المملكة سوف يقلل من خطر تراكم أكثر من خمسمائة ألف (911.111) طن من البلاستيك سنويا من المكب ويقلل من الضار وخمسمائة (911) طن من المركب المضاعفة التي تخلو من الهيدروكربون. وأظهرت نتائج محاكاة عشرين (71) عاماً من عمر الخلطات السفلتية قام حسنة لوليتي تتعرض الى أحمال ثقيلة من المركبات باستخدام المواد البلاستيكية المعاد تدويرها أكثر من الخلطات. حيث تؤكد نتائج المحاكاة لمعدل المتبقي على أن هذه المواد متفوقة على الخلطات التي تحتوي على المطاط المعاد تدويره عند درجة حرارة (27) مئوية في حالة فترات الوقت قصيرة عرضه للأحمال.

CHAPTER 1

INTRODUCTION

Introduction: This chapter covers the basis, motivations and objectives for this research. It starts with highlighting the statistics on RPW generation with respect to the kingdom of Saudi Arabia (KSA). The economic and environmental cost associated to the RPW were briefly discussed. The KSA asphalt polymer modification requirement given rise to polymer demand that can be supplemented or replaced by the RPW is highlighted. The main objectives of research towards the use of RPW for asphalt concrete (AC) modification were outlined.

1.1 BACKGROUND

The quantity of solid plastic waste generated from material packages like plastic bottle and similar utilities within the kingdom of Saudi Arabia (KSA) has skyrocketed. This is as result of the increased level of industrial packaging due to rapid industrialization and fast urbanization in the country. The associated cost of managing these solid wastes has also multiplied as the task has become difficult and enormous. The per capita waste generation is estimated at 1.5 to 1.8 kg per person per day [1]. Solid waste generation in the three largest cities Riyadh, Jeddah, and Dammam exceeds 6 million tons per annum which gives an indication of the enormity of the problem.

Meanwhile, the economic feasibility studies of processing and utilizing plastic waste in Saudi Arabia indicates of rate of return of more than 14% [2].

The local available asphalt binder in Saudi Arabia can only be utilized without modification, if the maximum pavement temperature at service condition is below 64°C. However, the 7-day maximum temperature was found to range between 64 to 76°C within the Kingdom [3]. In addition, the proportion of heavy trucks in the county's traffic has increased, and the variation in daily and seasonal temperature has become significant. Hence, all flexible pavement road construction at national level requires polymer-modified or similar asphalt binder, for an improved material characteristics and pavement performance.

Global demand towards shift from routine production and manufacturing processes has paved way for research that explored recycling potentials of several industrial and domestic wastes. Waste plastics, due to their non-degradable nature and high production rate, constitute a major environmental nuisance. The combined annual municipal solid waste generation of KSA exceeds 14,000,000 tones, with an average per capita of 1.4 kg/day [1, 4]. A review on the use of recycled solid waste shows that plastic waste represent 10% of the bulk municipal solid waste [5]. Government in KSA have established numerous collection point for various recycled waste. However, the full potential of these collected recycled waste is yet to be fully exploited [4]. Most common plastic waste (PW) are inert and hydrophobic material [6], which causes adverse environmental consequences by polluting pastoral land and water sources [7]. These plastic debris transmit toxic substances to the global food chain due to ingestion by lower

level organisms. Additional negative impact on cities esthetic which directly negates tourist attraction was also reported.

1.2 OBJECTIVES

The main objective of this research is to utilize domestic plastic wastes in the preparation of local asphalt mix. Specific objectives include the following:

1. To utilize local RPW to improve the performance of asphalt concrete and minimize costs associated with the use of expensive virgin polymers.

2. To determine the optimal RPW-virgin polymer (hybrid) that results in the highest possible Superpave plus performance grading.

3. To determine the best size and proportion of recycled polymer granules to be used for substituting some proportion of the asphalt concrete aggregate.

4. To model the rutting and fatigue performance of the RPW-modified asphalt concrete using mechanistic empirical flexible pavement analysis technique.

1.3 SIGNIFICANCE OF THE RESEARCH

There is a global environmental concern relating to natural raw material preservation, which is completely a function of how humans manage these resources. These non-renewable resources preservation can only be successful if the rate at which they are exploited is limited. This brings us to the unavoidable issue of waste disposal and recycling. Recycling has been identified as one of the vital course of action that will lead to natural resource sustainability.

1.3.1 DEMAND FOR ASPHALT MODIFICATION: *KSA Perspective*

Airport & highway pavement network of KSA is wide spread and each year new projects are adding to the network. The total estimated cost of the kingdom highway network was more than $80 billion as of 2010, with an average annual maintenance cost of up to a billion dollar [8]. These roads were built based on American Association of State Highway and Transportation Officials (AAHSTO) standard. The extremely hot climate is causing permanent deformation. The local asphalt binder can only produce a durable pavement suited to climate with 7 days maximum pavement temperature below 64°C [9]. While the seven day maximum pavement temperature within KSA was established to range between 64 and 76°C [3, 10], as shown in Figure 1.1. However, the lowest service temperature for the whole region is just -10^{o}C, which even the local unmodified asphalt binder could effortlessly resist as can be seen from Table 3.4. Hence, the high temperature related distresses are the major concern for the kingdom. The performance temperature zoning was a product of extensive research in adopting the

Strategic Highway Research Program (SHRP) performance base specifications for the Gulf region. From the map, almost all the major cities (Riyadh, Jeddah, Makkah, and Damman) require polymer-enhanced or similar asphalt binder. Research on the use of different commercial elastomer (SBS, Crumb rubber) and plastomers (LDPE, HDPE, polystyrene, polybilt) to attain the required performance was well documented [11-12]. Contractors have to resolve to polymer modification so as to meet the high temperature performance requirements set by the Ministry of Transport. However high cost of polymer modified binder (PMB) has been described as one of the major challenges in asphalt paving industry [13]. The economic potential of PW as replacement or supplement of commercial virgin polymer in modification of Arabian asphalts binder was yet to be explored.

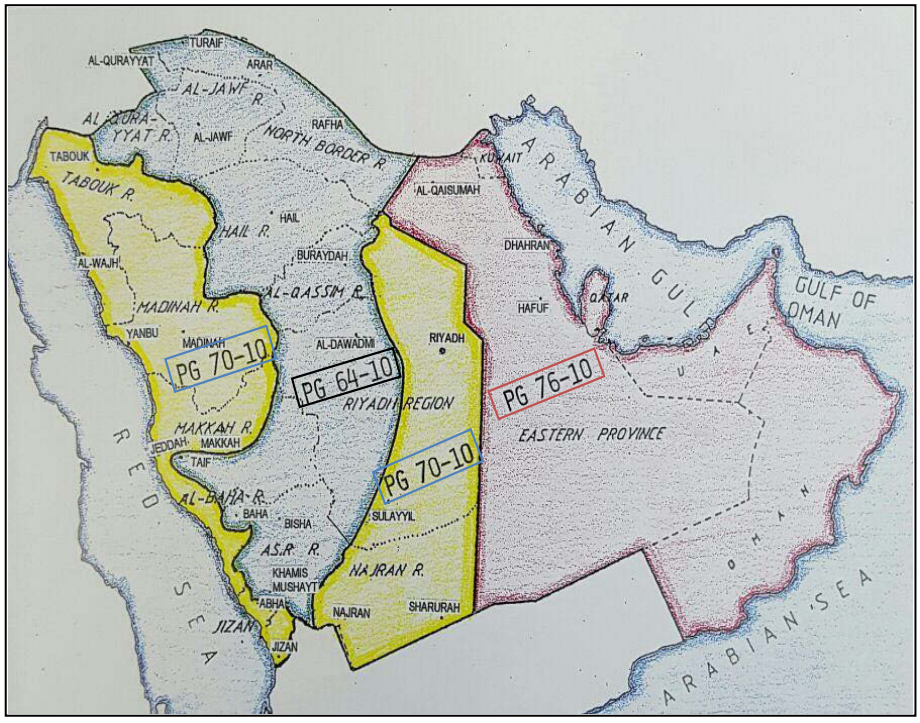

Figure 1.1: Temperature Zoning for Asphalt Performance Requirement KSA [3].

Summary: RPW have negative economic and environment impact in terms of proper handling and disposal. High amount of the RPW is generated globally each year, with combined annual municipal solid waste (MSW) generation of KSA exceeding 14,000,000 tones. A review on the use of recycled solid waste shows that plastic waste constitute 10% of the bulk MSW. The RPW have potential for use in the modification of AC. There is already a huge demand for asphalt polymer modification in KSA, due adverse climate and increased traffic load. The RPW will be utilized together with and in place of a virgin polymer to produce a cheaper and more durable AC for KSA climate.

CHAPTER 2

LITERATURE REVIEW

Introduction: The literature review is categorized into five main subheadings: i) literature addressing asphalt binder modification for enabling improved performance in road construction and other applications, such as roofing, and literature that aims to improve the performance of AC by partially replacing the aggregate component of the AC with RPW. ii) Current state of practice as regards the use of RPW in road construction globally, and the method of RPW collection by the eastern province municipality in KAS was also highlighted. iii) Past and current studies on polymer modified asphalt storage stability was also reviewed. iv) Studies on AC rutting and FN test, and v) Fatigue life of AC and related literature were finally presented.

2.1 USE OF RECYCLED PLASTIC WASTE (RPW) IN ASPHALT CONCRETE

More than 300 Million metric tons of plastic waste (PW) was globally generated annually as of 2014, this value is expected to keep rising [14]. Countries that has the best recycling rate records reuse about just 50%, while 90% of the plastic waste end in landfills in most Countries [14]. Among the high-tech recycling approaches are: Plastic-Waste-to-Fuel via pyrolysis [15] and Plastic-Waste-to-Energy via incineration [16]. But the major limitation of these advanced recycling options is their elimination of the plastic

waste without relieving the material demand of such. Thus, keeping the waste generation and related virgin plastic production emission growing. Moreover, the Plastic-Waste-to-Energy other disadvantage is related to the toxic emissions accompanying the combustion of several types of plastics [17]. The other popular but low-tech recycling alternative is the use of the recycled plastics wastes in construction or manufacturing processes instead of the virgin type. Several among this option relieved the demand for the virgin plastic materials at the same time disposing off the wastes.

Several research were carried out to explore the potential of PW in building and construction applications [5, 18-19]. Polymer modified asphalt is the key component of a high performance flexible pavement [20]. But due to the environmental and cost concern associated with the use of virgin polymer, PW are being explored as alternative for asphalt binder modifications [9, 21-25]. Some portion of the flexible pavement aggregate are also being replaced with PW [26-27]. A low density AC was obtained by substituting 20% by volume of aggregate without significant loss in marshal stability [28]. Up to 30% by volume of aggregate was replaced by low density polyethylene in dense graded flexible pavement [29]. The recorded lightness in weight was offset by loss in indirect tensile strength.

In past studies that explored the modification of asphalt binder using recycled polymer waste, the optimized polymer-asphalt mixing duration was reported to be greater than 2 hr at temperatures of 180 to 200°C [21]. When asphalt is subjected to high temperatures for an extended period of time, such as 2 hr, it will undergo oxidation [30]. Oxidation is responsible for the degradation of certain mechanical properties of asphalt

due to aging. Furthermore, a particle size of 1.18 to 2.36 mm seems to be preferred when RPW is used to partially replace AC aggregates [27, 31]. There is no experimental basis for this selection. Therefore, this preferred size might not be optimal. Another observation is the type of test conducted in most of the relevant studies. The current state-of-the-art performance tests were not typically used in previous research. A thorough and high quality study needs to be conducted in this research area.

2.1.1 RPW AS ASPHALT BINDER MODIFIER

Murphy et al. [25] used various polymers including polyethylene (PE), polypropylene (PP), ethylene vinyl acetate (EVA), styrene butadiene styrene (SBS), polyether polyurethane, truck tire rubber and ground rubber, as an asphalt modifier with the intention of obtaining an appropriate blend that will exhibit similar properties as Polyflex 75 (modified binder) and 100 penetration bitumen. Their experimental results provided satisfying blends containing LDPE and ethyl-vinyl acetate for further consideration because of the similarity of their properties to those of 100 penetration bitumen and Polyflex 75.

García-Morales et al. studied the rheological characteristics and microstructure of recycled EVA-modified bitumen [32]. Dynamic shear test was conducted in the linear visco-elastic region. Significant increase in storage and loss moduli values were observed at high temperature, indicating increased resistance to permanent deformation. Furthermore, micro-structural changes were also observed through optical microscopy and modulated differential scanning calorimetry (MDSC) for polymer content of up to

9% in the blends. This is related to the interaction between large swollen polymer particles and the other constituents of the asphalt.

The effect of hydrogen-peroxide-treated (ozonized) PVC pipe waste on the behavior of asphalt mastic has been reported [33]. Various samples were prepared from SBS-modified (20 to 30%wt.) bitumen with varying contents of coarse and micronized H_2O_2-treated PVC particulates (60-70%wt.) along with limestone dust (7-15%wt.). The ozonized PVC waste demonstrated a better performance in terms of improved viscoelastic properties (as indicated by dynamic mechanical analyses (DMA) and rheometer test results). This is attributed to the lower molecular mass and rougher and porous surface characteristics of the treated particles, as evidenced by UV-visible spectrometry and SEM measurements, which leads to a consistent and better particle-bitumen anchorage. A roof mastic composition of treated coarse and micronized PVC waste, isocyanate waste, limestone dust, anti-oxidant, rosin and SBS-modified bitumen that satisfied Indian specifications (IS 1195-90 Bitumen Mastic for Flooring) has been fully characterized.

Furthermore, the modification of an asphalt binder for roofing using PVC packaging waste has been conducted [34]. Samples from asphalt containing (0-10%wt. asphalt) PVC waste were subjected to low-temperature flexibility, elongation, tension, alkali and acid resistance, softening point, ductility and penetration tests during a 12-month aging cycle period. The results revealed positive performance improvements. This is related to FT-IR findings that show negligible differences in the locations and magnitudes of peaks in the absorption band between the modified and unmodified asphalt, which implies a compatible physical interaction among the PVC waste and light

oil asphalt constituents. Additional microscopic images showed the emergence of a disperse and continuous polymer-rich microstructure with increasing polymer content.

The effect of using recycled toner cartridge plastic waste on the properties and behavior of asphalt binder has been examined [22]. The research was funded by the Texas Department of Transportation in an attempt to improve the performance of hot mix asphalt and facilitate the recycling of toner cartridge waste. Three test road sections having different toner compositions were constructed at various locations. The toner level required to achieve different superpave performance grading were established for each type of toner waste. Bending beam rheometer results shows increased stiffness (m-value) for the modified asphalt, thus indicating increased susceptibility to lower-temperature cracking. A mixing time of 60-90 min was required to obtain a homogenous mix. However, the asphalt-toner blend exhibits lower thermal storage stability.

Ho Susanna et al. performed asphalt modification using combinations of three LDPE wax materials and three recycled LDPE materials [24]. The molecular weight and molecular weight distribution of recycled LDPE were observed to significantly affect the modified asphalt's hot storage stability and behavior at low temperature. Low-molecular-weight LDPE with wider molecular weight distributions was found to be more suited for asphalt modification compared to LDPE with higher molecular weight and a narrower molecular weight distribution.

An economic feasibility evaluation of the utilization and processing of mixed plastic waste (MPW) with or without vacuum residue (VR) under conditions characteristic of Saudi Arabia has been conducted [2]. The study established all the

associated costs related to the processing of MPW and conducted sensitivity and profitability analyses. The processing of MPW with VR at a capacity of 200,000 tons per year was found to be economically feasible under conditions found in Saudi Arabia. An internal return rate (IRR) value of 14.6% with a corresponding payback period of approximately 6 years and break-even capacity of 47.6% were estimated.

The feasibility and potential use of recycled waste polymer as a modifier in stone mastic asphalt (SMA) in Ireland has been investigated [21]. The study focused on increasing the market value of local commercially available recycled waste plastic and providing guidelines for and insight into the use of RPW for quality road construction in that country. Several types of RPWs were identified, including LDPE, medium-density PE (MDPE), and HDPE, which are mainly used for packaging and plastic bottles; PVC; PP; PET; and acrylonitrile butadiene styrene (ABS). Only three of the RWPs (PP, HDPE and LDPE) were successfully blended with the binder. The remaining polymers were found to be immiscible with the bitumen due to their high melting point, high density or low surface area. A straight-grade bitumen was selected for the study. The optimized bending time and temperature were 2.5 hr and 180°C at 4% HDPE content; this RPW blend showed the most promising results. The RPW was found to outperform the traditional mix when subjected to performance testing, such as wheel track and indirect tensile fatigue tests. However, the use of virgin polymer still yields better results than the RPW. The study recommended the blending of both RPW and virgin polymers, especially the elastomeric type, so as to compensate for the loss of elasticity of the RPW-modified asphalt. As with most similar studies, the mixing time of the RPW is long and could be very costly when large quantities of bitumen are needed for road projects. The

morphology of the binder has not been closely examined to determine the extent to which the RPW is blended. This could be performed with high-resolution imaging processes, such as SEM. The above point is important in regard to analyzing the effects of time, temperature and rate of shearing (which has not been mentioned) on the morphology. So, for all that is observed, the increased penetration and softening point of the binder could be mainly due to the oxidation of the binder as a result of the prolonged mixing time and not because of the homogeneous mixing of the RPW with the binder.

In a comparative analysis of the modifying effect of reactive and non-reactive polymers [35], the effect of recycled EVA and a combination of recycled EVA with LDPE (EVA/LDPE) on the rheology of asphalt was reported. The recycled EVA- and EVA/LDPE-modified asphalts show both increased losses and elastic modulii. Bitumen modified with 5% EVA/LDPE yields the maximum linear visco-elastic moduli within a temperature range of -10 to 50°C.

The micro-structure and properties of asphalt modified with PE waste have been investigated [23]. The homogeneity and dispersion of the PE waste in bitumen was improved through the addition of an organophilic Momtmorillomite (OMMT). The PE waste was collected from domestic garbage. The FT-IR results showed no change in the functional group of the modified asphalt, and SEM and fluorescence microscopy analyses showed a more homogenous micro-structure due to the addition of OMMT. As a result, an increased softening point and penetration with improved ductility were observed.

Up to 5% of 2 mm shredded LDPE collected from domestic waste has been utilized to modify an asphalt binder [36]. The mixing of the waste and the binder was

performed at 165°C with a shearing speed of 3,500 rpm. Fluorescent microscopy scanning (FMS) was employed to verify the homogeneity of the PE-modified binder. Three factors were the main focus of the examination: temperature effects on binder properties, the effects of the mixing duration on the binder properties, and the effects of the PE content on the asphalt binder properties. The results from conventional asphalt tests show slight changes in penetration and softening point values with increasing blending temperature. Increasing the blending temperature facilitates the PE-asphalt blend mixing, hence obtaining harder polymer-modified binder. As the PE content is increased, the rate at which the softening point and penetration increased was lower. It was shown that, by keeping blending time constant, the increase in PE content required higher temperatures for the development of modified asphalt. PE-modified binders were found to exhibit relatively lesser loss on heating, when compared to the neat asphalt binder. This result was possible because significant proportions of the high volatile fraction of the binder were absorbed and trapped within the swollen PE pellets.

Fang, C. et al. modify asphalt using a combination of packaging PE and rubber powder [37]. They performed rolling thin film oven (RTFO) tests and studied the aging mechanism using Fourier transform infrared spectroscopy (FTIR). They used rubber powder with a fineness range of 300–600 μm and waste PE with a chip size of 1.5 cm X 2.5 cm. The polymer-asphalt blending was performed at 180°C at four different combinations and percentages. A significant decrease in the ductility and an increase in the softening point were observed following the RTFO aging test. However, the results indicate changes in the ductility and softening point of modified asphalt due to the aging of the asphalt to be less significant than that of raw asphalt. The penetration variation of

modified asphalt is also smaller than that of raw asphalt, which is an indication of the lack of dependency of the penetration on the aging of modified asphalt to some extent.

Singh et al. studied the modification of asphalt using maleic anhydride and recycled LDPE [38]. They found significant increases in the softening point and some reduction in penetration due to modification with maleic anhydride. The difference was conspicuous when the base bitumen was modified with higher percentages of maleic anhydride. The viscosity of the maleated bitumen was found to be higher than that of bitumen without maleic anhydride and thus produced improved viscoelastic properties of the resulting blend. The recoverable blends composed of recycled LDPE and SBS displayed satisfactory softening points and low-temperature susceptibility.

2.1.2 RPW AC MODIFICATION VIA AGGREGATE SUBSTITUTION

In a review of the use of recycled solid waste material in asphalt pavement construction in the United Kingdom [5], a substantial proportion of the generated solid waste plastic that could be successfully utilized as a substitute for virgin aggregate in pavement construction was reported as not being recycled for this purpose. Several types of plastic waste could be used as fine aggregate if they pass the standard specification test for surface course aggregates. Recycled plastic mainly containing LDPE was used to substitute 30% of 2.36 mm to 5 mm aggregate in a dense bituminous macadam (DBM). This lowered the mix density by 16% and increased the mix Marshal stability by 250%. Smaller sized LDPE (0.3-0.92 mm) was also utilized as 15% of the aggregate in asphalt surfacing. This resulted in a higher retained stability of 15% and doubled the Marshal quotient. However, a higher binder content is required in this situation. Positive results

were also reported when PVC particles were used. But only limited performance tests were performed on AC modified using RPW aggregate. Fewer types of RWP were utilized as aggregate substitutes.

The effect of PET on the performance of stone mastic asphalt (SMA) has been reported [27]. Crushed PET waste 2.36 mm and smaller was incorporated into an SMA mix to substitute 0-1%wt. of the aggregate. The stiffness of the mix decreased at a higher PET waste content, whereas the fatigue life of the PET-modified SMA significantly improved.

A hybrid recycled waste containing 20% nitrile rubber and 80% PE was obtained by shred mixing (2.36 mm to 1.18 mm). The effect of the use of the waste on various mechanical properties of the AC was investigated [31]. Mix containing 8% of the waste by weight of the aggregate showed improved Marshal stability, Marshal quotient and retained stability. The indirect tensile strength of the modified mix increases by up to 50% as compared to the conventional mix. However, the modified mix exhibited a reduced rutting tendency based on results from a wheel track test.

Local recycled plastic (RP) in corporation with recycled aggregate pavement was utilized to investigate how to improve the efficiency and performance flexible pavement maintenance in Algeria [39]. The RP, which is mainly composed of plastic bottles and cable phone plugs, was obtained from a local plastic recycling company. Granular pellets of the RP material of approximately 4 mm were utilized as a substitute of up to 8% of the mix aggregate. However, the procedure of the asphalt mix preparation and the test

conducted on the prepared samples are not the current state of the art. The Marshall mix design and test procedure employed for this study could produce misleading results.

2.2 PLASTIC WASTE USED IN ROAD CONSTRUCTION

Certain states in India have used between 10% and 15% polythene plastic waste content to modify asphalt binder used in road construction. The available polythene waste was estimated to cover up to 134 km span of road. An equivalent savings of 35,000 to 45,000 Indian rupees per km of road was calculated. Good initial road performance was also reported, and improved long-term performance is also anticipated [40]. An extensive research on the use of PW waste for road construction has made it possible for Indian government to make it (PW) mandatory road construction material [41].

Several test roads of plastic waste modified asphalt concrete AC were constructed in the city of Vancouver, Canada [42]. Approximately 20% of the mix proportion was replaced with reclaimed asphalt and a wax derived from plastic waste. Various initial benefits, such as low cost and a reduced carbon footprint, related to the mix processing were reported. The performance results will be obtained in the near future.

2.2.1 Eastern Province Municipal Recycling Program KSA

The Eastern Province municipality in KSA has started a domestic waste recycling program as a part of its sustainable city initiatives. The recycling program is currently very limited and depends on sorting the domestic waste during collection using separate trash containers as shown in Figure 2.1. The recycling program will be expanded in the

near future by building waste separation and sorting plants that will help recycle 100% of the domestic waste in Al-Dammam, Al-Khobar, and Dhahran.

Figure 2.1: Typical Recycle Waste collection Bins setup by the Municipality.

2.3 STORAGE STABILITY OF MODIFIED ASPHALT BINDER

Static storage stability and compatibility of styrene-butadiene-styrene (SBS) modified asphalt binder was investigated in the past [43-44]. The modified asphalt binder stability was found to decrease with increasing SBS content, while the asphalt binders with more aromatic constituent happened to show more compatibility towards the SBS polymer. The use of softening point as phase separation parameter was also found to be inadequate. As a result, new separation index as a function of visco-elastic property of the binder was proposed [43]. The stability of asphalt binder modified with methacrylate-butilacrylate terpolymer (EGA), Virgin polyethylene, ethylene-propylene-diene terpolymer (EPDM) and SBS was also examine [45]. All the polymer showed some level of instability when stored in a static mode with time. In another research, the effect of molecular weight and molecular weight distribution on the storage stability and low

temperature properties of recycled low density polyethylene was explored [24]. Low molecular weight LDPE with wider molecular weight distribution exhibits superior properties than LDPE with higher molecular weight and narrow molecular weight distribution. No specific conclusion was made about content range of recycled LDPE that could possibly warrant stable asphalt blend. Later on, compatibility and storage stability of a polar monomer grafted SBS modified asphalt binder was reported [46]. The polarized SBS modified binder was found to be relatively more stable than the normal SBS modified asphalt binder. Addition of nano-clay was also reported to improve the storage stability of the SBS modified asphalt binder [47]. The reason given for this improvement was not due to prevention of phase separation, but rather the settling of the clay to bottom of the aluminum test tube. This compensates the difference in softening point that could be observed between the top and bottom samples, which occurs due to the migration of the SBS polymer to the surface. Hence, another reason that prompt the question of appropriateness of the static approach of testing of modified asphalt stability arise. In another study, effect of sulfur and base bitumen constituent on the stability of SBS modified asphalt has been examined [48]. Even though the variously utilized type of bitumen showed similar constituent proportions, the stability of their SBS modified blends differ. Addition of sulfur to the SBS modified asphalt helps retards phase separation through the formation of additional cross link within the polymer phase network (vulcanization). The storage stability examination in all the above mentioned studies was conducted in static mode.

The storage stability test employed by all the above mentioned studies, was based on the the American Society for Testing and Materials standard test for possible

separation of polymer phase from the asphalt (ASTM D5892). Due to several questions that this standard test could not address, it has been withdrawn since 2005. For example, the standard specified that the sample be statically stored in a cylindrical tube within an oven (163^{o}C) for some time and then cool to a freezing temperature. It is then cut into three part for the softening point of the top and bottm parts to be tested. But in reality the polymer modified asphalt undergoes a contious agitation in the storage tank, prior to mixing with aggregate [49]. This crutial factor, which can make or break the stability of a given polymer in an asphalt binder was not considered by the test. The specified test parameter (softening point) that measures the separation extent was found to be indequate [43]. Some studies suggeted that this method exaggerates the seperaration tendency of the modified asphalt [50]. An alternative test method that reflect actual field performance was proposed by a National Cooperative Highway Research Program (NCHRP) research under the Strategic Highway Research Program (SHRP), which has been evaluated by the Federal Highway Administration (FHWA) [49]. This alternative test method for storage stability was employed in this study.

2.4 RUTTING AND FLOW NUMBER TEST OF ASPHALT CONCRETE

Dynamic creep load test was found to correlate excellently with the rutting performance of asphalt mixtures [51]. The three main stages utilized in describing and modeling the permanent deformation of the asphalt material was earlier verified through field and laboratory studies [52]. Repeated load testing is now part of asphalt mix simple performance tests as Flow Number (FN) test [53]. This was the result of series of research

carried out under the National Cooperative Highway Research Program [51]. The FN test is being used as a measure of rutting resistance of asphalt pavement mixtures for quality control and assurance [54]. The asphalt repeated load test was also adopted as part of a provisional standard by American Association of State Highway and Transportation Officials as AASHTO: TP 79. Research were carried out to further standardize and accommodate various asphalt mix type such as warm mix asphalt [55]. The standardized test has accounted for different source of variation like testing loads, aggregate sizes, sample preparation for laboratory test specimens etc. However, there are still issues which are yet to be addressed, making it the focus of research in recent years.

Previous studies have identified some flaws of the FN test, resulting in inconsistent FN values, and proposed possible solutions [53, 56]. The inconsistency was found to be as a result of permanent strain data fluctuation, due to electric noise and elastic recovery property in case of rubber mix [53]. A simple stepwise approach that rearrange the permanent deformation curve (PDC) data increasingly was proposed [56]. Fitting the PDC data in to Francken model (FM) prior to FN estimation was recommended as the best alternative [53]. The later approach was ultimately and widely accepted as it is currently part of the AASHTO TP 79 standard. Further studies on the FN test include correlating the FN with secondary strain rate, in an attempt to minimize the test duration [57]. Genetic programming coupled with simulated annealing, multiple least square regression and support vector machine were used to modeled the FN of Marshall asphalt mixture test specimens [58-59]. Superpave asphalt mix volumetric parameters were also utilized as FN predictors [60]. But not all of these previous studies conducted were based on the current standardized test. Almost all of these research were conducted

on some old data base, that was acquired prior to the adaptation of the FN as a standard test, which was drafted and activated in 2009.

2.5 FATIGUE LIFE (FL) OF ASPHALT CONCRETE

The existing major standard methods for estimating the fatigue life of asphalt concrete (AC) are performed at constant temperature, continuous and constant load frequency [61-62]. Table 2.1 list the widely employed failure criteria for analyzing fatigue test data. The standard AC fatigue test is conducted on a 50 mm thick by 63 mm wide by 380 mm long AC beam, loaded at third points and subjected to repeated flexural bending (10 Hz), under a constant stress or strain until failure [61].

The traditional method of 50% stiffness loss fatigue life (N_50), the Rowe energy ratio approach (N_DRE) and the viscoelastic continuum damage approach (VECD) were compared [63]. Both N_50 and VECD fatigue life were found to be less than the fatigue life estimated by N_DRE approach. Thermo-mechanical fatigue life prediction model of cement asphalt mortar was presented in [64]. The Combined effect of loading frequency, temperature and stress level on the indirect tensile stress fatigue life of AC was investigated [65]. The effect of recycled asphalt pavement (RAP) on the fatigue life of asphalt concrete (AC) and asphalt binder was also investigated [66]. The RAP has a positive and negative impact on the fatigue life of the AC and the binder respectively.

Table 2.1: Different failure criteria for estimating asphalt fatigue life.

Methods	Equations	Description
Classical approach [61].	NA	Fatigue life (N_50) corresponds to the load cycle (N) at which 50% loss in AC stiffness is observed.
Dissipated energy ratio (DRE) approach [67].	$R_E = \frac{nw_o}{w_n}$ ...(2.1) $w_n = \pi\varepsilon_n\sigma_n \sin\delta_n$ ..(2.1a)	R_E is the energy ratio; n: number of load cycle; w_n: dissipated energy in the n^{th} cycle; w_o: dissipated energy in the initial cycle; ε_n, σ_n, δ_n and E_n^*: strain, stress, phase angle and complex modulus at the n^{th} cycle respectively. For (2.1), crack initiates at n (N_DRE) value corresponding to the peak of $R_E - n$ plot for controlled stress test, and at n value where the $R_E - n$ plots deviate from straight line for strain controlled test.
Rowe Energy ratio approach (N_DRE) [68].	$R_E = nE_n^*$ ...(2.1b) $R_E = \frac{n}{E_n^*}$ ...(2.1c)	(2.1) was later simplified and modified to (2.1b) and (2.1c). Equation (2.1b) and (2.1c) for stress and strain controlled test respectively. Crack initiation point is the same as in (2.1).
Change in dissipated energy ratio [69].	$\Delta R_E = \frac{(w_{n+1}-w_n)}{w_n}$ ...(2.2)	ΔR_E is the dissipated energy change ratio; w_n: dissipated energy in the n^{th} cycle; w_{n+1}: dissipated energy in the $(n+1)^{th}$ cycle.

Table 2.1: Different failure criteria for estimating asphalt fatigue life. (Cont'd)

Methods	Equations	Description
		The $\Delta R_E - n$ plot exhibits three distinct regimes. The first is characterise by rapid and continuous decrease of ΔR_E as n increases. The second regime shows a steady and relatively constant value of ΔR_E with increasing n. Then finally a sudden and rapid increase in ΔR_E. The beginning of stage three corresponds to initial crack formation.
Stiffness ratio (SR) approach [70].	$SR = \frac{nS_n}{S_o}$ ...(2.3)	n: number of load cycle; S_n: stiffness at n^{th} load cycle; S_o: initial stiffness corresponding to the 50th load cycle. The fatigue failure is said to occur at n value (N_SR) that corresponds to the maximum SR in the $SR - n$ plot.

Summary: The past studies on the use of RPW for asphalt binder or asphalt concrete modification are old and mostly used empirical test techniques, make several assumption without scientific justification and targeted only one or two of the RPW. A lot of these research give little or no attention to specific tests related asphalt concrete performance, but general viscoelastic characterization. Several countries have initiated research towards incorporating RPW to obtain a cheaper and durable AC design for their local climate. KSA Eastern province municipality has initiated a systematic RPW collection point that will facilitate and increase the rate plastic waste recycling. Past and current studies on polymer modified asphalt storage stability was also reviewed.

CHAPTER 3

METHODOLOGY

Introduction: This chapter describes the methodology followed in carrying out the various tasks involved in this research. The study has been divided into three phases. The first phase addresses the identification of RPWs that can be used in asphalt modification or replacement of aggregate, followed by the evaluation of RPW-modified asphalts. Different potential RPWs will be screened and selected based on thermal and rheological techniques. The second phase involves analysis of the performance and mechanical properties of RPW-modified AC mixtures composed of both pure binder and pure RWP or blended modified asphalt binder. The third phase includes data analyses and reporting. The overall work sequence and content has been summarized in the work flow chart a shown Figure 3.1. The RPW modified asphalt test experimental design was presented. The RPW-AC mix optimization and performance evaluation guide was also shown. The detail description of the test and analysis methods employed has been provided in the subsequent subheadings. Details of the AC mechanic-empirical performance modeling method adopted was also described.

3.1 DESCRIPTION OF WORK EXECUTION

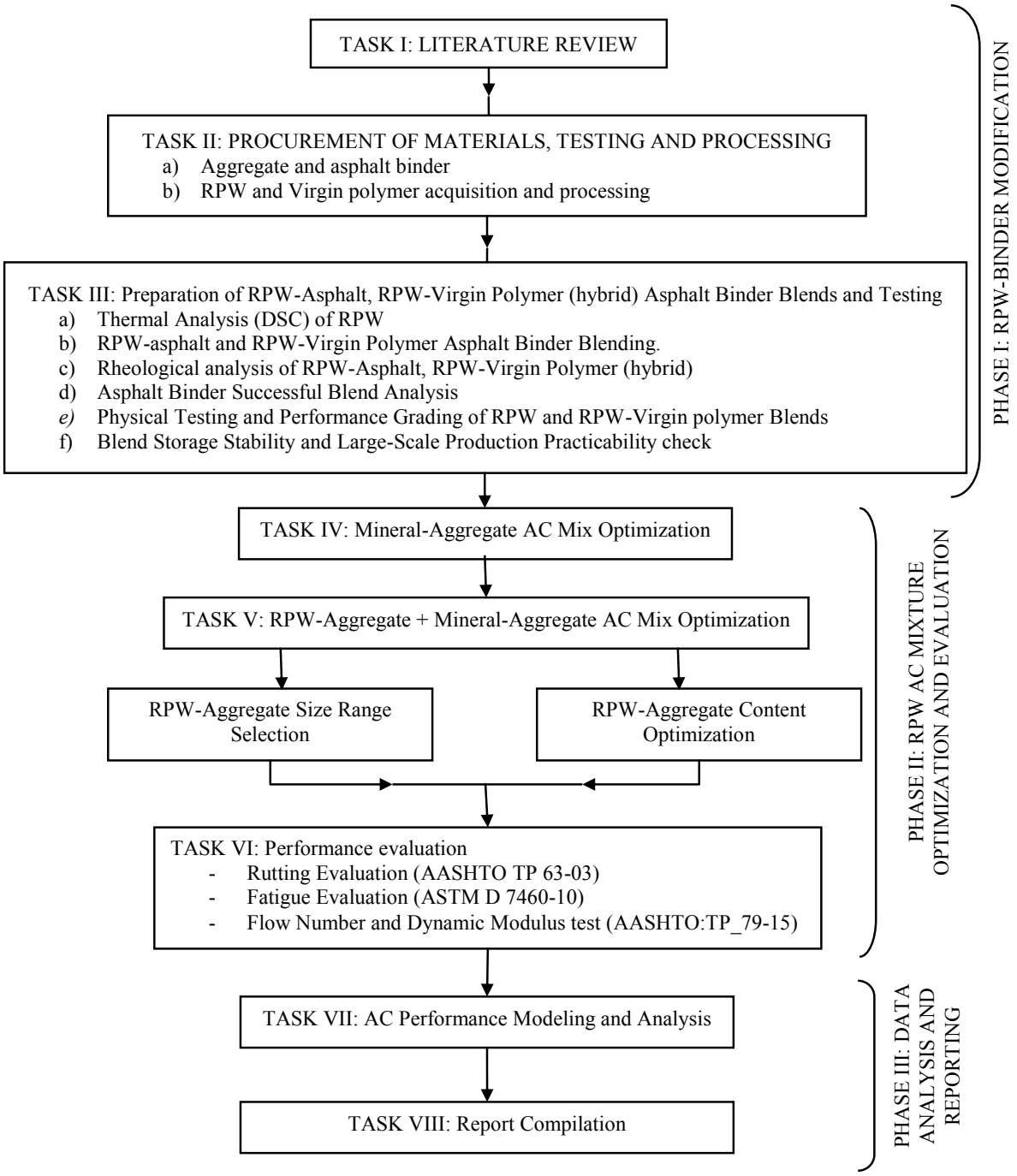

Figure 3.1: Work Flow Chart.

3.1.1 PHASE I: RPW BINDER MODIFICATION

The tasks for each phase of the research are listed under the appropriate heading. An initial set of sub-tasks of some of the main tasks are carried out concurrently.

3.1.1.1 TASK I: LITERATURE REVIEW

A thorough literature review of current and past research related to the use of RPW for asphalt modification has been carried out. The current practices and approaches related to research on RPW asphalt concrete from developed countries were also documented.

3.1.1.2 TASK II: PROCUREMENT OF MATERIALS, TESTING AND PROCESSING

A. Aggregate and Asphalt Binder: A neat asphalt binder, which was collected from local refineries, was used in this study. A common and local type of aggregate were also collected from the nearest quarry.

   The aggregate was analyzed for conformity with ASTM specifications for aggregates to be used for road construction. ASTM D1241-07: (Specific Gravity, Water Absorption, Soundness, angularity and L.A. Abrasion tests). The asphalt binder was characterized using the asphalt the Performance Grade tests (AASHTO MP-19) and (AASHTO TP-70).

B. RPW and Virgin Polymer Acquisition and Processing:

Local plastic waste were identified and handpicked from municipal waste collection program. These wastes were then processed for easier use. Virgin polymers, which include plastomeric Polybilt (PB) and elastomeric styrene butadiene styrene (SBS), were acquired from commercial source. The processing involves the following:

a. *Shredding and Grinding:* the RPWs were shredded, and some amount of the RPW was subjected to grinding using special plastic shredding and grinding machines. For example, RLDPE and RHDPE waste must be ground to the desirable size, depending on whether it will be used for blending with asphalt binder (fine) or for modifying the aggregate composition of asphalt concrete (AC).
b. *Cleaning:* washing and drying for the removal of organic materials.

Classification of the RPW into two groups according to the melting point: the first group with low melting points were selected for asphalt modification, whereas the second group were examined for potential use as aggregates replacement. Thermal analysis and characterization techniques was employed for this purpose. Differential scanning Calorimetry (DSC) was used to determine the melting point, and, accordingly, potential RPW candidates for asphalt modification as well as for aggregate substitution were identified.

3.1.1.3 Task III: Preparation of RPW-Asphalt Binder, RPW-Virgin Polymer (hybrid) Asphalt Binder Blends and Testing

RPWs with recycle labels 2, 4 and 5, which are RHDPE, RLDPE and RPP, respectively, will be the main focus in this task.

A. A differential scanning calorimeter (DSC) Q1000 was used to determine the melting point of the RPWs.

B. An ARES rheometer was used to determine the viscoelastic properties of the RPWs and virgin polymers modified asphalt binders.

C. RPW-asphalt and RPW-Virgin Polymer Asphalt Binder Blending.

For this particular task, a special air-tight and high-shear mixer (blender) with a shear speed of up to 5,000 rpm was acquired. This was necessary because most RPW cannot be easily blended with asphalt binder.

Preliminary Mixing of the RPW with the Binder: Various mixing duration for each type of RPW with the asphalt binder at temperatures above the RPW melting point was explored to determine the optimal mixing duration.

D. *Asphalt Binder Successful Blend Analysis:* samples prepared under various mixing were subjected to dynamic shear rheological (AASHTO PP6) and rotational viscosity (ASTM D 4402) tests. These results were plotted against the mixing duration for analysis.

E. Physical Testing and Performance Grading of RPW and RPW-Virgin polymer Blends

The viscoelastic performance properties of asphalt blends with various RPW contents (and in combination with a visco-elastic or viscos-plastic virgin polymer) was investigated. Table 3.1 shows the experimental design that was followed. The series of tests that were conducted are listed below.

1) Rotational viscosity test (ASTM D 4402)

2) Performance Grading (PG) of the modified asphalt binder ((AASHTO MP-19) and (AASHTO TP-70)).

Table 3.1: General Experimental Design for Asphalt Binder Testing.

Blend Type	% Recycled Plastic Waste (RPW)			
	2%	4%	6%	8%
RHDPE	H2	H4	H6	H8
RHDPE+1%SBS	H2S1	H4S1	H6S1	H8S1
RHDPE+1.5% SBS	H2S1.5	H4S1.5	H6S1.5	H8S1.5
RHDPE+2% SBS	H2S2	H4S2	H6S2	H8S2
RHDPE+1%PB	H2PB1	H4PB1	H6PB1	H8PB1
RHDPE+1.5%PB	H2PB1.5	H4PB1.5	H6PB1.5	H8PB1.5
RHDPE+2%PB	H2PB2	H4PB2	H6PB2	H8PB2
RLDPE	L2	L4	L6	L8
RLDPE+ 1% SBS	L2S1	L4S1	L6S1	L8S1
RLDPE+ 1.5%SBS	L2S1.5	L4S1.5	L6S1.5	L8S1.5
RLDPE+ 2% SBS	L2S2	L4S2	L6S2	L8S2
RLDPE+1%PB	L2PB1	L4PB1	L6PB1	L8PB1
RLDPE+1.5%PB	L2PB1.5	L4PB1.5	L6PB1.5	L8PB1.5
RLDPE+1.5%PB	L2PB2	L4PB2	L6PB2	L8PB2
RPP	P2	P4	P6	P8
RPP+1% SBS	P2S1	P4S1	P6S1	P8S1
RPP+1.5% SBS	P2S1.5	P4S1.5	P6S1.5	P8S1.5
RPP+2% SBS	P2S2	P4S2	P6S2	P8S2
RPP+1%PB	P2PB1	P4PB1	P6PB1	P8PB1
RPP+1.5%PB	P2PB1.5	P4PB1.5	P6PB1.5	P8PB1.5
RPP+2%PB	P2PB2	P4PB2	P6PB2	P8PB2
Two Replicate for each combination were tested				

F. Blend Storage Stability and Large-Scale Production Practicability check.

A thermal storage stability analysis (Section 3.3.5) of the asphalt modified using RPW and RPW-Virgin polymer was conducted on selected blends having acceptable PG grades from the previous sub-task. This is to determine whether

the minimum storage stability level is achieved. The obtained results served as a basis for the appropriate use and recommendation of the specific RPW used in the asphalt binder modification.

3.1.2 PHASE II: RPW AC MIXTURE OPTIMIZATION AND EVALUATION

RPWs with recycle labels of 1, 2, 3, 4, 5 and 6, namely, recycled Polyethylene recycled Terephthalate (RPET), recycled High density polyethylene (RHDPE), polyvinyl chloride (RPVC), recycled low density polyethylene (RLDPE), recycled polypropylene (RPP), and recycled polystyrene (RPS), were utilized in the following tasks.

3.1.2.1 Task IV: Virgin Aggregate Asphalt Concrete Mix Optimization

Asphalt concrete mixtures were designed and prepared for the control binder and nine selected modified binders: RHDPE, RLDPE, RPP, RHDPE+SBS, RLDPE+SBS, RPP+SBS, RHDPE+PB, RLDPE+PB, and RPP+PB. Modified binders that have the required PG will be selected from Phase I. The AC mixtures were prepared following the superpave volumetric mix design [71], and the optimal binder content are determined in each case which were then adopted in the next subtask. The first two columns of Table 3.2 showed the various mixtures to be designed.

3.1.2.2 Task V: RPW Aggregate + Virgin Aggregate AC Mix Optimization

The selected optimum blends from Phase-I was further utilized to design asphalt concrete mixtures containing both RPW aggregate and conventional aggregates. The optimal RPW aggregate size was first established. Three levels of RPW was then used as partial replacements of the fine aggregate for RPW content optimization. The percentage of the fine aggregates to be replaced depends are 5, 10, 20%. Table 3.2 provides an overview of the conceived experimental design.

Table 3.2: Experimental design of the AC mix optimization and performance evaluation.

Mix type	RPW contents			
	Virgin Aggregate	Aggregate + level 1 %RPW	Aggregate + level 2 %RPW	Aggregate + level 3 %RPW
Virgin Asphalt AC Mix	2 samples	2 samples	2 samples	2 samples
RHDPE - Optimal AC Mix				
RHDPE + SBS Optimal AC Mix				
RHDPE + PB Optimal AC Mix				
RLDPE Optimal AC Mix				
RLDPE + SBS Optimal AC Mix				
RLDPE + PB Optimal AC Mix				
RPP - Optimal AC Mix				
RPP + SBS Optimal AC Mix				
RPP + PB Optimal AC Mix				

3.1.2.3 Task VI: Performance evaluation

Fatigue and Rutting Performance Evaluation of the Most Prominent Mixtures:

Test samples for the various successful mixtures shown in Table 3.2 were prepared and tested using the following tests:

- Standard Test Method for Determining the Rutting Susceptibility of Asphalt Paving Mixtures Using the Asphalt Pavement Analyzer (APA) (AASHTO TP 63-03)
- Standard Test Method for Determining Fatigue Failure of Compacted Asphalt Concrete Subjected to Repeated Flexural Bending (ASTM D7460 - 10)
- Superpave Asphalt Mix Performance Tester (AMPT) for determining the dynamic modulus, flow time and flow number tests.

3.1.3 PHASE III: DATA ANALYSIS AND REPORTING

3.1.3.1 Task VII: Results Analysis and AC Performance Modeling

The results from the Superpave asphalt mix performance testing (AMPT) was utilized to simulate the service rutting and fatigue performance of the RPW-modified hybrid asphalt concrete mix using Finite Element based Mechanistic Empirical technique. The measured rutting and fatigue performance from Task VI is compared to the modeled service performance. The economic feasibility of developing the modified AC mix in terms of the costs and enhanced service life of the asphalt concrete structures was also assessed.

3.1.3.1 Task VIII: Report Compilation

A comprehensive and detailed report of all the findings, which will serve as a milestone for research related to RPW asphalt modification, has been prepared. This also include a full accounting of all the findings from the different levels of AC modification and a summary of how the findings for the various levels are related. The results are presented and documented in this report, in a format and style recommended by the graduate school dissertation template.

3.1.4 CODING Description for Experimental Samples

Table 3.3 summarizes the general coding system employed in results analysis throughout this report, including examples on how to interpret a given sample code.

Table 3.3: Coding and Nomenclature Table.

Name	RPW/Polymer	Code	Source/Nature
Recycled High Density Polyethylene	RHDPE	H	RPW
Recycled Low Density Polyethylene	RLDPE	L	RPW
Recycled Polypropylene	RPP	P	RPW
Styrene Butadiene Styrene	SBS	S	Commercial
Polybilt	PB	PB	Commercial
Example 1: L2 = 2%RLDPE; L4S1 = 4%RLDPE+1%SBS; P2=2%RPP etc. Example 2: L6_76(H) = 6%RLDPE_PG-Testing Temperature-(Heavy Traffic level)			
Asphalt Concrete (AC) Mix			
AC mixture Type	Description		
CRB_76	Crumb rubber modified asphalt binder AC		
5% RPW AC	Neat binder AC + %5 RPW aggregate etc		
5% RPET AC	Neat binder AC + %5 RPET aggregate etc		
Fresh+RPW	Neat binder AC + optimum RPW aggregate content		
L6_76(H)	L6_76(H) modified binder AC		
L6_76(H)+RPW	L6_76(H) binder AC + optimum RPW aggregate		
L4S1.5_76(H)+RPW	L4S1.5_76(H) binder AC + optimum RPW aggregate		
L6B1_76(H)+RPW	L6B1_76(H) binder AC + optimum RPW aggregate		
H4_76(H)+RPW	H4_76(H) binder AC + optimum RPW aggregate		
H2B1.5_76(H)+RPW	H2B1.5_76(H) binder AC + optimum RPW aggregate		
H4S1_76(H) +RPW	H4S1_76(H) binder AC + optimum RPW aggregate		
P2S1.5_(76)+RPW	P2S1.5_(76) binder AC + optimum RPW aggregate		

3.2 MATERIALS

3.2.1 Asphalt Binder and Commercial Polymers

The properties of the local asphalt binder utilized in this research are shown in Table 3.4. It is obtained from Riyadh refinery. Typical asphaltene, aromatics, saturates and resin proportion of local binder are 19, 25, 27, and 29% respectively. The performance grade of the local asphalt can be seen to satisfy less than 40% of KSA regions upper service temperature, according to the kingdom PG service temperature shown in Figure 1.1. It can also be noted that the local asphalt binder is only capable of withstanding a standard traffic level 'S' (< 10 million Equivalent Single Axle Loads) according to AASHTO MP-19. These are the main reason why polymer modification of the local asphalt is necessary for major road construction. Radial type styrene butadiene styrene (SBS) thermoplastic copolymer (Calprene C411) was used. This SBS is obtained by solution polymerization of 70/30 butadiene/styrene mix. SBS being the commonly adopted elastomer, and radial SBS being less stable than linear type served as bases for its selection. Plastomeric Polybilt_101 (PB) being once among the top recommended polymer by KSA ministry of transport (MOT) was utilized.

Table 3.4: Components proportion and PG grade of the neat asphalt binder.

Property	PG grade	PG^{+} grade (AASHTO MP-19)	Components Proportion			
			Saturates	Aromatics	Asphaltene	Resins
Value	64- 22	64 S - 22	27.23	24.72	19.22	28.83

3.2.2 Aggregates Properties and Gradations

Table 3.5 shows particle size distribution of the RPW aggregate Size 1 and 2 (S1 and S2) employed in this research. The gradation and properties of the mineral aggregates utilized are shown in Table 3.6, and Table 3.7 respectively. Aggregate properties such as toughness (Los Angelis abrasion), ability to establish a stable skeletal matrix (elongation and angularity) and acceptable organic content etc all have to meet the desired limit for superpave AC mix. The aggregates employed in this study have satisfied these requirement as shown in Table 3.7. The aggregates gradation also must fall within the established control points for Superpave Volumetric Mix Design [71], which they did as shown in Table 3.6. Out of the three gradations employed for this study, the two gradations (Gradation I and Gradation II) shown below were successfully adopted according to superpave volumetric mix design for the various AC mixtures. All the selected asphalt binders type yielded AC volumetric properties much closer to the superpave specification criteria with Gradation I (G1), while H4_76(H) and H4S1_76(H) works better with Gradation II (G2). Typical results and summary have been presented in Table 4.9 and Table 4.10. It can be clearly seen that Gradation II has lesser fine aggregate content than Gradation I. It will later be seen in the result section that H4_76(H) and H4S1_76(H) possessed relatively higher complex modulus than the rest of the RPW binders.

Table 3.5: RPW Aggregate Size Distribution.

Sieve sizes	No. 8	No. 10	No. 12	No. 16	No. 20	No. 30	No. 40
S1	47%	22%	7%	17%	3%	1%	1%
S2	68%	32%	*	*	*	*	*

Table 3.6: Aggregate gradation.

Sieve Size	%Passing Gradation I	%Passing Gradation II	Control point (Min.)	Control Point (max)
3/4"	100	100	100	--
1/2"	95.19	94.00	90	100
3/8"	81.81	79.50	--	--
No. 4	44.00	49.20	--	--
No. 8	31.49	30.20	28	--
No. 10	28.49	28.80	--	--
No. 16	22.11	25.50	--	--
No. 30	16.11	18.70	--	--
No. 40	12.40	13.60	--	--
No. 50	11.30	10.50	--	--
No. 80	9.00	6.50	--	--
No. 100	7.89	5.00	--	--
No. 200	5.19	3.50	2	10

Table 3.7: Properties of aggregate.

	Coarse Aggregate	Fine Aggregate	Filler	Crite -ria	Method
Bulk specific gravity	2.47	2.56	2.75	--	ASTM C127/C128
Apparent specific gravity	2.74	2.78	2.84	--	ASTM C127/C128
absorption	1.73	1.04	--	--	ASTM C127/C128
Los Angelis abrasion (%)	27%	--	--	⩽45	ASTM DC-131
Flat and elongated particles	0	--	--	⩽10	ASTM D4791
Coarse Aggregate Angularity	97/91	--	--	95/90	ASTM D5821
Fine Aggregate Angularity	--	45	--	⩾45	ASTM C1252
Sand Equivalent (%)	--	58	--	⩾45	ASTM D2419

3.2.3 Recycled Plastic Waste (RPW)

RPWs from municipality collection point and KFUPM student restaurant was obtained, sorted into similar category, screened and shredded. The plastic wastes were then processed for easier mixing (as AC concrete aggregate) and blending (in case of asphalt binder modification) as shown in Figure 3.3 Figure 3.4 , Figure 3.5 and Figure 3.6. The

shredded RPW waste was ground using a special grinding machine, as shown in Figure 3.2 below.

Figure 3.2: RPW grinder.

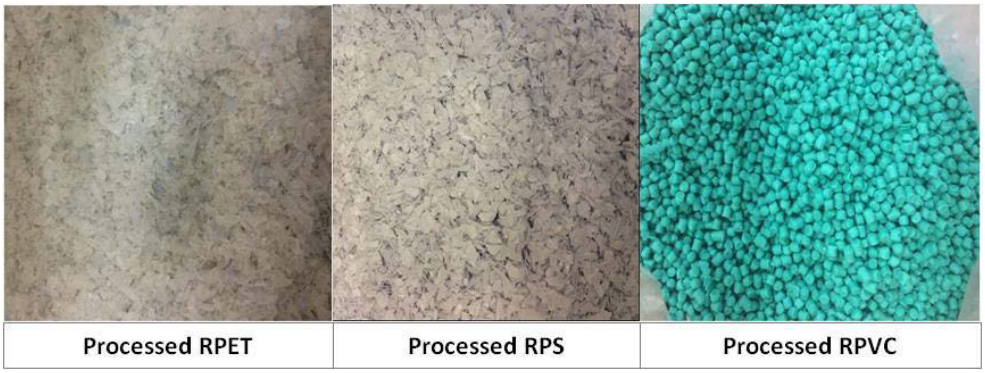

Figure 3.3: Processed Recycled PET, Recycled PS and Recycle PVC.

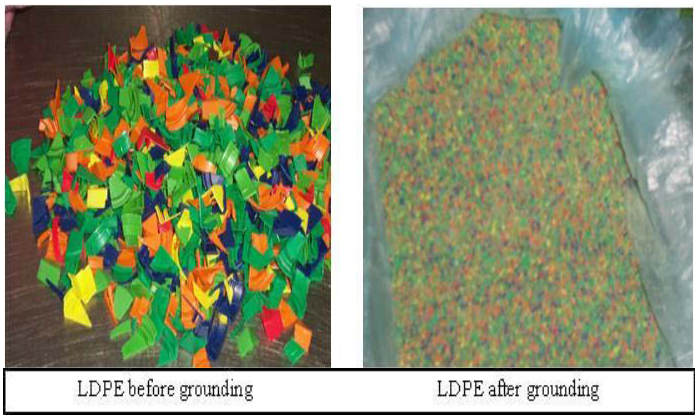

Figure 3.4: Recycled LDPE before and after grinding.

Figure 3.5: Recycled HDPE, before and after grinding.

Figure 3.6: Recycled PP, before and after grinding.

3.2.3.1 Relative Composition of the RPW in the RPW-Asphalt Concrete

The relative proportion of each RPW in the bulk of the RPW combination was established using a pilot survey result from various households at unique neighborhoods. Figure 3.7 shows typical sample images of wastes analyzed, and Figure 3.8 summarizes the procedure of estimating the various weight of the RPW from each sample. A total of 53 sample were analyzed, and 5% significant level was selected in calculating the confidence interval of the various RPW proportion.

Figure 3.7: Typical RPW Relative Proportion Survey Sampling Images.

Figure 3.8: Reference Approximate Weight of Sample RPWs.

3.3 TESTS AND METHODS

3.3.1 RPW Screening

Differential Scanning Calorimetry (DSC) (ASTM E1356 - 08) was employed to determine the exact melting point of the RPW. DSC Q 1000 model was used for these tests. The thermal analysis results served as bases for screening the RPWs. DSC measures the amount of energy absorbed or released by a sample when it is heated or cooled, providing quantitative and qualitative data on endothermic (heat absorption) and exothermic (heat evolution) processes. Figure 3.9 shows a sample result from a single heating and cooling test. The image of the DSC is shown in Figure 3.10.

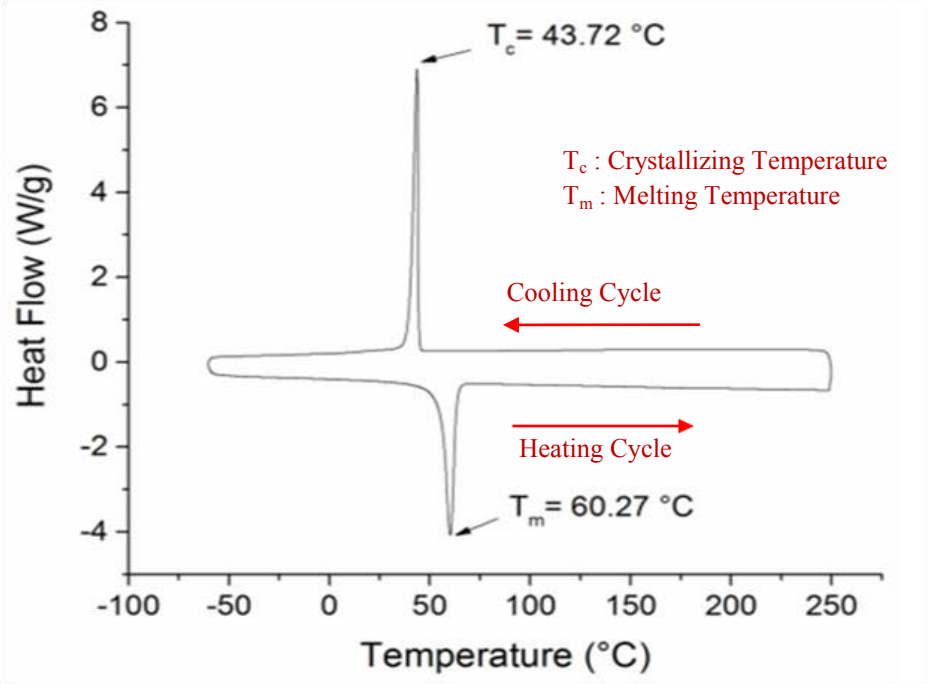

Figure 3.9: DSC Result Interpretation Sample.

Figure 3.10: Differential Scanning Calorimetric Machine.

The possibility of utilizing all available RPW for the asphalt binder modification was explored. Six common plastic waste were examined, viz: polyethylene terephthalate (PET) with recycled label of 1; high density polyethylene (HDPE) with recycled label of 2; polyvinyl chloride (PVC) with recycle label of 3; low density polyethylene (LDPE) having recycle label of 4; polypropylene (PP) with recycled label of 5; and polystyrene (PS) with recycled label of 6. Only RPW with melting point below 200^{o}C were considered suitable for the asphalt modification. But all of the RPW are utilized in AC

modification as aggregate substitute. The selectiveness in case of binder modification is purely based on the asphalt binder characteristics. When asphalt is subjected to high temperatures for an extended period of time, it will undergo oxidation [30]. Oxidation leads to aging of the asphalt, and aging is responsible for the degradation of vital properties of asphalt. But in the case of AC, the there is no need for the RPW to melt in the mix. So all the RPW can be employed in the AC modification via aggregate substitution.

3.3.2 Optimization of RPW-Asphalt Blending Duration

The RLDPE modified asphalt was obtained by hot blending both asphalt and the recycled plastic at 160^{o}C and around 5000 rpm shearing speed. The blend is first placed in an oven at 160^{o}C inside a sealed can, for 1 hr. Rotational viscosity test and dynamic shear rheometer test samples were obtained after 10 minutes blending time interval. The mixing was continued for up to 50 minutes. Figure 4.7 and Figure 4.8 shows the results.

The RHDPE and RPP modified asphalt were obtained by hot blending the asphalt and the recycled polymers at 180^{o}C and 190^{o}C respectively. The shearing speed of blender is about 5000 rpm. The blends are first placed in an oven at 160^{o}C inside a sealed can, for 1 hr. Rotational viscosity test and dynamic shear rheometer test samples were obtained after 10 minutes blending time interval. The mixing was continued for up to 70 minutes. Figure 4.7 and Figure 4.9 showed the plots of the results.

3.3.3 RPW-Asphalt Blending

A customized air-tight and high shear blender shown in Figure 3.11 was employed for the RPW-Asphalt blending. The blender can reach shearing speed up to 9000 rpm, and a temperature of up to 500^{o}C. The air tightness was to minimize or eliminate the oxidation of the blended RPW-asphalt during mixing at high temperature in the presence of air. 500 g of liquid asphalt was manually mixed with appropriate amount of RPW (RPP, RLDPE, or RHDPE), SBS/PB, or combination of both inside a 1000 ml metallic can. The can was sealed with aluminum foil, stored inside an oven at 160^{o}C for an hour to soften the added RPW, SBS/PB or both. The can was put inside a customized high shear blender at the appropriate blending temperature (Table 4.1), the mixture was then shear-blended at 5000 rpm for the applicable time (Table 4.1). The blending duration is 1 hour if the RPW requires less than 1 hour and is in combination with SBS.

3.3.4 Asphalt Performance Grading

DV-II Brookfield viscometer was employed to measure the RPWs modified asphalt viscosities (ASTM D4402). RPW-modified asphalts were subjected to a short term aging test (AASHTO T 240 or ASTM D2872) as per AASHTO PG requirements (AASHTO M 332-14). Dynamic shear analysis and MSCR tests were conducted on the modified asphalt using TA CSAII Dynamic Shear Rheometer (DSR) (AASHTO M 332-14, AASHTO TP 70-11). Further details of the tests and equipments involved in the performance grading of the modified asphalt binder are shown in the following sub-headings.

Figure 3.11: RPW-Asphalt Shear Mixer.

3.3.4.1 Viscosity test (ASTM D4402)

Viscosity test measures the torque required (T) to maintain a constant rotational speed (ω) of a cylindrical spindle that is submerged in the asphalt binder at a constant temperature of 135^{o}C. The measured torque is then converted to a viscosity and is displayed automatically by the rotational viscometer shown in Figure 3.12. Equation (3.1), equation (3.2) and equation (3.3) summarizes the working principles of the rotational viscometer.

$$\gamma = \frac{2\omega R_C^2 R_S^2}{\chi^2 (R_C^2 - R_S^2)} \quad (3.1)$$

$$\tau = \frac{T}{2\pi R_S^2 L} \quad (3.2)$$

$$\eta = \frac{\tau}{\gamma} \quad (3.3)$$

η = Rotational viscosity (Pa·s)

τ = Shear stress (N/cm^2)

γ = Shear rate (s^{-1})

T = torque (Nm)

L = Effective spindle length (m)

R_s = Spindle radius (m)

R_c = Container radius (m)

ω = Rotational speed (radians/second)

χ = Radial distance where shear rate is being calculated (m)

Figure 3.12: Rotational Viscometer setup.

3.3.4.2 Rolling Thin Film Oven test (RTFOT), (AASHTO T 240 and ASTM D 2872)

The Rolling Thin-Film Oven (RTFOT) simulates the short term aging of asphalt binder. Asphalt binder is exposed to temperatures within the range inside the mixing plant, in order to simulate manufacturing and placement aging. The RTFOT also provides a quantitative measure of the volatiles lost during the aging process. The volatiles loss is expressed as percentage of initial mass (35g) of the asphalt, and should not exceed 1%. Equation (3.4) provides the mathematical relationship for obtaining the mass loss. The RTFOT procedure involves putting un-aged asphalt binder samples contained inside cylindrical glass bottles into a rotating carriage within an oven. The oven temperature is maintained at (163°C), and the ageing process continue for 85 minutes. Typical image of the RTFOT machine is shown in Figure 3.13.

$$Volatiles\ Loss = \frac{M_1 - M_2}{M_1} \tag{3.4}$$

M_1: the initial mass of asphalt (35 g)

M_2: mass of asphalt at the end of the RTFO test (g)

3.3.4.3 Accelerated Aging of Asphalt Binder Using a Pressurized Aging Vessel (AASHTO R 28)

The RTFO aged asphalt binder is put in the pressure aging vessel (PAV) that has been preheated to the test temperature (100^{o}C). When the PAV nears the test temperature it is pressurized to 300 psi (2.07 MPa). After 20 hours of this treatment, the samples are removed and stored for future testing, from the degassed chamber. Figure 3.14 shows the major PAV equipment

Figure 3.13: Rolling Thin Film Oven (RTFO) tester.

Figure 3.14: Pressure Aging Vessel (PAV).

3.3.4.4 Dynamic Shear Rheometer test (DSR), (AASHTO T 315)

Dynamic shear rheometer test is used to characterize the elastic and viscous behavior of an asphalt binder. Equation (3.5) up to equation (3.9) describes the stress-strain viscoelastic behavior of asphalt. The test is used in the Super-pave asphalt binder PG specification. DSR test uses thin asphalt binder sample sandwiched in-between two parallel circular plates. The upper plate oscillates across the sample at 10 rad/sec (1.59 Hz) creating a shearing action, while the lower plate is fixed. Equation (3.10), (3.11) and (3.14) presents the mathematical relationship between the applied toque 'T', maximum stress and strain with the complex modulus for DSR test setup. The rutting parameter '$G^*/\sin\delta$' must be maximized for minimal dissipated energy per load cycle at high temperature. Likewise, the viscous component of the complex modulus '$G^*\sin\delta$' has to be minimized to eliminate fatigue cracking. Figure 3.15 shows a typical DSR machine.

$$\varepsilon = \varepsilon_o \sin(\omega t) \tag{3.5}$$

$$\sigma = \sigma_o \sin(\omega t + \delta) \tag{3.6}$$

$$G' = \frac{\sigma_o}{\varepsilon_o}\cos\delta \tag{3.7}$$

$$G'' = \frac{\sigma_o}{\varepsilon_o}\sin\delta \tag{3.8}$$

$$G^* = G' + iG'' \tag{3.9}$$

$$\sigma_o = \frac{2T}{\pi r^3} \tag{3.10}$$

$$\varepsilon_o = \frac{\theta r}{h} \tag{3.11}$$

$$G^* = \frac{\sigma_o}{\varepsilon_o} \tag{3.12}$$

$$W_c = \pi \sigma_o^2 \left[\frac{1}{G^*/\sin\delta} \right] \tag{3.13}$$

G^* : Complex shear modulus

ε_o: maximum applied strain

ε : sinusoidal strain function

ω : angular frequency (rad/s)

t : time (s)

σ_o: maximum applied stress

σ : sinusoidal stress function

δ : the phase angle, or the lag between applied strain and stress

G': storage or elastic modulus

G'' : loss or viscous modulus

T : maximum applied torque

r : specimen radius (either 4 or 12.5 mm)

θ : deflection (rotation) angle (rad)

h : specimen height (1 or 2 mm)

W_c : Dissipated energy per load cycle

Figure 3.15: Dynamic Shear Rheometer.

3.3.4.5 Multiple Stress Creep Recovery (MSCR) Test of Asphalt Binder Using DSR (AASHTO TP 70-11)

An RTFOT conditioned asphalt binder is employed for the test. The test is performed at the upper PG temperature established from the previous DSR PG according to the AASHTO T 315. The 25-mm parallel plate geometry is used with a 1-mm gap setting. The sample is tested in creep at two stress levels followed by recovery at each stress level. The stress levels used are 0.1 kPa and 3.2 kPa. The creep portion of the test

lasts for 1 second, which is followed by a 9-second recovery. Ten creep and recovery cycles are tested at each stress level. Figure 3.16 shows data plot for creep and recovery at creep stress of 0.1 kPa.

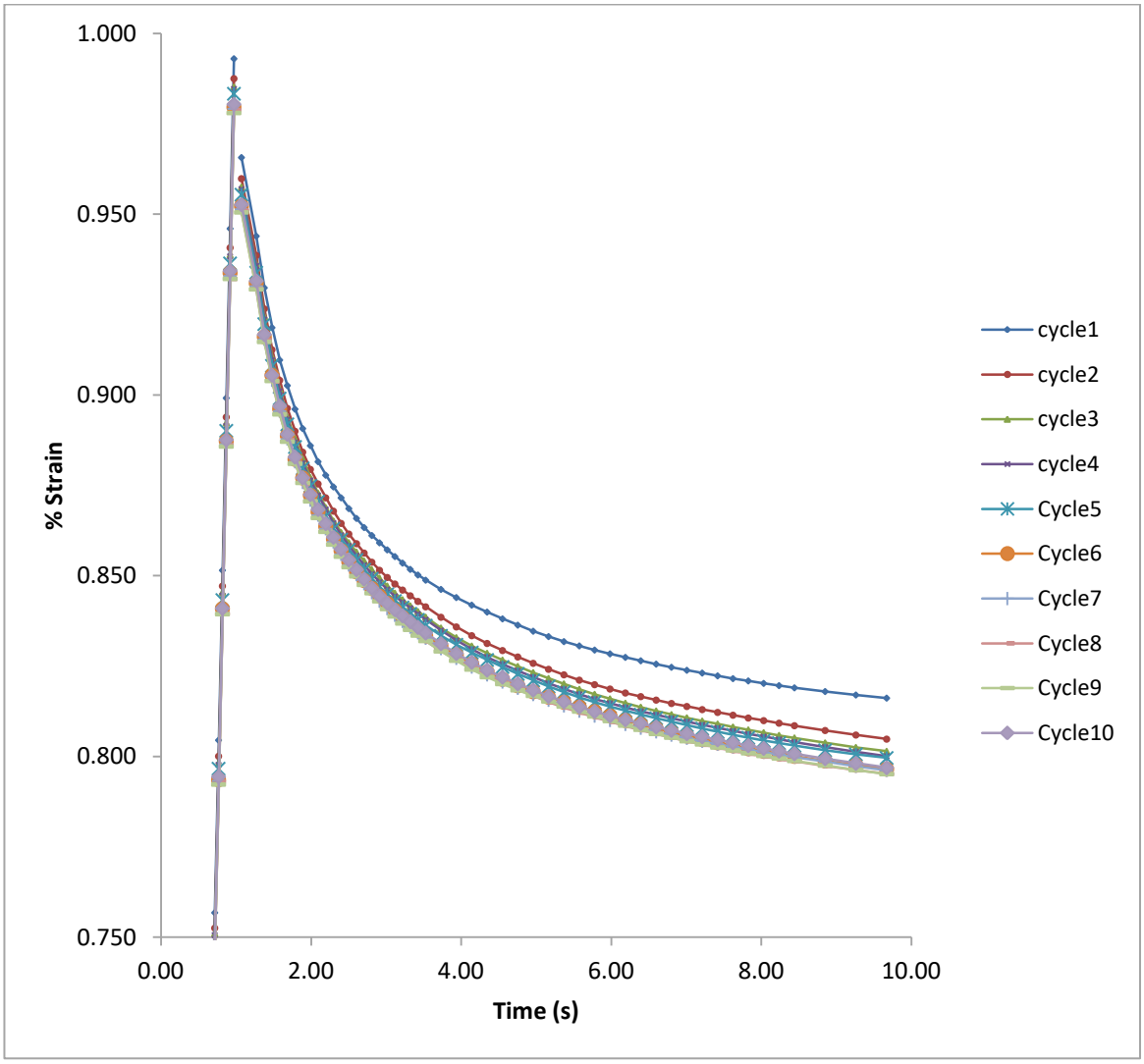

Figure 3.16: Data Plot Showing Creep and Recovery at Creep Stress of 0.1 kPa.

For each of the ten cycles, record the following:

The initial strain value at the beginning of the creep portion of each cycle; This strain shall be denoted as $\in_0$. The strain value at the end of the creep portion (i.e., after

1.0 second) of each cycle; This strain shall be denoted as $\in_c$. The adjusted strain value at the end of the creep portion (i.e., after 1.0 second) of each cycle ($\in_1$), which is calculated as follows:

$$\in_1 = \in_c - \in_0 \tag{3.14}$$

The strain value at the end of the recovery portion (i.e., after 10.0 second) of each cycle; This strain shall be denoted as $\in_r$. The adjusted strain value at the end of the recovery portion (i.e., after 10.0 seconds) of each cycle ($\in_{10}$), which is calculated as follows:

$$\in_{10} = \in_r - \in_0 \tag{3.15}$$

For each of the ten cycles, calculate the following at the creep stress level of 0.1 kPa:

Percent recovery $\in_r(0.1, N)$ for $N = 1$ to 10:

$$\in_r (0.1, N) = \frac{(\in_1 - \in_{10}) \times 100}{\in_1} \tag{3.16}$$

For each of the ten cycles, calculate the following at the creep stress level of 3.2 kPa:

Percent recovery $\in_r(3.2, N)$ for $N = 1$ to 10:

$$\in_r (3.2, N) = \frac{(\in_1 - \in_{10}) \times 100}{\in_1} \tag{3.17}$$

The average percent recovery at 0.1 kPa:

$$R_{0.1} = \frac{SUM\left[\in_r (0.1, N)\right]}{10} \quad \text{for } N = 1 \text{ to } 10 \tag{3.18}$$

The average percent recovery at 3.2 kPa:

$$R_{3.2} = \frac{SUM\left[\in_r (3.2, N)\right]}{10} \quad \text{for } N = 1 \text{ to } 10 \quad . \tag{3.19}$$

The percent difference in recovery between 0.1 kPa and 3.2 kPa:

$$R_{diff} = \frac{\left[R_{0.1} - R_{3.2}\right] \times 100}{R_{0.1}} \tag{3.20}$$

For each of the ten cycles at a creep stress of 0.1 kPa, calculate the non-recoverable creep compliance, $J_{nr}(0.1, N)$, kPa^{-1}, as strain/stress:

$$J_{nr}(0.1, N) = \frac{\in_{10}}{0.1} \tag{3.21}$$

For each of the ten cycles at a creep stress of 3.2 kPa, calculate the non-recoverable creep compliance, $J_{nr}(3.2, N)$, kPa^{-1}, as strain/stress:

$$J_{nr}(3.2, N) = \frac{\in_{10}}{3.2} \tag{3.22}$$

The average non-recoverable creep compliance at 0.1 kPa, $J_{nr_{0.1}}$, kPa^{-1}:

$$J_{nr_{0.1}} = \frac{SUM\left[J_{nr}(0.1, N)\right]}{10} \quad \text{for } N = 1 \text{ to } 10 \tag{3.23}$$

The average non-recoverable creep compliance at 3.2 kPa, $J_{nr_{3.2}}$, kPa^{-1}:

$$J_{nr_{3.2}} = \frac{SUM\left[J_{nr}(3.2, N)\right]}{10} \quad \text{for } N = 1 \text{ to } 10 \tag{3.24}$$

Table 3.8 and Table 3.9 presents the upper temperature performance grading scheme using the MSCR test results. The full provisional standard is now available as AASHTO M 332-14. The lower PG temperature procedure remain the same as in AASHTO T 315.

Table 3.8: Traffic Categories according to J_{nr} (AASHTO M 332-14).

Traffic Level	*Traffic Range and speed*	J_{nr} Requirements
Standard Traffic "S"	*< 10 million ESAL and > 70 km/h*	$J_{nr3.2}$, max 4.0 kPa^{-1} J_{nrdiff}, max 75%
Heavy Traffic "H"	10 to 30 million ESALs Slow traffic or (20 to 70 km/h)	$J_{nr3.2}$, max 2.0 kPa^{-1} J_{nrdiff}, max 75%
Very Heavy Traffic "V"	> 30 million ESALs or standing traffic (< 20 km/h)	$J_{nr3.2}$, max 1.0 kPa^{-1} J_{nrdiff}, max 75%
Extremely Heavy Traffic "E"	> 30 million and standing traffic (< 20 km/h)	$J_{nr3.2}$, max 0.5 kPa^{-1} J_{nrdiff}, max 75%

Table 3.9: Superpave Performance Grading Using MSCR Test (Extract of upper PG) (AASHTO M 332-14).

Performance Grade	PG 64						PG 70					
	10	16	22	28	34	40	10	16	22	28	34	40
Average 7-day max pavement design temp, °C[b]							<70					
Min pavement design temp, °C[b]	>–10	>–16	>–22	>–28	>–34	>–40	>–10	>–16	>–22	>–28	>–34	>–40
Original Binder												
Flash point temp, T 48, min °C	230											
Viscosity, T 316:[c] max 3 Pa·s, test temp, °C	135											
Dynamic shear, T 315:[d] G*/sinδ, min 1.00 kPa[e] test temp @ 10 rad/s, °C	64						70					
Rolling Thin-Film Oven Residue (T 240)												
Mass change, max, percent[f]	1.00											
MSCR, TP 70: Standard Traffic "S" Grade $J_{nr3.2}$, max 4.0 kPa^{-1} J_{nrdiff}, max 75% test temp, °C	64						70					
MSCR, TP 70: Heavy Traffic "H" Grade $J_{nr3.2}$, max 2.0 kPa^{-1} J_{nrdiff}, max 75% test temp, °C	64						70					
MSCR, TP 70: Very Heavy Traffic "V" Grade $J_{nr3.2}$, max 1.0 kPa^{-1} J_{nrdiff}, max 75% test temp, °C	64						70					
MSCR, TP 70: Extremely Heavy Traffic "E" Grade $J_{nr3.2}$, max 0.5 kPa^{-1} J_{nrdiff}, max 75% test temp, °C	64						70					

[a] MSCR test on RTFO residue should be performed at the PG grade based on the environmental high pavement temperature. Grade bumping is accomplished by requiring a lower J_{nr} value while testing at the environmental temperature.

[b] Pavement temperatures are estimated from air temperatures using an algorithm contained in the LTPP Bind program, may be provided by the specifying agency, or by following the procedures as outlined in M 323 and R 35, excluding the provisions for "grade bumping".

[c] This requirement may be waived at the discretion of the specifying agency if the supplier warrants that the asphalt binder can be adequately pumped and mixed at temperatures that meet all applicable safety standards.

3.3.5 Asphalt Storage Stability Test

450 g of modified asphalt was placed inside a 72 mm (diameter) and 232 mm high airtight metallic container. A butterfly-like blade was attached to a rotating rod, which was inserted and located 20 mm from the bottom of the can containing the modified asphalt. The temperature of the container was externally maintained at 165^{o}C, and the rod is rotated continuously at 250 rpm. DSR test samples were extracted from the top and bottom of the container, with the aid of 4mm glass tube attached to pipette suction rubber, at 0 and 48 hrs. The modified asphalt blend is likely to undergo phase separation if the separation index (3.25) of top and bottom differs by more than 20%. The degrading potential (significant deviation from actual polymer network structure or Rheopectic behavior etc.) of the modified asphalt blend is measure by the degradation ratio (3.26). The schematic of the laboratory asphalt stability test (LAST) is shown in Figure 3.17 below [49].

$$\text{Complex Modulus Separation Index 'SR(G*)'} = \frac{G^*_{top}}{G^*_{botom}} \tag{3.25}$$

$$\text{Complex Modulus Degradatio n Index 'DR(G*)'} = \frac{\left(G^*_{top} + G^*_{botom}\right)_{48hrs}}{\left(G^*_{top} + G^*_{botom}\right)_{0hr}} \tag{3.26}$$

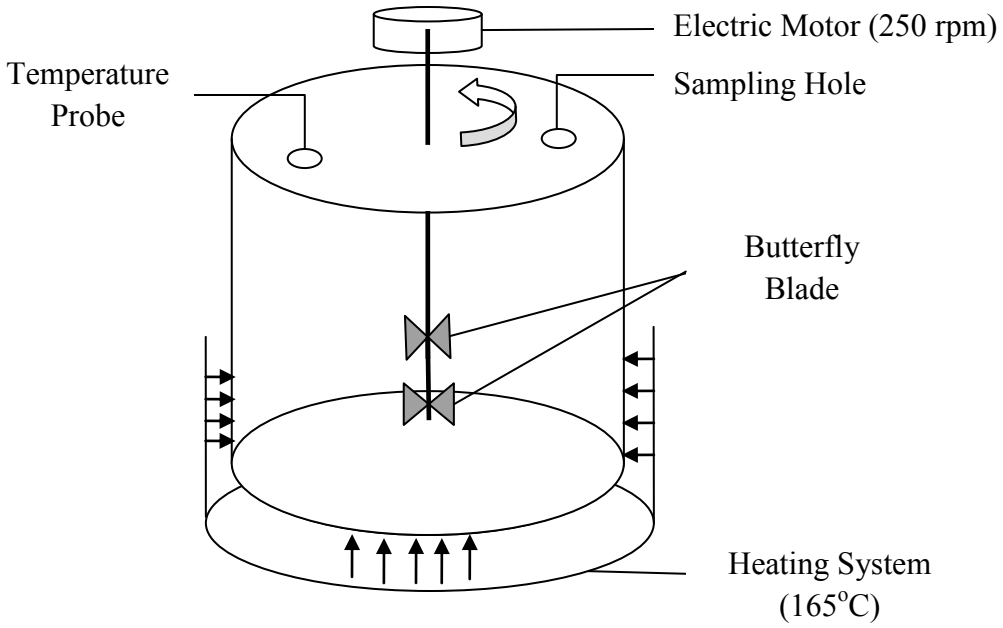

Figure 3.17: Storage Stability Schematic Test Set-up.

3.3.6 RPW-Asphalt Concrete Mix

Asphalt concretes mixtures with only RPW modified asphalt binder were first designed using the AC superpave mix design method [71]. Then, the hybrid RPW-asphalt concrete mixtures containing both RPW modified binder and RPW-aggregate as substitute of some portion of mineral-aggregate was obtained. Two different RPW size ranges S1 (No. 8 to No. 10) and S2 (No. 8 to No. 40) were analyzed for selection. Resilient modulus and moisture sensitivity test was employed for the RPW size range selection. Flow number test was employed for the optimization of the RPW content. Dynamic modulus test, flexural fatigue test, asphalt pavement analyzer, flow number and flow time test were employed to assess the performance of the hybrid RPW-asphalt concrete.

3.3.7 Asphalt Concrete Resilient Modulus, AMPT Dynamic Modulus and Rutting Performance Tests

Resilient Modulus (MR) Test for Asphalt Concrete Mix (ASTM D7369 - 11) was utilized to assess the relative effectiveness of the different sizes and content of RPW aggregate in asphalt concrete. Figure 3.18 shows the resilient modulus set-up. MR is defined as the ratio of applied stress to the recovered strain from diametrically dynamic loaded AC sample of 100 mm diameter by 63 mm height. Equation (3.27) presents the mathematical definition of MR. It is used as a measure of the AC elastic properties for design.

$$MR = \frac{\sigma}{\varepsilon_r} \tag{3.27}$$

MR : Resilient Modulus

σ : Maximum Applied Stress

ε_r : Recovered Strain

The dynamic modulus and flow number of AC was obtained in accordance with the Standard Method of Test for Determining the Dynamic Modulus and Flow Number for Asphalt Mixtures Using the AMPT [72]. The image of the AMPT is shown in Figure 3.19 below. The master curve plot for the dynamic modulus of the RPW-ACs was developed from dynamic modulus results of the asphalt mix performance test. Atleast 2 replicate samples are tested at three temperatures within a frequency of 0.01 to 10 Hz for the temperature frequency superposition curves [73]. The dynamic modulus was obtained under a confining stress of 180 kPa, an estimated stress similitude of those measured in

the field [74]. Further details on the rutting performance testing via the FN test and Asphalt Pavement Analyzer (APA) are outlined in the next sub-headings.

Figure 3.18: Resilient Modulus Test setup for bituminous material.

Figure 3.19: Asphalt Mix Performance Tester (AMPT).

Dynamic modulus test measures the stress-strain relationship of an asphalt mixture under continuous sinusoidal loading. Equation (3.28) and (3.29) summarizes the stress-strain relationship. The master curve of the AC mixture was developed using a symmetrical sigmoidal function (3.30a) along with Arrhenius shift factor (3.30b) for time temperature superposition [73].

$$E^* = |E^*| \sin \emptyset + i|E^*| \cos \emptyset \tag{3.28}$$

$$|E^*| = \frac{\sigma_o}{\varepsilon_o} \tag{3.29}$$

$$\log|E^*| = \delta + \frac{Max-\delta}{1+e^{\beta+\gamma\left(\log t+\frac{\Delta E_a}{19.14714}\left[\frac{1}{T}-\frac{1}{T_r}\right]\right)}} \tag{3.30a}$$

$$\log a(T) = \frac{\Delta E_a}{19.14714}\left[\frac{1}{T} - \frac{1}{T_r}\right] \quad (3.30b)$$

$$|E^*|_{max} = P_c\left[4{,}200{,}000\left(1 - \frac{VMA}{100}\right) + 435{,}000\left(\frac{VFAxVMA}{10{,}000}\right)\right] + \frac{1-P_c}{\left[\frac{\left(1-\frac{VMA}{100}\right)}{4{,}200{,}000} + \frac{VMA}{435{,}000xVFA}\right]} \quad (3.31)$$

$$P_c = \frac{\left(20+\frac{435{,}000xVFA}{VMA}\right)^{0.58}}{650+\left(\frac{435{,}000xVFA}{VMA}\right)^{0.58}} \quad (3.32)$$

Where:

$|E^*|$: Complex Modulus

$a(T)$: Shift Factor

P_c : Factor for limiting maximum dynamic modulus estimation

$\emptyset$: Phase angle

σ_o : Maximum applied stress

ε_o : Peak of recoverable axial strain

E^* : Dynamic Modulus

$|E^*|_{max}$: Limiting Maximum Mixture Dynamic Modulus

VMA : Void in Mineral Aggregate

VFA : Void Filled with Asphalt

T : Temperature

T_r : Reference Temperature (^{o}K)

Max: Limiting Maximum Modulus

t : Loading Time

$\delta, \beta, \gamma, \Delta E_a$: Fitting Parameter

3.3.7.1 Flow Number Test

The current standard FN test is conducted on a cored cylindrical asphalt mix test specimen of 4" diameter by 6" height. The unconfined sample is subjected to repeated sinusoidal load of 600 kPa deviatory stress, at an adjusted mix targeted service temperature. The sample is loaded for 0.1 second and allowed to rest for 0.9 second continuously, while the accumulated permanent strain is recorded. Figure 3.20 shows a typical asphalt mix permanent deformation curve (PDC). The sample initially deforms rapidly in the primary stage (densification), the strain accumulation then stabilizes in the secondary stage. Gradually, the strain accumulation rate rise again, when the aggregate start to slide past each other. This last stage is termed the shear deformation or tertiary flow, and the point at which it begins is termed the flow point. Finally, the obtained PDC should then be fitted in to Franken Model (FM) for FN estimation.

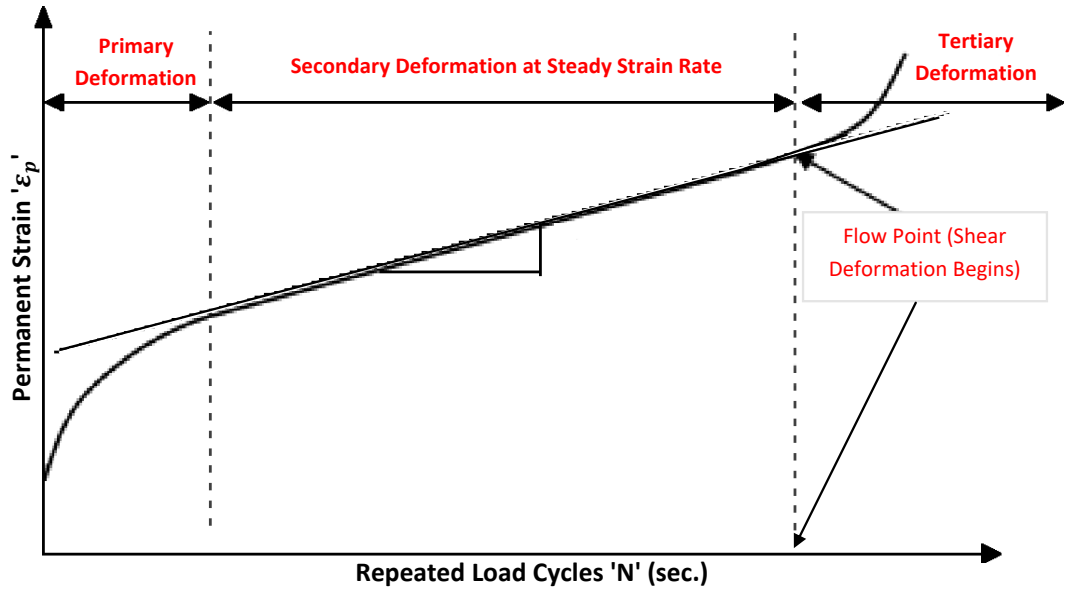

Figure 3.20: Concept of Flow Point and Permanent Deformation Curve of HMA.

3.3.7.2 Franken model (FM)

The FM is a combination of two types of functions, as presented in equation (3.33). The first part described the primary and secondary deformation, while the exponential function represent the tertiary deformation. The regression constants A, C and D are highly correlated for a giving PDC. The choice of FM as a standard model for FN estimation was prompted by its ability to successfully accommodate/fit all the three main permanent strain stage of the asphalt material [53].

$$\varepsilon_p = \mathrm{A} * \mathrm{N}^{\mathrm{B}} + C(e^{D*N} - 1) \tag{3.33}$$

$$\varepsilon_p'' = \mathrm{AB(B-1)} * \mathrm{N}^{(\mathrm{B-2})} + CD^2 * e^{D*N} \tag{3.34}$$

ε_p = Permanent Strain Sustained by the HMA test Sample

ε_p'' = Rate of change of the strain rate (second differential of ε_p with respect to N).

N = load cycle repetition in seconds

A, B, C & D are regression constants

3.3.7.3 Flow Number (FN) Estimation

FN is the number of load repetition corresponding to the flow point shown by the Asphalt Mixture Performance Test (AMPT) visual progress in Figure 3.21. It is the point of lowest strain rate as shown in Figure 3.21. This point also corresponds with the number of load cycle at which the rate of change of the strain rate or the sustained permanent strain acceleration (3.34) changes sign from negative (deceleration) to positive. It can be

easily obtained by solving (3.34) at $\varepsilon_p'' = 0$. The FN values obtained in this study were corrected using equation (4.17) based on the findings from Appendix A.

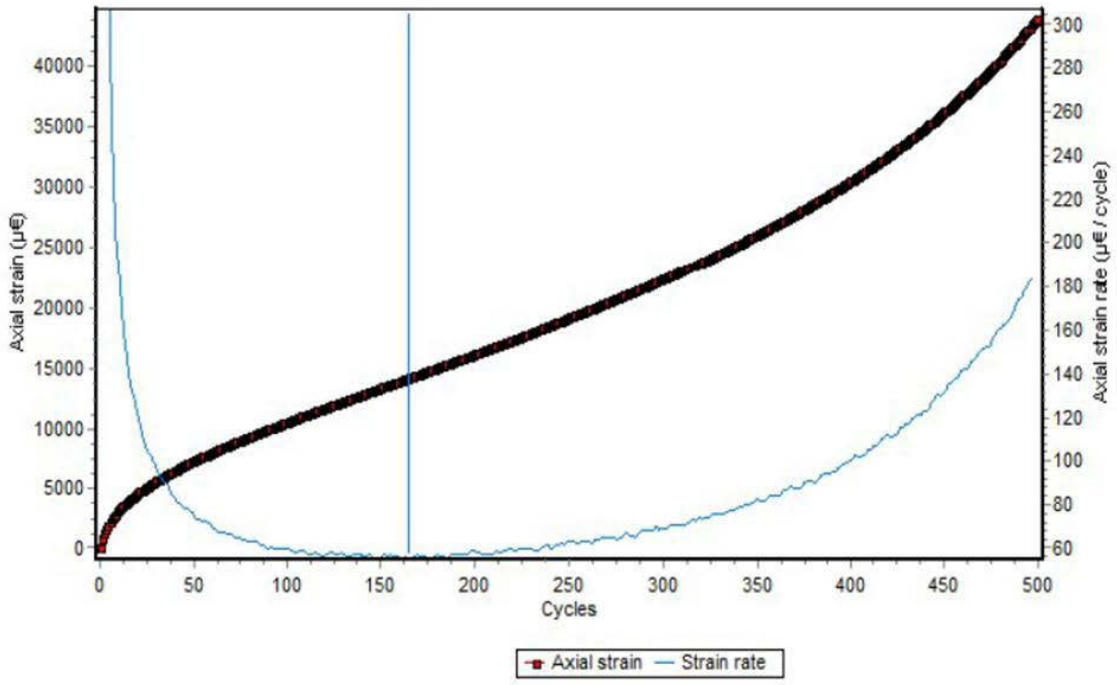

Figure 3.21: AMPT Flow Number Test Progress Visualization.

3.3.7.4 EFFECT OF TERTIARY FLOW LENGTH ON ASPHALT FLOW NUMBER

More than 360 FN data points was generated from atleast 20 HMA repeated load permanent deformation test data. The HMA test samples were obtained from two types of asphalt grades (PG 70 - 16 and PG 64 - 22). The asphalt mixtures were prepared and tested in accordance with Standard Method of Test for Determining the Dynamic Modulus and Flow Number for Asphalt Mixtures Using the AMPT (AASHTO TP 79-15).

The selected service temperature for the test were 56, 60 and 64^{o}C so as to cover the range of FN values recommended for various traffic categories by AASHTO TP 79-15.

In an attempt to investigate the effect of tertiary flow length on the FN, Gauss-Newton algorithm (GNA) was used to fit the various permanent deformation curves PDCs data in to Francken Model (FM), Modified Francken Model-1(MFM-1) and Modified Francken Model-2 (MFM-2) at various progressive point in to the tertiary deformation of the test sample, with Minitab 16^{TM}. These yielded several PDCs with FN values similitude of FN test of similar samples but tested and terminated at progressively increasing time within the tertiary flow stage. Only in this case, the effect of sample preparation, conditioning time, different operator has been eliminated. Consistent starting values, maximum allowable Iterations and convergent criteria was used throughout. The FN of each run was accurately calculated from the second derivative of the model fit, using WOLFRAM MATHEMATICA 8.0^{TM}.

3.3.8 Asphalt Pavement Analyzer (APA)

The rutting resistance of the RPW-Asphalt concrete was further studied with the aid of APA test equipment shown in Figure 3.22. The APA test was conducted based on AASHTO standard procedure for determining the rutting susceptibility of asphalt paving mixtures using the APA (AASHTO TP 63).

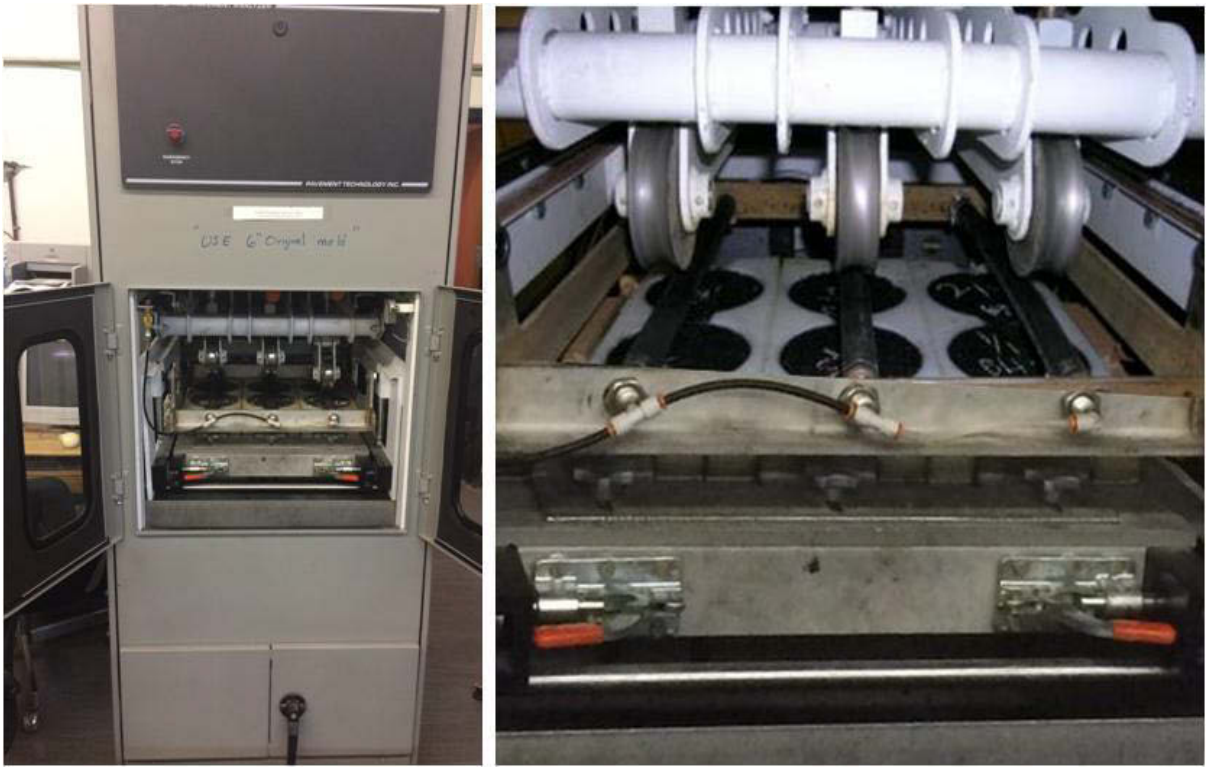

Figure 3.22: Asphalt Pavement Analyzer (APA).

3.3.9 Asphalt Concrete Fatigue Life Test

Sample preparation and testing for the AC fatigue life was done according to Standard Method of Test for Determining the Fatigue Life of Compacted Asphalt Mixtures Subjected to Repeated Flexural Bending [61]. Figure 3.23 shows Cooper made flexural fatigue tester used to conduct the fatigue tests. The Fatigue test was conducted in both controlled stress and strain mode, continuous load cycles (10Hz) and constant temperature. An applied tensile stress ranging between 400 to 1000 kPa was employed for the controlled stress AC fatigue test. For the strain control test, the fresh and CRB-76 ACs were tested at strain level ranging between 200 to 600 μst, while the AC containing RPW

as aggregate substitute are tested at higher strain ranging from 350 to 1000 μst due to their high flexural resilience.

$$\sigma_t = \frac{3aP}{b\mathrm{h}^2} \tag{3.35}$$

$$\varepsilon_t = \frac{12\delta \mathrm{h}}{3L^2 - 4a^2} \tag{3.36}$$

$$S = \frac{\sigma_t}{\varepsilon_t} \tag{3.37}$$

$$\varphi = 360\mathrm{fs} \tag{3.38}$$

Where:

σ_t : maximum tensile stress

a : space between inside clamps

P : applied load

S : Stiffness

b : average beam width

h : average beam height

ε_t: maximum tensile strain

δ : measured deformation

L : beam length between outside clamps

φ : phase angle (degrees)

f : load frequency (Hz)

s : time lag between maximum load and deflection

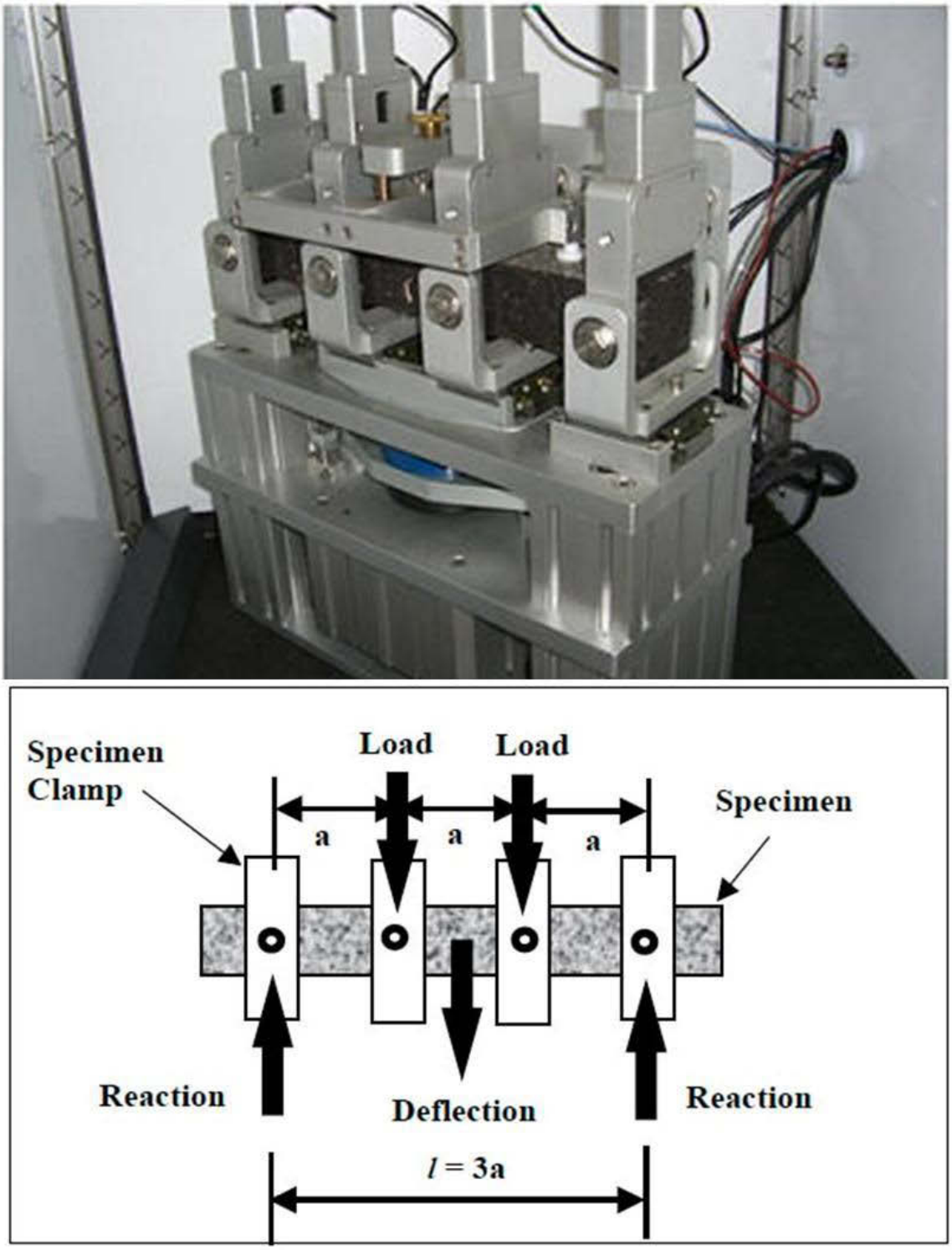

Figure 3.23: Fatigue Test Machines setup and schematics.

3.4 PERFORMANCE MODELING OF RPW-ASPHALT CONCRETE

AASHTO mechanistic-empirical pavement analysis and design method was employed for the AC life and performance simulation. Mechanistic-Empirical pavement design, unlike other purely empirical based pavement design methods, has the ability to utilize the measured visco-elastic property of pavement material [75]. It translates the mechanistic response of the pavement component in to performance parameter using empirically developed relationships called transfer functions. The transfer functions were calibrated by comparing their output with observed field performance data.

A 20 cm asphalt concrete pavement wearing course (as shown by Figure 3.24) was modeled for RPW modified asphalt binders and hybrid-RPW ACs. All parameters (layer thickness, traffic loading, climatic data etc) are kept constant for the different RPW modified binder and hybrid-RPW AC mixtures. The only property varied is the visco-elastic behavior of the hybrid-RPW AC mixtures. Average daily equivalent single axle load (ESAL) of 2200, with 5% annual growth was utilized. A 20 year design period, corresponding with cumulative 30 million ESAL was used. NCHRP 1-37A nationally calibrated coefficients were utilized in all cases.

The strain induced by the standard axle load in the pavement section (as shown by Figure 3.24), was obtained using WinJULEA software [76]. WinJulea is a windows version of the layered elastic program JULEA, which has been implemented in the AASHTO Mechanistic Empirical Pavement Design Guide for pavements [77]. Using the standard axle configuration, the critical elastic vertical and horizontal tensile strain at the

middle and the bottom of the AC layer respectively, directly under the wheel load were obtained. The dynamic modulus of the ACs was obtained as function of KSA seasonal average temperatures (23, 37, 45 and 27^{o}C) [78], at a frequency corresponding the desired traffic speed (10 km/h). The predominant loading frequency 'f_p' at the top, mid and bottom of the AC layer was obtained using field established relationship between vehicle speed 'V ' and loading time [79], using equation (39) and (40) respectively. Tensile strains at the bottom of the AC directly under the wheel, and at the top of the AC approximately 10 cm from the wheel center are computed for bottom-up and top-down fatigue cracking respectively. Compressive strain at the middle of the AC layer was also obtain for the for the rutting performance estimation. The obtained critical load responses are incorporated into the AASHTO rutting and fatigue models, for rutting and fatigue performance prediction.

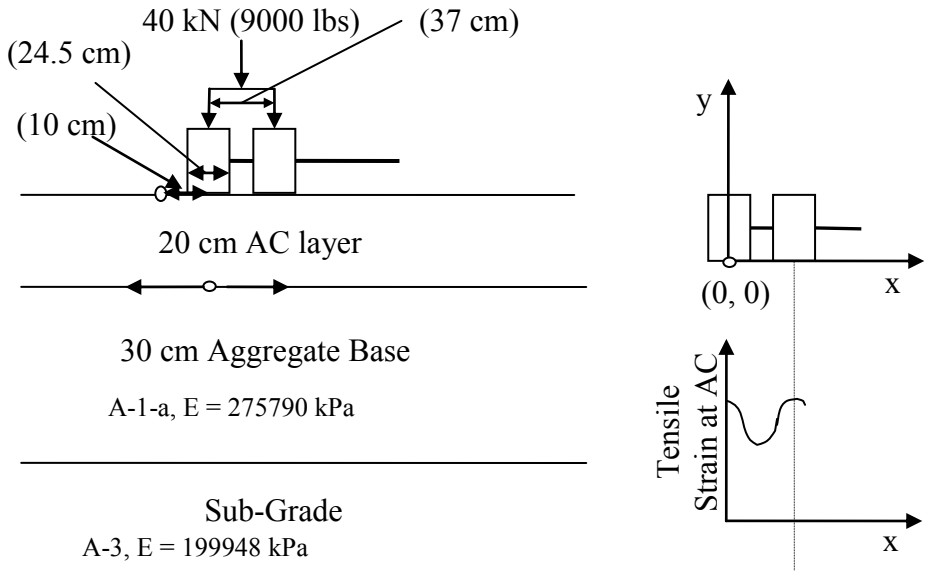

Figure 3.24: Pavement Section and Moving Load Orientation.

$$f_p = 0.218 * V \quad (39)$$

$$f_p = 0.468 * V \quad (40)$$

3.4.1 AC Rutting Performance Model and Transfer Function

Equation (3.41) represents the generalized AC rutting performance model [77]. Where ε_p is the accumulated vertical permanent deformation (mm/mm); ε_r: vertically imposed resilient strain on laboratory test sample to obtain ε_p (mm/mm); N is the number of cumulative load repetition; $T; D;\ H_{AC};\ k_z$: Layer temperature (^{o}C), depth below the surface, thickness of AC layer and depth confinement factor respectively.

$$\frac{\varepsilon_p}{\varepsilon_r} = k_z B_{r1}(10)^{k_{r1}}(33.8T)^{\beta_{r2}k_{r2}}N^{\beta_{r3}k_{r3}} \quad (3.41)$$

$$k_z = (C_1 + 39.3701C_2D)0.328196^{39.3701D} \quad (3.42)$$

$$C_1 = -161.0453H_{AC}^2 + 97.9055H_{AC} - 17.342 \quad (3.43)$$

$$C_2 = 26.6601H_{AC}^2 - 68.2323H_{AC} + 27.428 \quad (3.44)$$

$B_{r1} = 1;$

$k_{r1} = -3.35412;$

$\beta_{r2} = 0.55;$

$k_{r2} = 0.4791;$

$\beta_{r3} = 0.8;$

$k_{r3} = 1.5606$ are regression constants.

3.4.3 AC Fatigue Performance Model and Transfer Function

Equation (3.45) shows the general fatigue performance model employed for the fatigue performance estimation [77]. Where N_f is the number of load repetition to cracking, ε_t is

tensile strain at critical locations, $E_{AC}$is the dynamic modulus of AC layer (kPa), V_{be} is the effective asphalt binder content (by volume), V_a is the AC air void and $B_{f1} = 0.005;\ k_{f1} = 0.007566;\ k_{f2} = 3.9492;\ \beta_{f2} = 1;\ k_{f3} = 1.281;\ \beta_{f3} = 1$: are all regression constants.

$$N_f = 0.00432 k_{f1} C B_{f1} (\varepsilon_t)^{-k_{f2}\beta_{f2}} (E_{AC})^{-k_{f3}\beta_{f3}} \quad (3.45)$$

$$C = 10^{4.84\left[\frac{V_{be}}{V_a + V_{be}} 0.69\right]} \quad (3.46)$$

- For AC Top-Down Cracking:

$$FC_{Top} = 6.562 \left(\frac{C_3}{1 + e^{(C_1 - C_2 \log_{10}(100D))}}\right) \quad (3.47)$$

$$D = \frac{n}{N_f} \quad (3.48)$$

H_{AC}: Thickness of AC layer

FC_{Top}: Length of longitudinal crack (m/km)

D: Damage index

$C_1;\ C_2;\ C_3$: Nationally calibrated regression constants

- For AC bottom-up cracking

$$FC_{Bottom} = 0.18 \left(\frac{C_3}{1 + e^{\left(C_1 C_1' - C_2 C_2' \log_{10}(100D)\right)}}\right) \quad (3.49)$$

FC_{Bottom}: % lane area of cracking

$$C_2' = -2.40874 - 39.748(1 + 39.3701 H_{AC})^{-2.856} \quad (3.50a)$$

$$C_1' = -2C_2' \quad (3.50b)$$

3.5 ECONOMIC AND ENVIRONMENTAL BENEFITS ANALYSIS OF RPW-ASPHALT CONCRETE

3.5.1 Monetary Cost Analysis of RPW-Modified Asphalt Binder

A total of 12 promising treatments were selected for this purpose. Six of these treatments possessed an upper PG of 82, while the remaining 6 treatments are suited for environments with 76^{o}C seven day maximum pavement temperature or less. These treatments were compared with conventional polymer modified asphalt in terms of initial material cost. Local price of commercial polymer was obtain from SABIC, a local petrochemical company, and other local suppliers. International cost was obtained from ICIS market intelligence [80]. The recycled plastic price was established by contacting some small scale local plastic recyclers.

3.5.2 Environmental Benefit Estimation of RPW-Modified Asphalt Binder

Carbon and NMVOCs emission factors associated with the manufacturing process of virgin LDPE and HDPE, PB where obtained from Environmental Protection Agency publication [81-82]. Carbon emission factors associated with the production of SBS and PP were obtained from energy required in manufacturing and polymerization of their respective monomers (styrene, butadiene and propylene) [83]. The related emission factors of the recycled PW was obtained based on processing energy requirement for sorting, washing, shredding (to flakes), granulating (to granules) and finally grinding for

easier asphalt blending. Table 3.11 shows the capacity and power summary of the processing equipment involved. The emission accompanying each treatment was estimated relative to the total annual asphalt demand for pavement construction. The various factors are presented in Table 3.10.

Table 3.10: Emission Factors Summary.

Polymer	CO_2 ($MTCO_2e$/ton)	NMVOCs (kg/Ton)
LDPE	2.34	2.40
HDPE	1.95	2.30
PP	0.67	0.19
SBS	2.55	0.27
PB	2.42	2.40
rLDPE	$0.21x10^{-6}$	Negligible
rHDPE	$0.21x10^{-6}$	Negligible
rPP	$0.21x10^{-6}$	Negligible

Table 3.11: PW Processing Equipment Specification Summary.

Equipment	Capacity (kg/h)	Power (kW)
Shredder/Crusher	50 - 5000	7.5 - 250
Granulator	250 - 500	90 - 160
Grinder	100 - 200	4.0

Summary: The methodology followed in carrying out the various tasks involved in this research has been described. The study has been divided into three phases. The first phase addresses the identification of RPWs that can be used in asphalt modification or replacement of aggregate, followed by the evaluation of RPW-modified asphalts. Different potential RPWs will be screened and selected based on thermal and rheological techniques. The second phase involves analyses of the performance and mechanical properties of RPW-modified AC mixtures composed of both pure binder and pure RWP or blended modified asphalt binder. The third phase includes data analyses and reporting. The overall work sequence and content has been summarized in the work flow chart a shown Figure 3.1. The RPW modified asphalt test experimental design was presented. The RPW-AC mix optimization and performance evaluation guide was also explained. The detail description of the test and analysis methods employed was provided in the last subheadings. Details of AC mechanic-empirical performance modeling method adopted was also described.

CHAPTER 4

RESULTS AND DISCUSSION

Introduction: This chapter presents detail result discussion of all the tasks in this study. Sections covered include the RPW screening process, RPW asphalt binder blending optimization, performance grading of the RPW asphalt binder and storage stability analysis of the RPW asphalt binder. The superpave mix design of the RPW asphalt concrete, content and size range optimization of the hybrid RPW AC, and finally the results of effect of tertiary deformation length on the FN was also discussed. Each main subheading discusses an independent phase of this research.

4.1 RPW SCREENING RESULTS

The summary of the RPW screening is presented in Table 4.1. DSC analysis (ASTM E1356), Using *DSC Q 1000 model* yielded the melting point of the obtained RPW. The RPWs with melting point below 200^{o}C were selected as potential asphalt binder modifiers. 200^{o}C was considered the limit, since asphalt-polymer blending above this temperature for prolong duration results in excessive oxidation. Since aggregate are not required to fully integrate with the asphalt binder, all of the RPW are eligible for AC modification through aggregate substitution. The RPW-asphalt blending temperatures were obtained by adding approximately 45^{o}C to their corresponding melting points. This

was necessary in order to obtain a homogeneous RPW-asphalt blend within a reasonable time without over heating the binder.

The optimum blending duration of the RPW intended for asphalt binder modification (RPP, RLDPE and RHDPE) was obtained by measuring the viscosity and G*/sin δ of samples taken after time interval until there is no significant difference in the measure parameter. The next sub heading gives full detail of the blending time optimization process.

Table 4.1: Melting points of the RPWs.

RPW	Recycle label	Melting point (^{o}C)	Modification Role	Blending Temp. (^{o}C)
RPET	1	250	Aggregate only	--
RHDPE	2	132	Binder + aggregate	180
RPVC	3	300	Aggregate only	--
RLDPE	4	110	Binder + aggregate	160
RPP	5	162	Binder + aggregate	190
RPS	6	120	Aggregate only	--

4.1.1 RPW Differential Scanning Calorimetry Results

Results from Figure 4.1 shows the melting peaks for recycled polyethylene terephthalate (RPET) in the twin heating circles to be 249^{o}C. We can finally conclude that the melting point of RPET waste sample is 250^{o}C. This temperature level is beyond the suitable range of blending with asphalt binder. Thus the reason why RPET was not included among the utilized RPW for asphalt binder modification. However, RPET will still be adopted as RPW aggregate substitute for AC modification.

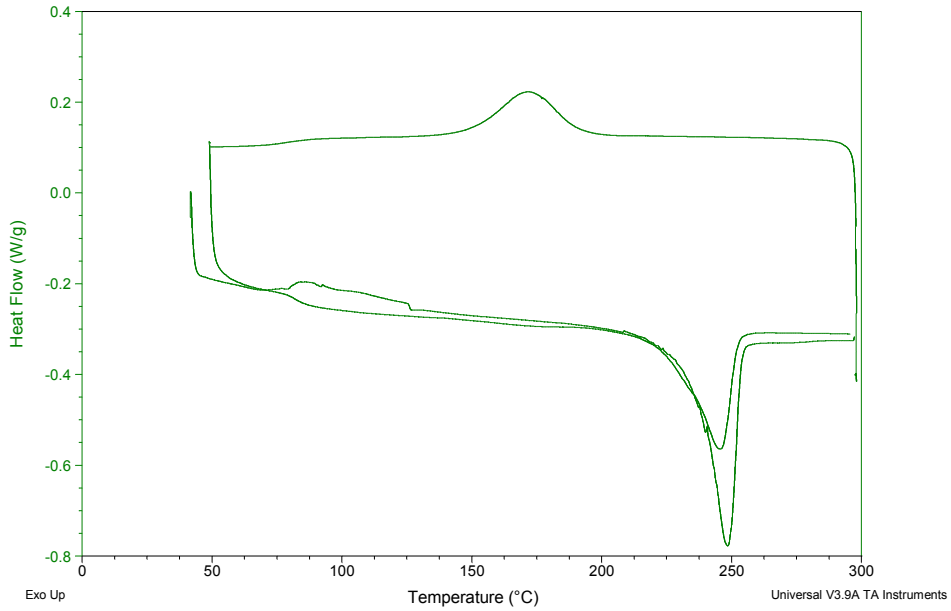

Figure 4.1: DSC thermal analysis results of RPET.

Figure 4.2 shows the melting peaks for recycled Low density polyethylene (RLDPE) in the twin heating circle to be around 110^{o}C. Hence we can conclude that the melting point of the RLDPE is 110^{o}C. This temperature level is within the suitable range of blending with asphalt binder. The selected blending temperature for RLDPE modified binder most be above this value. One of the twin heating curves shows some anomaly and possible decomposition after the melting peak, possibly due to forming of sample that results in intermittent closing of the lid of the pan. However, the other RLDPE heating curve does not show any sign of decomposing within the tested temperature range. The blending temperature was set at 160^{o}C (lower than 200^{o}C), approximately 50^{o}C above the melting point (110^{o}C).

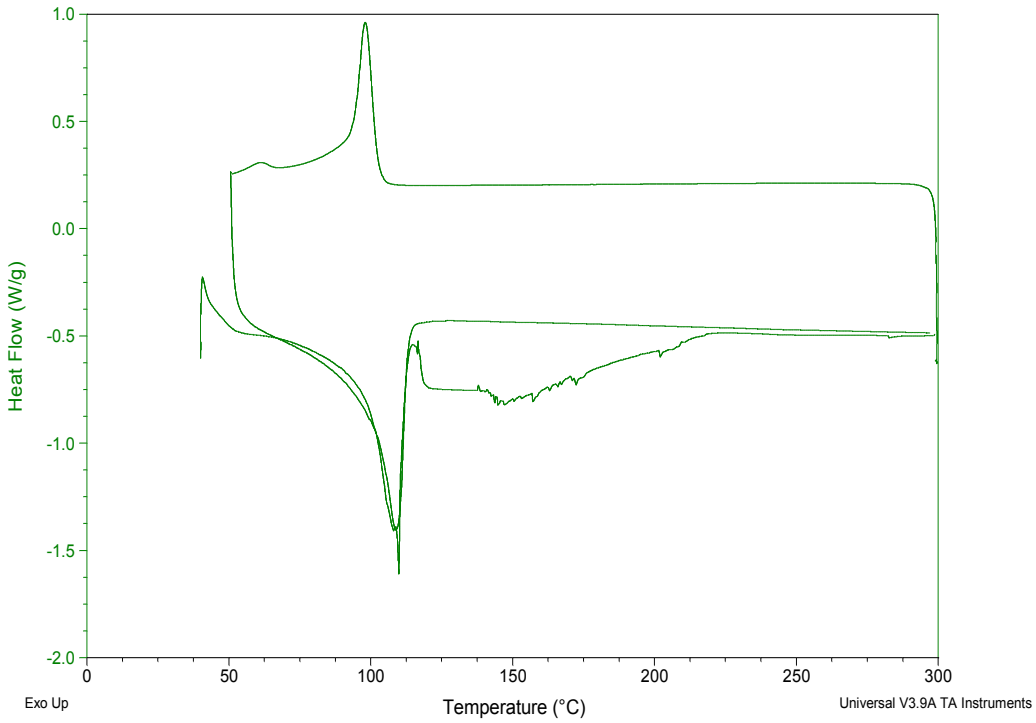

Figure 4.2: DSC thermal analysis results of RLDPE.

Results from Figure 4.3 shows the melting peaks for the recycled Polyvinyl chloride (RPVC) in the heating circles to falling just beyond the range of the test temperature 0 - 300^{o}C. Therefore, the RPVC melting point is considered to be approximately 300^{o}C, and cannot be practically blended with asphalt. The RPVC can only serve as aggregate replacement in the AC modification phase.

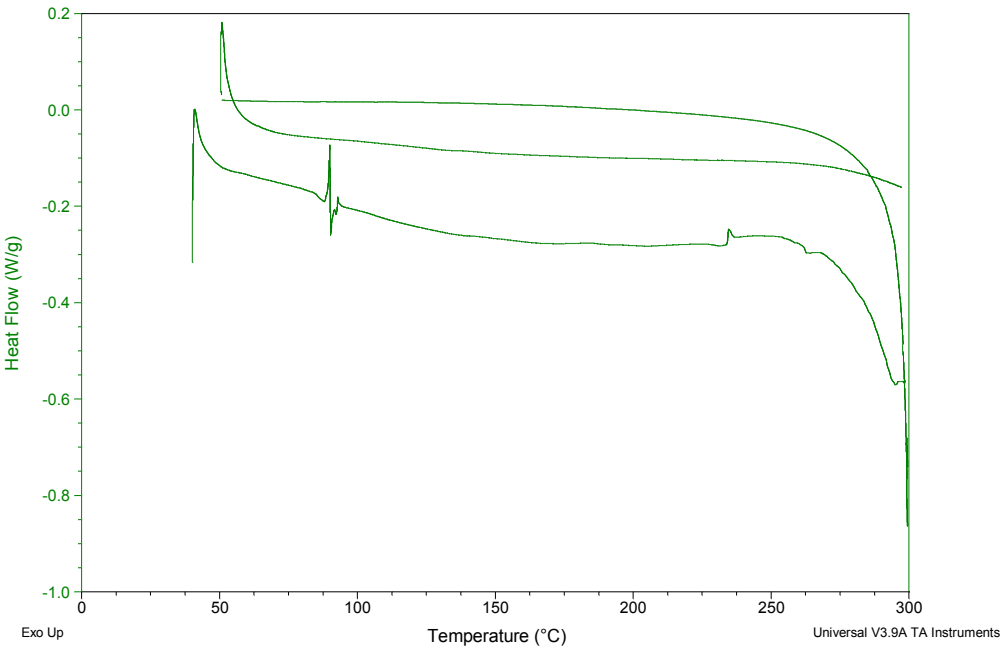

Figure 4.3: DSC thermal analysis results of RPVC.

Figure 4.4 shows the melting peaks for the recycled High density polyethylene (RHDPE) in the twin heating circle to be around 132^{o}C. Hence we can conclude that the melting point of the RHDPE is approximately 132^{o}C. This temperature level is within the suitable range of blending with asphalt binder. The selected blending temperature for RHDPE modified binder most be above this value for successful blending. Since the RHDPE does not show any sign of decomposing within the tested temperature range, the blending temperature was set at 180^{o}C (below 200^{o}), approximately 50^{o}C above the melting point.

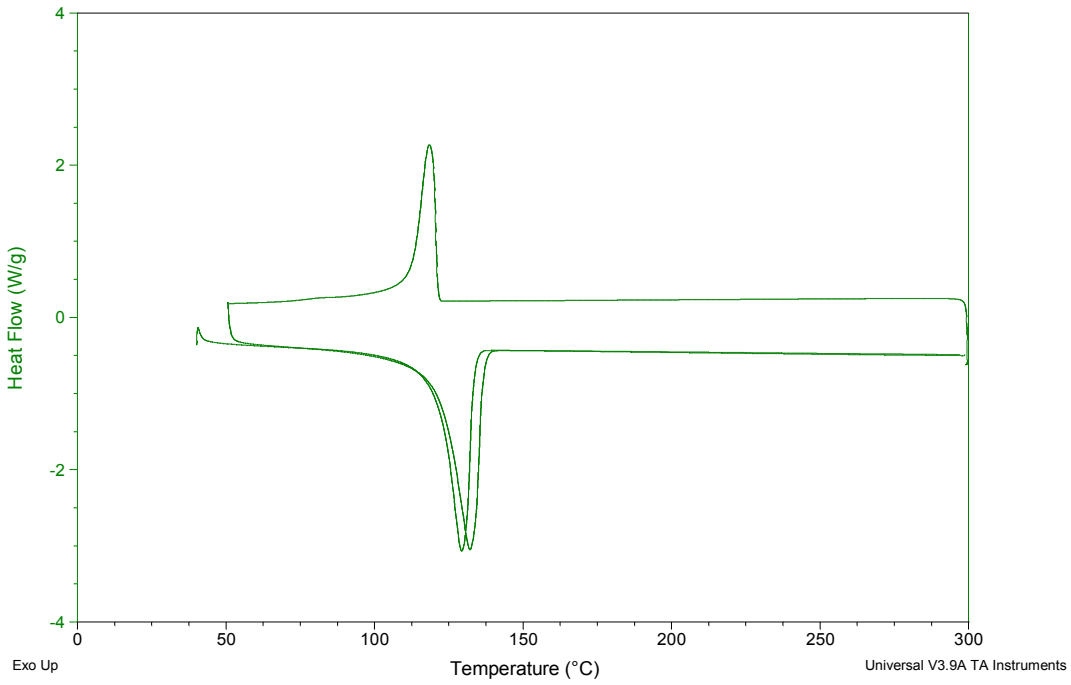

Figure 4.4: DSC thermal analysis results of RHDPE.

The melting peaks for the recycled polypropylene (RPP) in the twin heating circle could be observe to be around 162^{o}C as shown in Figure 4.5. Therefore the melting point of RPP is taken as 162^{o}C. This temperature level is also within the suitable range of blending with asphalt binder (below 200^{o}C). The selected blending temperature for RPP modified binder most be above this value. It can be observed that no decomposing occurs within the tested temperature range. Therefore, 190^{o}C (less than 200^{o}C and approximately 30^{o}C above the melting point) was finally selected for blending the RPP with the asphalt.

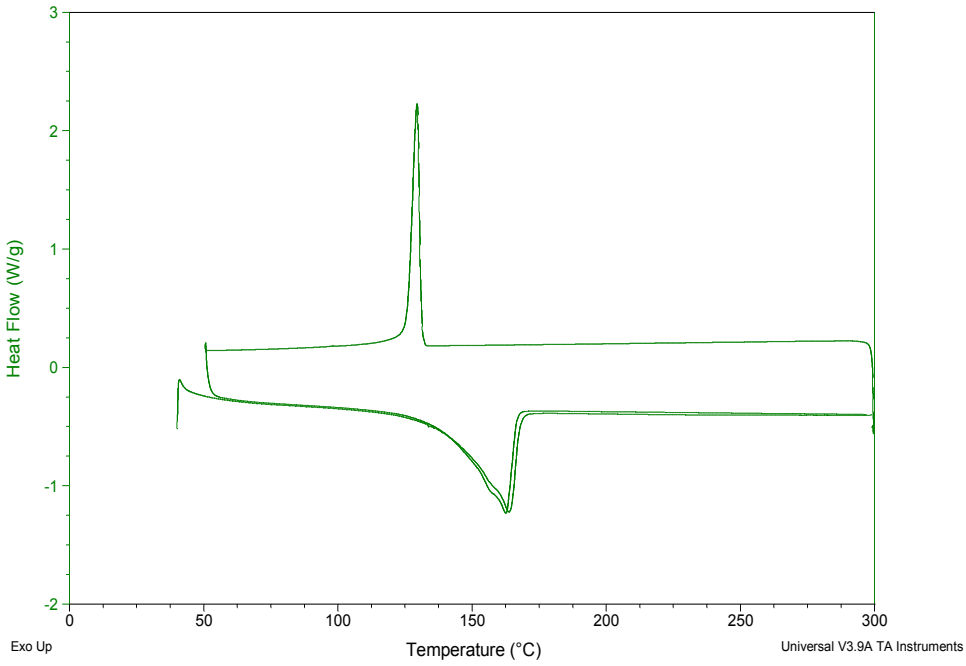

Figure 4.5: DSC thermal analysis results of RPP.

The melting point of the recycled polystyrene (RPS) is observed to be around 120^{o}C. Figure 4.6 below shows the DSC thermal of a polystyrene RPW sample. However, the polystyrene shows an early deep prior to the actual melting peaks, shown in Figure 4. This indicates the presence of some sort of impurity. We can conclude that the RPS is not 100% pure by composition. This could be due to presence of additive reagent for easier process of the original polymer at production stage. In any case, earlier trials shows RPS to be practically unsuitable for blending with asphalt binder. But this does not prevent its utilization as aggregate supplement in the AC modification phase.

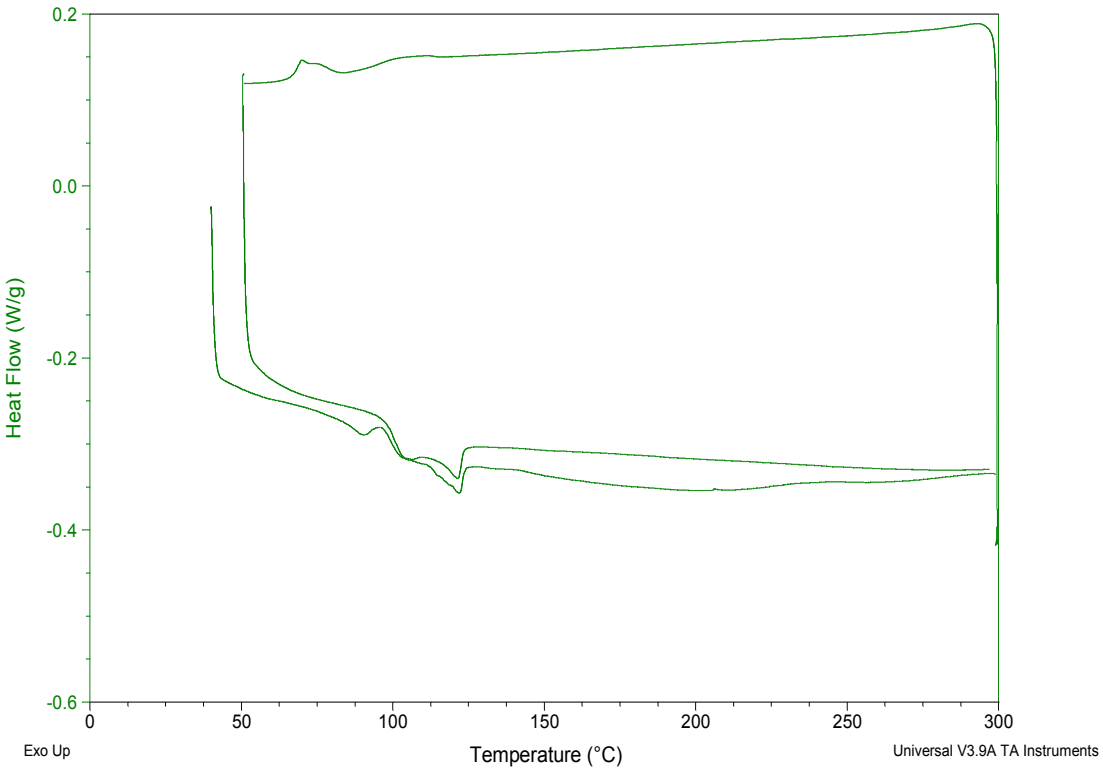

Figure 4.6: DSC thermal analysis results of RPS.

4.2 OPTIMIZATION OF RPW-ASPHALT BLENDING TIME RESULTS

After the selection of the RPW-asphalt blending temperature, the next task is the optimization of the blending duration. Two asphalt binder tests (rotational viscosity and dynamic shear modulus test) were selected for the blending time optimization. The viscosity test is conducted on RPW-asphalt at liquid state and temperature close to the AC compaction range (135^{o}C), while the dynamic shear modulus test is conducted on the semi-solid RPW-asphalt at close to AC service temperature (64 to 70^{o}C). The objective is to enable the establishment of a global optimum blending duration for the selected blending temperatures.

The variation of the viscosity with time at 4% content of PRW is shown in Figure 4.7. This plot was generated with the aim of establishing the optimum mixing duration of each RPW. As can be observed, there is a little increase in viscosity even for the neat asphalt binder, with increase in blending duration. This is due to the unavoidable, but limited oxidation that takes place while stirring the binder in an oxygen surrounded atmosphere (air) at high temperature. The RLDPE modified blend shows a relatively uniform viscosity after about 30 minutes of blending. This indicates that, the RLDPE polymer has already been dispersed thoroughly, such that additional shearing no longer changes the morphology of the blend. The change in viscosity of the RHDPE blend seems to stabilize after about 60 minute of shearing. The same trend as with the RHDPE blend can be observed with RPP modified asphalt binder.

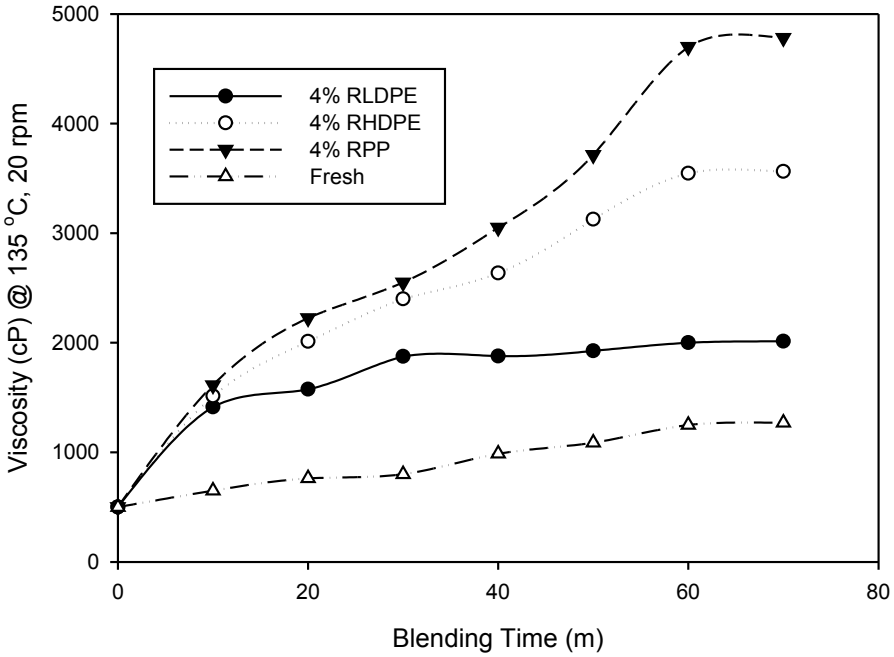

Figure 4.7: Viscosity-Time Variation at 4% RPW Loading.

The rutting parameter of RLDPE modified asphalt binder was plotted against the duration of mixing, as shown in Figure 4.8. Test results runs for 64 and 70^{o}C were shown. Both plots seem to stabilized after 20 minutes. This indicates that prolong blending after 20 minute could be counter-productive, as the little increase in the rutting parameter beyond 20 minutes could be due to the little but insignificant oxidation of the asphalt binder.

Figure 4.9 shows the rutting parameter of RHDPE and RPP modified binders plotted against duration of blending. The RPP modified asphalt curve can be observed to level relatively after 50 minutes of blending. Based on the observed trends for Figure 4.7, Figure 4.8 and Figure 4.9, the optimum blending time of RPP, RHDPE and RLDPE were selected to be 50, 60 and 30 minutes respectively as summarized in Table 4.2.

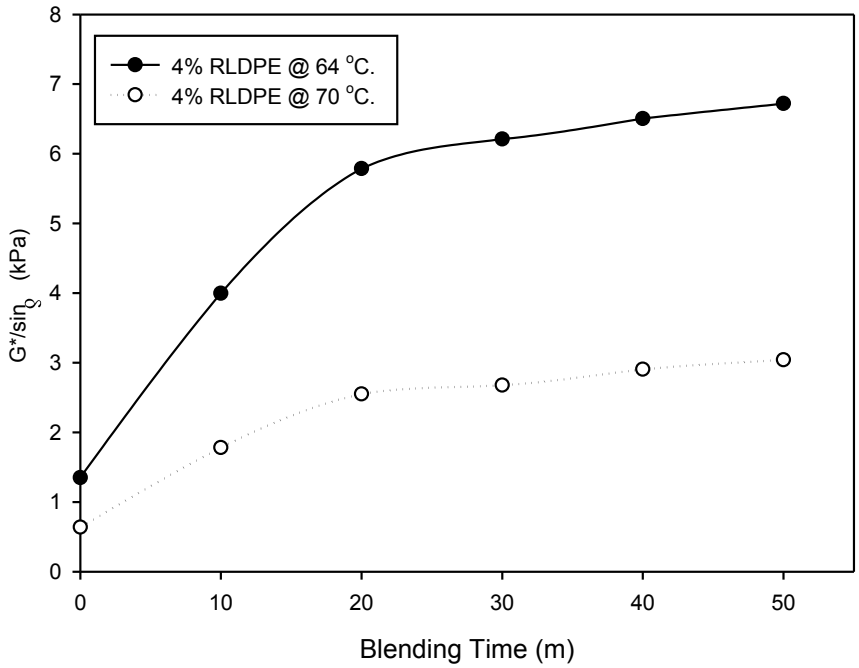

Figure 4.8: G*/Sinδ (kPa) vs. Blending Time for RLDPE Modified Asphalt.

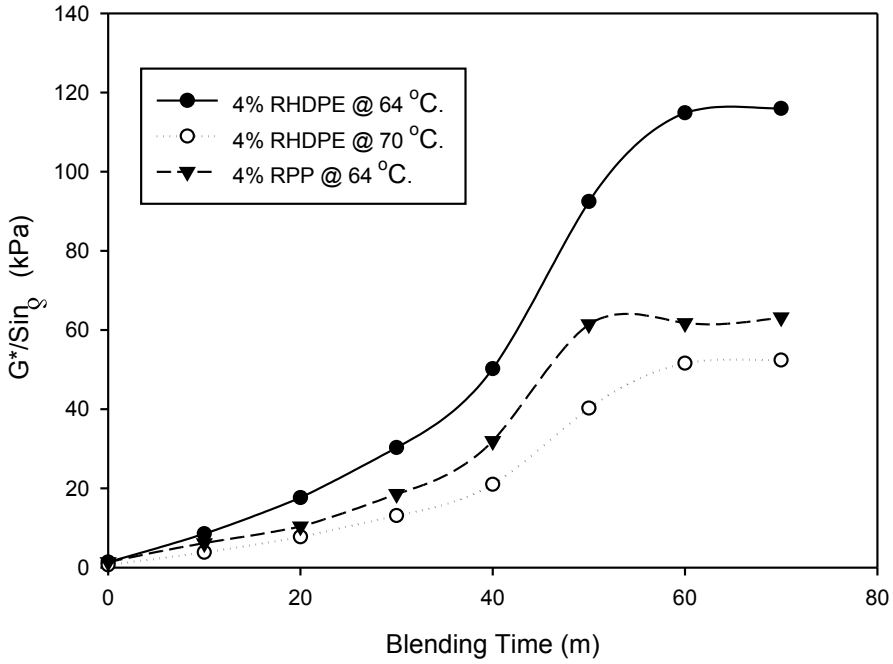

Figure 4.9: Rutting parameter vs. Blending Time RHDE and RPP Binders.

Table 4.2: Duration of RPW-Asphalt Blending.

RPW	Blending Duration
RHDPE	60 min.
RLDPE	30 min.
RPP	50 min.

4.3 ASPHALT PERFORMANCE GRADING

4.3.1 VISCOSITY TEST RESULTS

4.3.1.1 RPW Modified Asphalt Binder Viscosity

The viscosity variation at different level of the RPW content is shown in Figure 4.10. As expected, the viscosity increases with more RHDPE, RLDPE or RPP loading. However, the RHDPE modified asphalt has a relatively higher viscosity than its RLDPE and RPP counterparts. This is could be attributed to the difference in molecular structure, weight, and density. It can also be observed at RHDPE and RLDPE content above 7%, the viscosity exceeds the SHRP PG specified limit of 3000 Poise for convenient pumping activities. While the viscosity of the RPP modified asphalt binder remained within the stipulated limit, for RPP content below 8%.

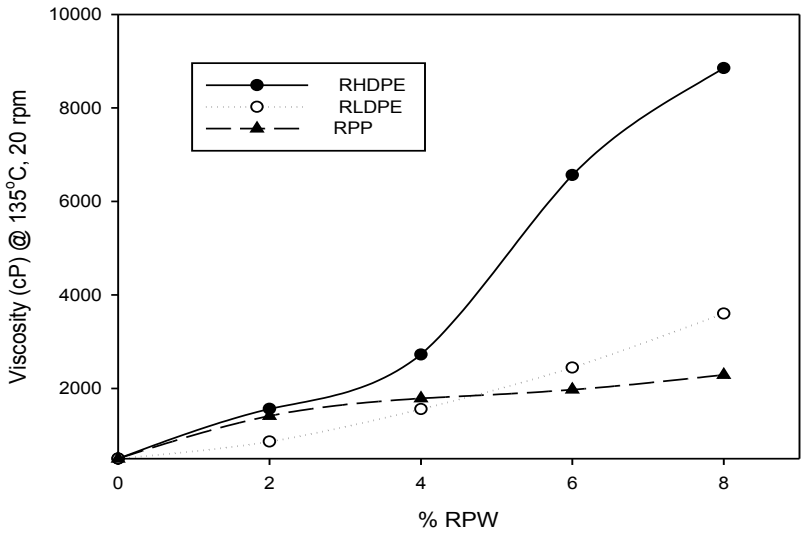

Figure 4.10: Viscosity of RPW Modified Asphalt Binders.

4.3.1.2 RLDPE + SBS Modified Asphalt Binders

The viscosity of a RLDPE-SBS binder appreciates with increase in either RLDPE or SBS, as can be observed from Figure 4.11. This is confirmed from the trends exhibited by blends containing either RLDPE or SBS alone. This increasing trend happened to be maintained by blends containing both RLDPE and SBS polymer, due to the constructive interaction between the RLDPE and SBS polymer micro-structural network. Their individual micro-structural linkage reinforced each other, and continue to develop more connections as either the RLDPE or SBS increases. This phenomena leads to an increased inter-layer movement resistance, which in turn translate to a more viscous modified binder. Most of the RLDPE-SBS blends meet the super-pave viscosity requirement limit. However, blends containing more than 6% RLDPE in addition to SBS failed to pass the viscosity criterion.

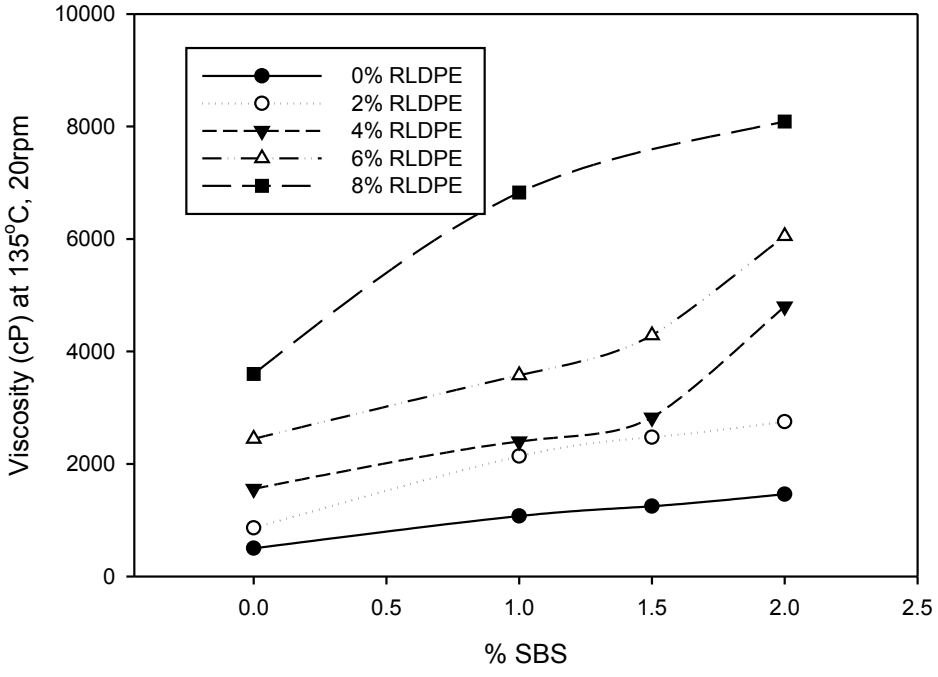

Figure 4.11: Viscosities of RLDPE-SBS modified binders.

4.3.1.3 RHDPE + SBS Modified Asphalt Binders

The trends observed for RHDPE-SBS blends are slightly different from those exhibited by RLDPE-SBS modified binders, as seen from Figure 4.12. Due to the high viscous nature of the RHDPE blends, for high content of RHDPE (above 4%), the SBS initially thins the RHDPE-containing blends. At high RHDPE content, SBS content below 1.5% is not sufficient for establishment of a critical RHDPE-SBS micro-structural network that will enable a constructive interaction. Hence the relatively less viscous and dispersed SBS phase incorporated in to the assembly ended up facilitating inter-layer movement. While above 1.5% SBS content there exist a more continuous SBS-RHDPE network that creates another dimension to the interlayer movement resistant. This leads to the development of a constructive interaction between the two additives. Seven top most viscous blends shown in this graphs have not met the super-pave viscosity criteria.

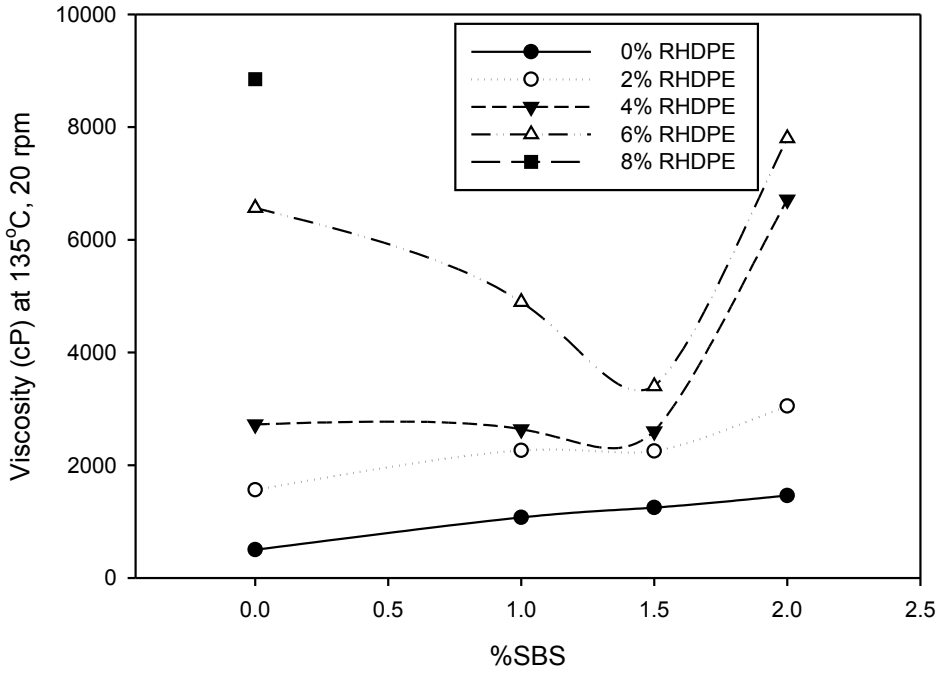

Figure 4.12: Viscosities of RHDPE-SBS modified binders.

4.3.1.4 RPP + SBS Modified Asphalt Binders

The impact of RPP and SBS on the viscosity of RPP-SBS modified asphalt blends is harmonious, as can be observed from Figure 4.13. Both SBS and RPP resulted in an increased viscosity at higher dosages. The rate of increase in the viscous component of the asphalt binder due to either RPP or SBS is relatively the same. For example, the viscosity of asphalt blend containing 2% SBS-only is approximately equals that containing 2% RPP-only. Therefore, there would not be significant difference in phase angle between the various micro-structural network. Unlike at higher RHDPE dosage in case of RHDPE-SBS asphalt binders, this enable and facilitates a constructive interaction between the SBS and RPP in the RPP-SBS modified asphalt blends. The only blends that could not meet the super-pave viscosity limit criterion are the 3 top most viscous combinations shown.

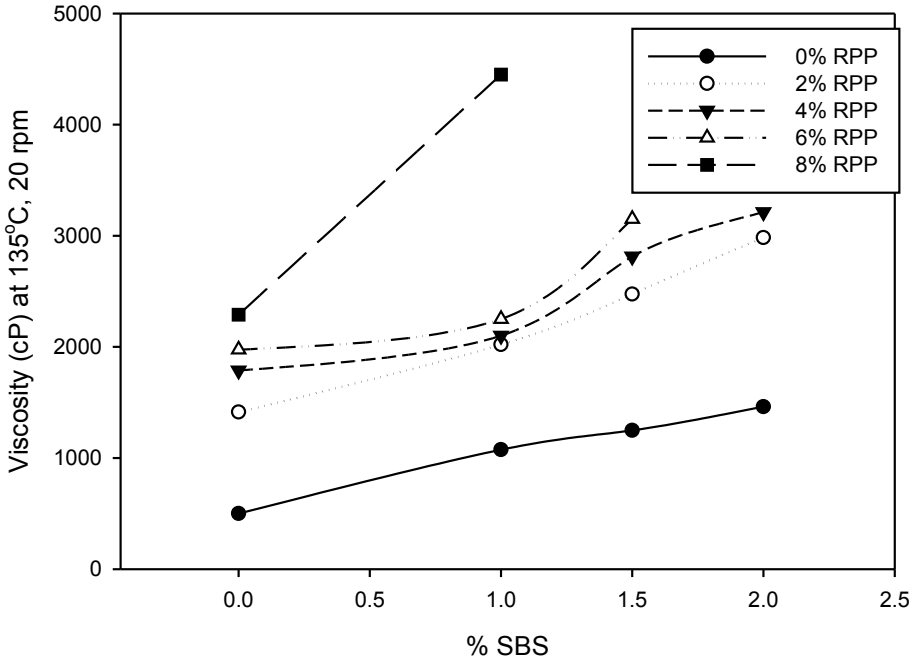

Figure 4.13: Viscosities of RPP-SBS modified binders.

4.3.1.5 RLDPE + PB Modified Asphalt Binders

The RLDPE-PB modified asphalt binders demonstrate increased viscosity with more RLDPE and PB, as shown by Figure 4.14. The viscosity increase due to PB is relatively slight when compared to RLDPE, as can be seen from blends containing either LDPE or PB alone. Increased viscosity due to PB tend to be more pronounced in blends with higher content of RLDPE. This could be as a results of much polymer-rich phase in the high RLDPE-containing asphalt binders. Most of the RLDPE-PB modified asphalt binders meet the super-pave viscosity limit, except the top six viscous blends.

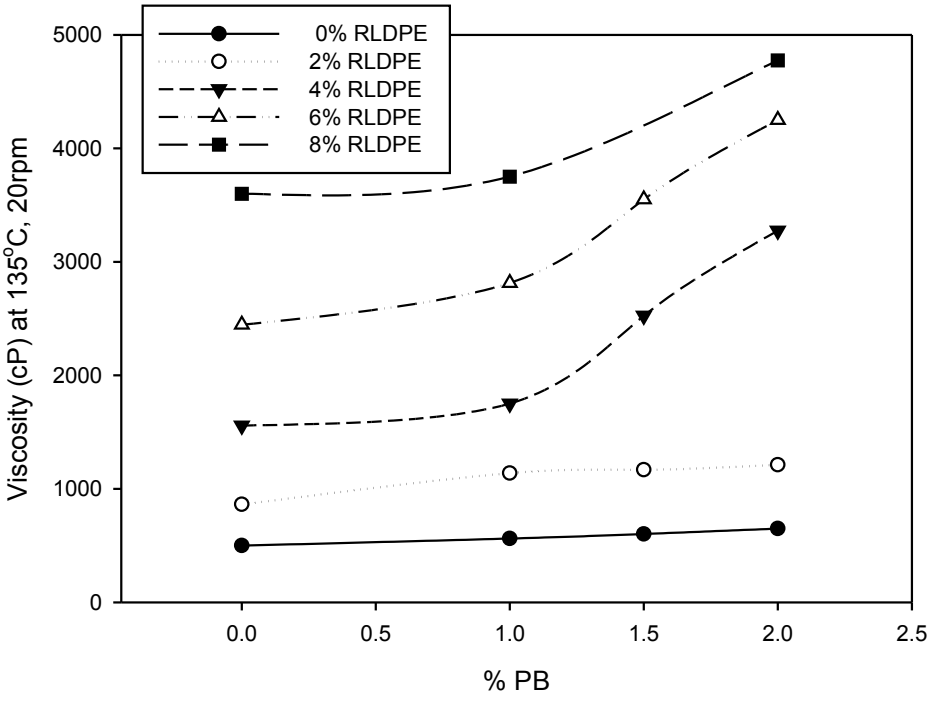

Figure 4.14: Viscosities of RLDPE-PB modified binders.

4.3.1.6 RHDPE + PB Modified Asphalt Binders

The RHDPE-PB blended asphalt binders exhibit lower viscosities than their RHDPE-only counter parts, as depicted in Figure 4.15. As can be observed, there is a decreasing viscosity trend as the PB content increases. The rate of decrease in viscosity is more rapid for asphalt blends containing higher RHDPE. Unlike the RLDPE blends, the RHDPE blends exhibits a very high viscosity (as high as 9000 cP for 8% RHDPE content). While on the other hand, PB can only results in a relatively slight viscosity increment. So for up to 4% of RHDPE containing blends, the mild PB was only successful in slightly lubricating RHDPE blends inter-layers. Hence resulting in reduced inter-layer friction resistance. However, for blends containing higher RHDPE dosage that have a continuous RHDPE micro-structural network. The resulting decrease in the interlayer friction translate into higher loss in viscosity. Hence, the PB here served a vital role that un-stiffen the viscous RHDPE modified asphalt binder. The topmost seven viscous blends shown did not meet the super-pave viscosity limits. That is, those blends containing more 4% RHDPE.

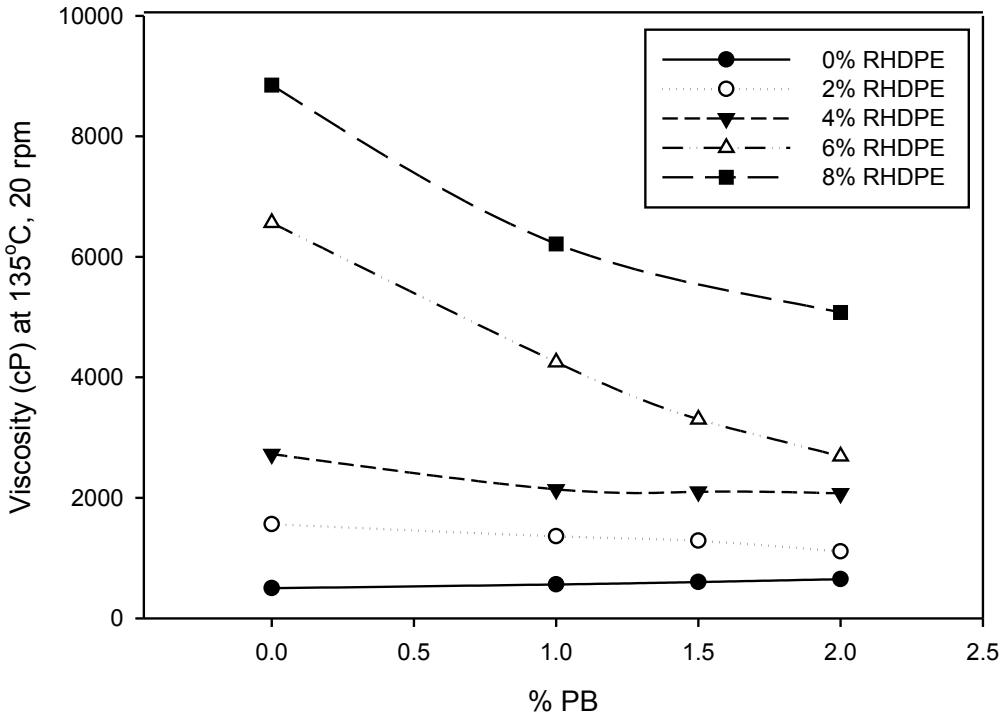

Figure 4.15: Viscosities of RHDPE-PB modified asphalt binders.

4.3.1.7 RPP + PB Modified Asphalt Binders

As previously established, adding RPP leads to more viscous asphalt binder. So also is adding PB polymer to a RPP modified asphalt binder, as can be seen from Figure 4.16. The only trend worth noticing here is the pronounced increment in viscosity due to increased PB content at higher dosages of RPP. This can be explained by zooming the phenomena to the micro-scale level. At lower content of both RPP and PB, the polymer phase is dispersed. But as both the RPP and PB content increases, there was a phase inversion. Hence the development of continuous RPP-PB polymer-rich phase and a disperse asphalt binder phase. The continuity of the RPP-PB micro-structure enables more interlayer movement resistance. This translate into much higher viscosity. The RPP-

PB modified asphalt binder fails to meet super-pave viscosity requirement from 4% RPP and 1.5% PB contents.

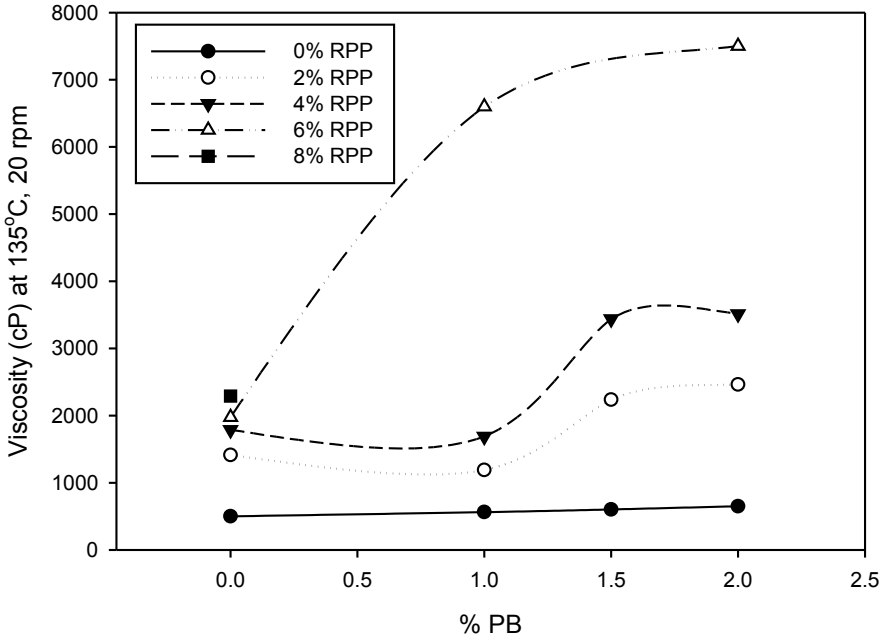

Figure 4.16: Viscosities of RPP-PB modified asphalt binders.

4.3.2 VISCOELASTIC PROPERTIES of RPW MODIFIED ASPHALT BINDER

4.3.2.1 Recycled Low Density Polyethylene Asphalt Blends

The rutting parameter ($G^*/\sin\delta$) and the phase angle (δ) plots of the RLDPE modified asphalt is shown in Figure 4.17. As can be anticipated, the rutting parameter increases with increasing RLDPE content and declined at higher temperature. The phase angle decreases at higher RLDPE loading, and increases with increasing temperature. The overall observation implied increased elastic properties and rutting resistance for the modified binder at increased RLDPE dosage.

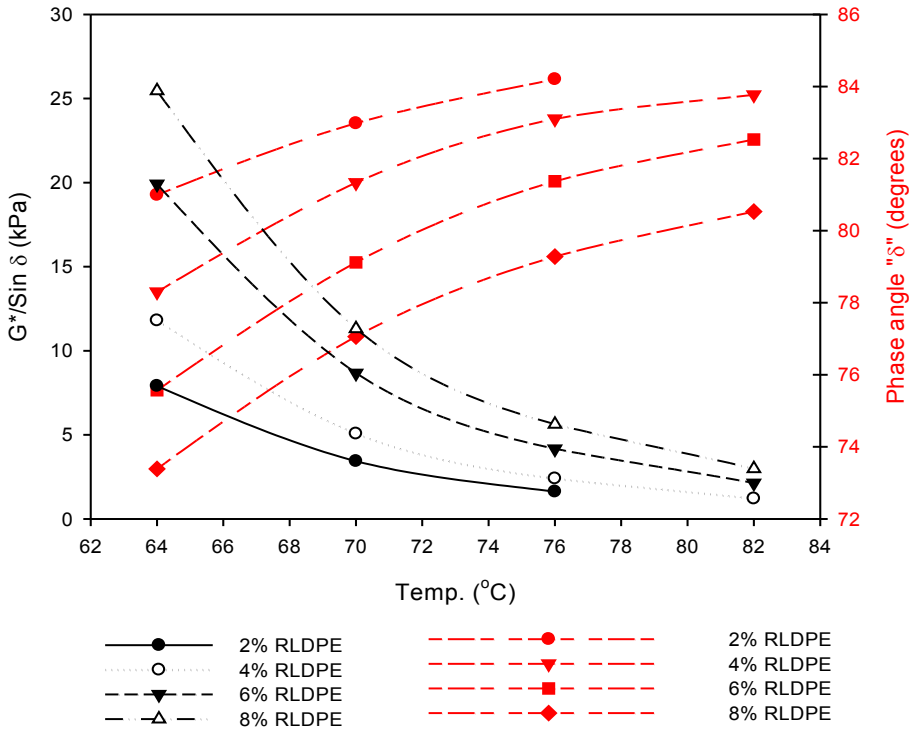

Figure 4.17: G*/sinδ and Phase Angle vs. Temperature for RTFO RLDPE Asphalt.

4.3.2.2 Recycled High Density Polyethylene Asphalt Blends

The rutting parameter and the phase angle plots of the RHDPE modified asphalt is shown in Figure 4.18. Similar trend as observed with RLDPE recycled waste can also be witnessed here. The rutting parameter increases with more RHDPE loading. But declined with increase in temperature. The phase angle respond in opposite manner. It decreases with more RHDPE contents and increases with increasing temperature. Based on this observations, it can be inferred that the rutting resistance and viscoelastic properties of the RHDPE binder improves with increase in RHDPE contents.

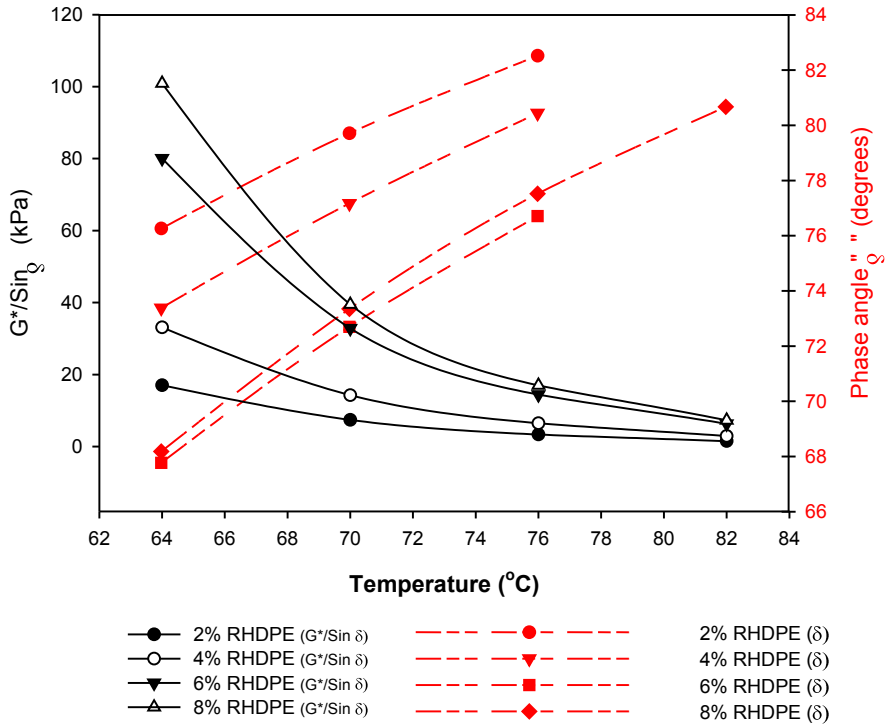

Figure 4.18: G*/sinδ and Phase Angle vs. Temperature for RTFO RHDPE Asphalt.

4.3.2.3 Recycled Polypropylene Asphalt Blends

The rutting parameter and the phase angle plots of the RPP modified asphalt is shown in Figure 4.19. The rutting parameter increases with increasing RPP content and declined at higher temperature. The phase angle decreases at higher RPP loading, and increases with increasing temperature. These observed trends indicate an improved rutting resistance and viscoelastic properties for the RPP modified asphalt with increasing RPP content.

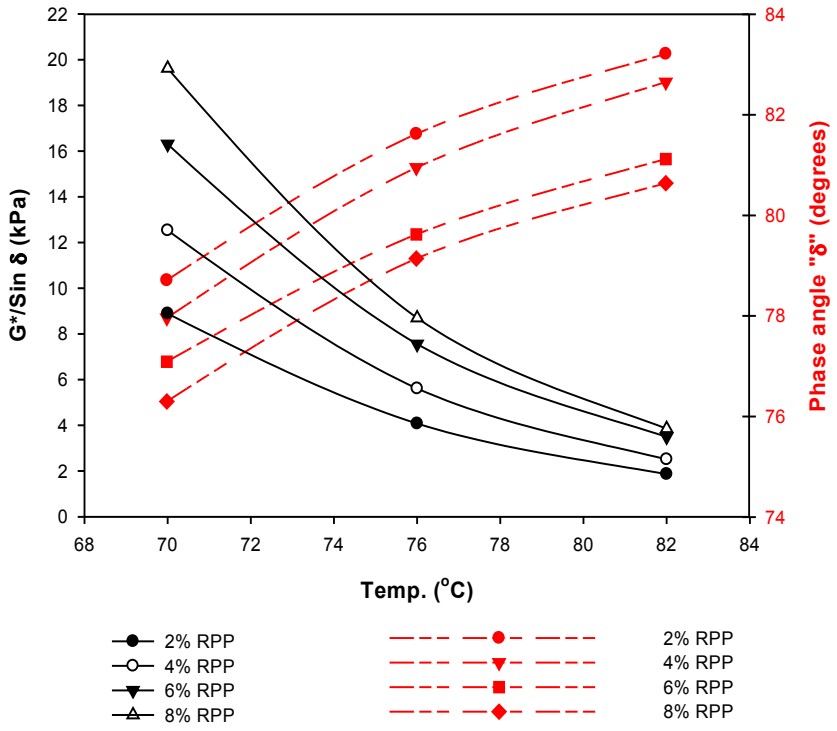

Figure 4.19: G*/sinδ and Phase Angle vs. Temperature for RTFO RPP Asphalt.

4.3.3 PERFORMANCE TEMPERATURE OF RPW MODIFIED ASPHALT

4.3.3.1 Performance Grade of the RPW-Modified Asphalt Binders

Table 4.3 shows the summary of the PG and PG^+ grades of the different recycled plastic modified asphalt binders. 2% dosage of RLDPE changes the upper PG of the neat binder to70, and its equivalent upper PG^+ grade is 60H. 4% and 6% RLDPE blends showed similar upper PG grade. The PG^+ grading system has the capability of further sub-categorizing blends of similar PG in to different traffic levels. Hence 4% and 6% RLDPE modified binder possesses PG^+ of 70H and 76H respectively. All the RLDPE blends did not meet the AASHTO TP 70 elastic recovery requirement. This is not surprising, because polyethylene in its self is not elastomeric in nature. For the same reason, similar outcome related to recovery was observed for RHDPE and RPP modified asphalt binders. However, according to the usual practice of verifying the PG of an Asphalt Binder (AASHTO PP6 and AASHTO M 332) the RPW have yielded a better performing binder. RLDPE and RPP content below 6% has satisfied the lower PG temperature requirement of KSA, while only 4% RHDPE content and below could meet KSA low PG temperature.

Figure 4.20 shows the plots of the upper PG temperature (UPGT) at which each blend failed. Identical pattern can be observed for the RHDPE and the RLDPE. Only that the RHDPE raises the PG temperature by far more, relative to RLDPE. The RPP yields blends with higher upper PG than the RLDPE, but higher than RHDPE modified binders only in some cases.

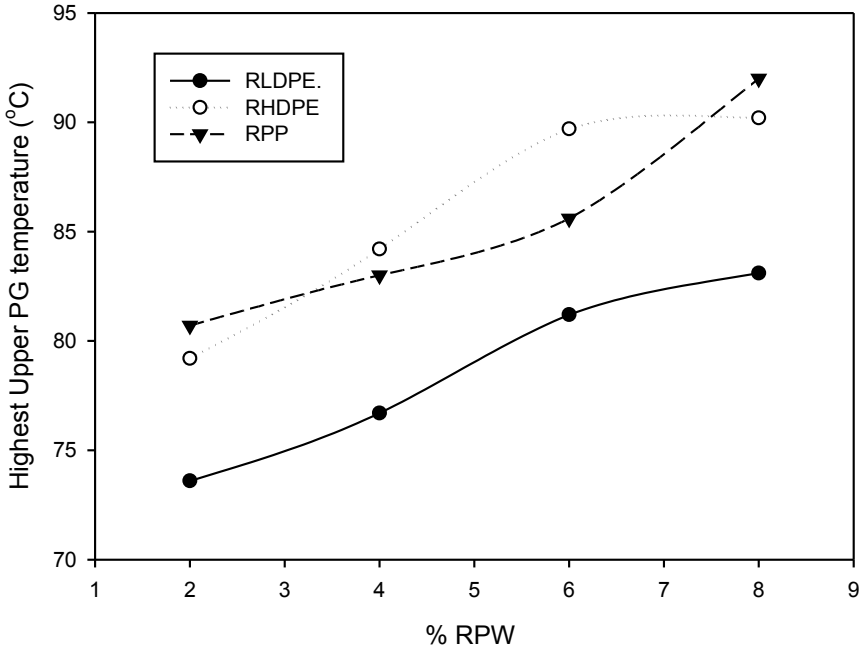

Figure 4.20: Upper PG Temperature vs. % RPW.

Table 4.3: Summary of RPW Modified Asphalt Performance Grade.

	RLDPE			
Composition	2%	4%	6%	8%
PG grade	70-18	76-12	76-10	82-6
PG^+ (MP 19-10)	64H; 70S-18	70H; 76S-12	76H-10	82S-6
PG^+ (TP 70-11)	Failed	Failed	Failed	Failed
	RHDPE			
Composition	2%	4%	6%	8%
PG grade	76-12	82-10	88 - *	88 - *
PG^+ (MP 19-10)	70H; 76S-12	76H; 82S-10	82H - *	82V- *
PG^+ (TP 70-11)	Failed	Failed	Failed	Failed
	RPP			
Composition	2%	4%	6%	8%
PG grade	76-12	82-10	82-10	88 - *
PG^+ (MP 19-10)	76S - 12	76H - 10	76H - 10	76V - *
PG^+ (TP 70-11)	Failed	Failed	Failed	Failed
*Upper PG only, and failed to meet viscosity specification requirement				

4.3.3.2 UPGT of RLDPE + SBS Modified Asphalt Binders

As can be seen from Figure 4.21, RLDPE results in blends with increases UPGT, but SBS raises the UPGT at relatively higher rate. This can be observed by comparing the lowest graph containing 0% RLDPE and 2% RLDPE blend corresponding to 0% SBS. Adding SBS to the RLDPE modified binder causes a continuous increment in UPGT. The addition of much stiffer SBS polymer into the existing RLDPE micro-structural network served to strengthen the matrix. The increased SBS content lead to the establishment of more SBS-SBS and SBS-RLDPE physical linkage. Hence the continuous increase in UPGT. The SBS serve as PG improving addition to the RLDPE blend.

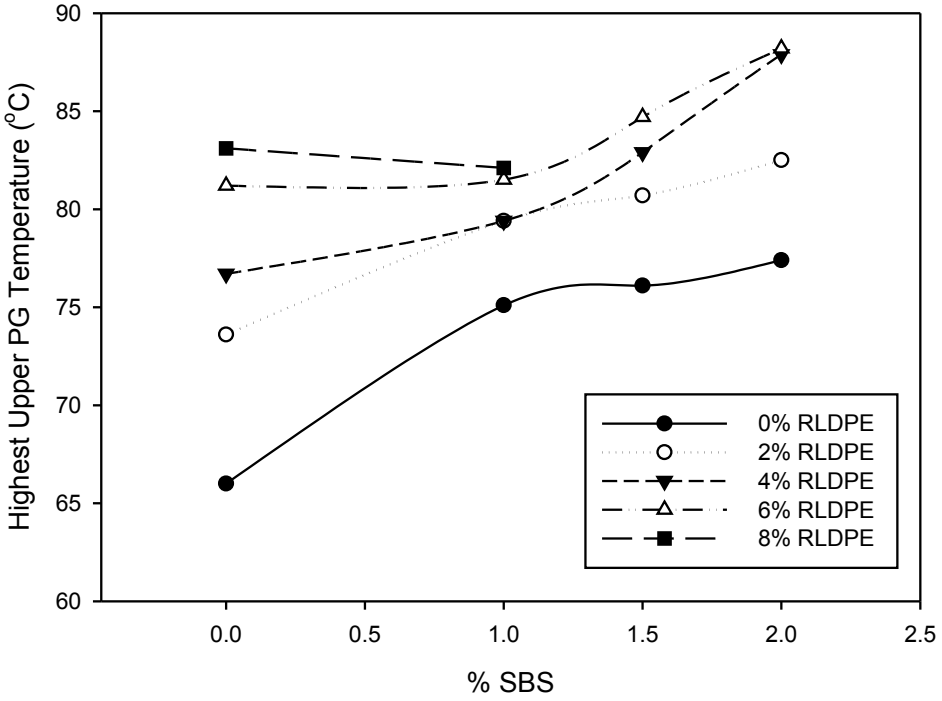

Figure 4.21: Upper Performance Grade Temperature of RLDPE-SBS binders.

4.3.3.3 UPGT of RHDPE + SBS Modified Asphalt Binders

The RHDPE results in blends with significant increase in UPGT, as seen from Figure 4.22 above. While on the other hand, SBS yield binders with increased UPGT, but at relatively lower scale than RHDPE. This can be confirmed by comparing blends containing 2% of each of modifiers alone. The RHDPE-SBS modified asphalt binders showed decreased UPGT at SBS content range below 1.5%. Then the pattern reverses afterwards, and the UPGT appreciate up to 2% SBS content. This trend has not been observed for RHDPE-SBS blend containing only 2% RHDPE. There is a slight continuous increase in UPGT all through. This is due to the fact that at 2% RHDPE content, the RHDPE micro-structural network is at a disperses state. No strong continuous RHDPE-RHDPE linkages were formed yet. Addition of the SBS helps improve the proportion of the dispersed polymer within the continuous weak asphaltic phase. Which in turn helps influence the thermal resistance of the blend towards the higher side of the polymers. But at RHDPE contents above 2%, there is an already establish continuous RHDPE micro-structural linkage within the asphalt. And the UPGT of the blend is more or less already influence towards that of much tougher RHDPE. Hence adding SBS to this assembly introduces relatively weak and dispersed spots within the already establish RHDPE network. This slightly weaken the overall stiffness and thermal resistance of the RHDPE blends at SBS content below 1.5%. However, as the SBS content increases beyond 1.5%. The then dispersed SBS spots became more connected and stronger. Hence the establishment of a constructive interaction between the RHDPE and SBS.

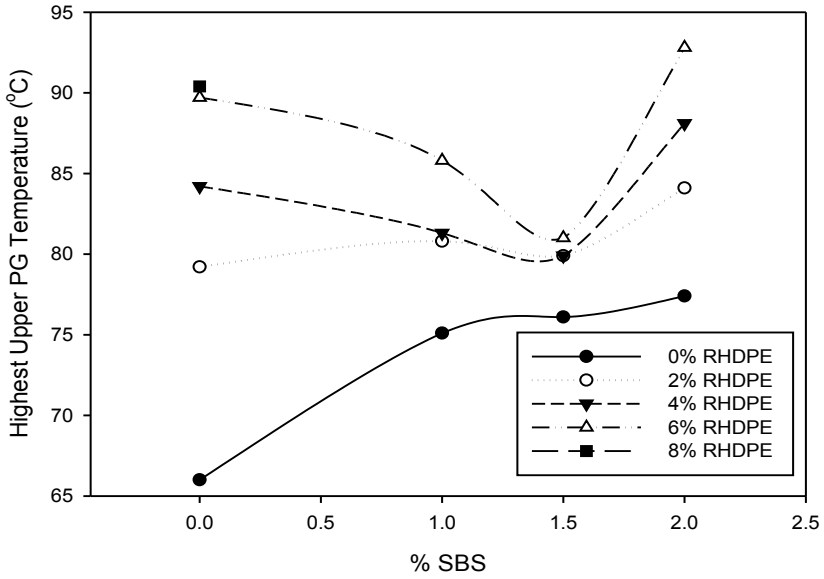

Figure 4.22: Upper Performing Grade Temperature of RHDPE-SBS binders.

4.3.3.4 UPGT of RHDPE + SBS Modified Asphalt Binders

The SBS results in steady UPGT increment from 1% to 2% content, as shown in Figure 4.23. However adding SBS to stiffer RPP modified binder results in initial UPGT decline, at SBS content below 1%, for up to 6% RPP binder content. But this loss trend in UPGT reverses at SBS content above 1%. This is a similar but less obvious case of RHDPE-SBS binder (Figure 4.22). Overall, the SBS does not affect the RPP modified asphalt binder UPGT significantly.

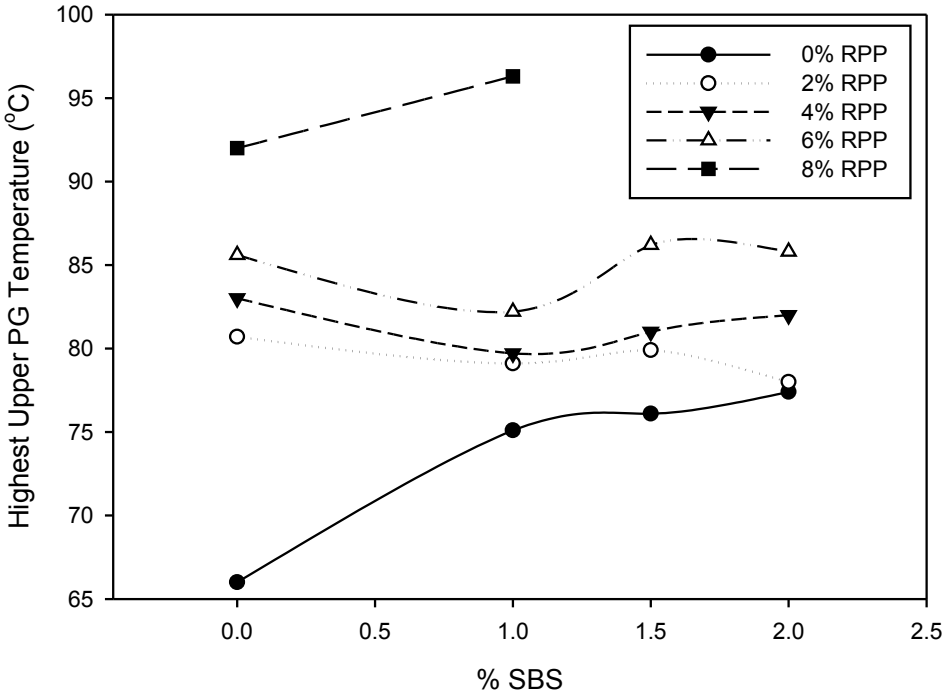

Figure 4.23: Upper Performing Grade Temperature of RPP-SBS binders.

4.3.3.5 UPGT of RLDPE + PB Modified Asphalt Binders

As shown in Figure 4.24, asphalt binders containing only RLDPE exhibit appreciable UPGT as the content increases (initial points on all graphs). This is also true with PB modified asphalt binders, even though the positive UPGT influencing strength is lower for PB when compared to RLDPE. For RLDPE content below 4%, the PB was only successful in slightly improving UPGT within the range shown. However as RLDPE content rises, the usual UPGT increasing trend of the PB ceases. And there is a decline in the UPGT up to almost 1.5% PB, then rise is observed. At lower RLDPE content (below 4%), the introduction of plastomeric PB in to the moderately stiff dispersed RLDPE micro-structural system results to a slightly reinforced stiffer RLDPE-PB matrix. This is in addition to the increased proportion of less thermal sensitive material than the asphalt

itself. Hence this lead a more temperature resistant blend with higher UPGT. But as the RLDPE content rises (above 4%), the RLDPE micro-structural network became more connected and stiffer. Therefore the introduction of the relatively softer plastomeric PB in to the well connected and much stiffer assembly, generates weak links and spots that yield more thermal sensitive hybrid RLDPE-PB matrix. Depending on the RLDPE content PB can either soften or stiffen RLDPE modified asphalt binder.

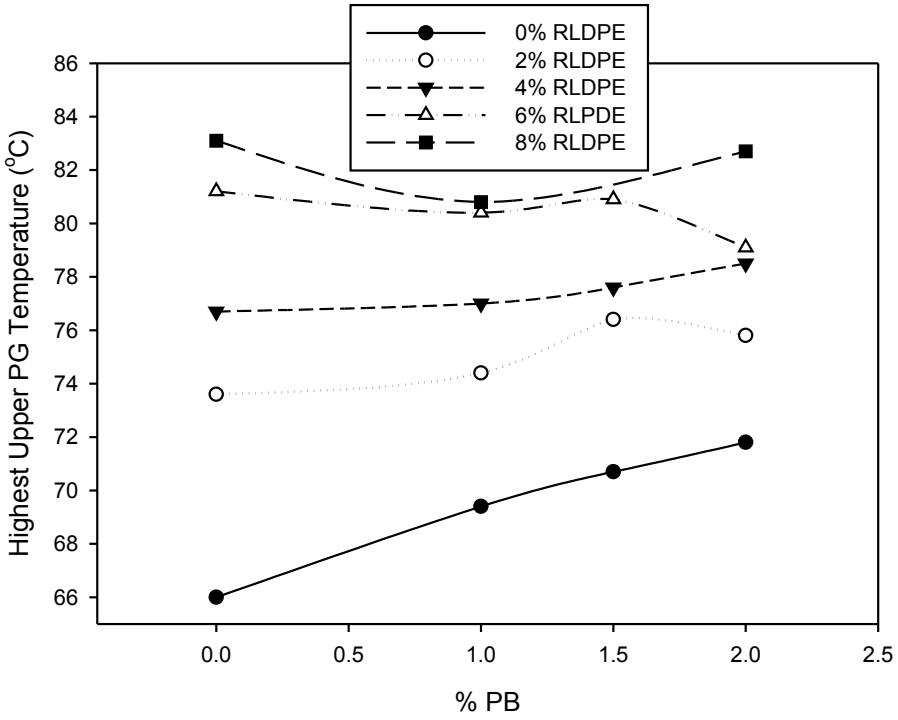

Figure 4.24: Upper Performing Grade Temperature of RLDPE-PB binders.

4.3.3.6 UPGT of RHDPE + PB Modified Asphalt Binders

As previously seen, the PB yield a steady increment in UPGT in the asphalt binder as the PB content increases. The increasing trend has not been maintained when the PB is added to RHDPE modified asphalt binder, as shown in Figure 4.25. There seem to be a

continuous slight decline then rise in UPGT for higher RHDPE content binders. The added PB polymer soften the existing RHDPE micro-structural matrix of the shown content ranging below 2%PB. This yield modified blends with slightly lower UPGT as compared to the RHDPE-only blends. The PB polymer showed a mild influence on the RHDPE modified binder in terms of UPGT.

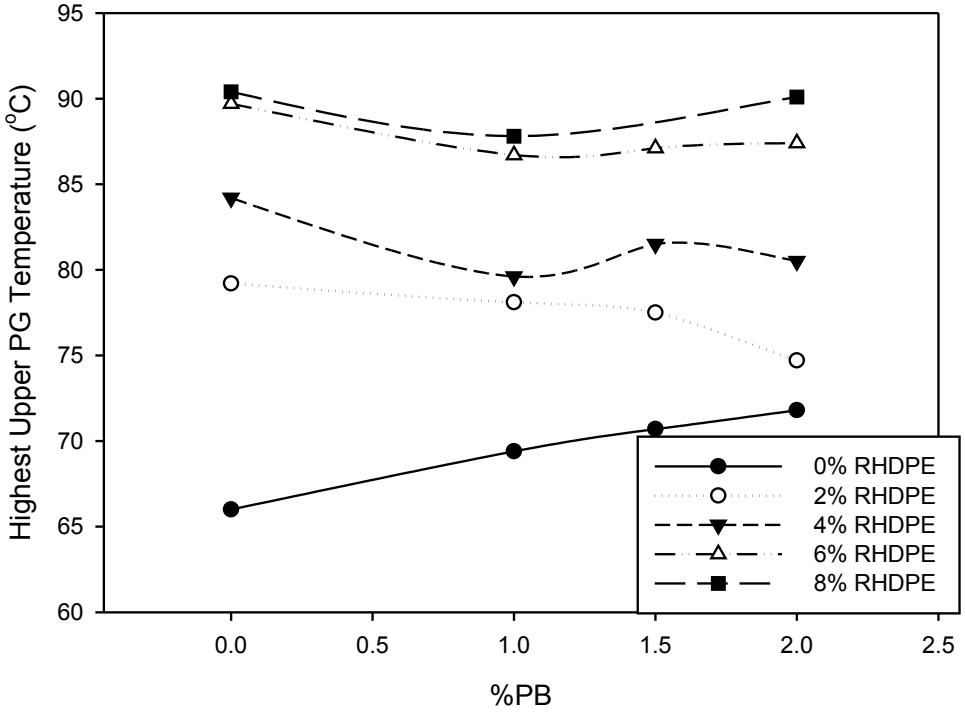

Figure 4.25: Upper Performance Grade Temperature of RHDPE-PB binders.

4.3.3.7 UPGT of RPP + PB Modified Asphalt Binders

Both PB and RPP modified asphalt binder demonstrate a steady UPGT increment with increasing PB or RPP dosages, within the range shown in Figure 4.26. This trend has been maintained for RPP-PB combination for PB content up to 1%. But slight decline in the UPGT is observed for RPP-PB blends containing more than 1% PB.

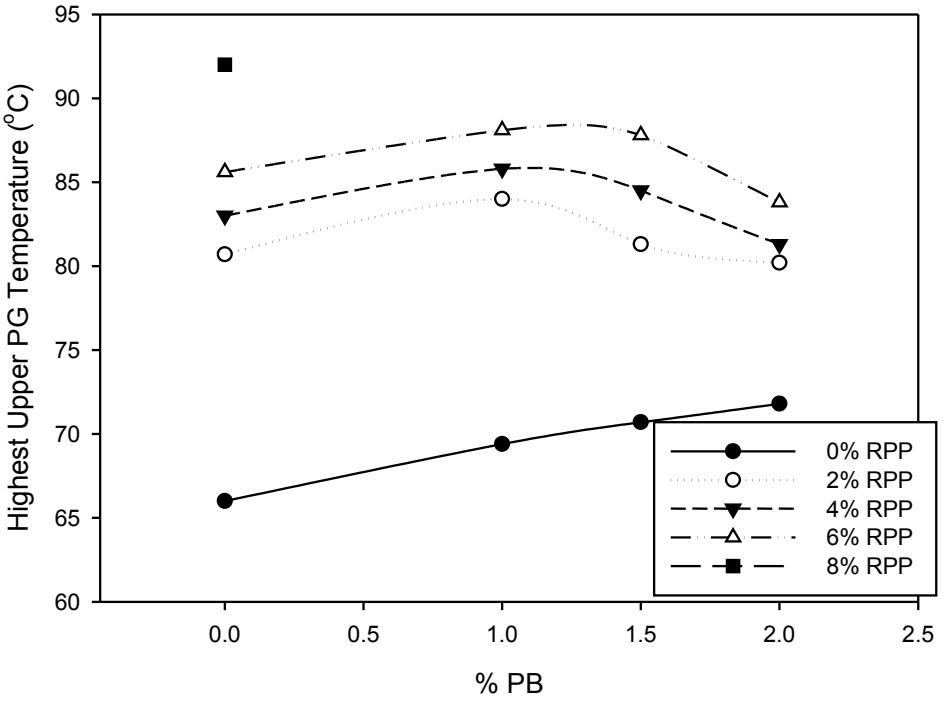

Figure 4.26: Upper Performance Grade Temperature of RPP-PB binders.

4.3.4 Elastic Recovery and Non-Recoverable Creep Compliance (J_{nr}).

4.3.4.1 Elastic Recovery and Jnr of RPW-blended asphalt

All the recycled plastic polymers blends could not meet the requirement of and elastomeric polymer modified asphalt binder set by AASHTO MP 70, as shown in Figure 4.27. As already mentioned, this recycled polymers should not be expected to behave completely different or better than their virgin counter parts. It is known than virgin polyethylene polymer and poly propylene are not elastomeric in nature. In order to compensate for their lack of elastic recovery, these recycled plastic waste need to be supplemented by some amount elastomeric polymer.

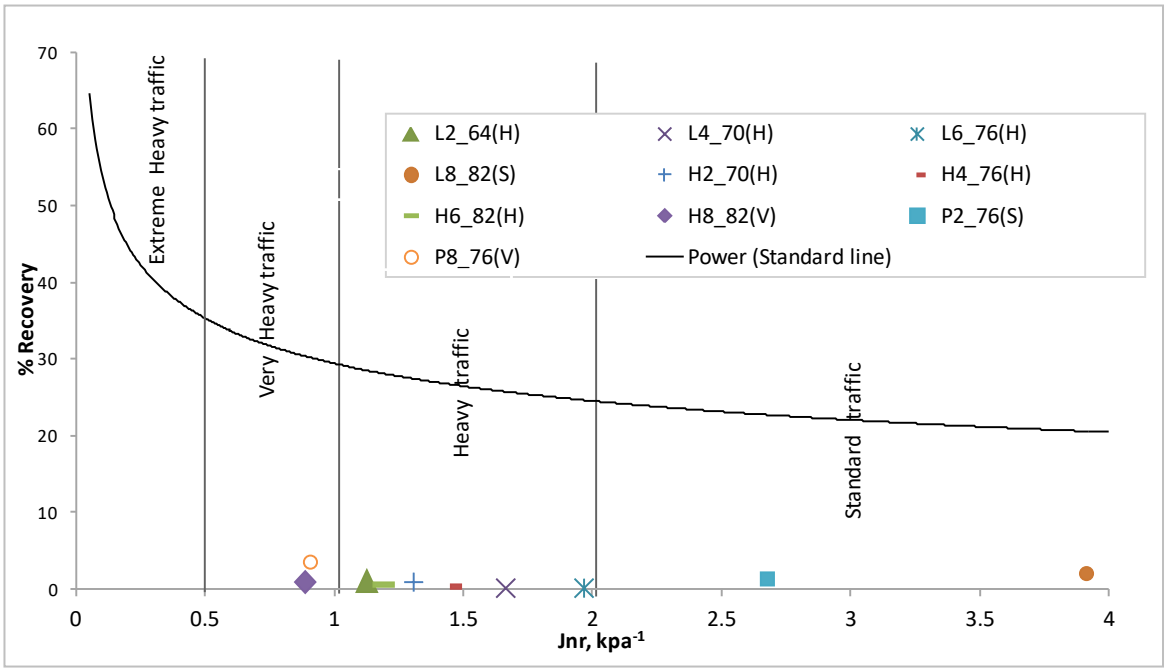

Figure 4.27: TP-70 Plots of RPWs modified asphalt binders.

4.3.4.2 Elastic Recovery and Jnr of RLDPE-PB modified asphalt binders

Figure 4.28 shows TP_70 plots of RLDPE-PB modified asphalt binders. The upper plot presents MSCR results obtained at 76^{o}C and the lower plot showed similar results but obtained at 70^{o}C. It can be seen that the addition of the plastomeric PB to the RLDPE modified bonder does not add to its recovery, as anticipated. It actually results in negative recovery due plastic flow especially at 76^{o}C. However, the non recoverable creep compliance (J_{nr}) tend to improve and the traffic level of the RLDPE modified blends is also seen to slightly increase with increasing PB. A typical example is that of L2PB1_70(S), L2PB1.5_70(H) and L2PB2_70(H) when compared. The RLDPE-PB binders mostly fall in to standard traffic category at 76^{o}C, while majority are suitable for heavy and very heavy traffic for 70^{o}C upper PG. In summary, the PB further aggregates the poor recovery characteristics of RLDPE shown by Figure 4.27, but result in slight J_{nr} improvement.

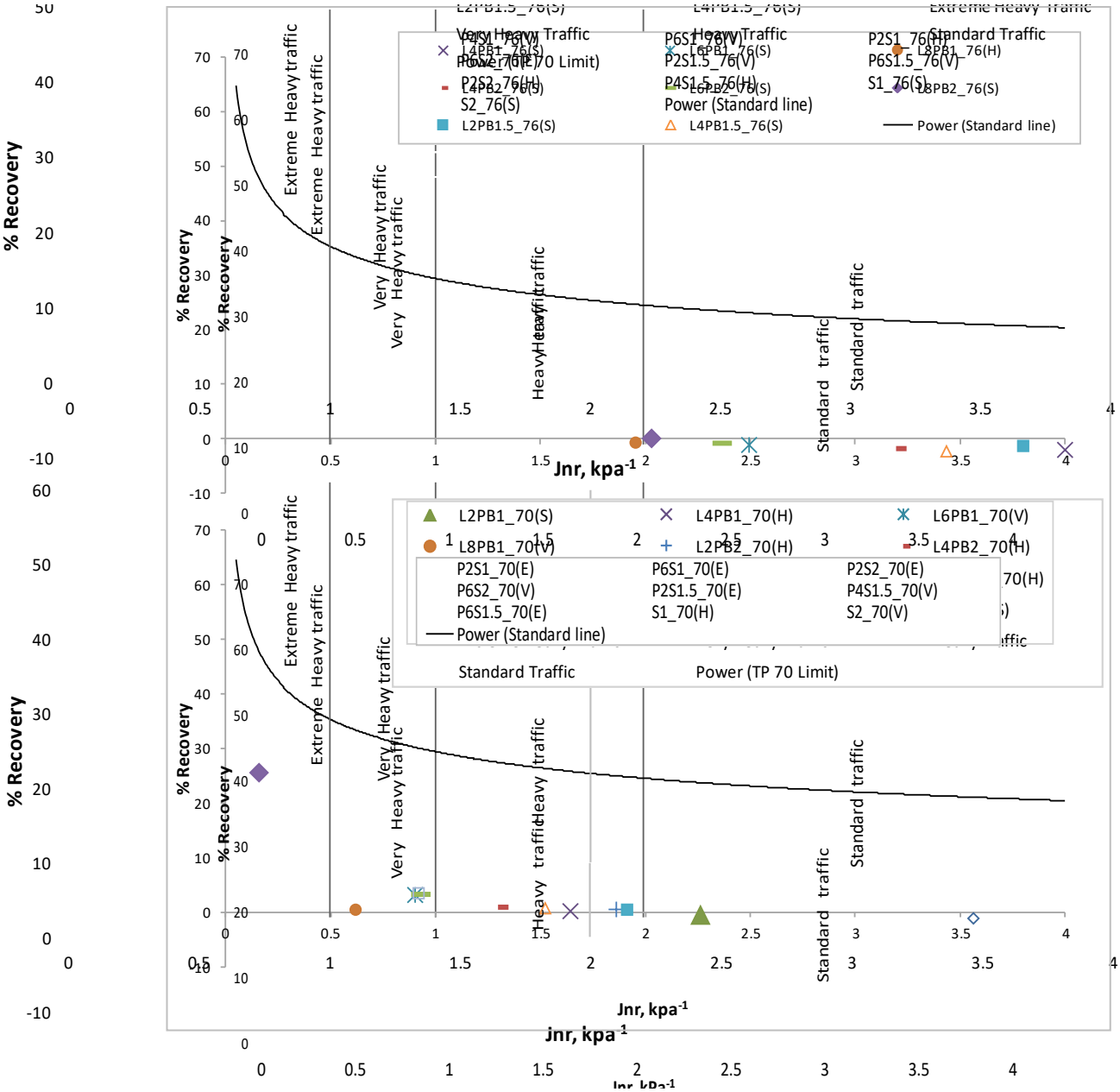

Figure 4.28: TP-70 Plots of RLDPE-PB modified asphalt binders.

4.3.4.3 Elastic Recovery and Jnr of RLDPE-SBS modified asphalt binders

Even though the RLDPE-SBS asphalt blends shown in Figure 4.29 did not meet the TP_70 requirement to be classified as elastomeric polymer modified asphalt binder. The RLDPE-SBS blends possessed significant and satisfactory recovery trait, especially

for environment with upper PG below 70°C. The addition of the SBS polymer results both in J_{nr} and recovery improvement. The hypothesis that lesser amount of virgin elastomer (SBS) might be required to obtain a given recovery (or pass the TP_70 requirement) for a certain PG, when compared to the amount required if elastomer/SBS alone is utilized has been found to be true for RLDPE. A good example is the recovery comparison of S1_70(H) and L2S1_70(V), or S2_70(V) and L4S2_70(E) etc. All RLDPE modified asphalt binders containing certain percentage of SBS, either have recovery equal or greater than the asphalt binder containing that same proportion of SBS alone, in addition to a better J_{nr}. The relative proportion of the elastomer to that of the RLDPE that will ensure greater recovery than when SBS alone is utilized will depend on factors such as: type of the SBB, asphalt, RLDPE and the targeted PG. But in this case, we can safely say, RLDPE content must be equal or greater than the SBS.

The elastomeric nature of the SBS polymer asphalt microstructure is the main reason for the above observation. The addition of the RLDPE to the asphalt binder yields a stiffer modified asphalt that is less train sensitive, but still having poor recovery. But introducing the SBS elastomeric microstructure within the existing RLDPE matrix raised the elastic component of the assembled microstructure and that of the asphalt binder at large. This type of combination has a stiffness added advantage over that consisting of only SBS. Since the MSCR test is stress controlled, which means applying a constant stress to a the test sample and measuring the corresponding strain. A less train sensitive RLDPE-SBS modified binder will sustain lower strain than the SBS-only modified binder containing same SBS proportion. As both type of blends possessed similar recovering tendency, the RLDPE-SBS blend find it easier to recover larger proportion of its strain

than the much deformed SBS-only modified binder. Hence the superior strain recovering trait of the SBS containing RLDPE binder over the SBS-only modified asphalt.

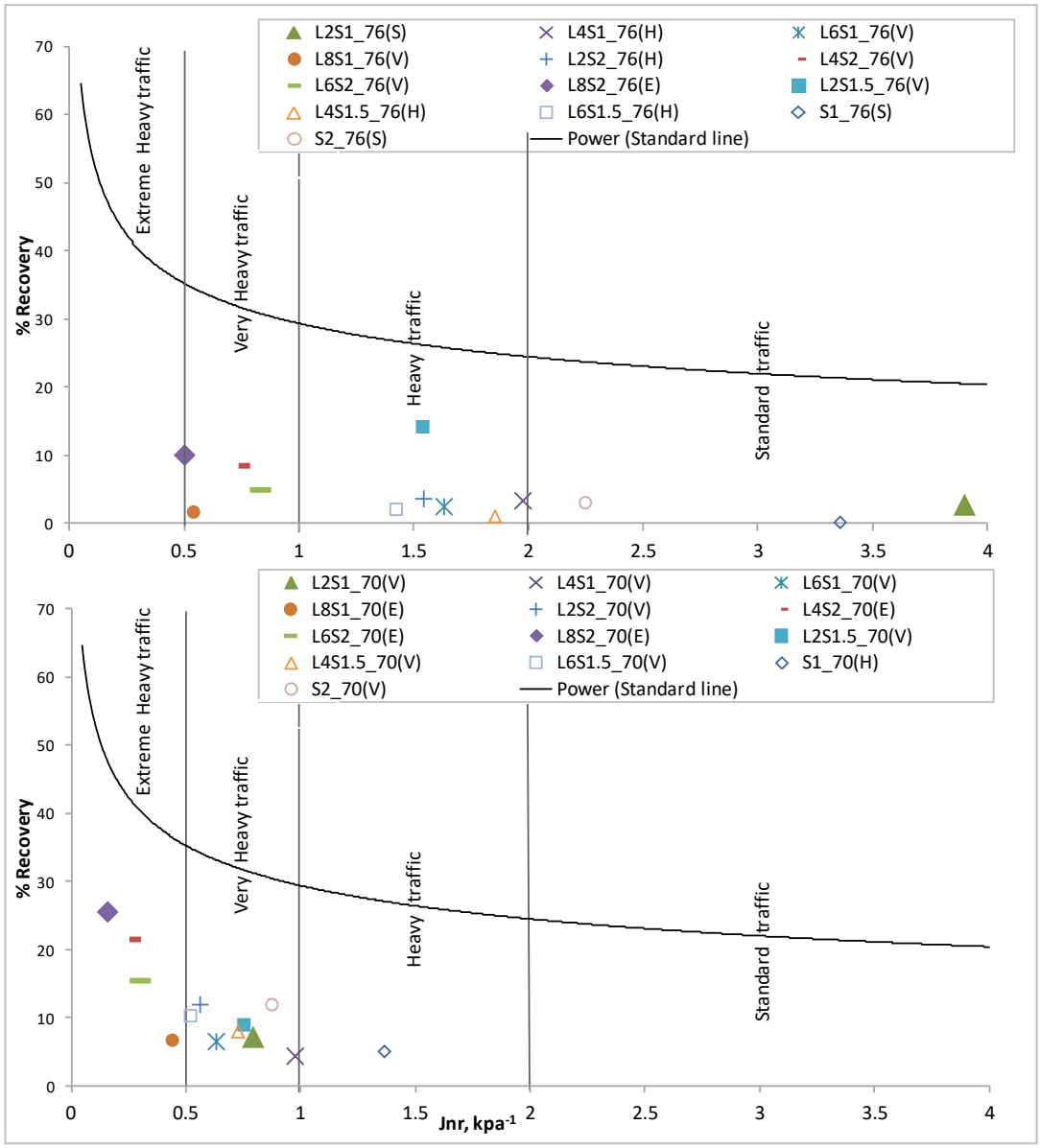

Figure 4.29: TP-70 Plots of RLDPE-SBS modified asphalt binders.

4.3.4.4 Elastic Recovery and Jnr of RHDPE-PB modified asphalt binders

Figure 4.30 show the TP_70 plots of RHDPE-PB asphalt binders. The introduction of PB to the RHDPE modified binder has little impact on the recovery. Two among the three blends with highest recovery as observed from the 70^{o}C results (lower plot) are highly viscous, as their viscosity results showed (Figure 4.10). Which means their observed gain in recovery might totally due to their stiff nature, since PB is not elastomeric polymer. Strain sustained by the less viscous blends is much higher. This viscous blends regained larger proportion of the relatively lesser strain they underwent. Most of the RHDPE-PB blends fall between extremely-heavy and very-heavy traffic category for environment with 70^{o}C upper PG, and between very-heavy and heavy traffic for environment with upper PG below 76^{o}C.

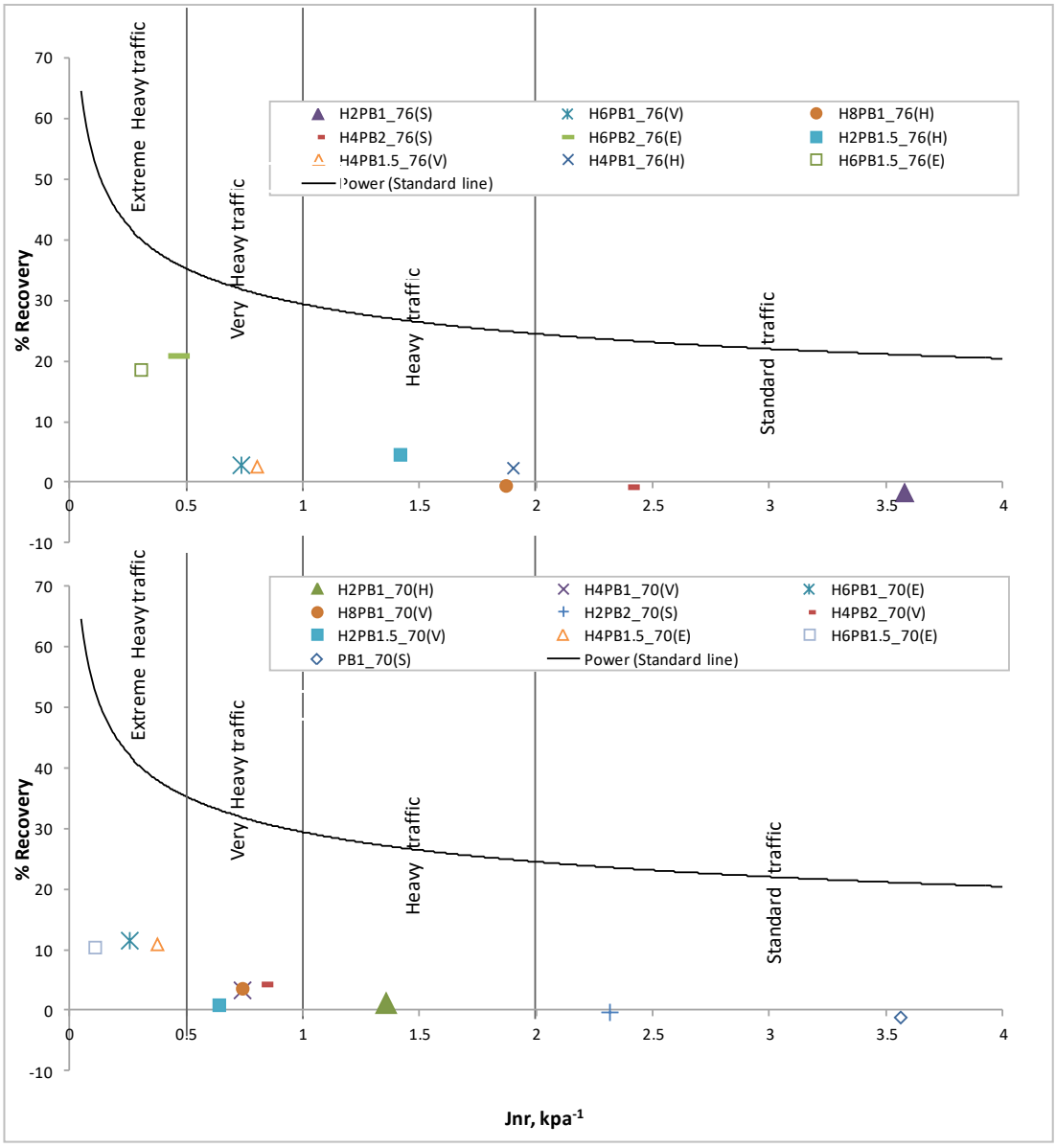

Figure 4.30: TP-70 Plots of RHDPE-PB modified asphalt binders.

4.3.4.5 Elastic Recovery and Jnr of RHDPE-SBS modified asphalt binders

The recovery versus non-recoverable creep compliance (J_{nr}) plot of RHDPE-SBS asphalt binders is shown by Figure 4.31. As anticipated, SBS has a positive impact on both the recovery and the J_{nr} characteristics of the RHDPE modified asphalt binder. It can

be observed that the SBS impact on recovery is more significant on the environment with upper PG below 70^{o}C. The possibility of utilizing the cheaper RHDPE as substitute of some portion of virgin elastomeric SBS to achieve a modified binder with satisfactory level of recovery is possible. Most the RHDPE blends containing certain proportion of SBS exhibited recovery equivalent to, or higher than asphalt binder containing same amount of SBS alone. For example, compare S1_70(H) with H2S1_70(H) and S2_70(V) with H4S1.5_70(V), H2S2_70(E) and H4S2_70(E). The RHPDE modified binders are highly viscous, as shown by their viscosity results (Figure 4.10). This made them relatively stiff as well. The added stiffness them less strain sensitive. When this property is combined with the recovering ability of the added SBS microstructure within that of the existing RHDPE, a hybrid microstructure with higher strain recovering ability than the asphalt blend containing same amount of SBS-only is produced.

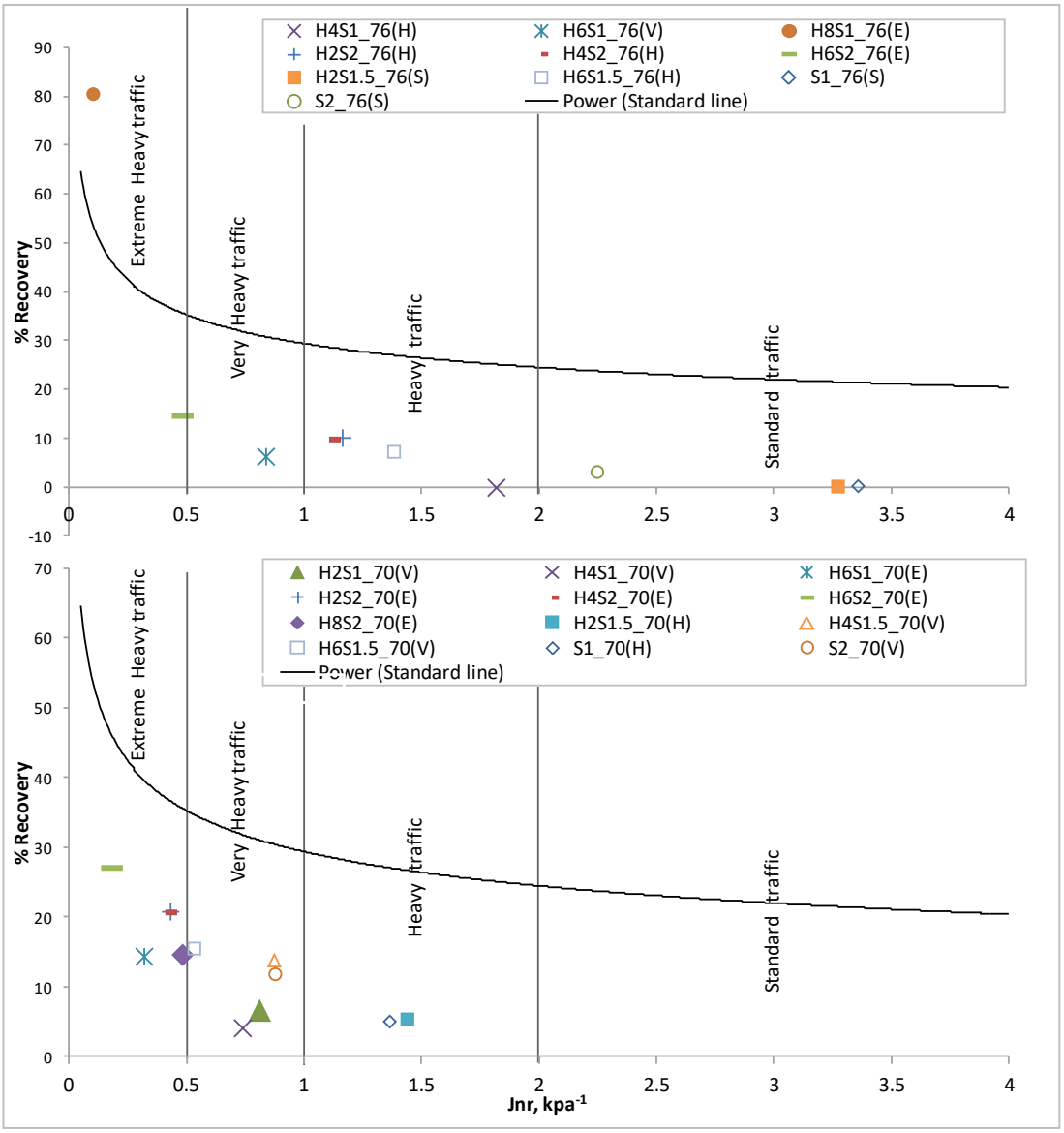

Figure 4.31: TP-70 Plots of RHDPE-SBS modified asphalt binders.

4.3.4.5 Elastic Recovery and Jnr of RPP-PB and RPP-SBS modified asphalt binders

The conclusion drawn regarding RLDPE and RHDPE on the possibility of minimizing amount of elastomeric polymer could not supported for RPP. The RPP-SBS plot in Figure 4.33 for environments with 70°C and 76°C seven days maximum pavement

temperature show J_{nr} and some recovery improvement due to the SBS presence. But no consistent trend could be observed. This might be attributed to the unstable nature of the RPP as will be seen in the storage stability section. The RPP-PB modified asphalt results shown in Figure 4.32 are even more inconsistent than the RPP-SBS results.

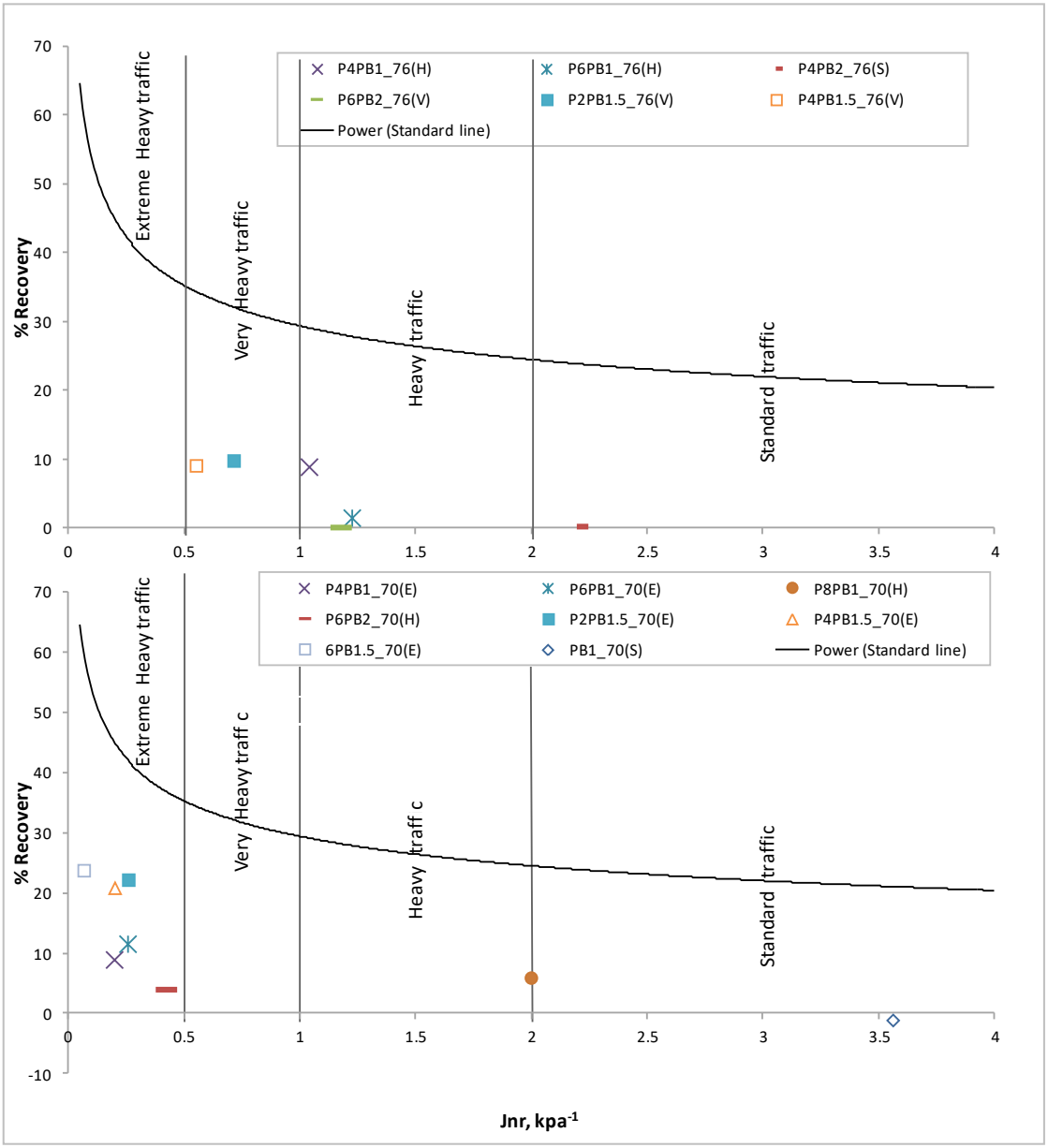

Figure 4.32: TP-70 Plots of RPP-PB modified asphalt binders.

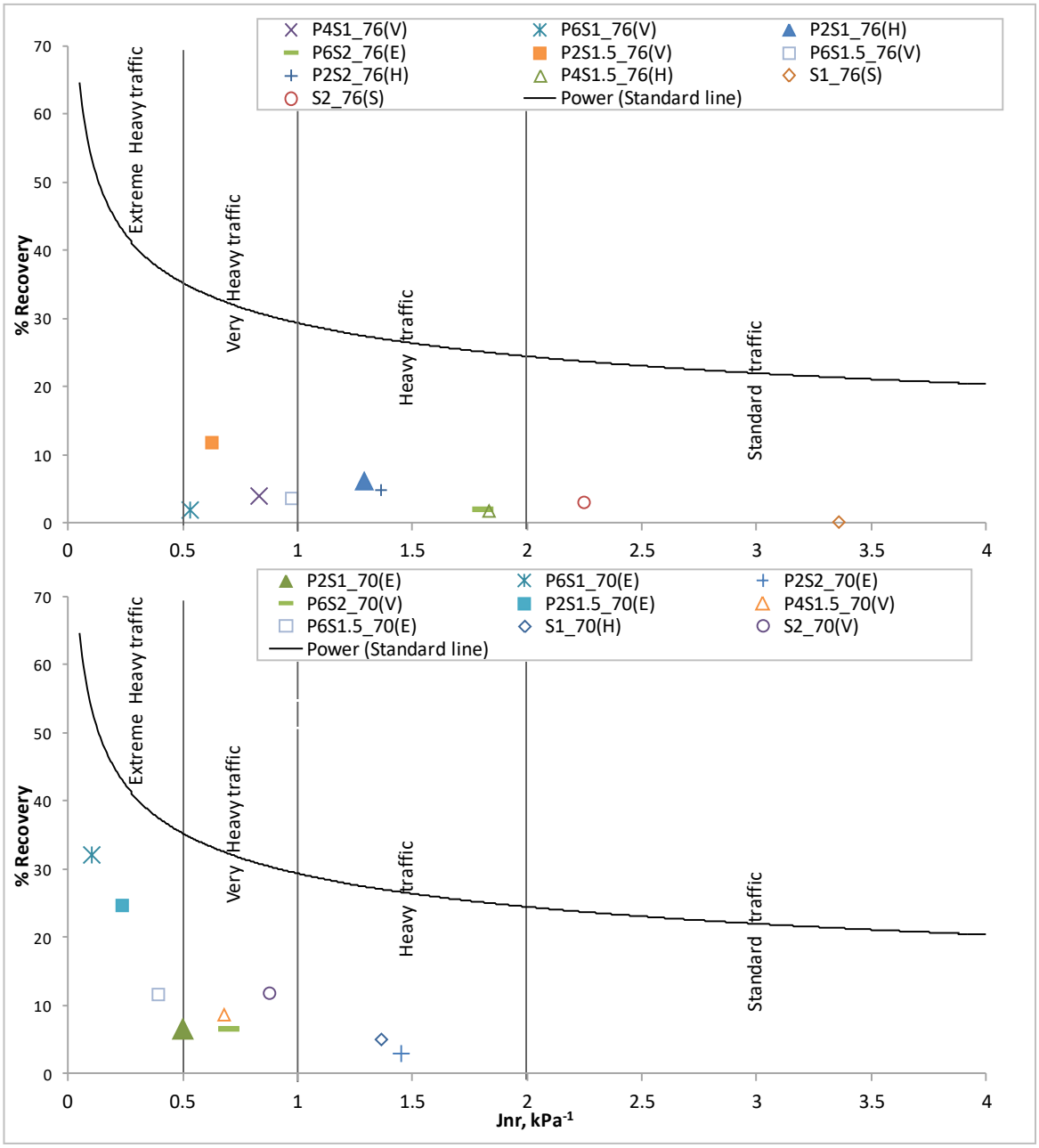

Figure 4.33: TP-70 Plots of RPP-SBS modified asphalt binders.

4.4 STORAGE STABILITY OF RPW MODIFIED ASPHALT

Table 4.4 shows the LAST phase angle separation ration (SR(δ)) at 0 hour, for the various categories of the RPWs modified asphalt binders. All the tested blends were found to be stable with respect to SR(δ) just after finishing the blending process. This should not come as a surprise, because the modified binder at this hour is more likely to show stable behavior. This is due to the fact that the resulting blends are just released from high shearing and constant agitation. The high agitation helps maintain an excellent RPWs and polymer homogeneity within the asphalt blends. Hence the top and bottom extracted sample exhibits almost the same phase angles at this hour.

Table 4.4: Complex Modulus and Phase Angle Separation Ratio at 0 hour, 75^{o}C.

Blend	G* (Pa)		δ (^{o}C)		Separation Ratio (SR)		Lower Limit	Upper Limit
	Top	Bottom	Top	Bottom	SR(G*)	SR(δ)		
L4_70(H)	6593	6762	78.91	78.52	0.97	1.00	0.8	1.2
L2S2_70(H)	1151	1140	68.9	68.71	1.01	1.00	0.8	1.2
H2_70(H)	3151	2905	64.91	65.73	1.08	0.99	0.8	1.2
H2PB1_70(S)	1540	1527	70.22	70.02	1.01	1.00	0.8	1.2
H2S1_70(H)	6171	6494	76.38	76.4	0.95	1.00	0.8	1.2
P2_70(H)	10166	6899	64.97	78.33	**1.47**	0.83	0.8	1.2
P2PB1_70(H)	2582	2530	80.59	80.51	1.02	1.00	0.8	1.2
P2S1_70(H)	3851	3742	79.17	79.52	1.03	1.00	0.8	1.2
L6_76(H)	6548	7437	77.21	78.93	0.88	0.98	0.8	1.2
L4S1.5_76(H)	1319	1242	69.78	67.09	1.06	1.04	0.8	1.2
L6B1_76(H)	3471	3299	79.66	79.14	1.05	1.01	0.8	1.2
H4_76(H)	4553	4246	78.13	78.91	1.07	0.99	0.8	1.2
H2B1.5_76(H)	2745	2856	80.18	79.86	0.96	1.00	0.8	1.2
H4S1_76(H)	4458	4236	77.93	78.84	1.05	0.99	0.8	1.2
P4_76(H)	9082	3480	67.02	78.01	**2.61**	0.86	0.8	1.2
P4B2_76(H)	3177	2960	77.3	79.03	1.07	0.98	0.8	1.2

The LAST complex modulus separation ratio (SR(G*)) marked two RPWs modified asphalt binder (P2_70(H) and P4_76(H)) with separation potential, as shown in Table 4.4. The data points of the SR(G*) plot are more scattered when compared to the SR(δ) data. This is an indication of how SR(G*) is more sensitive to separation tendency of polymer modified binders than the SR(δ), as both samples and data were extracted and obtained at the same time. Only the PP-only containing modified asphalt binders showed separation tendency just after the blends were prepared. This shows a compatibility issue between the asphalt binder and the RPP. It can be concluded that the top extracted sample is stiffer than the bottom extracted one, since the outlier data points falls above the upper limit. Which means the RPP in the asphalt binder moves upward to the surface as it is separating. The upward movement should be anticipated as the specific gravity of polypropylene ranges just below that of typical asphalt binder. Another thing worth noting is how displaced the outlier points are from the limit line. We can conclude that at this hour, the separation tendency of the RPP modified asphalt increases with more RPP content. Or, that the higher the RPP modified asphalt UPGT, the more likely it is to separate. And Since RPP modified asphalt containing either PB or SBS did not show similar trend as those containing RPP only, it can be concluded that the addition of either PB or SBS help minimize the possibility of early separation when utilizing RPP.

Table 4.5 shows the LAST phase angle separation ratio (SR(δ)) at after 48hrs under mild agitation. As observed from SR(δ) at 0 hour, almost all the blends showed significant amount of stability. Except the L2S2_70(H) that is just below the upper limit boundary, but still within the stable zone. When comparison compared to the SR(δ) results at 0 hour, where data point displacement from the centre mark (1) is higher, the

degree of stability happens to increase at this hour. But as previously observed, the SR(δ) is not the critical stability indicator. There is relatively small difference in phase angle as compared to complex modulus between top and bottom extracted samples.

Table 4.5: Complex Modulus and Phase Angle Separation Ratio at 48 hours, 75°C.

Blends	G* (Pa)		δ (°C)		Separation Ratio (SR)		Lower Limit	Upper Limit
	Top	Bottom	Top	Bottom	SR(G*)	SR(δ)		
L4_70(H)	6951	7449	73.89	72.74	0.93	1.02	0.8	1.2
L2S2_70(H)	998	911	63.74	53.52	1.10	1.19	0.8	1.2
H2_70(H)	2913	2904	58.78	59.41	1.00	0.99	0.8	1.2
H2PB1_70(S)	1491	1528	65.63	65.26	0.98	1.01	0.8	1.2
H2S1_70(H)	6920	6967	73.94	74.27	0.99	1.00	0.8	1.2
P2_70(H)	7551	7650	72.8	72.65	0.99	1.00	0.8	1.2
P2PB1_70(H)	3846	3800	76.67	76.51	1.01	1.00	0.8	1.2
P2S1_70(H)	5312	5429	72.32	72.43	0.98	1.00	0.8	1.2
L6_76(H)	7066	7084	74.89	79.72	1.00	0.94	0.8	1.2
L4S1.5_76(H)	1503	1404	68.38	68.43	1.07	1.00	0.8	1.2
L6B1_76(H)	3730	3855	78.25	78.79	0.97	0.99	0.8	1.2
H4_76(H)	5301	4806	76.90	79.38	1.10	0.97	0.8	1.2
H2B1.5_76(H)	3224	3180	78.76	78.13	1.01	1.01	0.8	1.2
H4S1_76(H)	4877	4462	76.55	77.13	1.09	0.99	0.8	1.2
P4_76(H)	12242	13173	61.66	61.81	0.93	1.00	0.8	1.2
P4B2_76(H)	4523	4992	76.22	75.96	0.91	1.00	0.8	1.2

The 48 hour LAST complex modulus separation ratio (SR(G*)) is also presented in Table 4.5. All categories of the RPWs modified asphalt blends' SR(G*) fall within the stable zone. This indicate promising stability trait. This includes those blends that previously showed separation tendencies at 0 hour. There is no controversy from the above observed results. But there is a strong indication of rheological changes that occur after 48hrs within the RPP modified binders. Moreover, what has been observed does not necessarily means that the blends are definitely stable. Since the SR captures only the

blends homogeneity by the relative comparison of the top and bottom extracted samples properties at a one time. It does not link the current (48 hrs) observed results with the previous (0 hr) results. The degradation ratio (DR) will help supplement the previous observation so as to reach a conclusive finding.

As previously observed from SR(δ) results, the phase angle separation ratio SR(δ) was not successful in sufficiently capturing instability (degradation) trait by the blends. Table 4.6 presents the DR(δ) results at 48 hours. All blends appeared to be non-degradable, which is not necessarily so, as the DR(δ) cannot be taken as the critical degradation indicator.

Table 4.6: Complex Modulus and Phase Angle Degradation Ratio.

Blends	**Degradation Ratio (DR)**				**SEPARATION STATUS**	**DEGRADATION STATUS**
	DR(G*)	DR(δ)	Lower Limit	Upper Limit		
L4_70(H)	1.08	0.93	0.8	1.2	STABLE	STABLE
L2S2_70(H)	0.83	0.85	0.8	1.2	STABLE	STABLE
H2_70(H)	0.96	0.90	0.8	1.2	STABLE	STABLE
H2PB1_70(S)	0.98	0.93	0.8	1.2	STABLE	STABLE
H2S1_70(H)	1.10	0.97	0.8	1.2	STABLE	STABLE
P2_70(H)	0.89	1.02	0.8	1.2	STABLE	STABLE
P2PB1_70(H)	**1.50**	0.95	0.8	1.2	STABLE	Degrading
P2S1_70(H)	**1.41**	0.91	0.8	1.2	STABLE	Degrading
L6_76(H)	1.01	0.99	0.8	1.2	STABLE	STABLE
L4S1.5_76(H)	1.14	1.00	0.8	1.2	STABLE	STABLE
L6B1_76(H)	1.12	0.99	0.8	1.2	STABLE	STABLE
H4_76(H)	1.15	1.00	0.8	1.2	STABLE	STABLE
H2B1.5_76(H)	1.14	0.98	0.8	1.2	STABLE	STABLE
H4S1_76(H)	1.07	0.98	0.8	1.2	STABLE	STABLE
P4_76(H)	**2.02**	0.85	0.8	1.2	UNSTABLE	Degrading
P4B2_76(H)	**1.55**	0.97	0.8	1.2	STABLE	Degrading

Table 4.6 also presents the complex modulus degradation ratio (DR(G*)) at 48 hours. As can be observed, not all the RPWs modified asphalt binders' DR(G*) fall within the acceptable degradation zone. Four blends (P2PB1_70(H), P2S1_70(H), P4_76(H), and P4PB2_76(H)) were found to show potential degradation trait with time during storage. As in the case of separation, the more the RPP content the higher degradation tendency. The higher the RPP content the further away the DR(G*) seemed from the upper acceptable limits (1.2). Micro-structural reorganization and possible time hardening due to continuous agitation is what could have led to the significant difference in the visco-elastic property between the sample extracted just after blending and those after 48 hours of mild agitation. Because none of the affected blends showed significant difference between top and bottom samples' visco-elastic properties at 48th hour. They have all passed the separation criteria. The early separation attribute of RPP modified asphalt binder is only seen on P2_70(H) and P4_76(H) SR(G*) plot at 0 hour (Table 4.4). However, RPP asphalt blends containing either SBS or PB did not show this behavior. The presence of extra SBS or PB micro-structural network within the RPP blend tend to slow the rate at which the RPP micro-structure reorganizes to move towards the asphalt surface. The only blend that failed to meet the separation criteria at 0 hour, but has met the degradation requirement is P2_70(H).

Hence, we can conclude that P2PB1_70(H), P2S1_70(H), P4_76(H), and P4PB2_76(H) are unstable due to their degrading tendency with time. P2_70(H) is only stable under mild agitation. RPP content above 2% will lead to an unstable modified asphalt binder. Addition of an elastomeric SBS and Plastomeric PB minimize the early separation of RPP

modified asphalt binder, but does not necessarily mean they are stable. As they have shown a potential degrading tendency with time. RHDPE and RLDPE modified asphalt binders (for RHDPE content below 4% and RLDPE content below 6%) whether containing either SBS or PB have shown good storage stability trait under mild agitation, both in terms of time degradation and separation.

4.5 COMPOSITION OF RPW IN THE RPW-ASPHALT CONCRETE

The bulk combination of the plastic wastes was employed for the AC aggregate substitution due to economic and practical reasons. Huge amount of the RPW is required for aggregate replacement in AC, and the cost associated with sorting the RPW into their categories is high and impractical. Besides, unlike in the case of asphalt binder modification, all the RPW are eligible for use as aggregate replacement. The summary of the pilot survey results of household waste on the various composition of the combined RPW is shown in Table 4.7. The combined RPW waste from households in Thuqba and Doha, Dhahran KSA was estimated to approximately consist of 33.7% PET, 25% HDPE, 3.8% PVC, 17.1% LDPE, 11.6% PP and 8.8% PS. The sample size required for a much reliable proportion estimate at 5 and 10% level of statistical significance was calculated from this survey. This can be observed that more sampling is required for a reliable data. However, since what was needed for this research is just an estimate, this results will suffice. The upper and lower confidence bound (UCB and LCB) for these estimated proportions is also estimated. Typical image of the combined RPW for AC modification via aggregate substitution is shown in Figure 4.34.

Table 4.7: Summary Results of Pilot Survey for RPW Composition.

Label	1	2	3	4	5	6	Sub-Total
Name	**PET**	**HDPE**	**PVC**	**LDPE**	**PP**	**PS**	
Sample 1	34.5	44.5	0.0	14.5	7.5	2.5	103.5
Sample 2	43.0	22.0	0.0	10.5	5.0	0.0	80.5
Sample 3	23.5	0.0	0.0	12.5	16.5	12.5	65.0
Sample 4	35.0	35.0	0.0	20.0	0.0	8.0	98.0
**	**	**	**	**	**	**	**
**	**	**	**	**	**	**	**
Sample 50	22.0	0.0	0.0	15.0	12.5	2.0	51.5
Sample 51	38.0	0.0	0.0	12.5	28.0	0.0	78.5
Sample 52	0.0	34.5	0.0	12.5	0.0	8.0	55.0
Sample 53	8.0	0.0	0.0	15.0	0.0	15.0	38.0
Sub-Total	1384.0	1028.0	155.0	702.0	477.5	360.0	4106.5
% Proportion	33.7	25.0	3.8	17.1	11.6	8.8	100.0
UCB	46.4	36.7	8.9	27.2	20.3	16.4	
LCB	21.0	13.4	0.0	7.0	3.0	1.2	
Required Sample size (5% SL)	390	288	59	216	150	112	
Required Sample size (10% SL)	275	203	42	152	106	79	
UCB: Upper Confidence Bound; LCB: Lower Confidence Bound; SL : Significance Level							

Figure 4.34: Image of Combined RPW aggregate substitute.

4.6 SUPERPAVE MIX DESIGN RESULTS OF RPW-ASPHALT CONCRETE MIX

4.6.1 Compaction and Mixing Temperature

The relationship between the RPW asphalt binder viscosities and temperature was established and presented in Figure 4.35. The recommended mixing and compaction asphalt viscosity ranges are 0.17 ± 0.02 and 0.28 ± 0.03 Pas, respectively. The mixing and compaction temperature for the various RPW asphalt binders were obtained within this range from the viscosity-temperature plots shown in Figure 4.35. The flow activation energy 'E' of the RPW-binders, a measure of required compaction effort related to the viscosity of the binder was obtained from Arrhenius equation (42) and presented in the Table 4.8. It can be observed that the flow activation energy of the various RPW-asphalt are not far from that of the crumb rubber binder. The H4 and P2S1.5 binders showed the highest required compaction energy when compared to the rest of the binders at the temperature. It can be concluded that all the RPW asphalt binder mixtures, with the exception of H2B1.5, will require a slightly higher compaction effort than the crumb rubber mix at the same temperature.

$$\ln \eta = \frac{\mathrm{E}}{\mathrm{R}}\left(\frac{1}{\mathrm{T}}\right) + \mathrm{A} \qquad (4.1)$$

Where: η: viscosity (Pa.s), T: Temperature (^{o}K), E: flow activation energy, $R = 8.314\ \mathrm{J.mol^{-1}K^{-1}}$ and A is the plot intercept.

Table 4.8: Flow Activation Energy of the RPW Binder.

Asphalt	E/R (mol.K)	E (kJ/mol)
L6_76(H)	3733.057	31.04
L4S1.5_76(H)	3757.454	31.24
L6B1_76(H)	3698.489	30.75
H4_76(H)	3997.77	33.24
H2B1.5_76(H)	3392.98	28.21
P2S1.5_76(H)	4034.27	33.54
CRB_76	3643.38	30.29

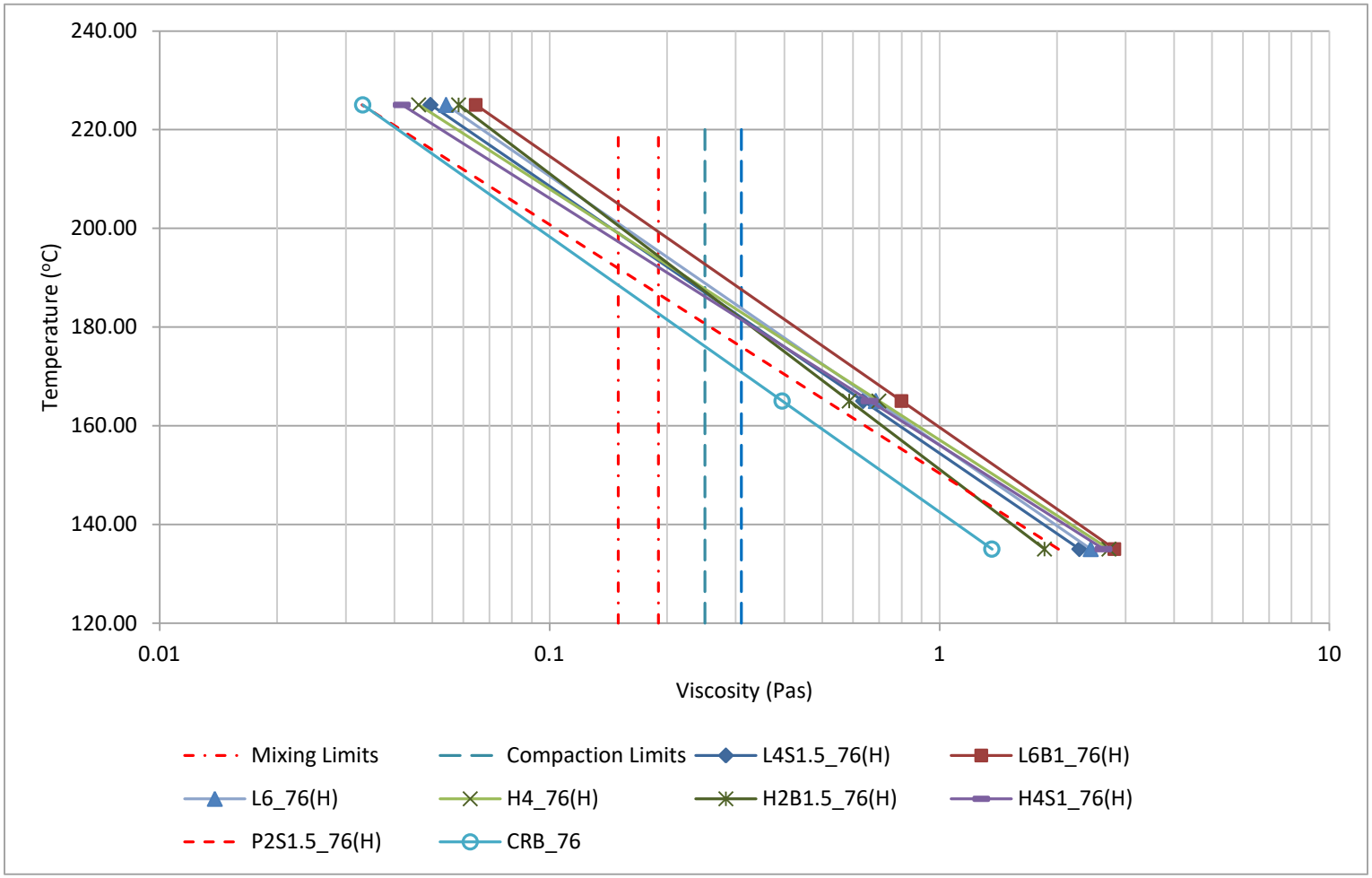

Figure 4.35: Compaction and Mixing Temperature Ranges For RPW AC.

4.6.2 Mix Design Summary and RPW-AC Mixtures Parameters

Table 4.9 present the selection of aggregate gradation results for L6_76(H). The criteria are air void, void in mineral aggregate (VMA), void filled with asphalt (VFA), level of compaction relative to the maximum theoretical density (%G_{mm}) at three stages of the pavement life, namely N_{design}, $N_{initial}$ and $N_{max.}$ Three trial gradations G1, G2, and G3 (Table 3.6) were checked, and G1 happened to be the best option based on the design criteria. G1 yielded a mix with air void, VFA, VMA and level of compaction much closer to the target criteria than both G2 and G3. The G1 gradation was selected for the optimum asphalt binder content determination phase. Similar approach was employed for the remaining AC mixtures.

Due to the unstable nature of the RPP modified binder, only the P2S1.5 binder was selected for AC mix design phase, just for reference purpose. The summary of the superpave mix design of the RPW asphalt concretes was presented in Table 4.10. All the important volumetric properties of the mixtures such as the VMA, VFA, optimum asphalt content and selected gradation, percent maximum theoretical density (G_{mm}) at N_{design}, $N_{initial}$ and N_{max}, in addition to the mixing and compaction temperature for each mix were outlined. The moisture durability test result for the mixtures is shown in Figure 4.36. All the RPW modified asphalt mixture met the minimum retained strength index (RSI) of 80%, with the L6_(76) mix retaining almost all its indirect tensile strength.

Table 4.9: Sample Gradation Selection Results for L6_76(H).

Design Criteria	*G1*	*G2*	*G3*	Target Criteria
%G_{mm}(N-Initial)	86.7	83.7	90.4	< 89 %
%G_{mm}(N-Design)	95.2	91.3	97.4	= 96 %
%G_{mm}(N-Maximum)	97.6	94.1	95.8	< 98 %
%Air Voids(N-Design)	4.8	8.7	2.6	= 4 %
%VMA(N-Design)	19.00	19.08	15.81	≥ 15
%VFA(N-Design)	68.81	54.18	83.65	65 % - 75 %
Dust Proportion	0.88	0.75	2.08	(0.6 to 1.2) %
Selected Gradation	√			

Table 4.10: Superpave Mix Design Results Summary.

tl ahps e pyTBrdnlB	n cata drG	**Optimum Asphalt Content (%)**	**AM**	**AF**	**mGG%**			**Mixing Temp. (^{o}C)**	**Compaction Temp. (^{o}C)**
					ipyp	**iTBt**	**i GhN**		
Fresh	G1	0.80	02.01	29.71	82.21	57.11	58.80	160	135
L6_76(H)	G1	9.07	02.71	29.88	82.81	57.11	58.00	200	190
L4S1.5_76(H)	G1	9.78	07.55	27.21	82.87	57.11	52.70	195	185
L6B1_76(H)	G1	9.71	07.57	20.58	88.99	57.11	52.87	200	190
H4_76(H)	G2	9.21	08.99	29.78	88.98	57.11	52.59	195	185
H4S1_76(H)	G2	9.71	07.07	20.20	88.07	57.11	58.07	195	185
P2S1.5_(76)	G1	9.07	17.78	28.87	88.17	57.11	58.71	190	175
CRB_(76)	G1	9.00	17.31	20.07	**	**	**	185	175

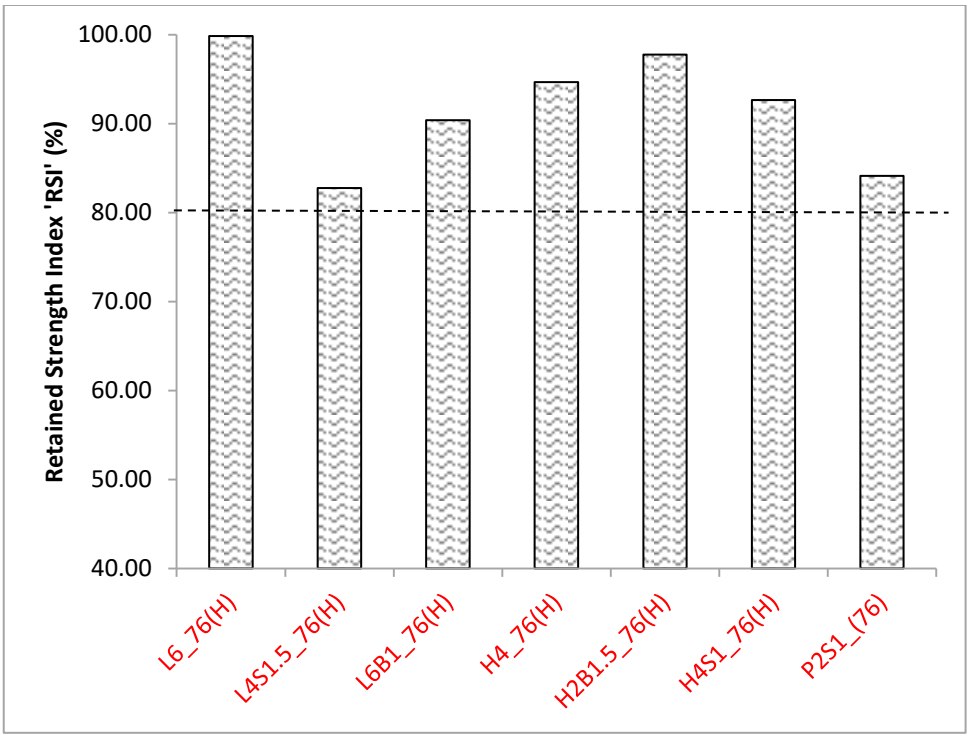

Figure 4.36: Moisture Sensitivity Results of the RPW Modified Asphalt Binders.

4.6.3 Optimum Size and Quantity of RPW for Aggregate Substitution

The RPW size range for aggregate substitution was selected based on the resilient modulus, indirect tensile strength, and moisture sensitivity of the AC. Two size ranges S1 (No. 8 to No. 10) and S2 (No. 8 to No. 40) were compared. Based on the neat AC gradation size range, only 10% of the aggregate is replaceable by S1, and as high as 20% of the aggregate can be replaced by S2. Hence AC mix with 5 and 10% of S1 RPW, 10 and 20% S2 RPW as aggregate were prepared. The prospect of having the opportunity to incorporate larger volume of the S2 RPW into the AC is an initial advantage of S2 over S1. But this is not a strong deciding criteria for the final selection. From Figure 4.37, It is obvious that the RPW generally resulted in lower RM value. But AC containing S2 RPW is the most negatively affected in terms of RM (S2-10% vs. S1-10%). However, the rate

of decline in RM for S1 containing AC is higher. This can be observed if the drop in RM from 10 to 20% increment in S2 RPW content is compared to that observed for 5 to 10% increase in S1 RPW content. No conclusive decision could be deduced from the ITS results, apart from the fact that for the same amount of RPW content, the S1 yielded AC with a slightly higher ITS than S2. But looking at the most vital test result, which is the moisture durability test shown in Figure 4.38, the S2 RPW holds better promise of an excellent AC mix. AC containing up to 10% S1 RPW cannot even meet the minimum moisture resistance requirement of 80% RSI. The S1 RPW lacks smaller RPW sizes with higher surface area. These small size RPW are present in S2 RPW, they facilitates aggregate-RPW bond formation that enhance resistance to moisture effect of AC. Based on these observations, the S2 (No. 8 to No. 40) RPW was selected as the preferred RPW size range to be adopted for all the RPW AC modification via aggregate substitution.

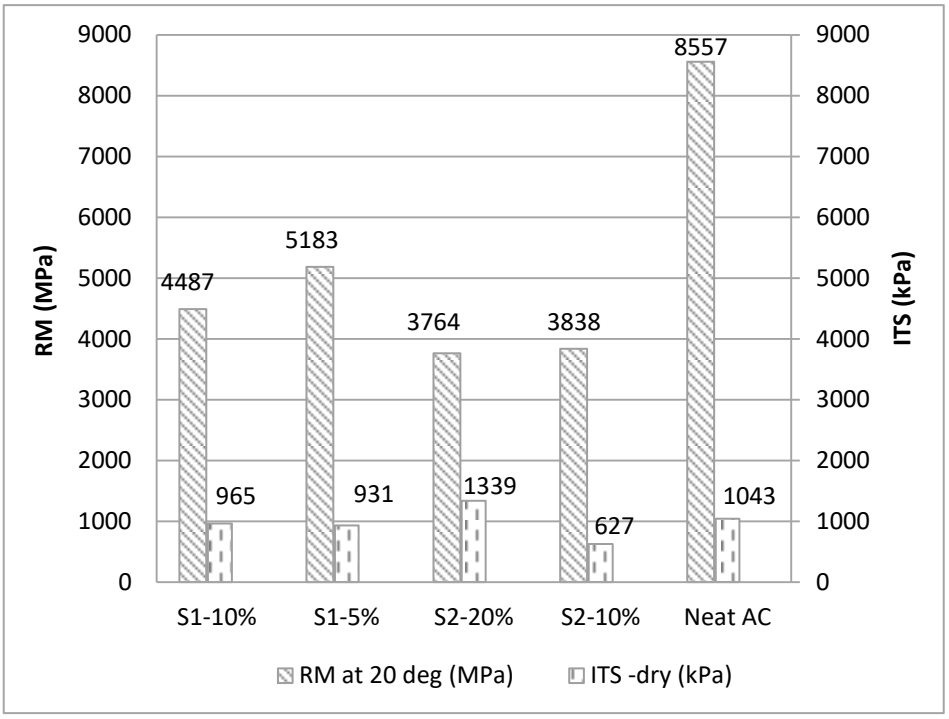

Figure 4.37: RPW Size Range For aggregate Substitution Results Plots.

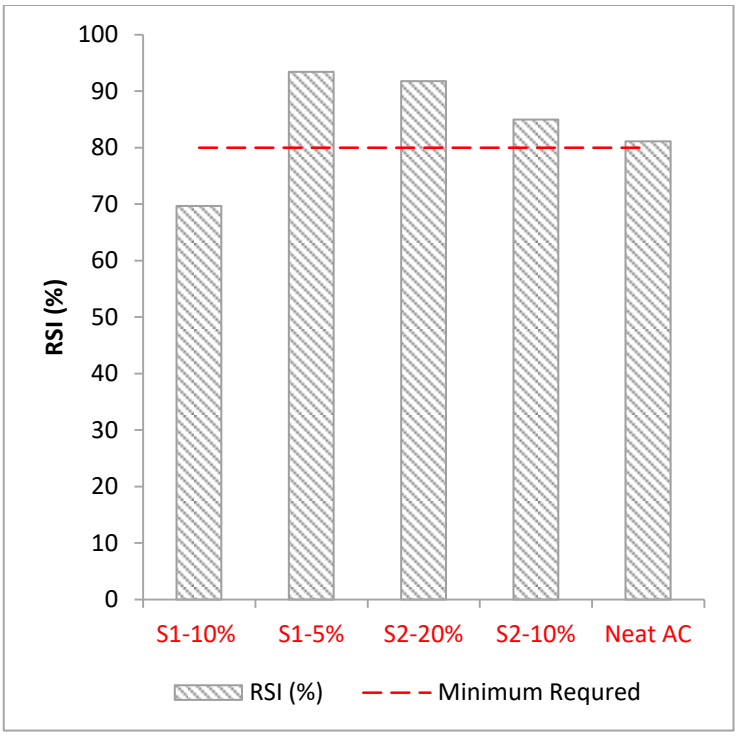

Figure 4.38: Retained Strength Index for RPW-aggregate Mixtures (S1 and S2).

Based on the previous observed trend of RPW content effect on the RM, ITS and RSI of the AC, a much reliable test parameter, capable of clearly showing an optimum RPW content is required. Since the RPW resulted in more plastic behavior with higher content, the flow number test was selected for the RPW content optimization. Figure 4.39 shows the RPW content optimization results. In addition to the control mix, three AC mix containing different levels of RPW content (5, 10 and 20%) were prepared and subjected to repeated dynamic load flow test. It can be clearly observed that the FN increases with increase in RPW at lower content. At higher dosage of the RPW, the FN then begin to decline, specifically after 9.5% RPW content. At RPW content below 9.5%, most of the added RPW goes in to fill the existing VMA of the AC, hence enhancing the asphalt binder resistance to permanent deformation. The overall AC structure is mostly stone-on-stone with RPW and asphalt binder filling the VMA. This resulted to an overall increased

resistance to permanent deformation of the AC, corresponding to higher FN value. However, as the RPW content keep increasing, the VMA is completely filled. This forces the excess RPW to create space between the larger aggregates, resulting in mostly stone-on-RPW AC structure. Hence the reduced resistance to permanent deformation. The strain at flow plot shows the highest strain sustained by the RPW-AC to correspond to 5% RPW content. After which the strain continuously decline with more RPW content. No significant decline in sustained strain was observed beyond 9.5% RPW content, and the lesser sustained strain recorded for 20% RPW was actually due to the fact that the 20% RPW containing AC could not last as long as the 10% RPW containing AC before flowing. This further confirm the superiority of the AC containing 9.5% RPW in terms of resistance to rutting. Finally, we can conclude that the optimum RPW content is observed to be **9.5%**.

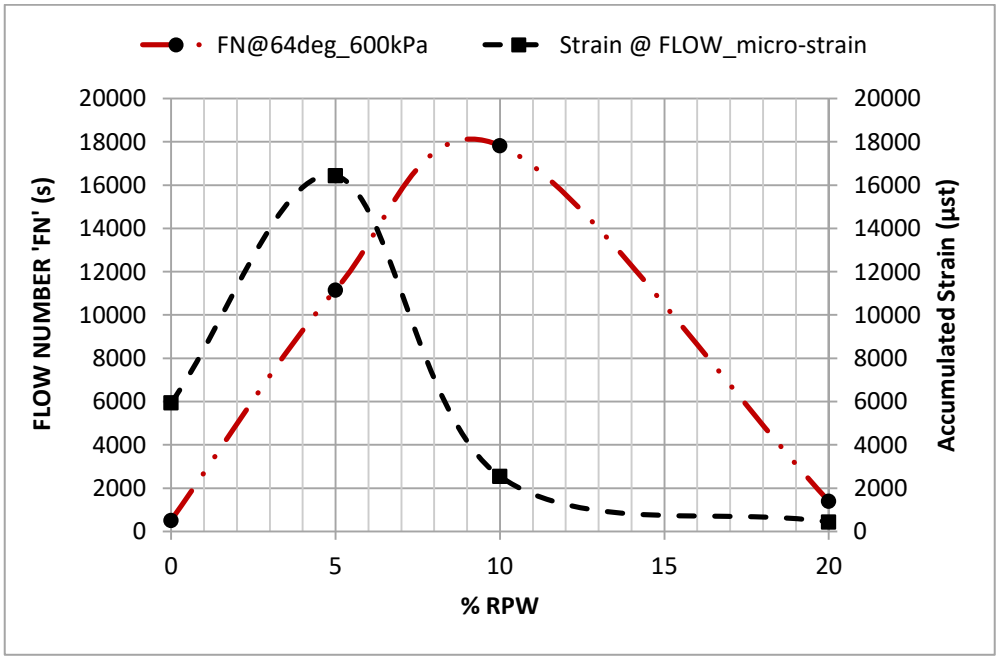

Figure 4.39: Optimum RPW Content for Aggregate Substitution.

4.7 RPW-AC AND HYBRID-RPW AC PROPERTIES AND PERFORMANCE

The following subheadings will present the mechanistic and performance properties of the RPW-ACs and hybrid-RPW-ACs. The RPW-ACs are those ACs obtained by modifying the asphalt binder alone using the RPW, while the hybrid-RPW-AC is an AC obtained by substituting some proportion of the RPW-AC mineral aggregate with RPW aggregates.

4.7.1 Resilient Modulus and Indirect Tensile Strength of RPW-Asphalt Concrete

The resilient modulus (RM) of an AC is the measure of it elastic response to dynamic load, while the indirect tensile strength (ITS) measure the diametrical splitting strength of the AC. Figure 4.40 shows the RM and the ITS of the RPW-modified asphalt binder mixture. The ITS was obtained during the moisture sensitivity test of the various mixtures. The various AC mixtures showed little variation in their ITS. Even though the RM is not a performance parameter, and there are so many concern on its reliability, some are still using it as a design parameter. P2S1.5_(76) and L6_(76) showed the highest RM, while H4_(76) exhibits the lowest RM. Since the PG of these binders is the same, and the last two binders are purely made from plastomeric polymer, the difference in RM can better be understood by studying the mixtures aggregates gradation. Both P2S1.5_(76) and L6_(76) mixtures have gradation (G1) aggregate structure, while H4_(76) has a G2 structure. The mix design is purely based on the volumetric properties, and thus

gradations suitable for different binders could have different effect on the RM of these mixtures.

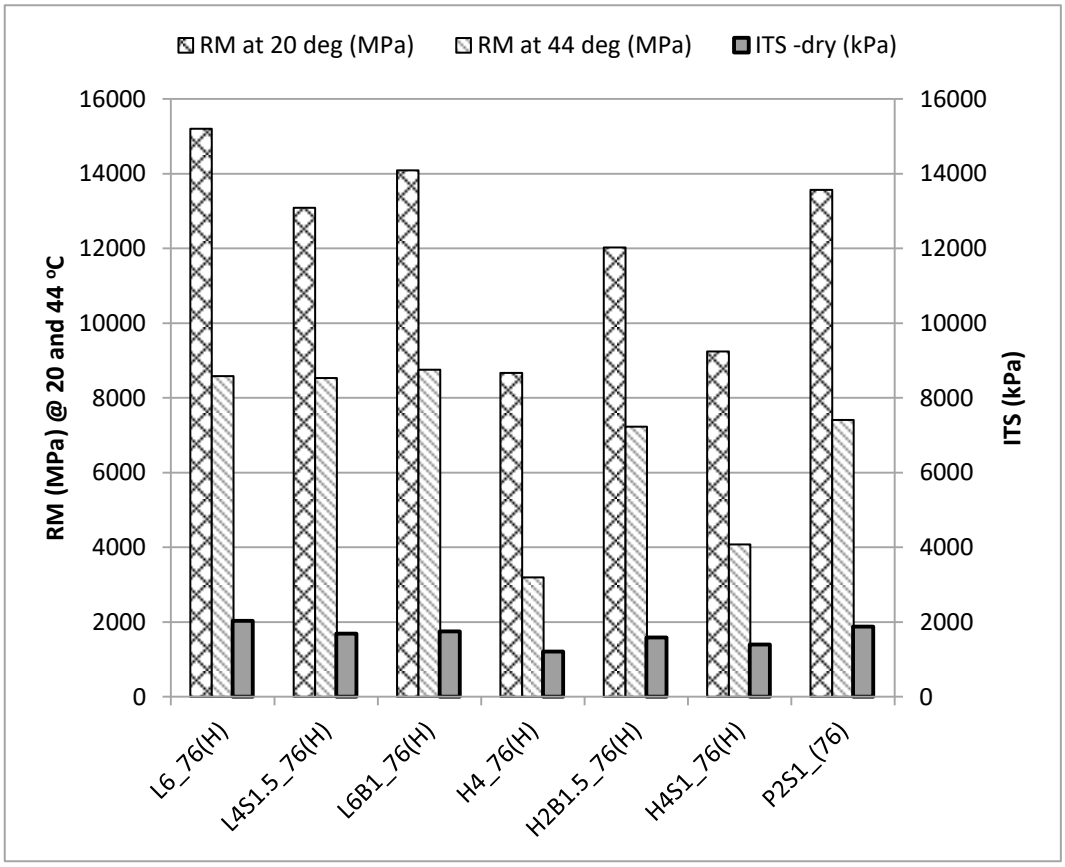

Figure 4.40: Resilient Modulus of RPW-Asphalt Concrete.

4.7.2 Dynamic Modulus of RPW-Asphalt Concrete

The dynamic modulus variation of the various AC mixtures with temperature and at different loading frequencies were presented and analyzed under this subheading. Figure 4.41 presents dynamic modulus for ACs containing 5, 10 and 20% RPW aggregate, along with that of ACs containing 5 and 10% RPET-only aggregate, at 10 HZ.

The reason for comparing these RPW aggregate containing ACs with those containing, RPET-only aggregate is: several previous research on asphalt concrete modification via aggregate substitution focused on isolated RPET as aggregate substitute. It can first of all be observed that the AC mix containing 10% RPW demonstrated the highest dynamic modulus. This is a further confirmation of the optimum RPW content from previous results. It is also clear that the RPW containing ACs (5 and 20%) possessed higher dynamic modulus at higher temperature and lower dynamic modulus at lower temperature than the Fresh mix. This trait is an indication of better fatigue and rutting performance of the AC with RPW aggregate when compared with the fresh ACs. The RPET aggregate ACs were the least in terms of dynamic modulus at all temperature level.

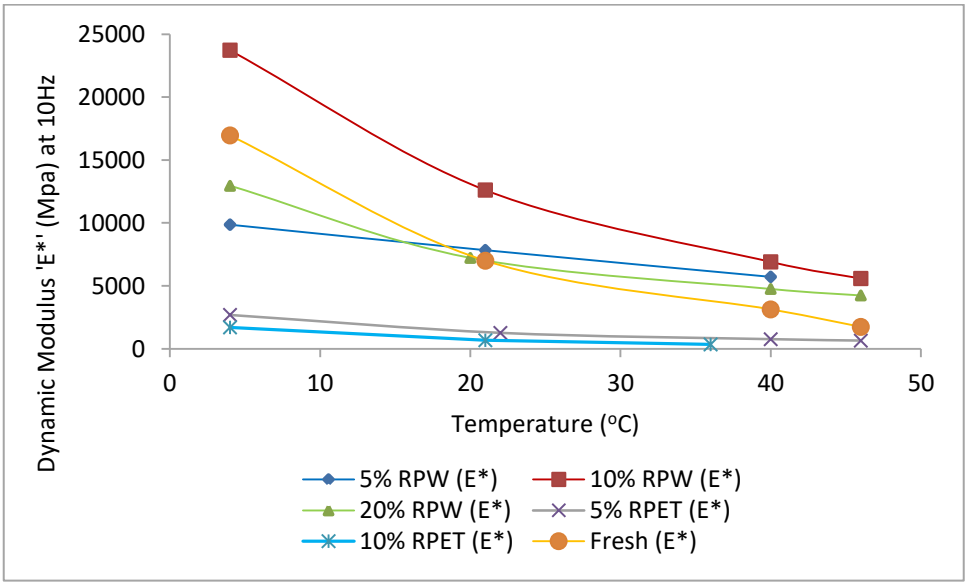

Figure 4.41: Dynamic Modulus of RPW-aggregate-AC and RPET-only-AC at 10 Hz.

Figure 4.42 shows the dynamic modulus of RPW-aggregate-ac constant temperature plots at 10Hz. The optimum RPW content can be clearly identified from this graphs. The results point at approximately 10% RPW content as the optimum, once again.

The relative gap in dynamic modulus of the RPW-aggregate ACs due to RPW content become more pronounced as the temperature increases.

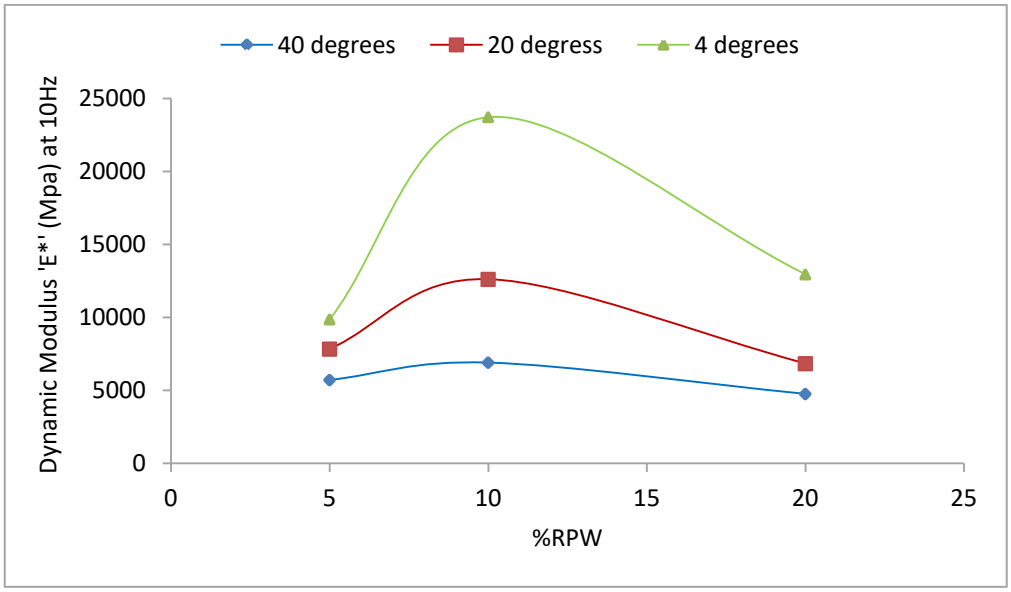

Figure 4.42: Dynamic Modulus of RPW-aggregate-AC Constant Temperature Plot (at 10Hz).

Figure 4.43 shows the corresponding phase angle of the AC mixture previous presented in Figure 4.41. The phase angle results reflects the exactly the trend previous observed, with only a slight difference. The 20% RPW AC compete more closely with the 10% RPW AC in terms of elasticity at higher temperature. The fact is that even though the former possessed a relatively lower dynamic modulus, it contains higher RPW aggregate, which made less temperature sensitive, as can be observed from their in individual dynamic modulus curve slope (Figure 4.41).

The dynamic modulus and phase angle plots of the crumb rubber modified asphalt binder mixture at various frequencies are shown in Figure 4.45. The CRB_76 mix shows a maximum dynamic modulus of approximately 27,000 MPa at 4^{o}C and 10 Hz frequency.

The lowest dynamic modulus was observed at 0.01 Hz and 50°C, a value of approximately 1,000 MPa.

Similar to Figure 4.42, Figure 4.44 presents the phase angle of RPW-aggregate-AC Constant Temperature Plot (at 10Hz). At all temperature levels, the AC containing 10% RPW-aggregate showed the highest elastic response, corresponding to the least phase angle. This further confirms the global nature of the optimum RPW aggregate content previously established.

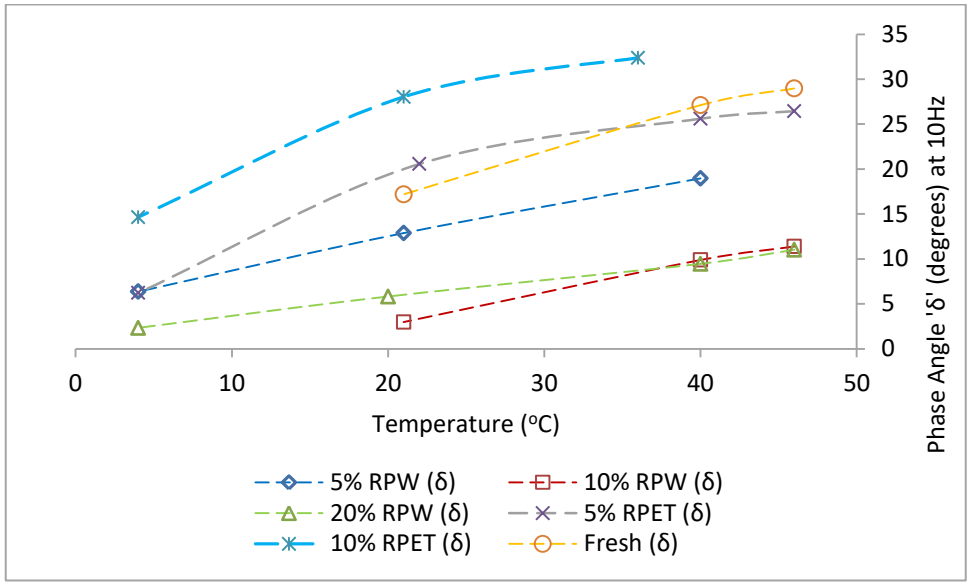

Figure 4.43: Phase Angle of RPW-AC and RPET-only-AC at 10 Hz.

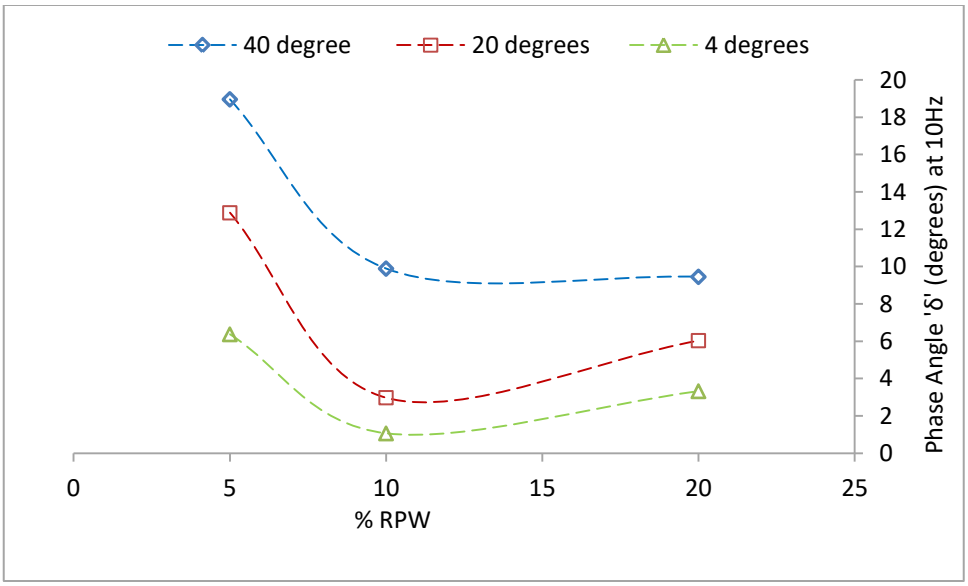

Figure 4.44: Phase Angle of RPW-aggregate-AC Constant Temperature Plot (at 10Hz).

Figure 4.46 also presents both phase angle and dynamic modulus of the P2S1.5_76(H)+RPW AC mixture at varying frequencies and temperatures. The observed trends are as expected: higher modulus at lower and higher frequency, or lower modulus at higher temperature lower frequency. However, these trends are better when this AC mixture (P2S1.5_76(H)+RPW) is compared to the CRB_76 mix observed high and low dynamic modulus in Figure 4.45. There is an overall lower dynamic modulus at lower temperature and higher at higher temperature. The phase angle range are also much lower in the P2S1.5_76(H) mix. A much comprehensive results and analysis will follow in the master curve plots of these AC mixtures

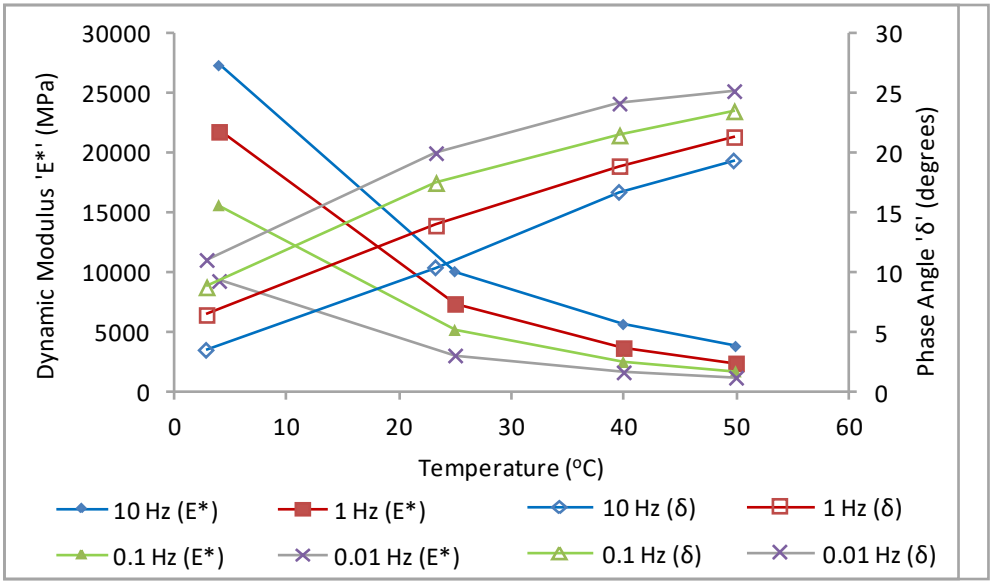

Figure 4.45: Dynamic Modulus and Phase Angle of CRB_76 AC.

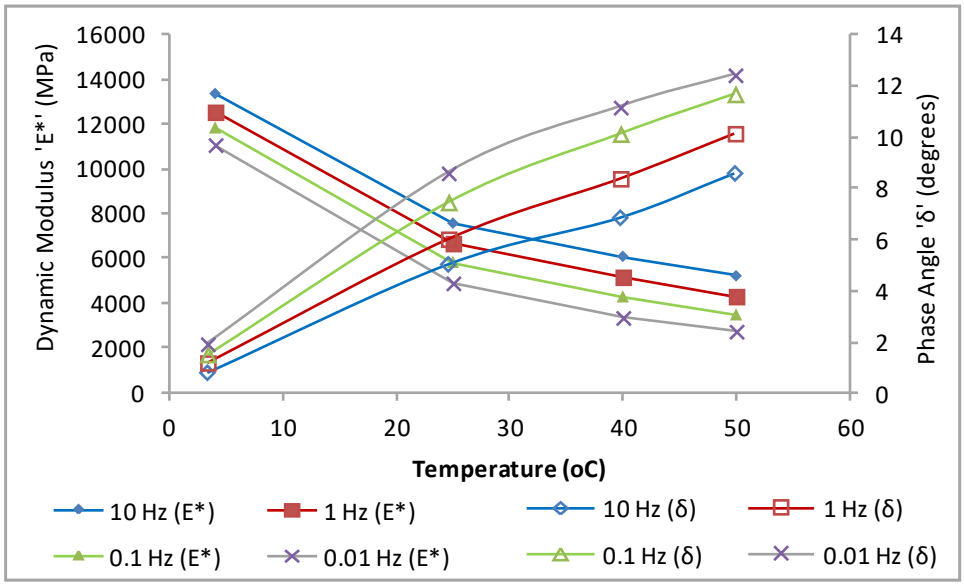

Figure 4.46: Dynamic Modulus and Phase Angle of P2S1.5_76(H)+RPW AC.

Similarly, the phase angle and dynamic modulus plots of the H2PB1.5_76(H)+RPW was also depicted by Figure 4.47. Highest and lowest dynamic modulus of approximately 10,000 MPa and 2,000 MPa were observed at (4°C, 10 Hz) and (50°C, 0.01 Hz) respectively. This is an even better trend than that observed for

P2S1.5_76(H)+RPW (Figure 4.46) when compared to the CRB_76(H) mixture. That is moderate stiffness at lower temperature and higher frequency, and high stiffness at high temperature under low frequency loading. The presence of the RPW aggregate in these two mixture has played a vital role in their observed frequency temperature behavior.

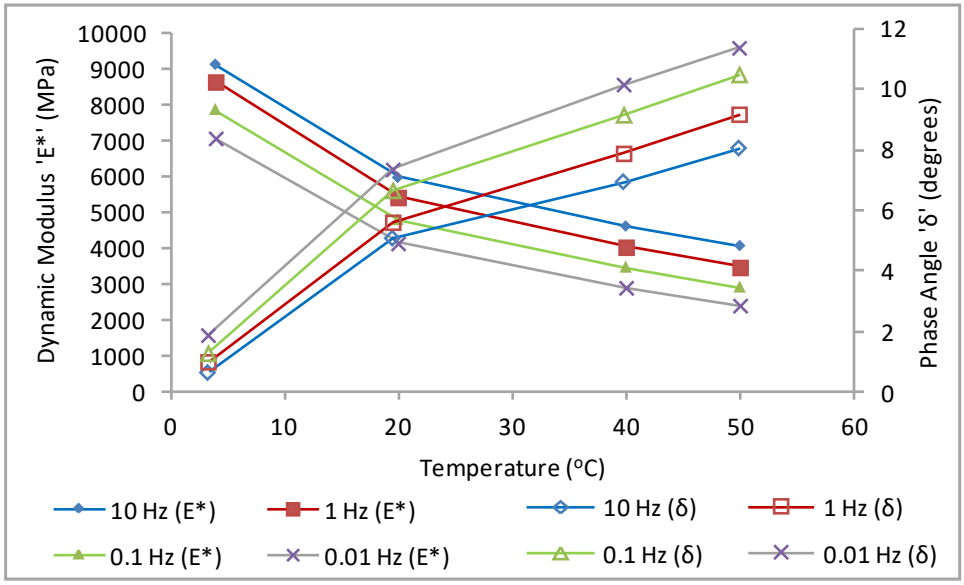

Figure 4.47: Dynamic Modulus and Phase Angle of H2PB1.5_76(H)+RPW AC.

Figure 4.48 and Figure 4.49 presents the dynamic modulus and phase angle plots of H4S1_76(H)+RPW and L4S1.5_76(H)+RPW AC mixtures, respectively. The maximum and minimum dynamic modulus of approximately 14,000 MPa and 2,000 MPa were observed at (4°C, 10 Hz) and (50°C, 0.01 Hz) respectively, for H4S1_76(H)+RPW AC. Likewise, maximum and minimum dynamic modulus of approximately 10,000 MPa and 1,500 MPa were observed at (4°C, 10 Hz) and (50°C, 0.01 Hz), respectively, for L4S1.5_76(H)+RPW AC. These observed values are relatively better than those observed for the CRB_76(H) mixture. However, it also appears that the L4S1_76(H)+RPW

exhibits the lowest dynamic modulus at high temperature low frequency range relative to the previously analyzed ACs containing RPW aggregates.

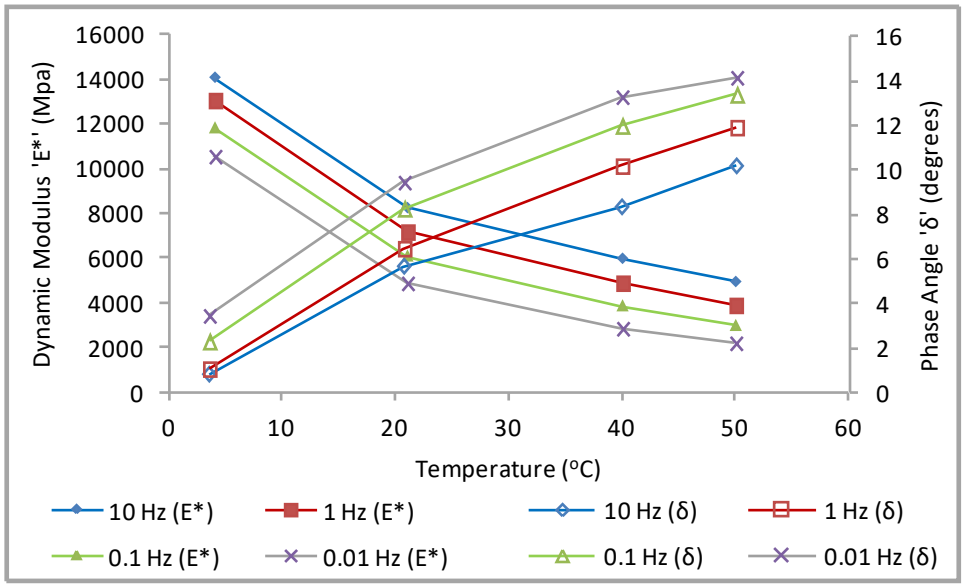

Figure 4.48: Dynamic Modulus and Phase Angle of H4S1_76(H)+RPW AC.

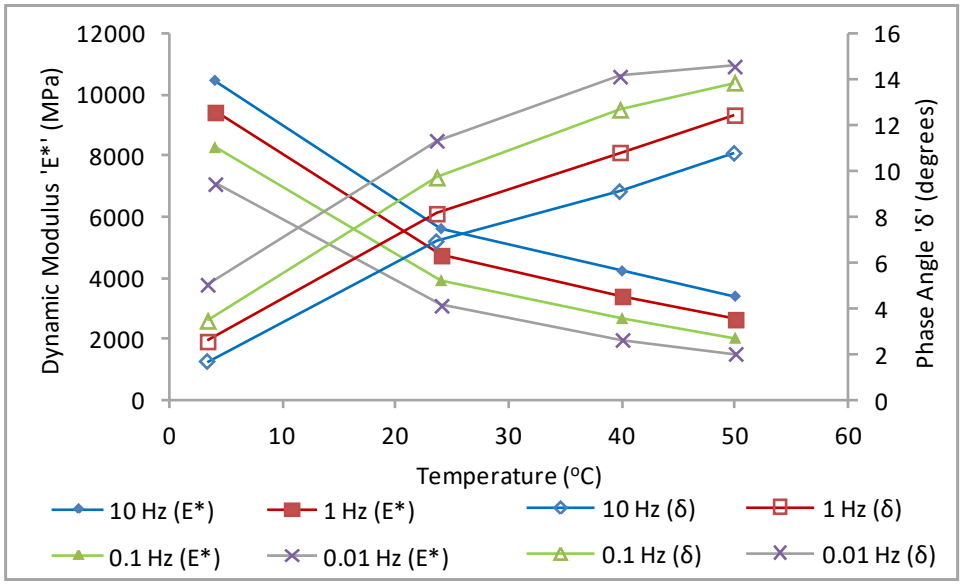

Figure 4.49: Dynamic Modulus and Phase Angle of L4S1.5_76(H)+RPW AC.

Figure 4.50 and Figure 4.51 also presents the dynamic modulus and phase angle plots of L6_76(H)+RPW and H4_76(H)+RPW AC mixtures respectively. Similar

previously observed trends can also be noticed for both mixtures. In all cases, the results explained in terms of the dynamic modulus were also reflected in the phase angle.

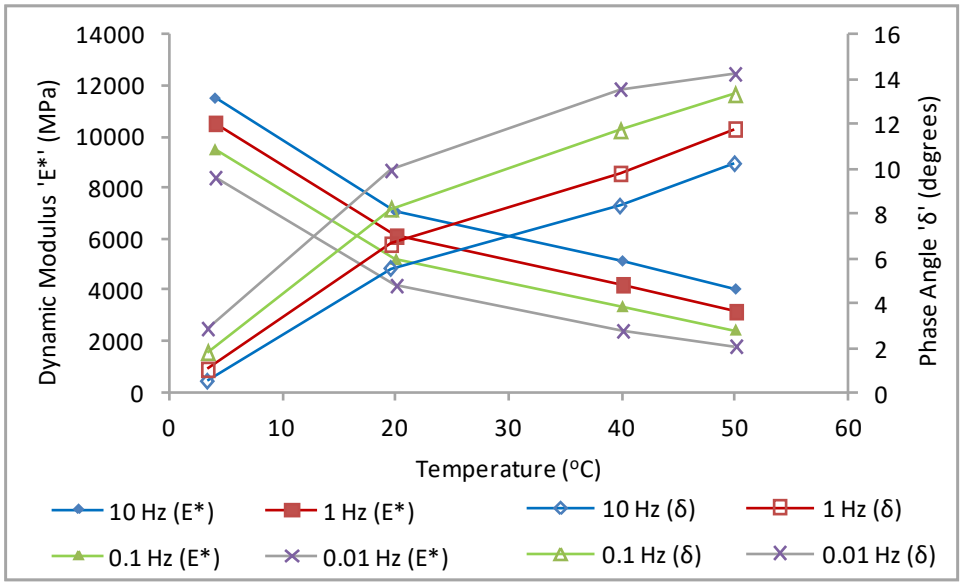

Figure 4.50: Dynamic Modulus and Phase Angle of L6_76(H)+RPW AC.

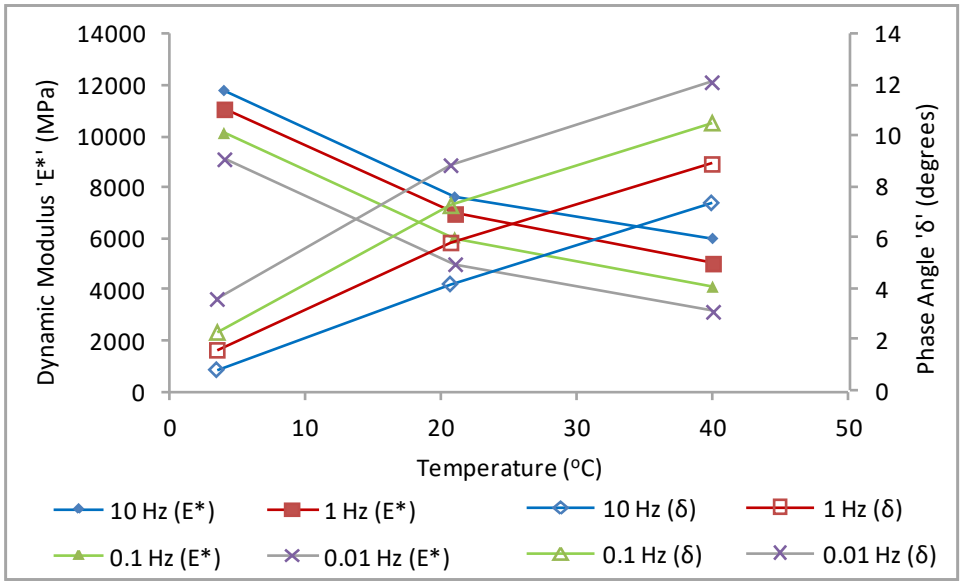

Figure 4.51: Dynamic Modulus and Phase Angle of H4_76(H)+RPW AC.

4.7.2.1 Master Curves of RPW-Asphalt Concrete

The master curve plot for the dynamic modulus of the RPW-ACs was developed from dynamic modulus results of the asphalt mix performance test. At least 2 replicate samples are tested at three temperatures within a frequency range of 0.01 to 10 Hz for the temperature frequency superposition curves [73]. The dynamic modulus was obtained under a confining stress of 180 kPa, an estimated stress similar to that measured in the field [74].

Figure 4.52 shows the master curves of the AC mixture containing the combined RPW aggregate and those containing only RPET aggregate, both compared with fresh AC. As stated earlier, the reason for RPET-aggregate-only mixture comparison is that for some reason, most previous research focused on using RPET solely as aggregate replacement. We have observed that one cannot be able to replace up to 10% of the aggregate in dense graded mix with RPET without compromising the original superpave mix design asphalt content. However for the combined RPW (containing all the various PW), substantial proportion of aggregates could be replaced without losing the binding ability of the mixture, hence needing no additional asphalt binder. This is due to the presence of thermoplastic PW in the combined RPW which tend to also serve as binder to some extent. The thermoplastic PW aggregates tend to partially melt and bind itself to the mineral aggregates during mixing and compaction period. Since RPET is thermosetting with high melting temperature in nature, the mixing and compaction temperature did little to improve bonding between the RPET aggregate and the actual mineral aggregate.

Observing the RPW aggregate containing mixtures (5% RPW, 10% RPW and 20% RPW) in Figure 4.52 will further confirm the optimal RPW aggregate content of around 10% RPW previously established by flow number test of the RPW-mixtures. The time-temperature superposition behavior of the RPW-mixtures was improving from zero RPW content (fresh mix) up to the 10% RPW content. Then a decline in the overall dynamic modulus was observed after the 10% RPW content as seen from the 20% RPW curve. Comparing the RPW-AC and the RPET AC, it can be observed that the RPW aggregates-containing ACs are viscoelastically superior to the RPET-only aggregate-containing AC mixtures. Observing the 5 and 10% contents of the different ACs will confirm this statement. So it can now be said, employing a combine PW for aggregate substitution is better than isolation of an all RPET for the same purpose. This is not to mention the cost and practical issue related to sorting for one individual PW.

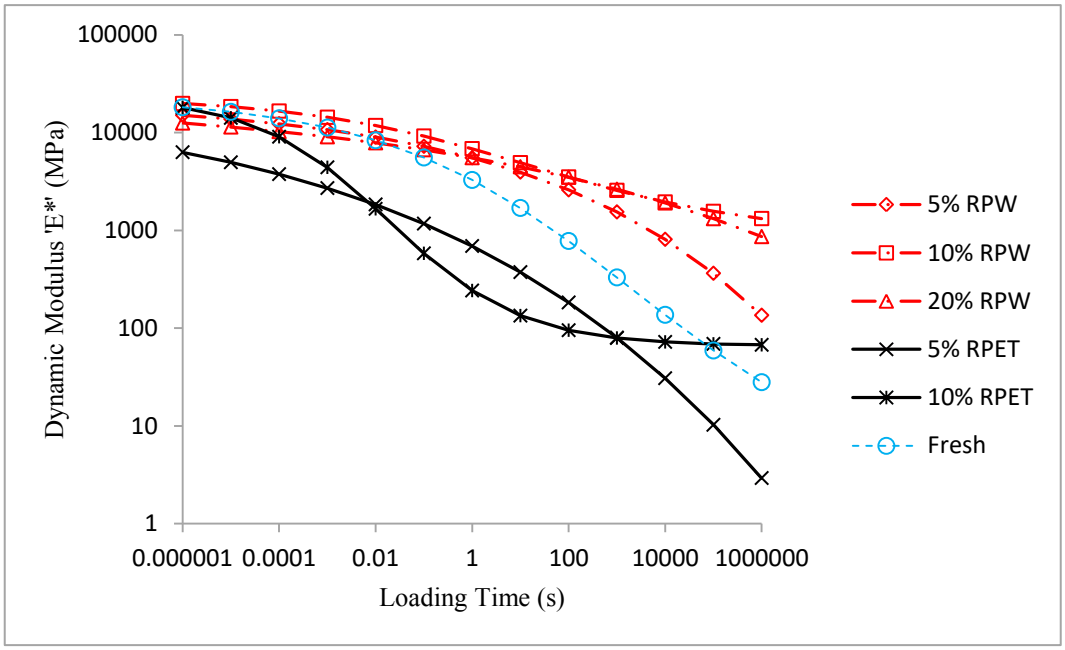

Figure 4.52: Master Curve Dynamic Modulus of RPW-AC and RPET-only-AC.

The phase angle plots of the RPW- and RPET-aggregate mixtures is shown in Figure 4.53. Even though the 10% and 5% RPET ACs exhibited lower dynamic modulus performance than the fresh AC in Figure 4.52, the 5% RPET-aggregate containing mixture shows a slightly lower phase angle than the fresh AC, an indication of better elastic properties. However, the RPW-aggregate mixtures maintain their superior performance by exhibiting less plastic property than the RPET-only aggregate containing mixtures.

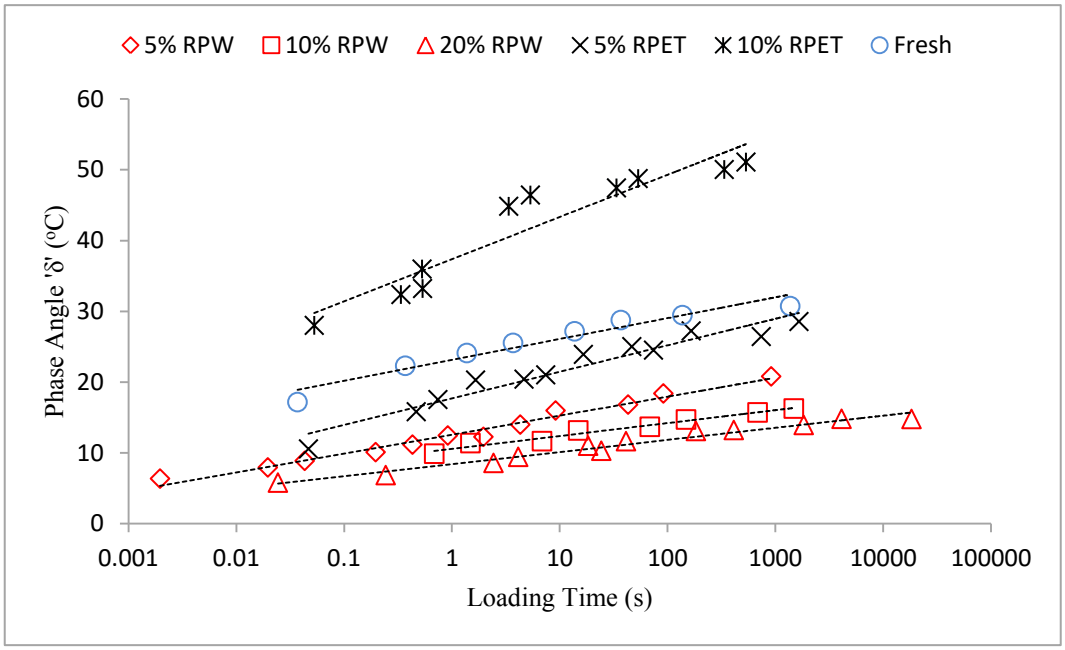

Figure 4.53: Phase Angle of RPW-AC and rPET-only-AC.

The master curve of the hybrid RPW-AC, containing both RPW aggregates and RPW-modified binder is shown in Figure 4.54. First of all, all the RPW-aggregate containing mixtures showed higher dynamic modulus than the conventional crumb rubber modified binder mix (CRB_76) at higher loading time (slow traffic), a loading range that is the most detrimental for the AC. The CRB_76 is the RPW-mix equivalent that is currently being used and recommended for road construction in KSA. The CRB_76

exhibited a higher modulus at lower loading time (higher frequency), a loading time range that impose the least damage to the AC. Both the RPW-aggregate mixture and CRB_76 outperform the fresh/plain asphalt. Among the RPW-aggregate mixtures, the L4S1.5 mix showed the least modulus and P2S1.5 exhibits the highest modulus followed by H2B1.5 mixture in the low loading frequency (high loading time) range.

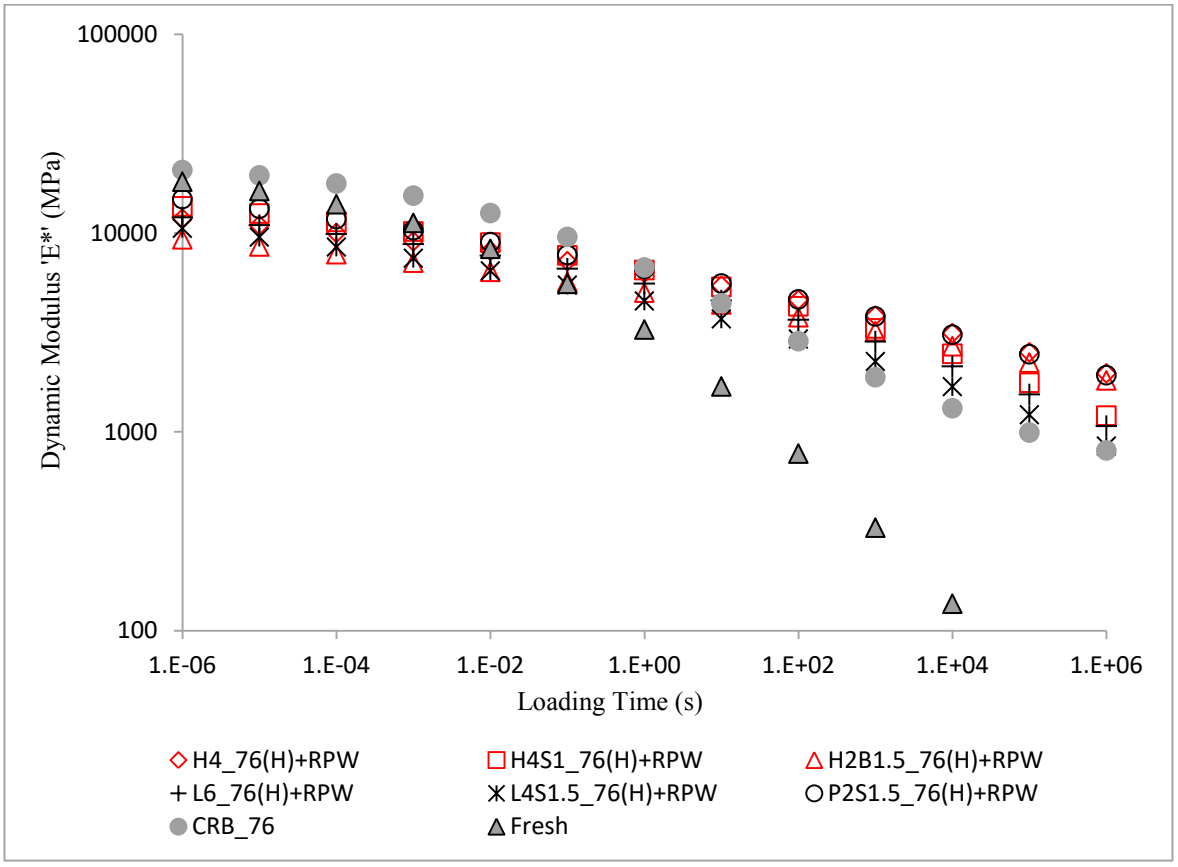

Figure 4.54: Master Curve Dynamic Modulus Plot of Hybrid RPW-AC and Crumb Rubber AC.

Phase angle versus loading time plots for the hybrid RPW-AC and the reference ACs (CRB_76 and fresh) is shown in Figure 4.55. The advantage and the added edge of the hybrid RPW-aggregate mixture over the reference AC is more obvious in this plot. The crumb rubber and fresh asphalt mixtures showed the highest plastic behavior, while

all the hybrid RPW-ACs demonstrate approximately uniform and relatively less deviation from elastic properties.

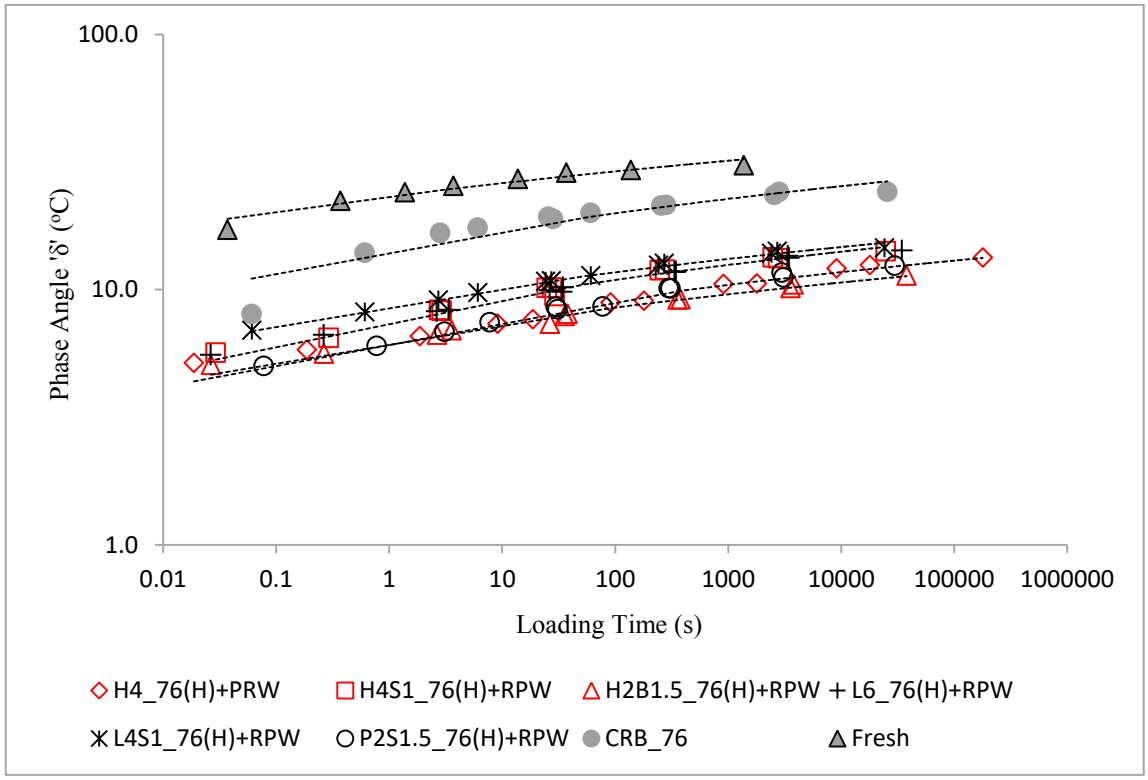

Figure 4.55: Phase Angle of RPW-AC and Crumb Rubber AC.

4.3.4.2 Mathematical Models Relating PRW Content, Test Temperature and Frequency with Dynamic Modulus and Phase Angle

Table 4.11 and Table 4.12 presents regression models relating dynamic modulus phase angle to %RPW/RPET, test frequency and temperature. The regression analysis was run at 5% significant level using MiniTab16 statistical software. All predictors significantly influence their parent models. Better correlation was obtained after linearizing the parameters using log function.

Table 4.13 presents the mathematical correlating the dynamic modulus (4.4 a) and phase angle (4.5 a) for hybrid-RPW AC with mix volumetric properties and test conditions. All predictors including void in mineral aggregate (VMA), void filled with asphalt (VFA) and percent of asphalt content (Pb) significantly influence the dynamic modulus and the phase angle. These model are valid for any AC mix made with a 76 (H) - 12 RPW modified asphalt binder and an optimum aggregate content of 9.5%.

Table 4.14 presents the dynamic modulus master curve models for the various ACs. Excellent fit were obtained for all the ACs, with the exception of 10% RPET AC, which happens to demonstrate significant lack of fit (having Se/Sy > 0.4). Apart from higher asphalt content requirement, relatively lower dynamic results was initially observed for this mix (Figure 4.41).

Table 4.11: Models Relating RPW Content, Test Temperature and Frequency with Dynamic Modulus and Phase Angle.

$\log_{10}(E^*) = 3.97 - 0.421\log_{10}(Temp.) - 26.4(\%RPW)^2 + 6.78(\%RPW) + 0.130\log_{10}(Freq.)$ (4.2)	
S = 0.0717295, R² = 89.3%, R²(adj) = 87.9%	
Predictor	*P-value*
Constant	*0.000*
$log_{10}(Temp.)$	*0.000*
$(\%RPW)^2$	*0.000*
$\%RPW$	*0.000*
$log_{10}(Freq.)$	*0.000*
$\log_{10}(\delta) = 1.77 - 1.19\log_{10}(Temp.) - 9.35(\%RPW) + 32.4(\%RPW)^2 - 0.0687\log_{10}(Freq.) + 0.687(log_{10}(Temp.))^2$ (4.3)	
S = 0.0540757, R² = 90.7%, R² (adj) = 89.2%	
Predictor	*P-value*
Constant	*0.000*
$log_{10}(Temp.)$	*0.000*
$(\%RPW)^2$	*0.000*
$\%RPW$	*0.000*
$log_{10}(Freq.)$	*0.000*
$(log_{10}(Temp.))^2$	*0.000*

Table 4.12: Models Relating RPET Content, Test Temperature and Frequency with Dynamic Modulus and Phase Angle.

$\log_{10}(E^*) = 4.36 - 0.931\log_{10}(Temp.) - 5.87(\%RPET) + 0.266\log_{10}(Freq.)$ (4.4)	
S = 0.176743, R² = 82.3%, R² (adj) = 79.7%	
Predictor	*P-value*
Constant	*0.000*
$log_{10}(Temp.)$	*0.002*
$\%RPET$	*0.001*
$log_{10}(Freq.)$	*0.000*
$\log_{10}(\delta) = 0.422 + 0.350\log_{10}(Temp.) + 6.29(\%RPET) - 0.0752\log_{10}(Freq.)$ (4.5)	
S = 0.0433541 R² = 95.4% R² (adj) = 94.7%	
Predictor	*P-value*
Constant	*0.000*
$log_{10}(Temp.)$	*0.000*
$\%RPET$	*0.000*
$log_{10}(Freq.)$	*0.000*

Table 4.13: Models Relating Dynamic Modulus and Phase angle to Volumetric Properties and Test Condition for Hybrid RPW ACs.

$\log_{10}(E^*) = 16.2 - 0.846\log_{10}(Temp.) + 0.100\log_{10}(Freq.) - 14.8(\frac{VMA}{100}) - 26.1\left(\frac{VFA}{100}\right) + 84.1(\frac{Pb}{100})$ (4.4 a)	
S = 0.106121, R² = 81.3%, R² (adj) = 79.7%	
Predictor	*P-value*
Constant	*0.000*
$log_{10}(Freq.)$	*0.000*
$log_{10}(Temp.)$	*0.000*
$VMA/100$	*0.000*
$VFA/100$	*0.000*
$Pb/100$	*0.000*
$\log_{10}(\delta) = -12.2 + 0.528\log_{10}(Temp.) - 0.0565\log_{10}(Freq.) + 14.9\left(\frac{VMA}{100}\right) + 35.9\left(\frac{VFA}{100}\right) - 98.8(\frac{Pb}{100})$ (4.5 a)	
S = 0.0942066 R² = 75.7% R² (adj) = 73.6%	
Constant	*0.000*
$log_{10}(Freq.)$	*0.000*
$log_{10}(Temp.)$	*0.000*
$VMA/100$	*0.000*
$VFA/100$	*0.000*
$Pb/100$	*0.000*

Table 4.14: Dynamic Modulus Models for Fresh RPW-aggregate and Hybrid-RPW ACs.

$\log\|E^*\| = \delta + \frac{Max-\delta}{1+e^{\beta+\gamma\left(\log t+\frac{\Delta E_a}{19.14714}\left[\frac{1}{T}-\frac{1}{T_r}\right]\right)}}$ (MPa)							
AC Type	Max	Delta (δ)	Beta (β)	Gamma (γ)	ΔE_a	R^2	*Se/Sy
5%RPW	21654.60	-542.111	-4.923	0.2220	123268.6	0.9954	0.0555
10%RPW	23109.30	14.544	-0.517	0.4154	107150	0.9420	0.1966
20%RPW	23109.30	-226.743	-4.055	0.1426	206991.5	0.9923	0.0719
5%RPET	23109.30	-184.875	-2.940	0.1708	111528	0.9532	0.1766
10%RPET	23109.30	6.767	1.255	0.7284	93320.67	0.3957	0.6347
Fresh	22917.86	-2.995	-1.303	0.3884	145893	0.9395	0.2009
CRB_76	23108.35	13.016	-0.718	0.4678	185770.7	0.9981	0.0353
L6_76(H)+RPW	22697.66	-189.999	-3.911	0.1335	195748.4	0.9952	0.0566
L4S1.5_76(H)+RPW	22977.89	-99.873	-3.204	0.1258	183899.9	0.9986	0.0301
H4_76(H)+RPW	22363.13	-33.613	-2.658	0.1199	251038.8	0.9572	0.1689
H2B1.5_76(H)+RPW	23256.24	-167.704	-3.709	0.0875	198929.2	0.9978	0.0382
H4S1_76(H)+RPW	23108.35	-93.261	-3.402	0.1487	184715.9	0.9984	0.0328
P2S1.5_76(H)+RPW	65146.34	-294.050	-3.827	0.0738	190824.6	0.9895	0.0837

*Se/Sy is the ratio of the standard error of predicted variable to the standard deviation of the independent variables

4.7.3 Rutting Performance of RPW-Asphalt Concrete

Two test methods were employed to analyzed the rutting performance of the RPW-aggregate mixtures, namely: the asphalt pavement analyzer (APA) and the AMPT flow number test. The APA test method is older and mostly employed specification and quality assurance, while the AMPT FN test method is more recent and still used for research and development purpose.

4.7.3.1 Flow Number of RPW-Asphalt Concrete

The FN test results of the various RPW-aggregate-containing AC mixtures and the reference ACs are shown in Table 4.15. None of the hybrid RWP-aggregate mixture flowed within the standardized test period of 10,000 seconds. The test was conducted at the highest operating temperature of the machine (64^{o}C). While the main reference mixture (CRB_76) shows a relatively very early flow at 1117 seconds. The CRB FN value falls within the range of AC mixtures eligible for extremely heavy traffic. The FN test results presented did not disqualify the CRB_76 as an excellent mix, but only shows an even superior super-performing RPW-aggregate containing AC mixture. Even though the hybrid RPW-AC did not flow, they have sustained some permanent deformations, which has been recorded at the end of the test. Comparing these permanent strains of the hybrid RPW-ACs with that of 4% SBS (another excellent conventional AC mix that did not flow under similar test condition), will further shows how excellent these mixtures are. The SBS mix sustained approximately 5000 μst permanent strain at the end of the test, while most of the hybrid RPW-ACs just about a quarter of this strain.

Table 4.15: Flow Number and Flow Time Test Results of RPW-ACs.

AC Type	FN (s)	Strain@10000s (μst)	FT (s)
Fresh	508	**	140
CRB_76	1117	**	**
Fresh+RPW	17825	**	**
4% SBS	No Flow	5003	No Flow
L6_76(H)+RPW	No Flow	1824	No Flow
L4S1.5_76(H)+RPW	No Flow	1742	No Flow
L6B1_76(H)+RPW	No Flow	1660	No Flow
H4_76(H)+RPW	No Flow	1536	No Flow
H2B1.5_76(H)+RPW	No Flow	1527	No Flow
H4S1_76(H)+RPW	No Flow	1504	No Flow
P2S1.5_(76)+RPW	No Flow	1360	No Flow

4.7.3.2 Asphalt Pavement Analyzer Results

The APA test results of the RPW-AC and the reference ACs are presented in Figure 4.56. The test deformation limit, the usual standard for various highway ministries was set at 6 mm (0.25"). The fresh asphalt mixture which was tested at 64^{o}C, seems to just barely remain within limit up to the end of the test (8000 seconds). Recalling that the fresh mix has a PG of 64, 64^{o}C was the recommended testing temperature. The RPW-ACs and the CRB_76 were tested at 70^{o}C (the highest operating temperature of the machine). The RPW-ACs showed better resistance to permanent deformations than the CRB_76. They exhibited approximately the same deformation trends.

Figure 4.57 presents correlation between the APA rut depth at 8000 cycles, Dynamic modulus and the AMPT FN test strain at 10,000 seconds for the AC containing RPW aggregate. A better correlation between rut-depth and FN-strain could be observed. Even though the RPW AC sustained very little rutting deformation from the APA test, the two different tests have a very good agreement.

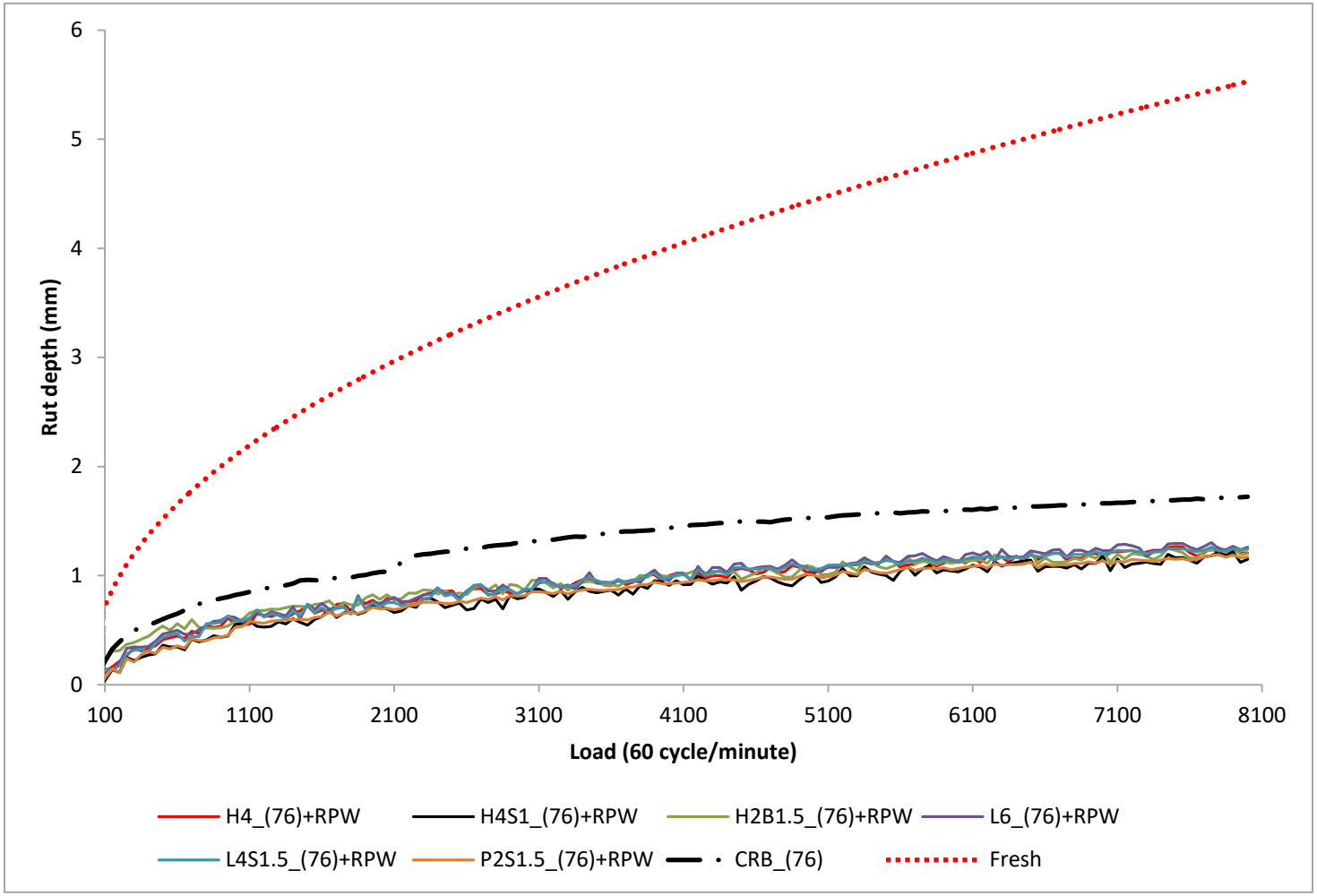

Figure 4.56: Asphalt Pavement Analyzer Permanent Deformation of RPW-AC and Crumb Rubber AC.

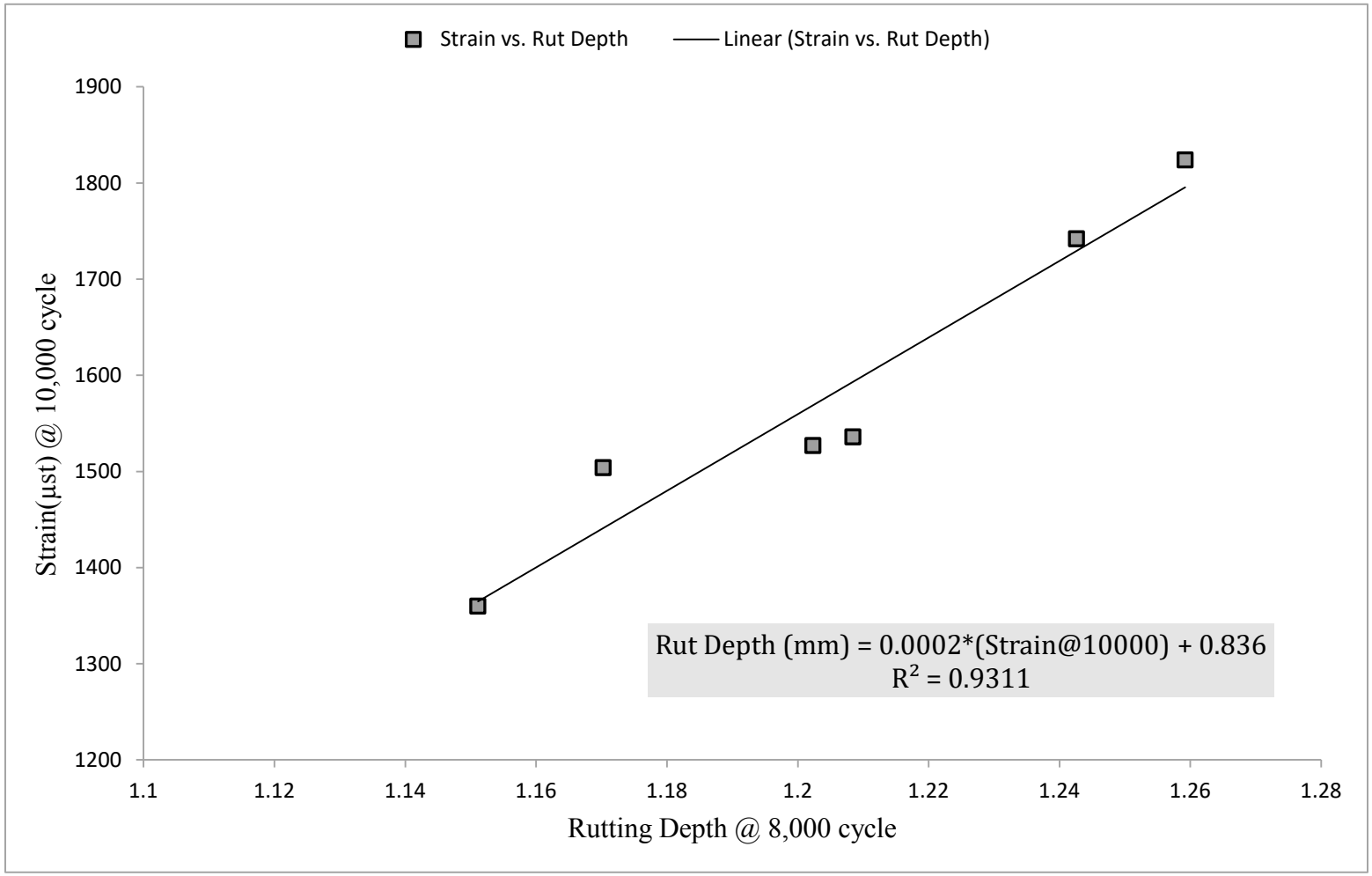

Figure 4.57: Correlation Between the APA Rut Depth, Dynamic Modulus and the AMPT FN test Strain @1000s.

4.7.4 Fatigue Life of RPW-Asphalt Concrete

The fatigue performance of the various ACs in this study was obtained at intermediate temperature (20^{o}C) using both controlled stress and strain test. Figure 4.58 shows the fatigue life of fresh AC, crumb rubber modified AC and fresh-AC-containing RPW aggregates under controlled strain test. As expected, the CRB_76 possessed longer fatigue life than the fresh AC. However, the presence of the RPW aggregate in the fresh+RPW mix has more than doubled the fresh AC fatigue life. The fresh+RPW fatigue life is at a completely different level. The melted thermoplastic RPW waste aggregates in the fresh+RPW mix have further reinforced the aggregate-aggregate and aggregate-mastic interfaces. This interfaces are where the fatigue cracks initiates, before propagating into the AC core. Any delay in the crack initiation will add to the fatigue life.

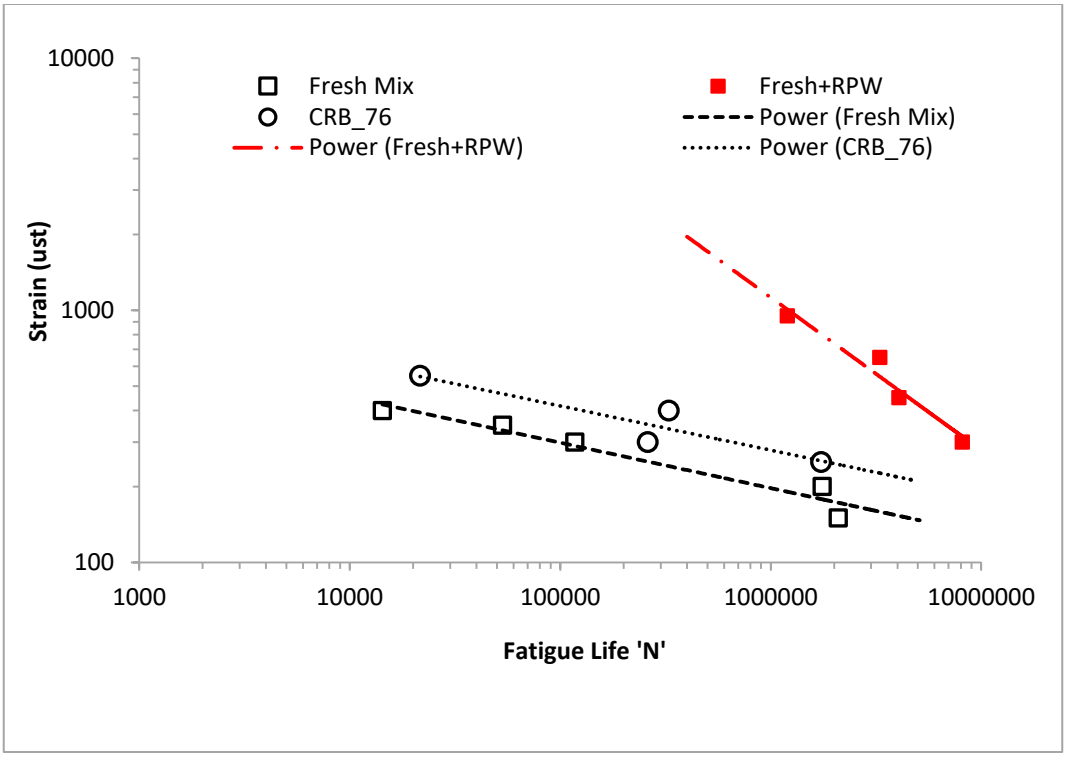

Figure 4.58: Controlled Strain Fatigue Life of RWP-AC and Crumb Rubber AC.

Figure 4.59 presented the strain controlled fatigue life of the hybrid RPW-AC along with those presented previously in Figure 4.58. It can be observed that the hybrid-RPW-ACs fatigue performance are not far beyond that of the fresh+RPW mix. In fact some of the hybrid-RPW-ACs fatigue life performance is a little below that of the fresh+RPW AC. This clearly indicates that the significant improvement in fatigue life of the ACs containing RPW aggregates is significantly related to the RPW aggregate content of the mixtures. The following observations in terms of relative performance of the various hybrid-RPW-ACs, CRB_76 and fresh AC mix were made:

- H4_76(H)+RPW mix showed the highest fatigue life among the hybrid-RPW-ACs at applied tensile strain level above 730 μst, while H4S1_76(H)+RPW out perform all the hybrid-RPW-ACs at 730 μst tensile strain and below (Figure 4.59). The presence of the 1% elastomeric SBS polymer in the H4S1_76(H)+RPW is responsible for its overall improvement in fatigue performance. It is important to note that both H4S1_76(H)+RPW and H4_76(H)+RPW have similar gradation (G2).
- It can also be noted that for hybrid-RPW-ACs with G1 aggregate structure, that L4S1.5_76(H)+RPW outperform the L6_76(H)+RPW at all strain level (Figure 4.59). This has further confirmed the previous observation that hybrid-RPW-ACs with elastomeric SBS content tend to have better fatigue resistance.
- P2S1.5_76(H)+RPW AC mix (with G1 aggregate structure) shows the least fatigue life among all the hybrid-RPW-ACs (Figure 4.59). This outcome cannot be disassociated with the unstable and high stiff nature of the RPP modified asphalt binder.

- H2B1.5_76(H)+RPW (with G1 aggregate structure) is the second least performing hybrid-RPW-ACs after P2S1.5_76(H)+RPW AC mix (Figure 4.59).
- All the hybrid-RPW-ACs showed better fatigue performance than the CRB_76 at applied tensile strain level above 150 μst (Figure 4.60).
- All the hybrid-RPW-ACs demonstrated higher fatigue resistance than the fresh AC mix at applied strain above 100 μst. As 100 μst is a strain level within the vicinity of the fatigue endurance limit for conventional AC mix (75 μst), it can be said that all the hybrid-RPW-ACs possessed better fatigue resistance than the fresh AC.

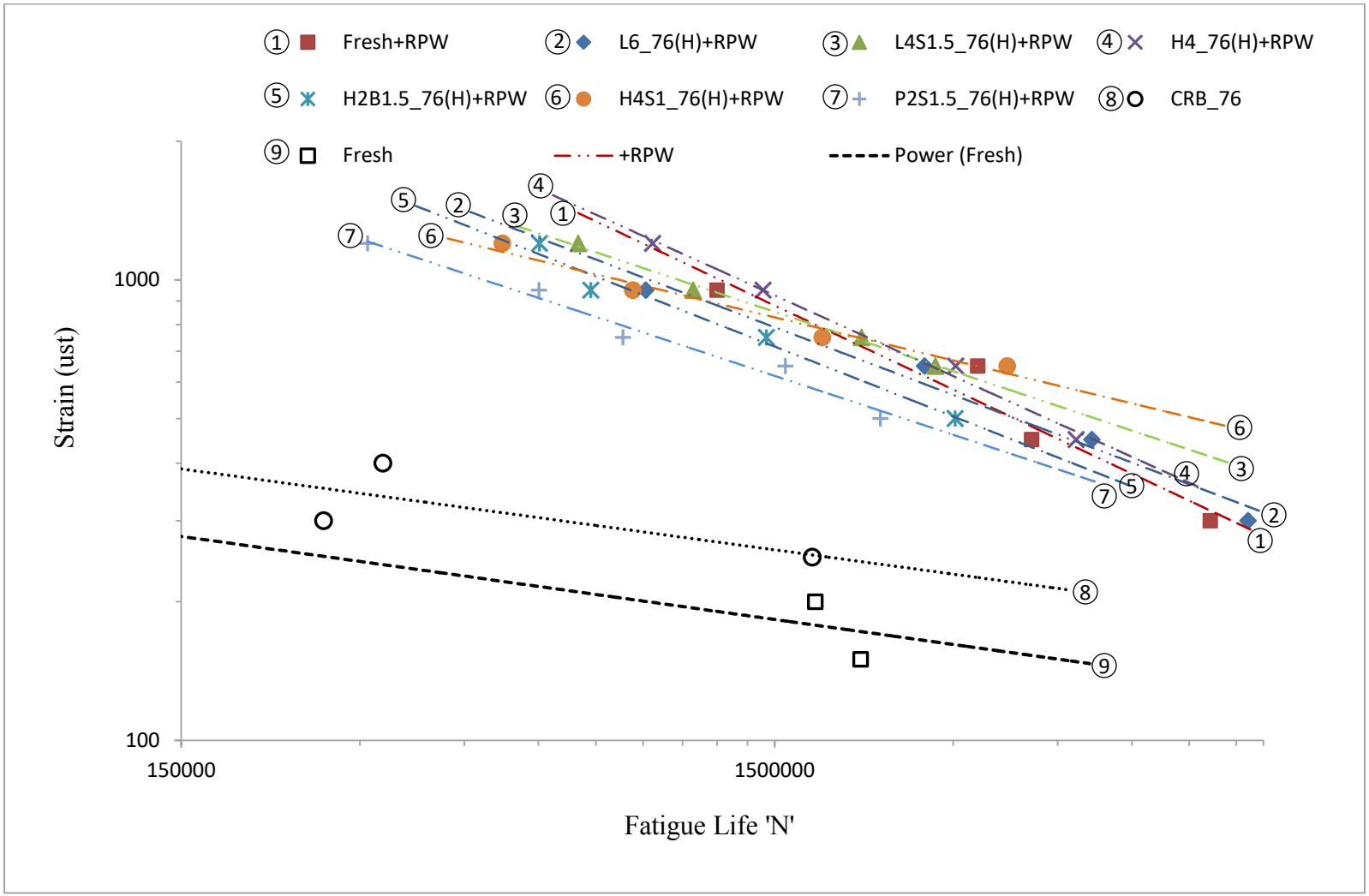

Figure 4.59: Controlled Strain Fatigue Life of Hybrid RPW_AC.

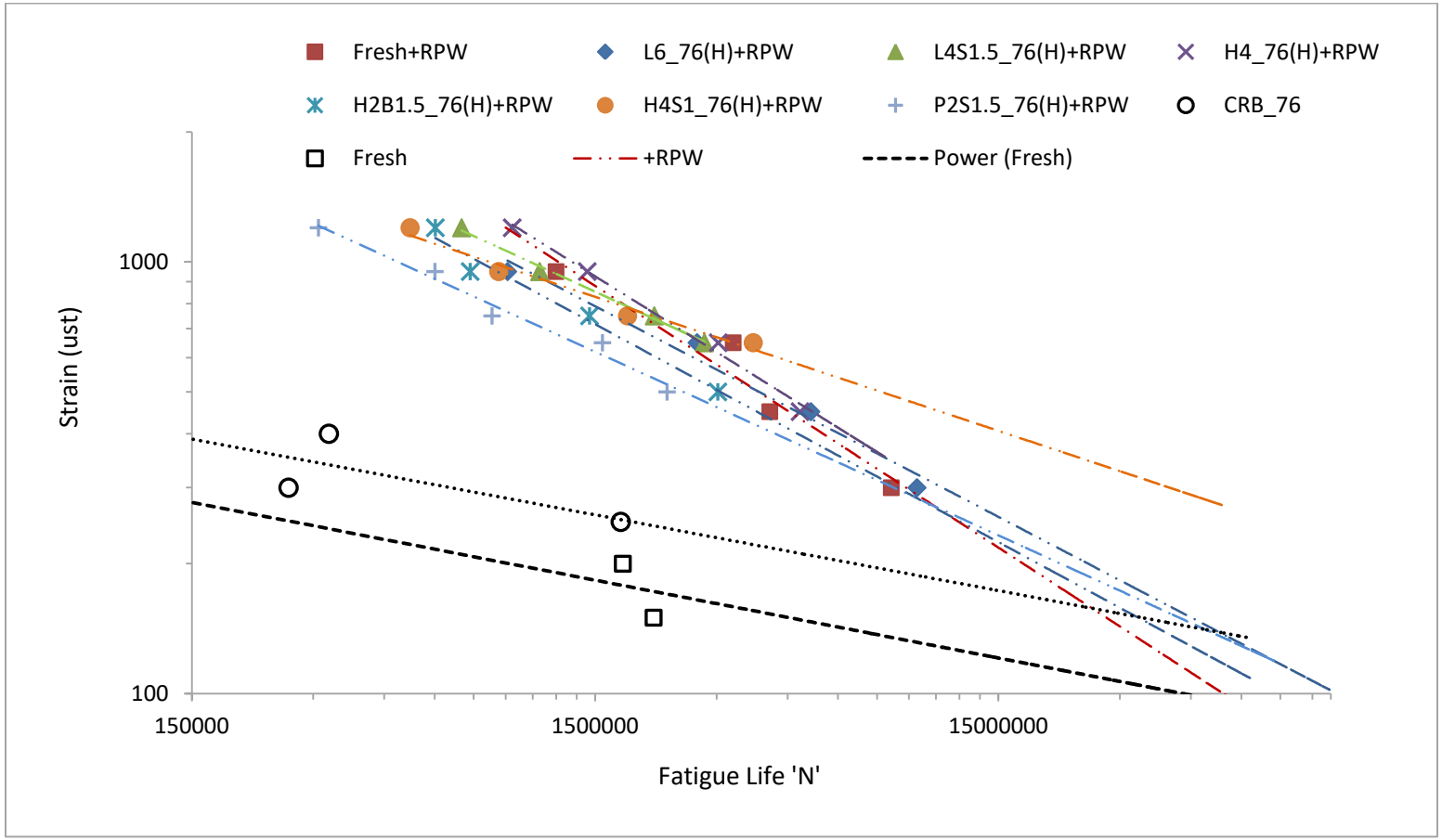

Figure 4.60: Controlled Strain Fatigue Life of Hybrid RPW_AC (Extended).

Figure 4.61 shows the fatigue life of fresh AC, crumb rubber modified AC and fresh-AC-containing RPW aggregates for both stress and strain controlled fatigue test. It can be generally observed that the controlled stress fatigue life results are relatively lower than the controlled stress fatigue performance. The stress controlled fatigue test maintained a constant applied stress and the tensile strain keeps increasing, while the strain controlled test applied a constant strain and the measured stress keeps increasing until failure. Unlike in the case of strain controlled test, the amount of dissipated energy per load cycle keeps increasing in the case of the stress controlled test, hence the reason why the stress controlled fatigue life are relatively shorter. The difference in magnitude between the applied strain (strain controlled) and the initial measure strain should also be noted here. The applied strain in this case (especially for the fresh+RPW mix) are higher than the record initial tensile strain for the stress controlled test. This is because in the stress controlled, the applied stress induces a relative lower strain and grows to the maximum at the end of the test. This factor makes the comparison a little less fair. However, it has been clearly established that the stress controlled fatigue life is lower than the strain controlled.

The one important observation worth noting is the relative sensitivity of the different AC mixtures to the fatigue test modes. The Fresh+RPW mix is more affected significantly by the stress controlled mode test than the CRB_76 and the Fresh Mix. This is due to the fact that the applied strain (600 - 1200 μst) for the controlled strain test are relatively much higher than the initial measured strain in the stress controlled test (200 - 400 μst). The applied strain for the other AC mixture ranges between 200 - 500 μst.

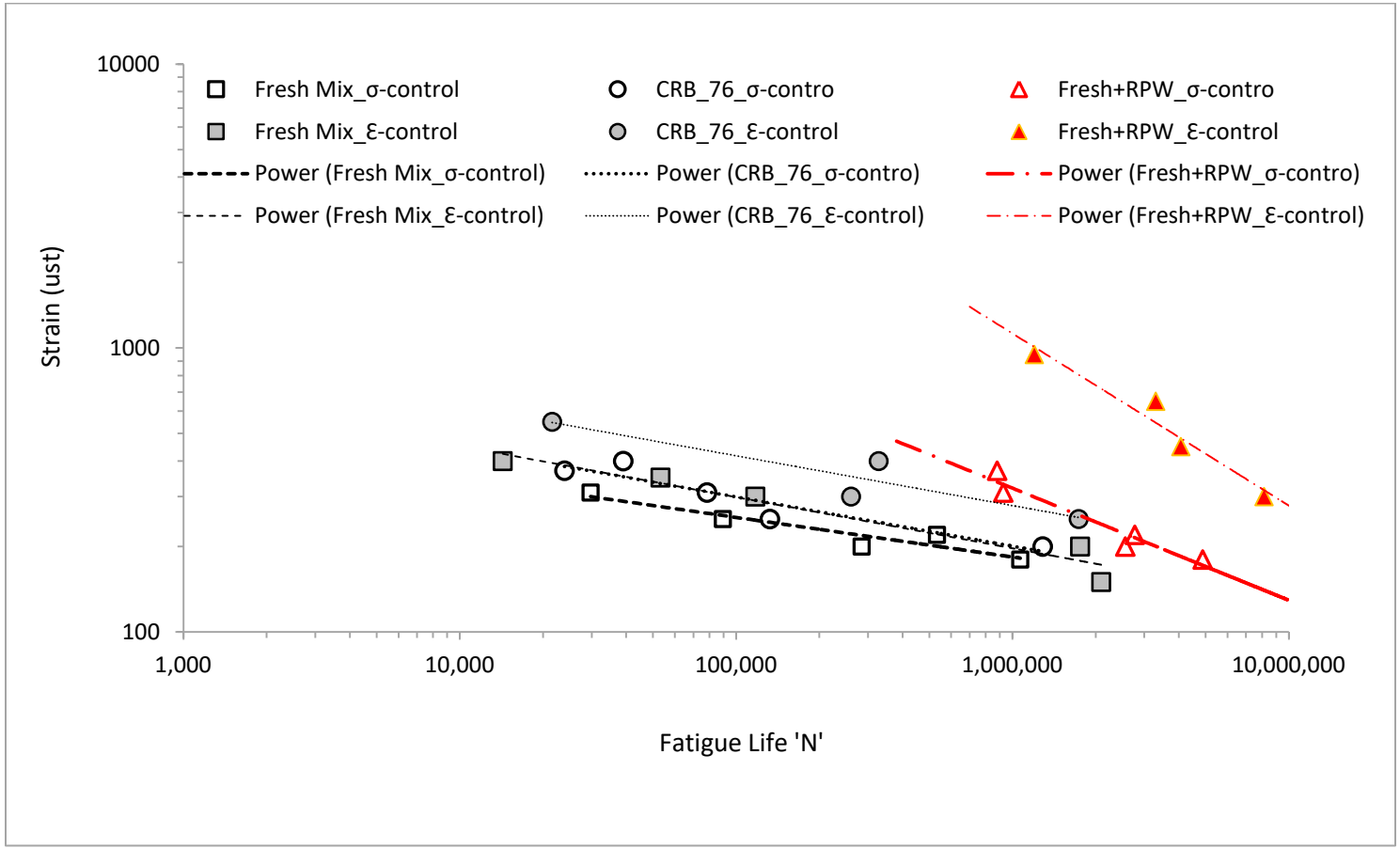

Figure 4.61: Controlled Stress and Controlled Strain Fatigue Life of RWP-AC and Crumb Rubber AC Compared.

Figure 4.62 presents the controlled stress fatigue life of hybrid-RPW-AC versus the initial measured applied strain. The same fatigue life result was plotted against the applied stress as shown in Figure 4.63. The relative performances of the various AC mixtures is slightly different from the strain controlled test results. Both Figure 4.62 and Figure 4.63 showed good correlation between the applied load repetition and the fatigue life. However, the initial strain plot (Figure 4.62) showed a much clearer fatigue life trend. The following inferences were deduced:

- The CRB_76 AC has better fatigue resistance than the fresh at measured applied strain above 140 μst, while the Fresh+RPW AC also out-perform the CRB_76 at strain above 140 μst (Figure 4.62). However, there was intersection between the CRB_76(H) and Fresh Mix AC fatigue performance curve in the stress versus load repetition curve (Figure 4.63). It should be noted that these AC mixtures have similar aggregate gradation, G1.
- All the hybrid-RPW-ACs showed better fatigue resistance than the CRB_76 at induced strain level above 120 μst (Figure 4.62). However, this measured strain could possibly correspond to a low applied stress not capable of inducing cumulative fatigue damage.
- The best performing mix among the hybrid-RPW-ACs is H4S1_76(H) at strain level below 650 μst. But the Fresh+RPW AC showed better performance above this strain level.
- As previously observed in the stain controlled test results. The least performing AC mix among the hybrid-RPW-ACs is the P2S1.5 above 270 μst induced strain. But H2B1.5_76(H)+RPW showed the least fatigue performance below 270 μst.

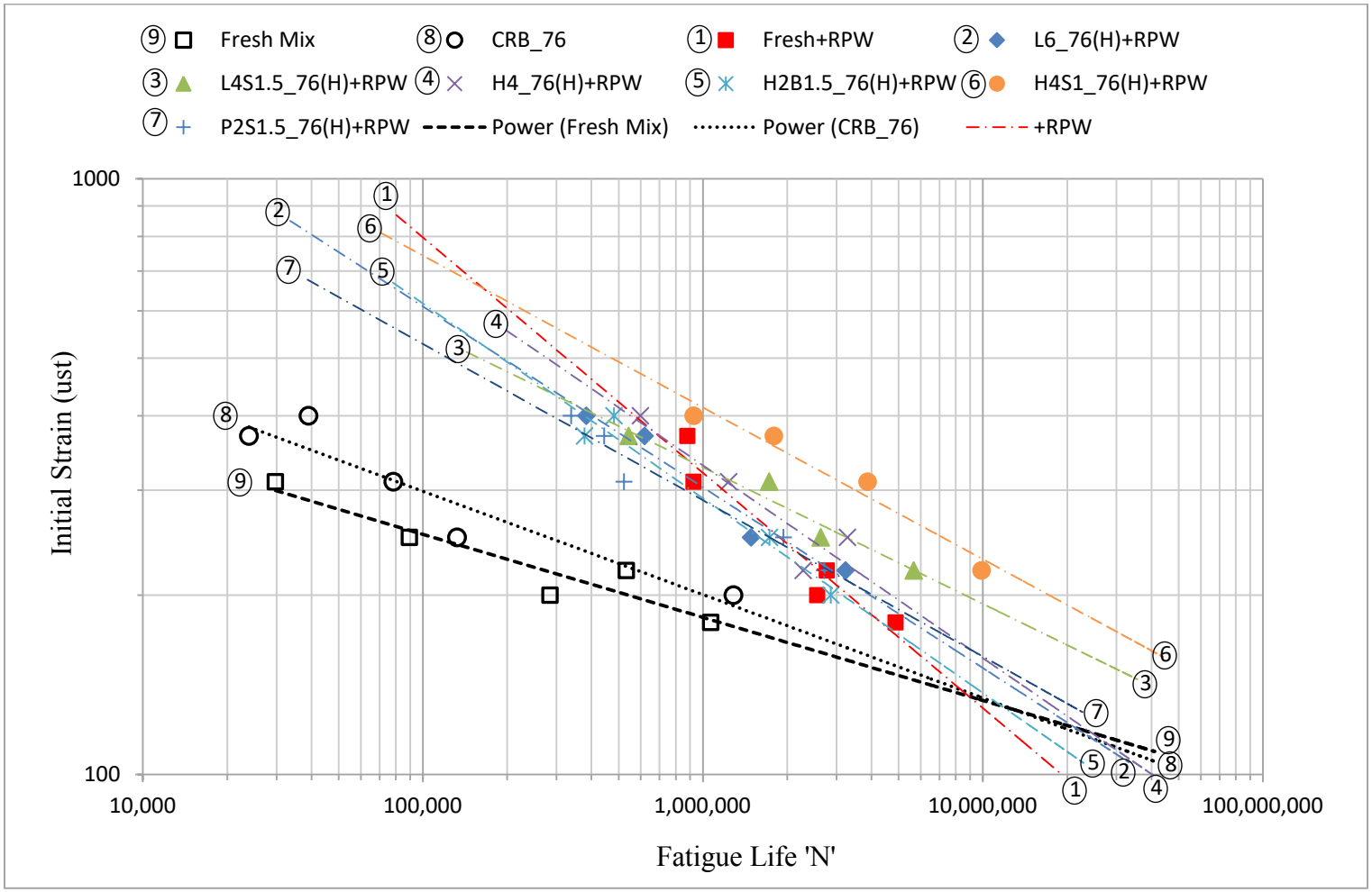

Figure 4.62: Controlled Stress Fatigue Life of Hybrid RPW_AC (Initial Strain vs. N).

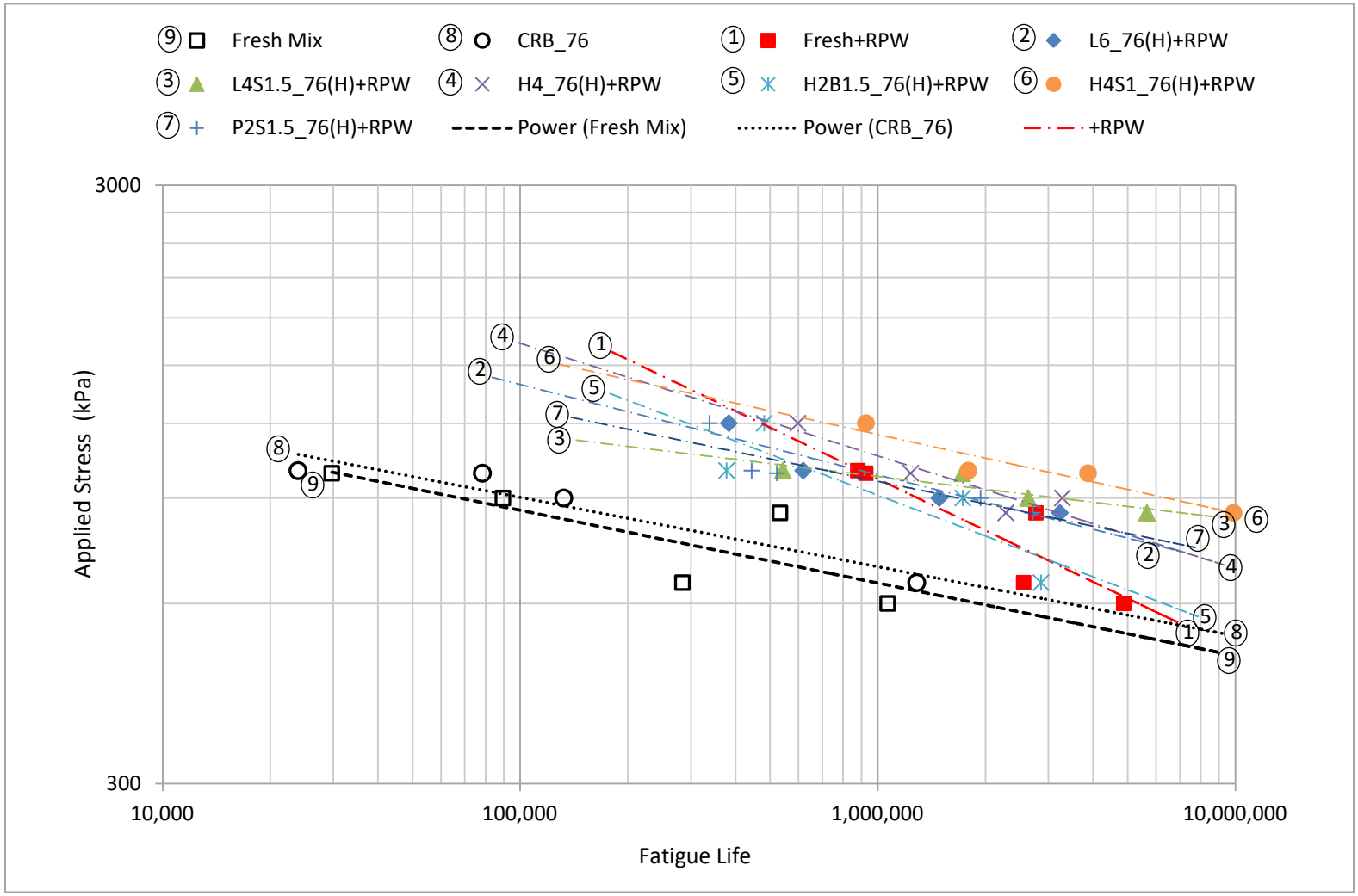

Figure 4.63: Controlled Stress Fatigue Life of Hybrid RPW_AC (Applied Stress vs. N).

Table 4.16 shows S-N fatigue performance models of the various AC mixtures for stress and strain controlled test. A good power model fit could be observed for both test modes. However, the strain controlled test showed better correlation as previously seen from the S-N curve plots. A tabular results presentation of the fatigue lives are presented in the appendix.

Table 4.16: S-N model fit equations for the various RPW- and Reference ACs for stress and strain controlled test

AC Mix ID	Controlled Strain		Controlled Stress	
	Fatigue Models	Model Fit	Fatigue Models	Model Fit
Fresh Mix	$N_f = \frac{5.7300 * 10^{18}}{\varepsilon^{5.5556}}$	$R^2 = 0.9404$	$N_f = \frac{1.4796 * 10^{24}}{\sigma^{6.5856}}$	$R^2 = 0.6443$
Fresh+RPW	$N_f = \frac{1.1300 * 10^{11}}{\varepsilon^{1.6500}}$	$R^2 = 0.944$	$N_f = \frac{6.9900 * 10^{12}}{\sigma^{2.300}}$	$R^2 = 0.8067$
CRB Mix	$N_f = \frac{7.5667 * 10^{19}}{\varepsilon^{5.6818}}$	$R^2 = 0.8487$	$N_f = \frac{8.9053 * 10^{24}}{\sigma^{6.7118}}$	$R^2 = 0.9177$
L6_76(H)+RPW	$N_f = \frac{1.2944 * 10^{12}}{\varepsilon^{2.0491}}$	$R^2 = 0.9754$	$N_f = \frac{3.5033 * 10^{15}}{\sigma^{3.1791}}$	$R^2 = 0.886$
L4S1.5_76(H)+RPW	$N_f = \frac{1.0679 * 10^{13}}{\varepsilon^{2.3364}}$	$R^2 = 0.9942$	$N_f = \frac{4.022 * 10^{16}}{\sigma^{3.4664}}$	$R^2 = 0.807$
H4_76(H)+RPW	$N_f = \frac{2.2067 * 10^{11}}{\varepsilon^{1.7182}}$	$R^2 = 0.9811$	$N_f = \frac{4.0821 * 10^{13}}{\sigma^{2.8482}}$	$R^2 = 0.8621$
H2B1.5_76(H)+RPW	$N_f = \frac{6.6980 * 10^{11}}{\varepsilon^{1.9802}}$	$R^2 = 0.976$	$N_f = \frac{1.6747 * 10^{15}}{\sigma^{3.1102}}$	$R^2 = 0.7448$
H4S1_76(H)+RPW	$N_f = \frac{3.9432 * 10^{15}}{\varepsilon^{3.2258}}$	$R^2 = 0.9718$	$N_f = \frac{4.1302 * 10^{19}}{\sigma^{4.3558}}$	$R^2 = 0.9024$
P2S1.5_76(H)+RPW	$N_f = \frac{5.5975 * 10^{12}}{\varepsilon^{2.33529}}$	$R^2 = 0.9597$	$N_f = \frac{2.1485 * 10^{16}}{\sigma^{3.4829}}$	$R^2 = 0.886$

4.7.4.1 Mathematical Correlation Between Fatigue Life, Dynamic Modulus and Phase Angle

Table 4.17 and Table 4.18 presents correlations fatigue life (N_f), applied load (stress (σ) and strain (ε)), dynamic modulus (E^*) and phase angle (δ) for hybrid-RPW-ACs and reference ACs respectively. The regression analysis was run at 5% significant level using MiniTab statistical software. Better statistical correlation was observed for controlled strain test results. All the predictors (strain/stress, dynamic modulus and phase angle) correlated significantly with the fatigue life in the controlled strain test mode. However the phase angle happen to also correlate significantly with another predictor, necessitating its elimination from the correlation equation. The dynamic modulus showed P-value greater than 5%, signally little or no influence on the fatigue life for the controlled stress correlation of the hybrid-RPW_AC. Similar outcome can be observed for the reference AC correlation results presented in Table 4.18.

Table 4.17: Fatigue Life, Dynamic Modulus and Phase Angle Correlation for Hybrid-RPW-ACs.

Controlled Strain	$\log_{10}(N_f) = 8.99 - 2.00\log_{10}(\varepsilon) + 0.594\log_{10}(E^*) + 0.918\log_{10}(\delta)$ (4.6)	
	S = 0.100024, R² = 93.6%, R² (adj) = 92.9%	
	Predictor	*P-value*
	Constant	*0.000*
	$\log_{10}(\varepsilon)$	*0.000*
	$\log_{10}(E^*)$	*0.043*
	$\log_{10}(\delta)$	*0.000*
Controlled Stress	$\log_{10}(N_f) = -355 - 4.24\log_{10}(\sigma) + 191\log_{10}(E^*) + 1.38\log_{10}(\delta) - 24.4\sqrt{\log_{10}(\delta)}$ (4.7)	
	S = 0.240771, R² = 69.1% , R² (adj) = 64.0%	
	Predictor	*P-value*
	Constant	*0.011*
	$\log_{10}(\sigma)$	*0.000*
	$\log_{10}(E^*)$	*0.009*
	$\log_{10}(\delta)$	*0.003*

Table 4.18: Fatigue Life, Dynamic Modulus and Phase Angle Correlation for CRB_76 and Fresh AC.

Controlled Strain	$\log_{10}(N_f) = 7.54 - 5.08\log_{10}(\varepsilon) + 2.62\log_{10}(E^*) + 0.00\log_{10}(\delta)$ (4.8)	
	S = 0.289469 R²= 90.8% R² (adj) = 87.8%	
	Predictor	*P-value*
	Constant	*0.032*
	$\log_{10}(\varepsilon)$	*0.012*
	$\log_{10}(E^*)$	*0.000*
	$\log_{10}(\delta)$	*0.000*
Controlled Stress	$\log_{10}(N_f) = 12.1 - 3.42\log_{10}(\sigma) + 1.04\log_{10}(\delta)$ (4.9)	
	S = 0.272539 R² = 58.8% R² (adj) = 53.8%	
	Predictor	*P-value*
	Constant	*0.008*
	$\log_{10}(\sigma)$	*0.000*
	$\log_{10}(\delta)$	*0.032*

4.8 RESULTS OF PERFORMANCE MODELING OF RPW-ASPHALT CONCRETE

The performance modeling of the RPW AC was formulated for the hybrid-RPW ACs made with RPW-modified binders having upper PG of 76 heavy traffic (30 million ESAL, Table 3.8). The upper PG of 76 was selected because of the climate requirement in Eastern Region of KSA. The fatigue and rutting performance of 20 cm hybrid-RPW ACs wearing course (as shown by Figure 3.24) was modeled. Average seasonal temperature conditions typical of KSA climate was utilized [78]. All parameters (layer thickness, traffic loading, climatic data, etc) are kept constant for the hybrid-RPW AC mixtures. The only property varied is the visco-elastic behavior of the hybrid-RPW AC mixtures. Average daily equivalent single axle load (ESAL) of 2200, with 5% annual growth was utilized. A 20 year design period, corresponding to 30 million cumulative ESAL was used.

4.8.1 Rutting and Fatigue Performance Analysis

The strain induced by the standard axle load in the pavement section (as shown in Figure 3.24), was obtained using WinJULEA software [76]. WinJulea is a windows version of the layered elastic program JULEA, which has been implemented in the AASHTO Mechanistic Empirical Pavement Design Guide for pavements [77]. Using the standard axle configuration, the critical strain were obtained at the bottom (for fatigue) and mid section (for rutting) of the AC layer, 20 cm and 10 cm below the surface, directly under the wheel load. AC layer modulus and Induced strain corresponding to average

monthly temperatures were estimated. These parameters were incorporated in to the rutting and fatigue models (3.41) and (3.45) respectively, for performance prediction.

Figure 4.64 shows the rutting performance results of the hybrid-RPW AC mixtures relative to fresh and crumb rubber AC mixtures. A handful of the hybrid-RPW AC mixtures exhibited higher resistance rutting than the CRB_76 and fresh. This trend was already observed from the master curve laboratory test results. Overall, the hybrid-RPW AC mixtures did not show any significant rutting throughout the pavements lives. This has a lot to do with their relatively low temperature sensitivity when compared to the control and reference mixtures. The RPW aggregates along with the RPW-modified asphalt binder have lead to ACs with significantly reduced temperature susceptibility. H4_76(H)+RPW and P2S1_76(H)+RPW showed the highest rutting resistance, while L4S1.5_76(H)+RPW shows the least resistance to rutting among the hybrid-RPW AC mixtures. Figure 4.65 shows the correlation between 20 years predicted rutting and laboratory APA rutting results. Excellent correlation was observed as seen from Figure 4.65.

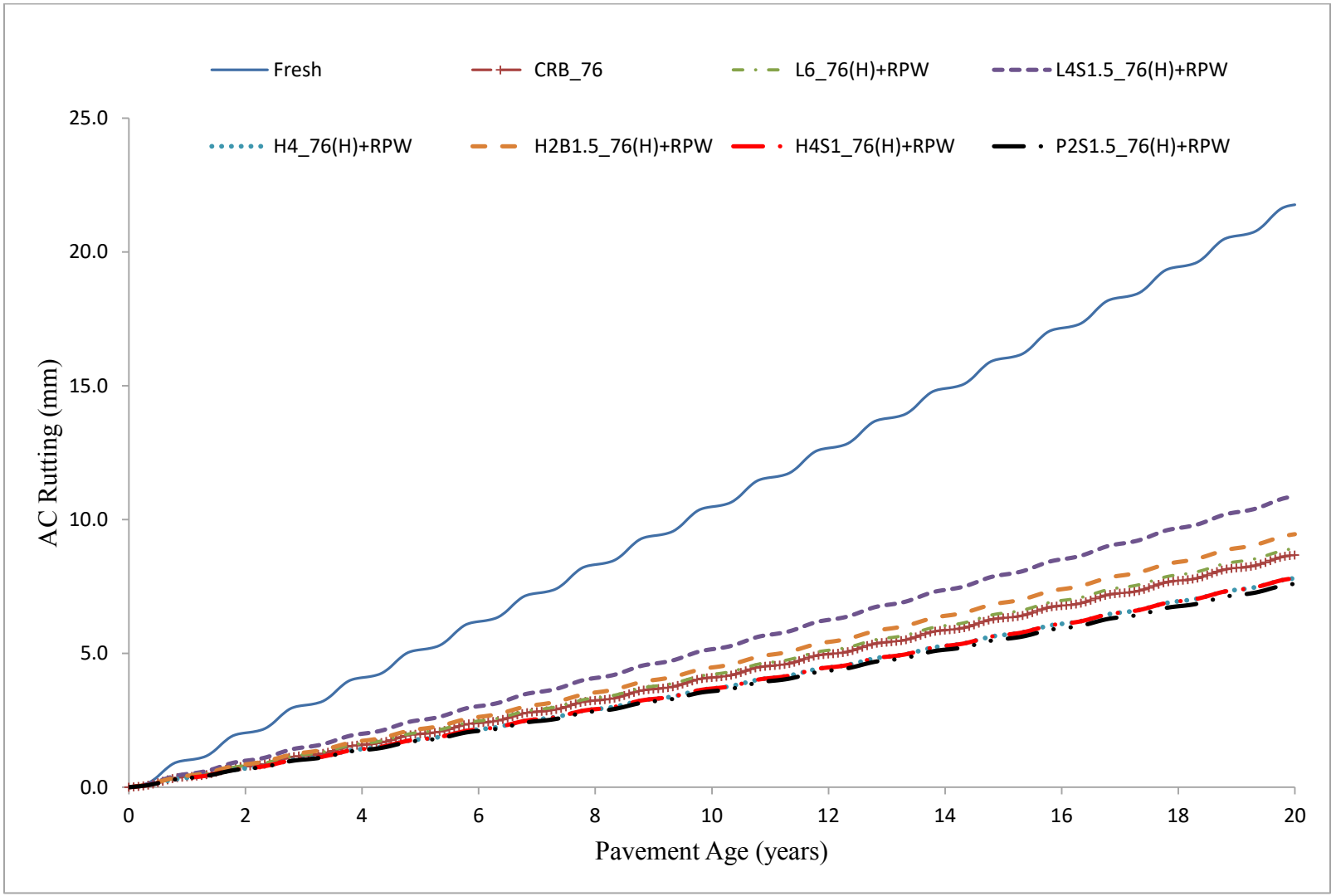

Figure 4.64: Rutting Performance simulation of Hybrid-RPW-AC.

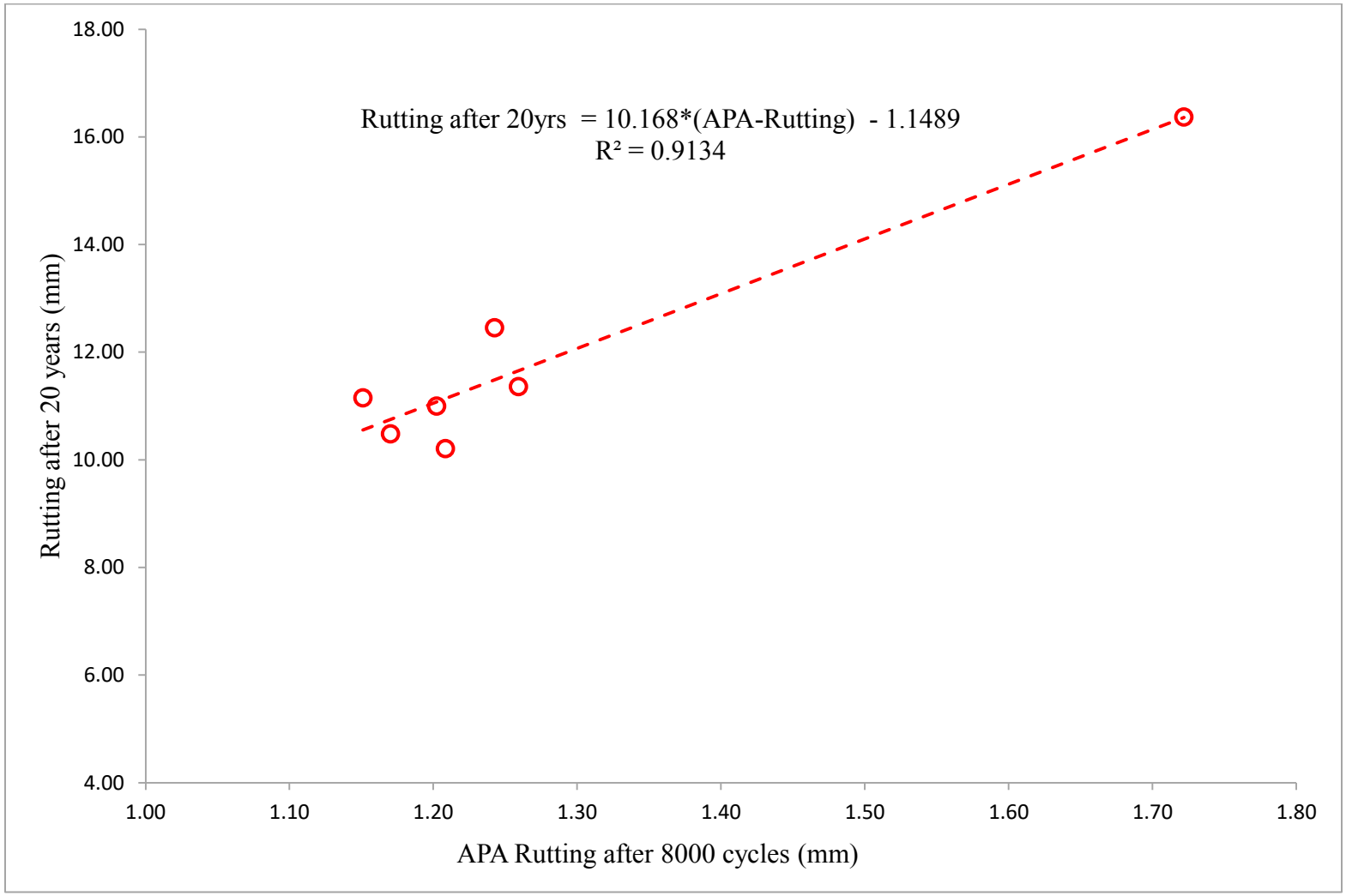

Figure 4.65: Correlation between rutting after 20yrs and laboratory APA rutting results.

Figure 4.66 shows the bottom-up fatigue cracking distress for the reference ACs and hybrid-RPW-ACs. The H4_76(H)+RPW, H4S1_76(H)+RPW and P2S1.5_76(H)+RPW showed lower alligator cracking than the CRB_76(H) and the remaining AC mixtures. This observation is in agreement with the laboratory fatigue test results for controlled stress. Similar performance hierarchy was observed in the dynamic master curve (Figure 4.54) for the hybrid-RPW-AC at higher loading time. Figure 4.67 shows the corresponding longitudinal (surface-down) cracking for the hybrid-RPW-AC. Similar trend as observed for the alligator cracking can also be seen in the surface-down cracking. However, the AC mixtures showed a negligible amount of longitudinal cracking, which is typical of rutting-resistant AC.

The fatigue models developed for the various AC mixture was used to check the observed trends for the AASHTO fatigue model. Using the standard axle configuration, the critical strain was obtained at the bottom of the AC layer, 20 cm below the surface, directly under the wheel load. These critical load responses was incorporated into the developed fatigue models (Table 4.16) for the percent consumed fatigue life estimation. The ratio of the cumulative ESAL at 10, 16 and 20 years to the allowable (fatigue life) was obtained. Table 4.19 presents the percentage of the consumed fatigue life of the various ACs at different time within their design periods. The last column of Table 4.19 shows the induced strain at the bottom of each AC layer, obtained at intermediate temperature. The induced strains are all below 100 μst, a range where the crumb rubber AC (CRB_76) can compete with the hybrid-RPW AC mixtures. Figure 4.68 shows the fatigue life deterioration plots for the various ACs. As previously observed from the laboratory fatigue test analysis, all the hybrid-RPW AC mixtures showed more fatigue

endurance than the fresh AC. Most of the hybrid-RPW AC mixtures (H4S1_76(H)+RPW, P2S1.5_76(H)+RPW and H4_76+RPW) outperformed the CRB_76 AC mixture with respect to fatigue failure resistance. H4S1_76(H)+RPW showed the highest resistance to fatigue failure, this was also observed from the laboratory fatigue test results. These results is in good agreement with the previous trend observed for the predicted bottom-up and top-down fatigue results using the AASHTO method.

Table 4.19: Percentage of Fatigue Life Consumed for the Various Pavements

AC Type /Age (years)	10	16	20	Induced Strain (μst)
H4_76(H)+RPW	1.448%	3.722%	6.204%	-44.7876
H4S1_76(H)+RPW	0.064%	0.164%	0.274%	-44.1072
H2B1.5_76(H)+RPW	3.868%	9.945%	16.575%	-49.374
L6_76(H)+RPW	2.638%	6.783%	11.304%	-49.4172
L4S1.5_76(H)+RPW	3.132%	8.053%	13.421%	-55.3068
P2S1.5_76(H)+RPW	1.192%	3.065%	5.108%	-42.4944
CRB_76+RPW	1.667%	4.285%	7.142%	-53.3988
Fresh AC	9.751%	25.075%	41.792%	-85.7988

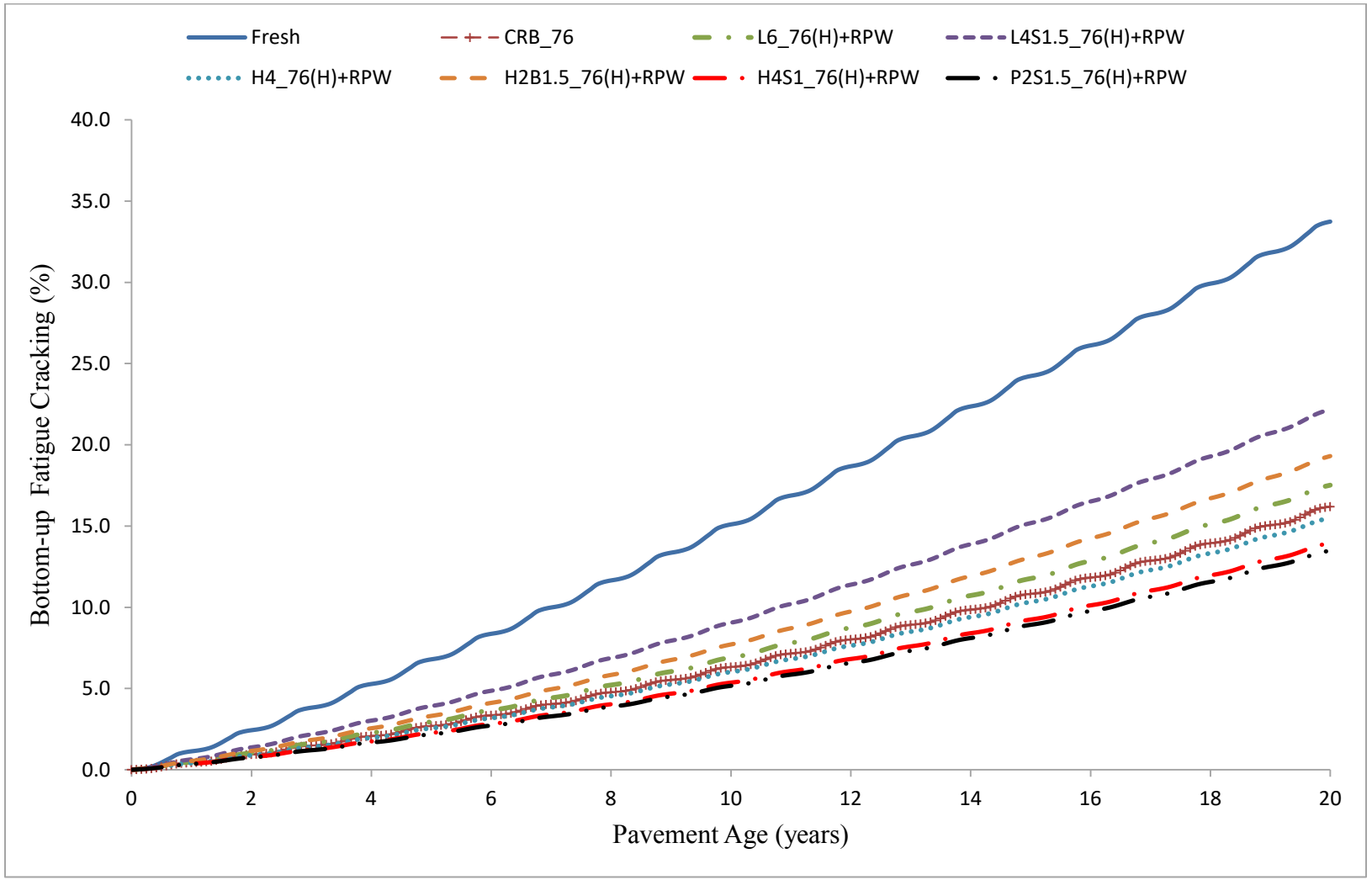

Figure 4.66: Bottom-up (Alligator) Cracking Performance of the Hybrid-RPW-ACs.

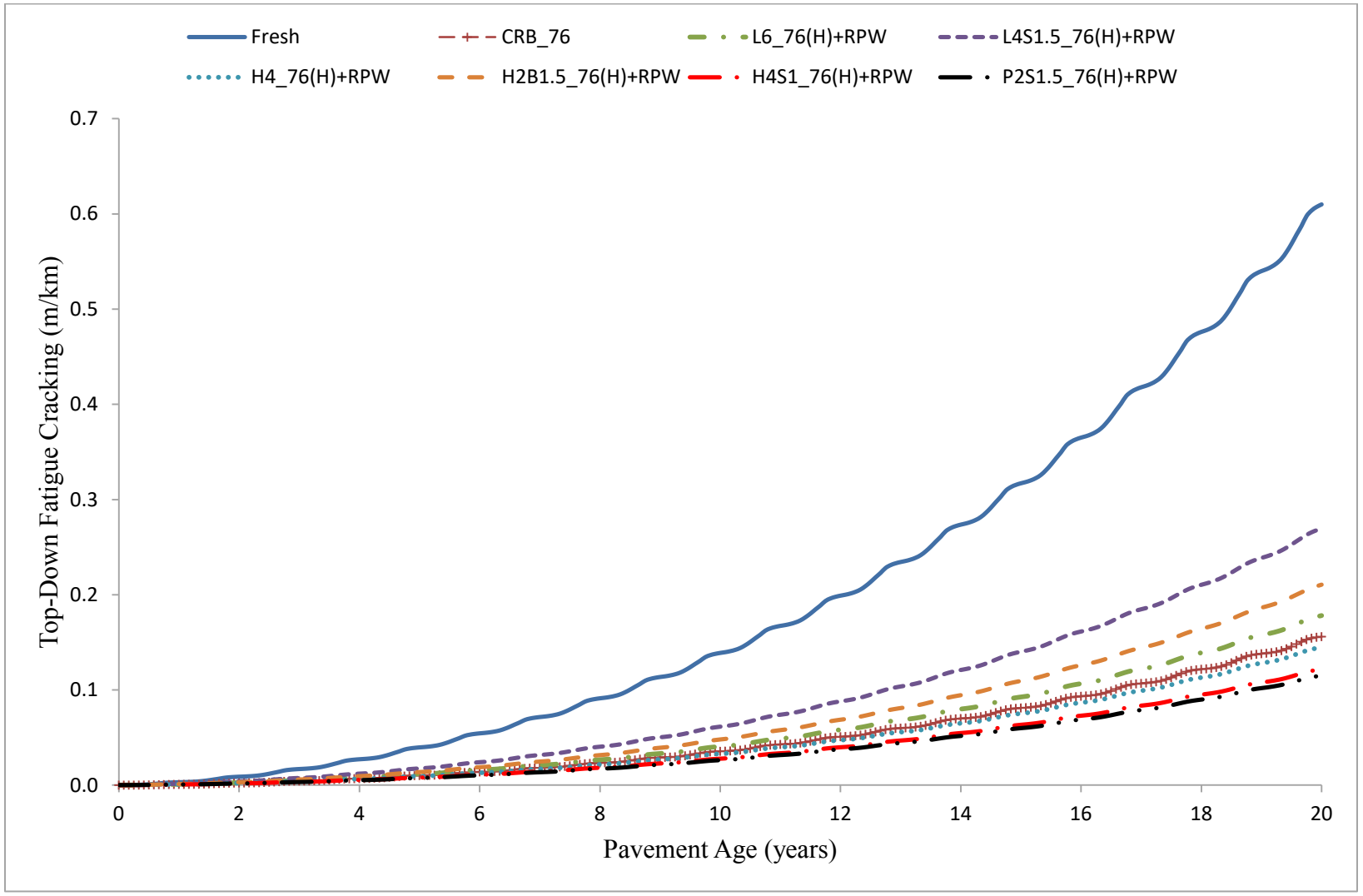

Figure 4.67: Surface Down Longitudinal Cracking Performance of the Hybrid-RPW-ACs.

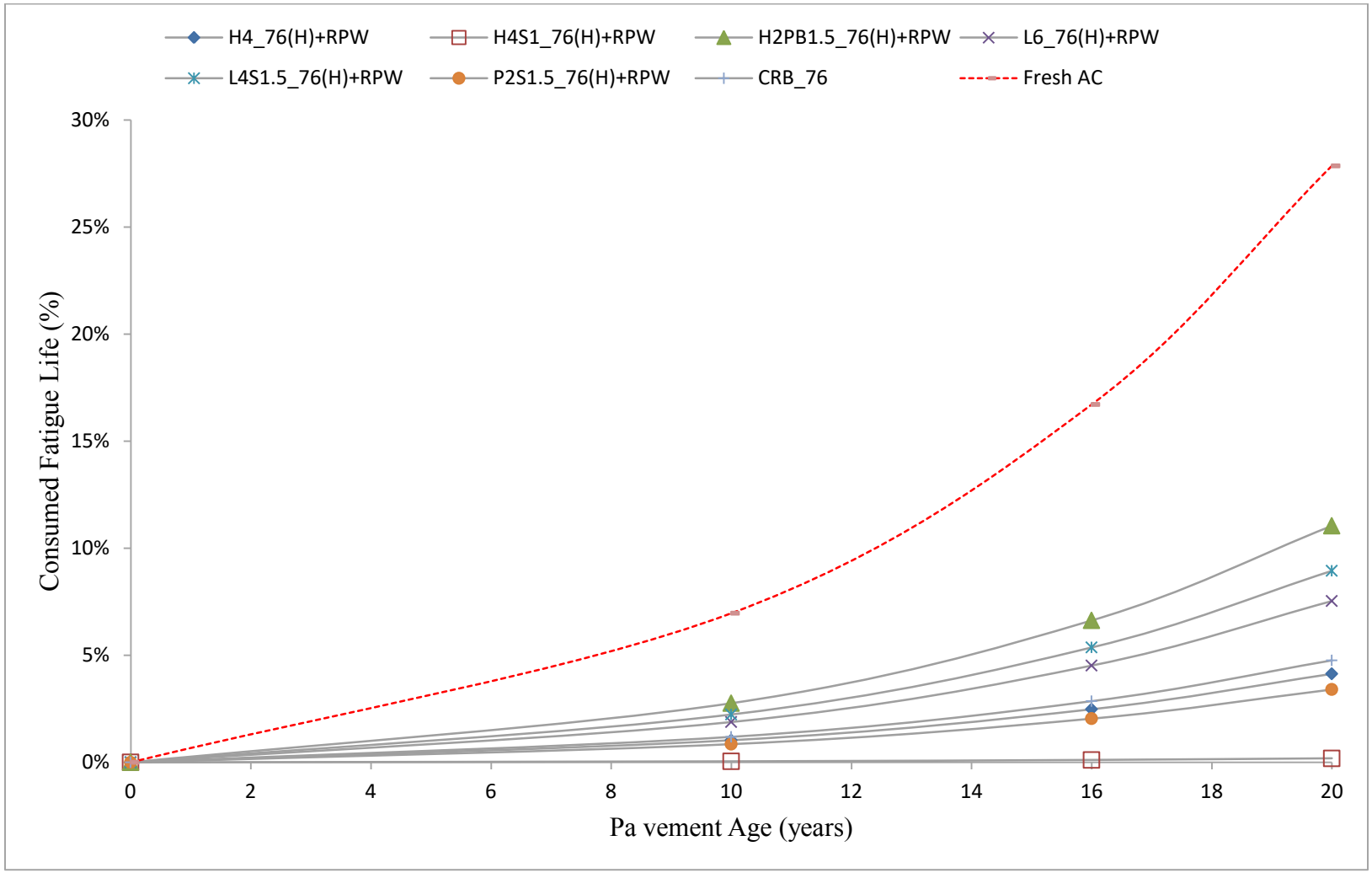

Figure 4.68: Percent Fatigue Life Consumed vs. Time for Hybrid-RPW-ACs.

4.9 ECONOMIC AND ENVIRONMENTAL BENEFITS OF RPW-ASPHALT CONCRETE

A comparative economic and environmental analysis in terms of initial material cost, carbon and non methyl volatile organic compound (NMVOCs) emission was conducted for the various RPW modified asphalt, with respect to conventional virgin polymers asphalt binder and reference CRB. The estimate was limited to the binder due to the fact that only an overall life cost cycle analysis could reflect the value of the RPW replacement of the mineral aggregate. The mineral aggregate is cheaper than the RPW aggregate. But the extended life cost savings due to the RPW aggregate should offset this material cost.

4.9.1 COST ANALYSIS

Based on the market price of recycled plastic and the virgin polymer, a comparative study has been conducted. The amount of polymer (recycled and virgin) required to reach HPT of 82^{o}C and 76^{o}C was determined. The initial polymer cost for six different PW-modified asphalt with 82^{o}C HPT was estimated and compared to two conventional PMA containing only SBS and PB virgin polymers, in Figure 4.69. Generally, a 15% or more saving in initial cost of material could be made when PW is used as a supplement or replacement of either SBS or PB. As high as 20% and 25% of the of polymer cost could be reduced if SBS and PB should be completely replace by RHDPE, respectively.

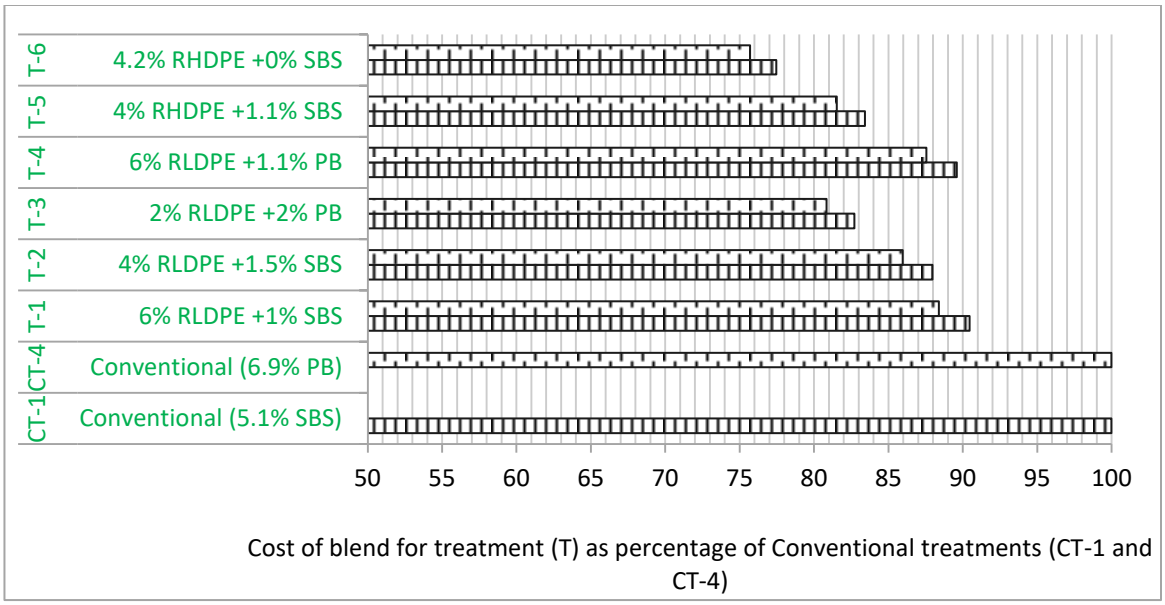

Figure 4.69: Cost Comparison of PW-Asphalt with Conventional Virgin Polymer Asphalt for 82ºC HPT.

Figure 4.70 showed the cost comparison plots of another 6 potential PW-modified asphalt with 76^{o}C HPT. The low material cost of recycled plastic should be anticipated. But the significant saving in the initial polymer cost of the modified asphalt associated with replacing the conventional SBS or PB cannot be overlooked. Similar cost cutback of 22% is also observed for the 76^{o}C HTP set of treatments.

The relatively large quantity of CRB required to achieve the same PG as the RPW, has counterbalanced the lower price advantage of the CRB over the RPW. Figure 4.71 shows cost comparison of some purely RPW-modified asphalt binders with conventional CRB_76 and CRB_82 blends equivalents. It can be seen that most of the RPW-modified asphalt binders are cheaper in terms of initial polymer cost. However, the cheaper price of the CRB and the comparably larger amount needed has a better tendency of increasing quantity of the modified asphalt produced.

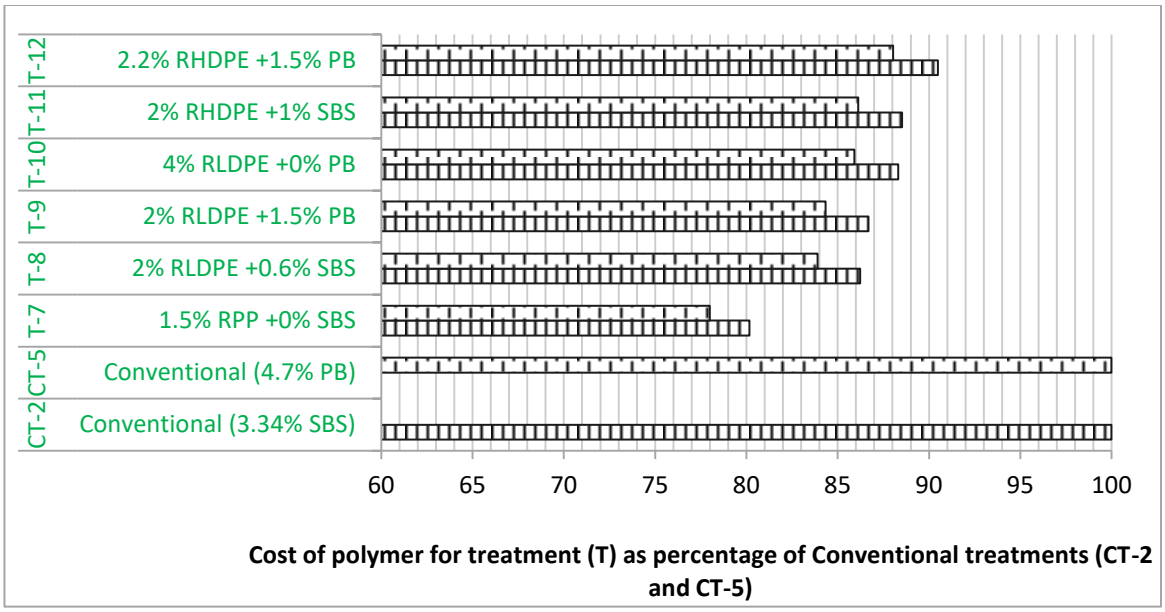

Figure 4.70: Cost Comparison of PW-Asphalt with Conventional Virgin Polymer Asphalt for 76ºC HPT.

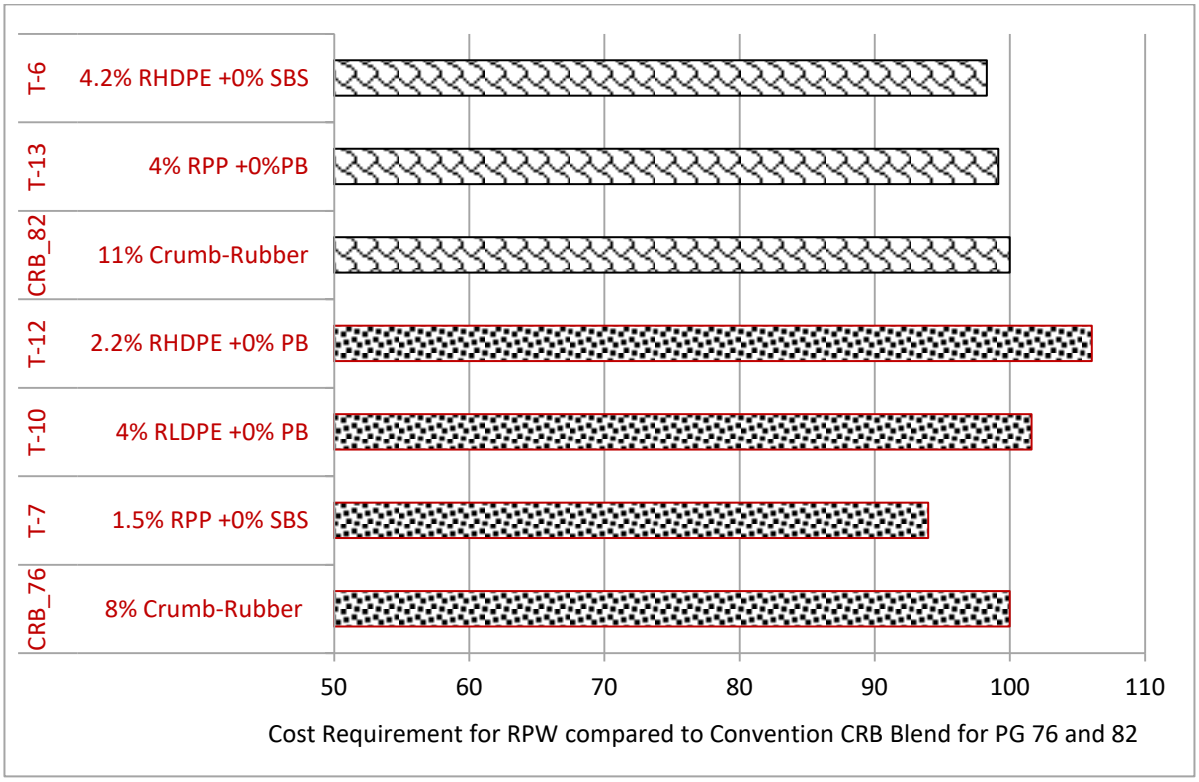

Figure 4.71: Cost Comparison of PW-Asphalt with Conventional Crumb Rubber Asphalt for PG 76 and 82.

4.9.2 ENVIRONMENTAL BENEFITS

Global asphalt demand was estimated at around 120 Million metric tons, with an annual appreciation forecast of approximately 4% from 2015 [84]. The combined KSA annual asphalt consumption both from importation and local refineries was estimated at around 4.6 Million metric tons [85]. Eighty five percent of these asphalt goes in to road construction, while roofing, waterproofing and other miscellaneous activities consume the rest [13, 84]. On average [13], six percent polymer equivalent of 80% of the road construction asphalt is required for the major KSA cities. Which Means, KSA annual polymer demand for road construction amounts to 187,680 tons, as of 2015. However, the plastic waste generated each year is more than 7 times the current virgin polymer demand. Manufacturing a single ton of any commercial polymer from virgin source is accompanied by major environmental emissions (see Table 3.10). Carbon and NMVOCs emission are few but critical among the substances emitted during these manufacturing processes.

Figure 4.72 shows the CO_2 and NMVOCs emissions that will results annually if the selected treatments of PW-asphalt with 82^{o}C HPT and if the incorporated PW were to be replaced by their exact virgin equivalent, are to be used as asphalt polymer modification options in KSA. Their equivalent conventional PMA emission results are also shown. The emission gap between the PW-modified asphalt binder compared to either the conventional PMA or an exactly virgin polymer equivalent of each treatment is too wide to ignore. Some of the PW-asphalts have negligible CO_2 and NMVOCs emission. This is the green way, the answer to challenges of the modern construction

approaches. Adopting this alternative polymer modification could eliminate up to 500,000 million metric ton of carbon emission and 500 tons of non-methane volatile organic compounds from our precious atmosphere every year. In general, 27 million metric tons of carbon emission could be prevented, for each ton of virgin polymer replaced with recycled one. Similar but relatively lower emission cutbacks could be observed for treatments with 76°C HPT as shown in Figure 4.73. This is due to fact the quantity of polymer required to achieve 82°C HPT is higher than that required for 76°C. In all cases, tremendous amount of CO_2 and NMVOCs could be eliminated if the right treatment is selected.

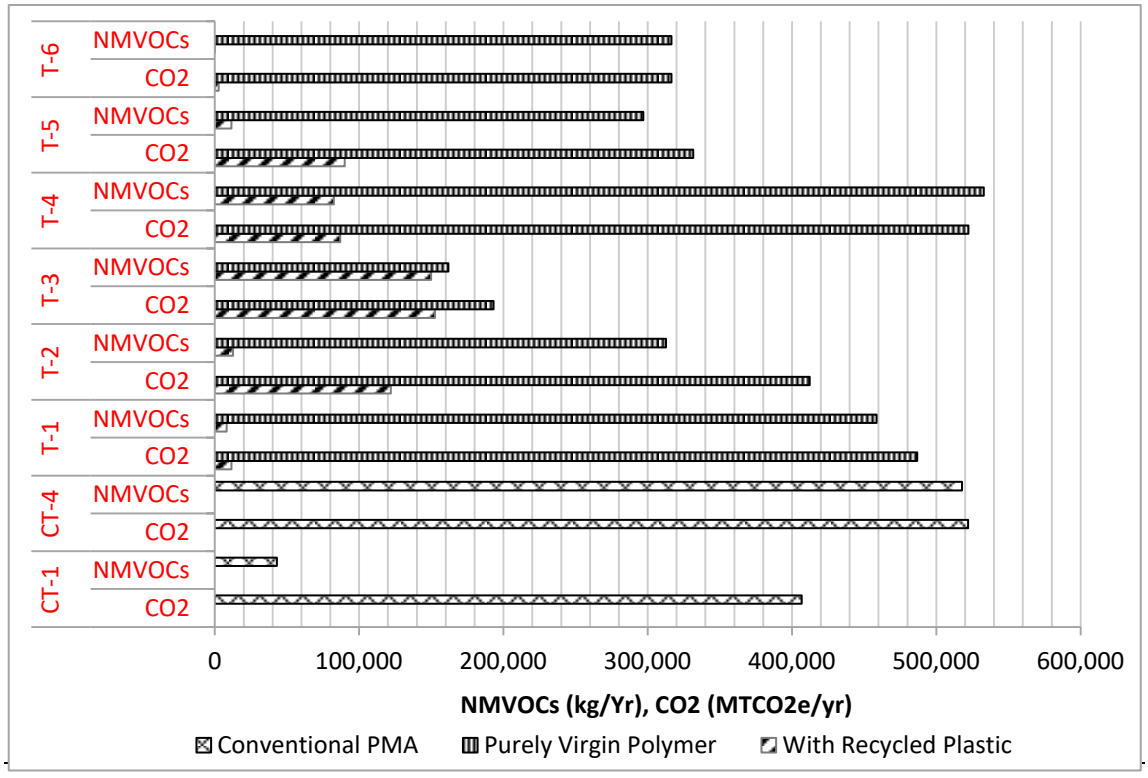

Figure 4.72: Emission Analogy for Treatments Meeting 82°C HPT.

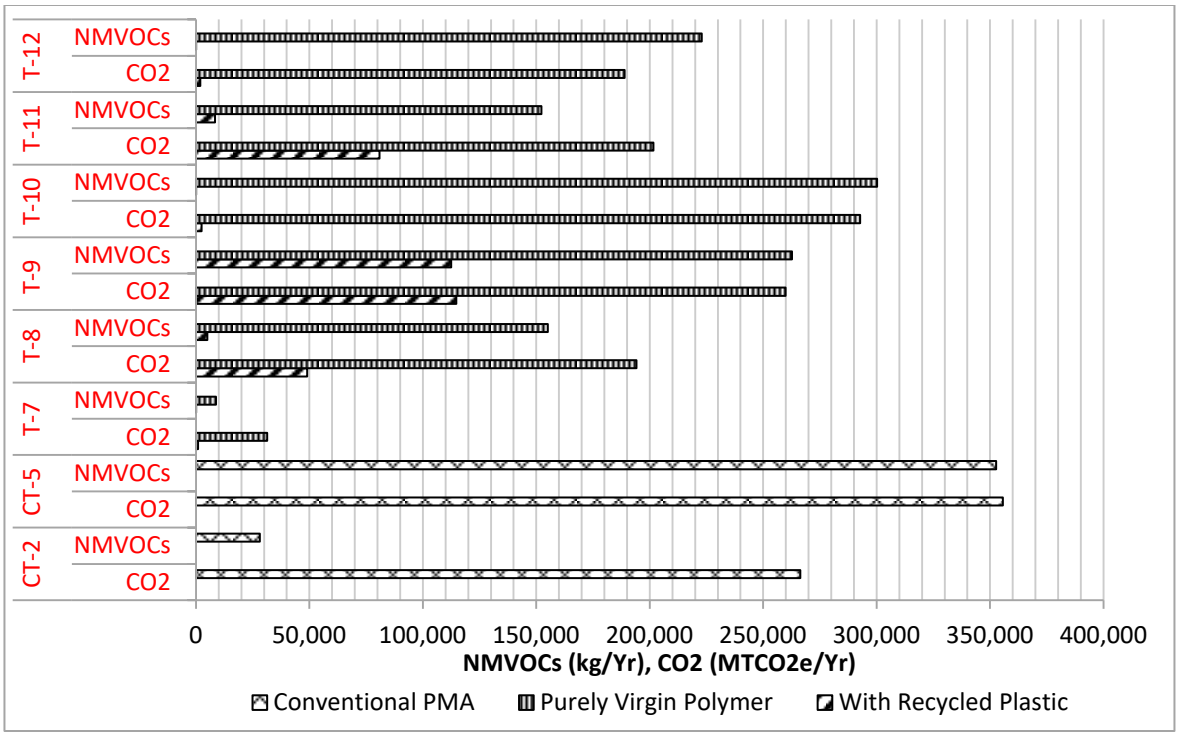

Figure 4.73: Emission Analogy for Treatments Meeting 76°C HPT.

Summary: The use of RPW as a supplement and replacement of virgin polymer in modification of Arabian asphalt has been studied. Significant improvements in the rutting parameter which directly translate in to an improved high temperature performance of the RPW-modified asphalt binder was observed. Although the RPWs yielded blends with higher and better PG than the local neat binder, these RPWs need to be supplemented by some amount of elastomeric polymer In order to compensate for their lack of elastic recovery. The RHDPE and RLDPE could be utilized along with an elastomeric SBS to achieve a higher recovery and strain resistance, than that which could be achieved if same amount of SBS alone is used. RPP below 2% content is only stable under mild agitation, and content above 2% will lead to an unstable modified asphalt binder. However, RHDPE and RLDPE modified asphalt binders for RHDPE content below 4% and RLDPE content below 6%, have shown good storage stability. Up to 25%

saving in initial cost of material could be made when PW is used as a supplement or replacement of virgin polymer. The RPW size ranging between No. 8 to No. 40 was found to be the best for RPW AC modification via aggregate substitution. The optimum RPW aggregate content was observed to be 9.5% by weight of the mineral aggregate. The RPW aggregates-containing ACs are viscoelastically superior to the RPET-only aggregate-containing AC mixtures. None of the hybrid RWP-aggregate mixture flowed within the standardized FN test period of 10,000 seconds. The hybrid-RPW ACs have also showed better resistance to permanent deformations than the CRB_76 when subjected to repeated wheel load test using the APA. The melted thermoplastic RPW waste aggregates in the fresh+RPW mix have further reinforced the aggregate-aggregate and aggregate-mastic interfaces. These interfaces are where the fatigue cracks initiates, before propagating into the AC core. The delay in the crack initiation has added to the fatigue life of the fresh+RPW AC. The significant improvement in fatigue life of the hybrid-RPW ACs is mainly due to the RPW aggregate content of the mixtures. The simulation results further confirms inferences made from laboratory test results that the hybrid-RPW ACs are only superior to the CRB_76 AC for higher loading time scenario. This fact indicates that the hybrid-RPW AC are much suitable to a predominantly hot climate location.

CHAPTER 5

CONCLUSIONS AND RECOMMENDATIONS

This chapter summarizes the conclusive findings from the phases and independent subheadings of this study. The first subheading presents RPW binder modification discoveries, where excellent PG and rutting parameters were observed for a relative cheaper RPW-modified asphalt binder. The major findings on the hybrid RPW-AC fatigue and rutting performance was summarized in the next following subheading. Finally the overall findings on the effect of tertiary deformation length on FN, and the new proposed FN refinement method was presented.

5.1 RPW Modification of Asphalt binder

The use of RPW as a supplement and replacement of virgin polymer in modification of Arabian asphalt has been studied. Majority of the asphalt RPW-asphalts demonstrate excellent constructability in terms of high temperature viscosity. Significant improvements in the rutting parameter which directly translate in to an improved high temperature performance of the RPW-modified asphalt binder was observed.

Most of the RPWs modified asphalt met the superpave viscosity requirement. Asphalt blends containing more than 4% RHDPE and in addition to SBS did not meet the super-pave viscosity criteria. Blends containing more than 6% RLDPE in addition to SBS failed to pass the viscosity criterion. Eight percent RPP blend containing more than 0.5%

SBS, 6% and 4% RPP blend in combination with SBS above 1.5% did not pass the super-pave viscosity limit criterion

It can be concluded that the upper PG limit increases by almost one level for every 2% increase in the RLDPE or RHDPE content. The improvement of the rutting performance indicator is more significant in the RHDPE samples than in the RLDPE and RPP blends. Although the RPWs yielded blends with higher and better PG than the local neat binder, all the RPWs could not meet the elastic recovery requirement for polymer modified asphalt binder set by AASHTO TP 70. In order to compensate for their lack of elastic recovery, these recycled plastic waste need to be supplemented by some amount of elastomeric polymer.

All the RPWs yields modified asphalt with improved high temperature performance. Even though the RPWs modified binders lack sufficient strain recovering ability, RLDPE and RHDPE could be utilized along with an elastomeric SBS to achieve a higher recovery and strain resistance, than that which could be achieved if same amount of SBS alone is used. Further investigation into the lower temperature performance of these RPWs modified asphalt combinations for regions with extremely low temperature climate is recommended.

RPP below 2% content is only stable under mild agitation, and content above 2% will lead to an unstable modified asphalt binder. Addition of an elastomeric SBS and Plastomeric PB minimize the early separation of RPP modified asphalt binder, but does not necessarily yield stable asphalt binders. As they have shown a potential degrading tendency with time. RHDPE and RLDPE modified asphalt binders (for RHDPE content

below 4% and RLDPE content below 6%) whether containing either SBS or PB have shown good storage stability trait under mild agitation, both in terms of time degradation and separation.

All the presented RLDPE-SBS and RLDPE-PB modified asphalts have met 70^{o}C upper service temperature requirement, a requirement for Medina, Riyadh and Makkah. Two percent rHDPE is enough to satisfy 70^{o}C high temperature performance requirement when utilized to modify the Arab asphalt binder. Much adverse high temperature climate like that of the KSA eastern province requires atleast 3.5% rHDPE modified asphalt binder to satisfy its high temperature specification. Only Two percent of rPP is required to yield similar asphalt binder that can endure 76^{o}C high temperature asphalt binder performance limit.

Up to 25% saving in initial cost of material could be made when PW is used as a supplement or replacement of virgin polymer. As high as 20 and 22% of the polymer cost could be reduced, should RHDPE be used as complete replacement. Adopting recycling alternative of polymer modification in KSA alone could eliminate up to 500,000 million metric ton of carbon emission and 500 tons of non-methane volatile organic compounds every year. In general, 27 million metric tons of carbon emission could be prevented, for each ton of virgin polymer replaced with recycled one.

5.2 Rutting and Fatigue Performance of Hybrid RPW-AC

The combined RPW waste from households in Thuqba and Doha, Dhahran KSA was estimated to approximately consist of 33.7% RPET, 25% RHDPE, 3.8% RPVC, 17.1% RLDPE, 11.6% RPP and 8.8% RPS. This composition was employed for RPW aggregate in this study.

Based on experimental parameters like RM and ITS, the S2 (No. 8 to No. 40) RPW appeared to be the best RPW size range, and was adopted for all the RPW AC modification via aggregate substitution.

According to the observed trend of RPW content effect on the RM, ITS and RSI of the AC, none of the mentioned test parameter is reliable or capable of clearly showing an optimum RPW aggregate content. However the FN test has proved adequate in this regard, and the optimum RPW aggregate content was observed to be 9.5%.

It has been observed that the ACs containing combined RPW aggregates are viscoelastically superior to the RPET-only aggregate-containing AC mixtures. All the Hybrid-RPW-ACs showed higher dynamic modulus than the conventional crumb rubber modified binder mix (CRB_76) at lower loading frequency (slow traffic), a loading time range that is the most detrimental for the AC. The CRB_76 is the RPW-mix equivalent that is currently being used and recommended for road construction in KSA. However, the CRB_76 exhibited a higher modulus at higher loading frequency only, a loading rate range that imposes the least damage to the AC.

None of the hybrid RWP-ACs flowed within the standardized FN test period of 10,000 seconds. While the main reference mixture (CRB_76) shows a relatively very early flow at 1117 seconds. The hybrid RPW-ACs also showed better resistance to permanent deformations than the CRB_76 when subjected to repeated wheel load test using the APA. However, they exhibited approximately the same deformation trends and all are far away from the deformation limit of 6 mm (within one-third of the limit).

As expected, the CRB_76 possessed longer fatigue life than the fresh AC. However, the presence of the RPW aggregate in the fresh+RPW mix has more than doubled the fresh AC fatigue life. The melted thermoplastic RPW waste aggregates in the fresh+RPW mix have further reinforced the aggregate-aggregate and aggregate-mastic interfaces. These interfaces are where the fatigue cracks initiate before propagating into the AC core. The delay in the crack initiation has added to the fatigue life of the fresh+RPW AC.

The hybrid-RPW-ACs fatigue performance are not far beyond that of the fresh+RPW mix. In fact of the hybrid-RPW-ACs fatigue life performance is a little below that of the fresh+RPW AC. This clear indicates that the significant improvement in fatigue life of the ACs containing RPW aggregates is mainly due to the RPW aggregate content of the mixtures.

Below are the outline of the major strain controlled fatigue test findings in details:

- H4_76(H)+RPW mix showed the highest fatigue life among the hybrid-RPW-ACs at applied tensile strain level above 730 µst, while H4S1_76(H)+RPW out perform all the hybrid-RPW-ACs at 730 µst tensile strain and below. The presence of the

1% elastomeric SBS polymer in the H4S1_76(H)+RPW is responsible for its overall improvement in fatigue performance. It is important to note that both H4S1_76(H)+RPW and H4_76(H)+RPW have similar gradation (G2).

- It can also be noted that for hybrid-RPW-ACs with G1 aggregate structure, that L4S1.5_76(H)+RPW outperform the L6_76(H)+RPW at all strain level. This has further confirmed the previous observation that hybrid-RPW-ACs with elastomeric SBS content tend to have better fatigue resistance.
- P2S1.5_76(H)+RPW AC mix (with G1 aggregate structure) shows the least fatigue life among all the hybrid-RPW-ACs. This outcome cannot be disassociated with the unstable and high stiff nature of the RPP modified asphalt binder.
- H2B1.5_76(H)+RPW (with G1 aggregate structure) is the second least performing hybrid-RPW-ACs after P2S1.5_76(H)+RPW AC mix.
- All the hybrid-RPW-ACs showed better fatigue performance than the CRB_76 at applied tensile strain level above 150 µst.
- All the hybrid-RPW-ACs demonstrated higher fatigue resistance than the fresh AC mix at applied strain above 100 µst. As 100 µst is a strain level within the vicinity of the fatigue endurance limit for conventional AC mix (75 µst), it can be said that all the hybrid-RPW-ACs possessed better fatigue resistance than the fresh AC.

Below are the outline of the major stress controlled fatigue test findings in details:

- The CRB_76 AC has better fatigue resistance than the fresh at measured applied strain above 140 µst, while the Fresh+RPW AC also out-perform the CRB_76 at strain above 140 µst. However, there was intersection between the CRB_76(H) and Fresh

Mix AC fatigue performance curve in the stress versus load repetition curve . It should be noted that these AC mixtures have similar aggregate gradation, G1.

- All the hybrid-RPW-ACs showed better fatigue resistance than the CRB_76 at induced strain level above 120 μst. However, this measured strain could possibly correspond to a low applied stress not capable of inducing cumulative fatigue damage.
- The best performing mix among the hybrid-RPW-ACs is H4S1_76(H) at strain level below 650 μst. But the Fresh+RPW AC showed better performance above this strain level.
- As previously observed in the stain controlled test results. The least performing AC mix among the hybrid-RPW-ACs is the P2S1.5 above 270 μst induced strain. But H2B1.5_76(H)+RPW showed the least fatigue performance below 270 μst.

The 20-year simulation results of the RPW modified AC has shown an overall excellent performance of the RPW modified binder AC mixture, in terms of rutting and fatigue damage for low intermediate and high temperature climate. It can be concluded that the RPW modified binder AC mixtures showed satisfactory performance for the harshest climate in KSA. The simulation results further confirms inferences made from laboratory test results that most of the hybrid-RPW ACs are superior to the CRB_76 AC for higher loading time scenario (i.e. high temperature, or slow traffic or both). This brings us to the conclusion that the hybrid-RPW AC are much suitable to a predominantly hot climate location.

Summary: The lack of elastic recovery on the purely RPW modified binders was successfully improved by incorporating minor proportion of elastomeric virgin polymer (SBS). Even though the RPWs modified binders lack sufficient strain recovering ability, RLDPE and RHDPE could be utilized along with an elastomeric SBS to achieve a higher recovery and strain resistance, than that which could be achieved if same amount of SBS alone is employed. Some of the RPP modified asphalt binder (content above 2%) were found to be unstable. A RPW size ranging between No. 8 and No. 40 was found to be the best for AC modification via aggregate substitution. An optimum RPW AC aggregate substitute of 9.5% was established. All the RPW-aggregate containing mixtures showed higher dynamic modulus than the conventional crumb rubber modified binder mix (CRB_76) at lower loading frequency. None of the hybrid RWP-aggregate mixture flowed within the standardized FN test period of 10,000 seconds. The presence of the RPW aggregate in the fresh+RPW mix has more than doubled the fresh AC fatigue life. Adopting recycling alternative of polymer modification in KSA alone could eliminate up to 500,000 million metric tons of carbon emission and 500 tons of non-methane volatile organic compounds every year. The 20 years simulation results of the RPW modified AC has shown an overall excellent performance of the RPW modified binder AC mixture. The simulation results further confirms inferences made from laboratory test results that the hybrid-RPW ACs are only superior to the CRB_76 AC for higher loading time scenario (i.e. high temperature, or slow traffic or both). Finally, it is concluded that the hybrid-RPW AC are much suitable to a predominantly hot climate location.

References

1. Zafar, S. *Solid Waste Management in Saudi Arabia. EcoMena Articles*. 2013; Available from: http://www.ecomena.org/solid-waste-management-in-saudi-arabia/.

2. Rahman, F., et al., *Catalytic Processing of Waste Plastics With/Without Petroleum Resid—An Economic Evaluation.* Energy Sources, Part A: Recovery, Utilization, and Environmental Effects, 2006. **28**(15): p. 1353-1363.

3. Al-Abdul Wahhab, H.I., et al., *Development of performance-based bitumen specifications for the Gulf countries.* Construction and Building Materials, 1997. **11**(1): p. 15-22.

4. Ouda, O.K.M. and H.M. Cekirge, *Roadmap for Development of Waste-to Energy Facility in Saudi Arabia.* American Journal of Environmental Engineering, 2013. **3**(6): p. 6.

5. Huang, Y., R.N. Bird, and O. Heidrich, *A review of the use of recycled solid waste materials in asphalt pavements.* Resources, Conservation and Recycling, 2007. **52**(1): p. 58-73.

6. Scott, G., *'Green' polymers.* Polymer Degradation and Stability, 2000. **68**(1): p. 1-7.

7. Thompson, R.C., et al., *Plastics, the environment and human health: current consensus and future trends.* Philosophical Transactions of the Royal Society of London B: Biological Sciences, 2009. **364**(1526): p. 2153-2166.

8. Mubaraki, M.A., *Predicting Deterioration for the Saudi Arabia Urban Road Network*, in *Civil Engineering*. 2010, University of Nottingham: Nottingham. p. 271.

9. Dalhat, M.A. and H.I. Al-Abdul Wahhab, *Performance of Recycled Plastic Wastes Modified Asphalt binder in Saudi Arabia.* International Journal of Pavement Engineering. DIO: 10.1080/10298436.2015.1088150, 2015.

10. Al-Abdul-Wahhab, H.I., et al. *Adaptation Of Shrp Performance Based Binder Specifications To The Gulf Countries*. in *Proceedings of the 4th Saudi Engineering Conference*. 1995: KAU.

11. Al-Dubabe, I.A., et al., *Polymer Modification of Arab Asphalt.* Journal of Materials in Civil Engineering, 1998. **10**(3): p. 161-167.

12. Al-Abdul-Wahhab, H.I., et al., *Performance Modification of Saudi Asphalt Binder Using SABIC Polymer*, in *Sixth Saudi Engineering Conference*. 2002, KFUM: Dhahran p. 15.

13. Zhu, J., B. Birgisson, and N. Kringos, *Polymer modification of bitumen: Advances and challenges.* European Polymer Journal, 2014. **54**: p. 18-38.

14. Gourmelon, G., *Global Plastic Production Rises, Recycling Lags*. 2015, World Watch Institute: Washington, D.C. p. http://www.worldwatch.org/global-plastic-production-rises-recycling-lags-0.

15. Wong, S.L., et al., *Current state and future prospects of plastic waste as source of fuel: A review.* Renewable and Sustainable Energy Reviews, 2015. **50**: p. 1167-1180.

16. Ouda, O.K.M., et al., *Waste-to-energy potential in the Western Province of Saudi Arabia.* Journal of King Saud University - Engineering Sciences, 2015. **http://dx.doi.org/10.1016/j.jksues.2015.02.002**.

17. Katami, T., et al., *Formation of PCDDs, PCDFs, and Coplanar PCBs from Polyvinyl Chloride during Combustion in an Incinerator.* Environmental Science & Technology, 2002. **36**(6): p. 1320-1324.

18. Saikia, N. and J. de Brito, *Use of plastic waste as aggregate in cement mortar and concrete preparation: A review.* Construction and Building Materials, 2012. **34**: p. 385-401.

19. Siddique, R., J. Khatib, and I. Kaur, *Use of recycled plastic in concrete: A review.* Waste Management, 2008. **28**(10): p. 1835-1852.

20. Yildirim, Y., *Polymer modified asphalt binders.* Construction and Building Materials, 2007. **21**(1): p. 66-72.

21. Casey, D., et al., *Development of a recycled polymer modified binder for use in stone mastic asphalt.* Resources, Conservation and Recycling, 2008. **52**(10): p. 1167-1174.

22. Yildirim, Y., D. Hazlett, and R. Davio, *Toner-modified asphalt demonstration projects.* Resources, Conservation and Recycling, 2004. **42**(3): p. 295-308.

23. Fang, C., et al., *Combined modification of asphalt with polyethylene packaging waste and organophilic montmorillonite.* Polymer Testing, 2012. **31**(2): p. 276-281.

24. Ho, S., et al., *Study of recycled polyethylene materials as asphalt modifiers.* Canadian Journal of Civil Engineering, 2006. **33**(8): p. 968-981.

25. Murphy, M., et al., *Bitumens modified with recycled polymers.* Materials and Structures, 2000. **33**(7): p. 438-444.

26. Ahmadinia, E., et al., *Performance evaluation of utilization of waste Polyethylene Terephthalate (PET) in stone mastic asphalt.* Construction and Building Materials, 2012. **36**(0): p. 984-989.

27. Baghaee Moghaddam, T., M.R. Karim, and T. Syammaun, *Dynamic properties of stone mastic asphalt mixtures containing waste plastic bottles.* Construction and Building Materials, 2012. **34**(0): p. 236-242.

28. Gandjidoust, H., A. Hassani, and A.A. Maghanaki, *Use of plastic waste (poly-ethylene terephthalate) in asphalt concrete mixture as aggregate replacement.* Waste Management and Research, 2005. **23**(4): p. 322+.

29. Zoorob, S.E. and L.B. Suparma, *Laboratory design and investigation of the properties of continuously graded Asphaltic concrete containing recycled plastics aggregate replacement (Plastiphalt).* Cement and Concrete Composites, 2000. **22**(4): p. 233-242.

30. Fang, C., et al., *UV-Aging Resistance of Packaging Waste PE Modified Asphalts.* Polymer-Plastics Technology and Engineering, 2009. **48**(9): p. 945-949.

31. Sangita, et al., *Effect of waste polymer modifier on the properties of bituminous concrete mixes.* Construction and Building Materials, 2011. **25**(10): p. 3841-3848.

32. García-Morales, M., et al., *Linear Viscoelasticity of Recycled EVA-Modified Bitumens.* Energy & Fuels, 2003. **18**(2): p. 357-364.

33. Singh, B., M. Gupta, and H. Tarannum, *Mastic of polymer-modified bitumen and poly(vinyl chloride) wastes.* Journal of Applied Polymer Science, 2003. **90**(5): p. 1347-1356.

34. Fang, C., et al., *Modification of waterproofing asphalt by PVC packaging waste.* Journal of Vinyl and Additive Technology, 2009. **15**(4): p. 229-233.

35. Navarro, F.J., et al., *Bitumen modification with reactive and non-reactive (virgin and recycled) polymers: A comparative analysis.* Journal of Industrial and Engineering Chemistry, 2009. **15**(4): p. 458-464.

36. Punith, V. and A. Veeraragavan, *Behavior of Reclaimed Polyethylene Modified Asphalt Cement for Paving Purposes.* Journal of Materials in Civil Engineering, 2011. **23**(6): p. 833-845.

37. Fang, C., et al., *Aging properties and mechanism of the modified asphalt by packaging waste polyethylene and waste rubber powder.* Polymers for Advanced Technologies, 2013. **24**(1): p. 51-55.

38. Singh, B., et al., *Polymer-modified bitumen of recycled LDPE and maleated bitumen.* Journal of Applied Polymer Science, 2013. **127**(1): p. 67-78.

39. Melbouci, B., S. Sadoun, and A. Bilek, *Study of Strengthening of Recycled Asphalt Concrete by Plastic Aggregates.* International Journal of Pavement Research and Technology, 2014. **7**(4): p. 280-286.

40. Gulati, V. (2010) *Indian state uses plastic waste for road construction*. **http://southasia.oneworld.net/news/indian-state-uses-plastic-waste-for-road-construction#.WClk3EC7rmQ**.

41. Menon, A. (2016) *Roads Made of Plastic Waste in India? Yes! Meet the Professor Who Pioneered the Technique.* **http://www.thebetterindia.com/43685/plastic-waste-in-road-construction-plastic-man-india-prof-vasudevan/**.

42. Ridden, P. (2012) *The streets of Vancouver are paved with ... recycled plastic*. **http://newatlas.com/vancouver-recycled-plastic-warm-mix-asphalt/25254/**.

43. Lu, X. and U. Isacsson, *Compatibility and storage stability of styrene-butadiene-styrene copolymer modified bitumens.* Materials and Structures, 1997. **30**(10): p. 618-626.

44. Chen, J.S., M.C. Liao, and C.H. Lin, *Determination of polymer content in modified bitumen.* Materials and Structures, 2003. **36**(9): p. 594-598.

45. Pérez-Lepe, A., et al., *Influence of the processing conditions on the rheological behaviour of polymer-modified bitumen ☆.* Fuel, 2003. **82**(11): p. 1339-1348.

46. Fu, H., et al., *Storage stability and compatibility of asphalt binder modified by SBS graft copolymer.* Construction and Building Materials, 2007. **21**(7): p. 1528-1533.

47. Galooyak, S.S., et al., *The Effect of Nanoclay on Rheological Properties and Storage Stability of SBS-Modified Bitumen.* Petroleum Science and Technology, 2011. **29**(8): p. 850-859.

48. de Carcer, Í.A., et al., *Storage stability of SBS/sulfur modified bitumens at high temperature: Influence of bitumen composition and structure.* Construction and Building Materials, 2014. **52**: p. 245-252.

49. Youtcheff, J., N. Wijayatilleke, and A. Shenoy, *Evaluation of the Laboratory Asphalt Stability Test*. 2005, Federal Highway Administration. p. FHWA-HRT-04-111.

50. Li, P., L. Liu, and Z. Sun, *Research on the Storage Stability Test Method of SBS Modified Asphalt*, in *Proceedings of the 2010 International Conference on Intelligent Computation Technology and Automation - Volume 03*. 2010, IEEE Computer Society. p. 178-181.

51. Witczak, M., *Simple Performance Tests: Summary of Recommended Methods and Database*. 2005, National Cooperative Highway Research Program (NCHRP): Washinton DC. p. 25.

52. Zhou, F., T. Scullion, and L. Sun, *Verification and Modeling of Three-Stage Permanent Deformation Behavior of Asphalt Mixes.* Journal of Transportation Engineering, 2004. **130**(4): p. 486-494.

53. Biligiri, K., et al., *Rational Modeling of Tertiary Flow for Asphalt Mixtures.* Journal of the Transportation Research Board, 2007: p. pp. 63–72.

54. Dongré, R., J. D'Angelo, and A. Copeland, *Refinement of Flow Number as Determined by Asphalt Mixture Performance Tester.* Journal of the Transportation Research Board, 2015: p. pp. 127–136.

55. Rodezno, M.C., R. West, and A. Taylor, *Flow Number Test and Assessment of AASHTO TP 79-13 Rutting Criteria.* Journal of the Transportation Research Board, 2015: p. pp. 100–107.

56. Goh, S.W. and Z. You, *A simple stepwise method to determine and evaluate the initiation of tertiary flow for asphalt mixtures under dynamic creep test.* Construction and Building Materials, 2009. **23**(11): p. 3398-3405.

57. Goh, S., et al., *Determination of Flow Number in Asphalt Mixtures from Deformation Rate During Secondary State.* Journal of the Transportation Research Board, 2011: p. pp, 106–112.

58. Alavi, A.H., et al., *Formulation of flow number of asphalt mixes using a hybrid computational method.* Construction and Building Materials, 2011. **25**(3): p. 1338-1355.

59. Yan, K.-z., D.-d. Ge, and Z. Zhang, *Support Vector Machine Models for Prediction of Flow Number of Asphalt Mixtures.* Int. J. Pavement Res. Technol, 2014. **7**(1): p. 10.

60. Apeagyei, A.K., *Flow number predictive models from volumetric and binder properties.* Construction and Building Materials, 2014. **64**: p. 240-245.

61. AASHTO:T321, *Standard Method of Test for Determining the Fatigue Life of Compacted Asphalt Mixtures Subjected to Repeated Flexural Bending*. 2014, AASHTO: Washington, DC 20001

62. ASTM:D7460-10, *Standard Test Method for Determining Fatigue Failure of Compacted Asphalt Concrete Subjected to Repeated Flexural Bending*. 2010, ASTM International: West Conshohocken, PA.

63. Tarefder, R.A., D. Bateman, and A.K. Swamy, *Comparison of fatigue failure criterion in flexural fatigue test.* International Journal of Fatigue, 2013. **55**: p. 213-219.

64. Qiu, K., et al., *Thermo-mechanical coupling effect on fatigue behavior of cement asphalt mortar.* International Journal of Fatigue, 2013. **51**: p. 116-120.

65. Al-Khateeb, G.G. and K.A. Ghuzlan, *The combined effect of loading frequency, temperature, and stress level on the fatigue life of asphalt paving mixtures using the IDT test configuration.* International Journal of Fatigue, 2014. **59**: p. 254-261.

66. Mannan, U.A., M.R. Islam, and R.A. Tarefder, *Effects of recycled asphalt pavements on the fatigue life of asphalt under different strain levels and loading frequencies.* International Journal of Fatigue, 2015. **78**: p. 72-80.

67. Pronk, A.C. *Comparison of 2 and 4 Point Fatigue Tests and Healing in 4-Point Dynamic Bending Test Based on the Dissipated Energy Concept*. in *Eighth International Conference on Asphalt Pavements* 1997. Seattle, Washington.: Transportation Research Board.

68. Rowe, G.M. and M.G. Bouldin., *IMPROVED TECHNIQUES TO EVALUATE THE FATIGUE RESISTANCE OF ASPHALTIC MIXTURES*, in *2nd Eurasphalt & Eurobitume Congress* 2000, Proc.0081.uk: Barcelona.

69. Carpenter, S., K. Ghuzlan, and S. Shen, *Fatigue Endurance Limit for Highway and Airport Pavements.* Transportation Research Record: Journal of the Transportation Research Board, 2003. **1832**: p. 131-138.

70. Abojaradeh, M., *Effective Fatigue Models for Arizona Asphalt Concrete Mixtures. PhD Dissertation*, in *Civil Engineering*. 2003, Arizona State University: Tempe, AZ.

71. AASHTO:M323, *Standard Specification for Superpave Volumetric Mix Design*. 2013, AASHTO: WASHINTON DC, 2001.

72. AASHTO:TP_79-15, *Standard Method of Test for Determining the Dynamic Modulus and Flow Number for Asphalt Mixtures Using the AMPT,* . 2015, AASHTO.: Washington, DC 20001

73. Bonaquist, R. and D. Christensen, *Practical Procedure for Developing Dynamic Modulus Master Curves for Pavement Structural Design.* Transportation Research Record: Journal of the Transportation Research Board, 2005. **1929**: p. 208-217.

74. Hajj, E., et al., *Estimation of Stress Conditions for the Flow Number Simple Performance Test.* Transportation Research Record: Journal of the Transportation Research Board, 2010. **2181**: p. 67-78.

75. Li, Q., et al., *Mechanistic-empirical pavement design guide (MEPDG): a bird's-eye view.* Journal of Modern Transportation, 2011. **19**(2): p. 114-133.

76. Hossain E.I, N., D. Singh, and M. Zaman P.E, *Dynamic Modulus-based Field Rut Prediction Model from an Instrumented Pavement Section.* Procedia - Social and Behavioral Sciences, 2013. **104**: p. 129-138.

77. ARA, *Guide for the mechanistic empirical design of new and rehabilitated pavement structures*. 2004, Transportation Research Board of the National Academies: Washington, DC.

78. Wheatherbase, *Monthly Wheather Average Summary*. 2017, CantyMedia: Dammam, Saudi Arabia.

79. Ulloa, A., et al., *Equivalent Loading Frequencies for Dynamic Analysis of Asphalt Pavements.* Journal of Materials in Civil Engineering, 2013. **25**(9): p. 1162-1170.

80. ICIS, *ICIS Pricing: Petrochemical, energy and fertilizer market intelligence*. 2014, ICIS.

81. EPA, *Plastics*, OCSPP, Editor. 2010, Environmental Protection Agency: U.S.

82. Kuenen, J., et al., *EMEP/EEA emission inventory guidebook*, in *2.B Chemical industry*, E.E. Agency, Editor. 2013, EEA: Copenhagen K.

83. Saygın, D., et al., *CHEMICAL AND PETROCHEMICAL SECTOR*, in *Potential of best practice technology and other measures for improving energy efficiency*. 2009, INTERNATIONAL ENERGY AGENCY. p. 60.

84. Freedonia. *World Asphalt - Demand and Sales Forecasts, Market Share, Market Size, Market Leaders*. 2014 Study #: 3129]; 429]. Available from: http://www.freedoniagroup.com/World-Asphalt.html.

85. United-Nation, *Energy and Renewables: UN Statistics Division Energy Statistics Database for Saudi Arabia.* 2013, KNOEMA.

APPENDIX A

A.0 EFFECT OF TERTIARY DEFORMATION ON ASPHALT FLOW NUMBER 'FN'

To illustrate the effect of test termination time on the FN, a single permanent deformation curve (PDC), fitted to FM at consecutively increasing test termination time were plotted, and extended beyond their actual test termination time. The 5 test termination durations are 740, 860, 980, 1110 and 1510 seconds respectively. The tertiary flow has already commences within each of these test time (visibly), and the results of the data fit will have shown from the exponential component of the Models if otherwise.

A.1 Francken Model Illustration

The Francken model (FM) response to the test termination time illustration is shown by Figure A.1. The FN values of each plot is presented in the parenthesis attached to the corresponding test termination time in the plot legend. The FN is seen to be increasing with increase in testing duration. Looking beyond 1500 seconds, will make the observer accept the variation and understand the reason behind it. Each curve fits into a different curve, depending on the initiating deformation data length. Figure A.2 presents the second differential plots with the FN clearly shifting to the right. This is a much obvious case selected for illustration, with emphasis at commencement of the tertiary flow for a mix with a moderate tertiary deformation rate. However, this trend or variation should not be witnessed, as any ideal model or method of estimating the FN should yield a unique FN value as soon as the shear deformation begins.

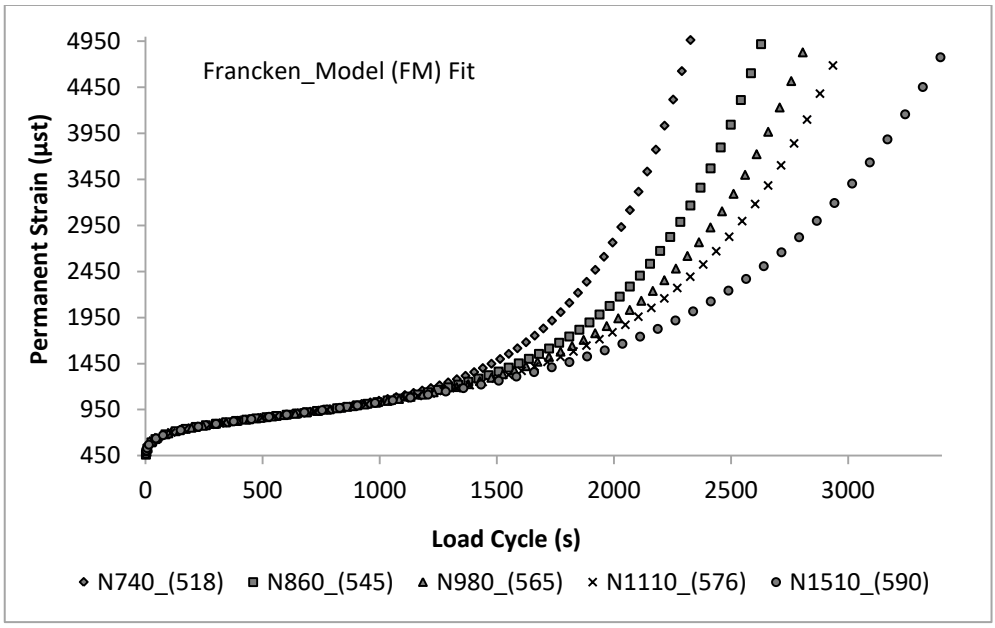

Figure A.1: Permanent Strain Data Fitted in to FM at Increasing level of the Tertiary Flow.

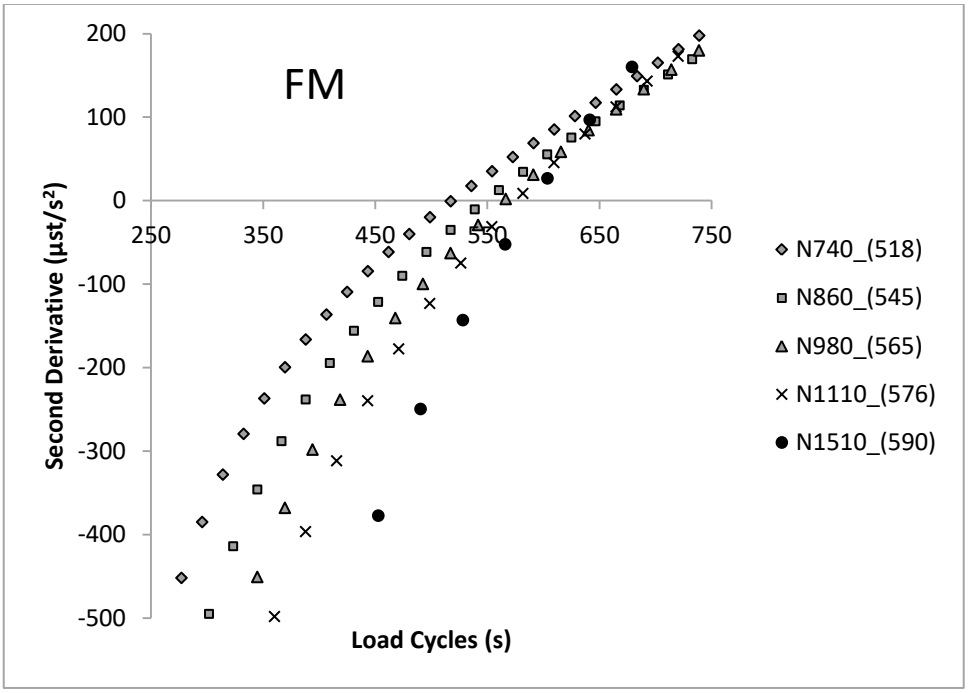

Figure A.2: Second Derivative of FM Fitted data Showing Increasing FN as Tertiary Flow Progresses.

A.1.1 FN Variation with Higher Test Termination Time Explanation and Implication

Based on the FM fitted data plots in Figure A.1, each previous curve got fitted in to a parent curve with a lower tertiary deformation rate or curvature than the subsequent curve. This resulted to each subsequent curve leading the previous curve. And each curve will have a FN number corresponding to its parent curve, not the initiating data curve. The FM exponential part is responsible for the high deformation rate of the parent curves. A different mix with an extremely high tertiary deformation rate (like double exponential, very unlikely) will results in an opposite trend. The implication is: regardless of what time or strain the test is terminated, extending the test duration (if possible) might results in the deformation data getting attached to a parent curve with FN significantly different to the actual asphalt mix FN. For several obvious reasons, this is a race that cannot be won by extending the test duration. This is the cost of mathematizing the permanent deformation data, which was generally agreed to be a necessity. But it is also just another issue with another solution. The FM was modified to yield two different models (MFM-1 and MFM-2) with the view of minimizing the effect of testing time on the FN.

A.2 Modified Francken Model -2 (MFM-2)

Equation (4.10) represent the MFM-2, a modified FM with the $\sqrt{N}$ instead of N in the exponential part, otherwise, all other parameters remain the same. This was intended for a model with slower tertiary deformation rate than FM.

$$\varepsilon_p = \mathrm{A} * \mathrm{N}^{\mathrm{B}} + C * (e^{D*\sqrt{N}} - 1) \tag{4.10}$$

$$\varepsilon_p'' = \frac{e^{\mathrm{D}\sqrt{N}}\mathrm{CD}(\sqrt{N}-1)\sqrt{N}+4\mathrm{AB}(B-1)N^{\mathrm{B}}}{4N^2} \tag{4.11}$$

ε_p = Permanent Strain Sustained by the HMA test Sample

ε_p'' = Rate of change of the strain rate (second differential of ε_p with respect to N).

N = load cycle repetition in seconds

A, B, C & D are regression constants

Figure A.3 presents similar analysis as that in Figure A.1, but this time around the data was fitted using MFM-2. The objective of slowing down the tertiary deformation of the parent curve has been obviously achieved when both Figure A.1 and Figure A.3 are compared. And the second objective, which was to minimize the effect of testing duration on FN was also actualized as can be observed. The highest FN recorded was 576 for a test time of 1510 seconds as opposed to 590 in the case of FM model fits. The questions still remain: is this enough? how general is this improvements? These questions shall be addressed in the subsequent paragraphs.

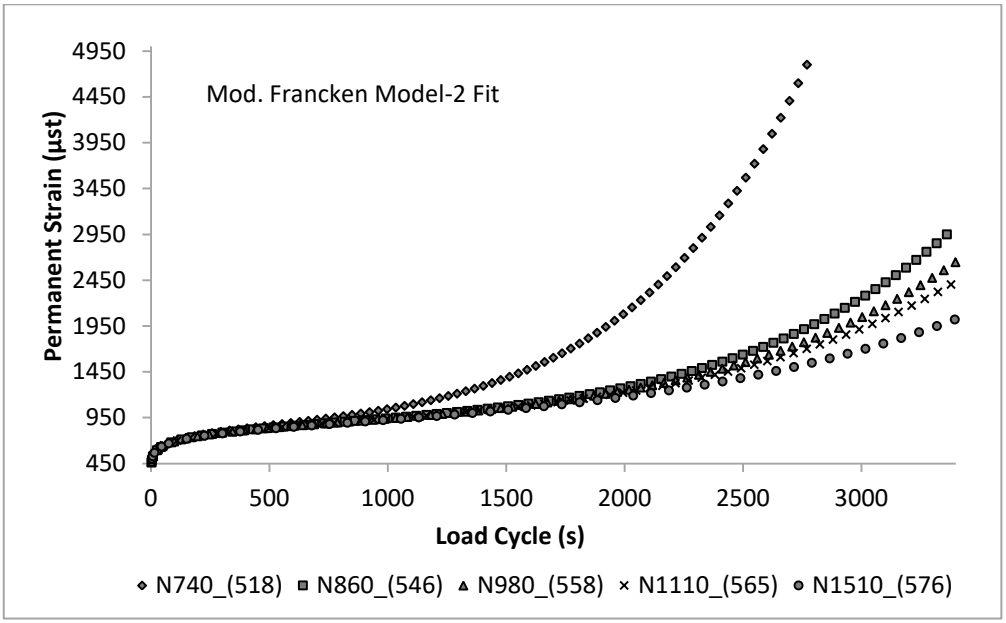

Figure A.3:Permanent Strain Data Fitted in to MFM-2 at Increasing level of the Tertiary Flow.

A.3 Modified Francken Model-1 (MFM-1)

Equation (4.12) represent the other FM modification MFM-1. Major changes were made to the FM in this case. The third constant in FM (which is C) was replaced with the independent variable (the load cycle 'N'). This is a further attempt to slow down the rate of tertiary deformation of the FN test data fit parent curve, by slightly linearizing the exponential component of the FM. All other parameters remain the same.

$$\varepsilon_p = \mathrm{A} * \mathrm{N}^{\mathrm{B}} + N * (e^{D*N} - 1) \quad . \tag{4.12}$$

$$\varepsilon_p'' = 2\mathrm{D} * e^{\mathrm{D}*N} + \mathrm{D}^2 N * e^{\mathrm{D}*N} + \mathrm{AB}(B-1)N^{B-2} \tag{4.13}$$

ε_p = Permanent Strain Sustained by the HMA test Sample

ε_p'' = Rate of change of the strain rate (second differential of ε_p with respect to N).

N = load cycle repetition in seconds

A, B & D are regression constants

The same data sets as analyzed with FM and MFM-2 was refitted using MFM-1 in similar manner, and the results is shown in Figure A.4. A completely different and opposite curve order and FN variation trend was observed for the data set. The parent curves exhibit slightly lesser tertiary deformation rate than the initiating strain data curves. Hence, instead of leading the previous parent curves as in the FM and MFM-2 case, the subsequent parent curves are lagging the previous ones. This results in reversing the increasing effect of the test termination time on FN to declining trend. And range of FN variation has further been narrowed. This was possible due the much lower curvature or turning rate of the MFM-1.

The intended purpose of the FM modifications has now been achieved with even more surprises, atleast for this specific case. The observed models diversity is worth exploring, with the view of finding solution to the previous outline problem. Nonetheless, there is an implication that accompanied these discoveries. First, the degree or range of curvature of the models is curve specific and inborn to their mathematical structure. However, permanent deformation behavior for different mix cannot be predicted, it depends on several factors (testing temperature, material quality, applied stress etc). Which means, any of these models could behave in whichever way (decreasing FN, increasing FN or even perfect), depending on the nature of the PDC data.

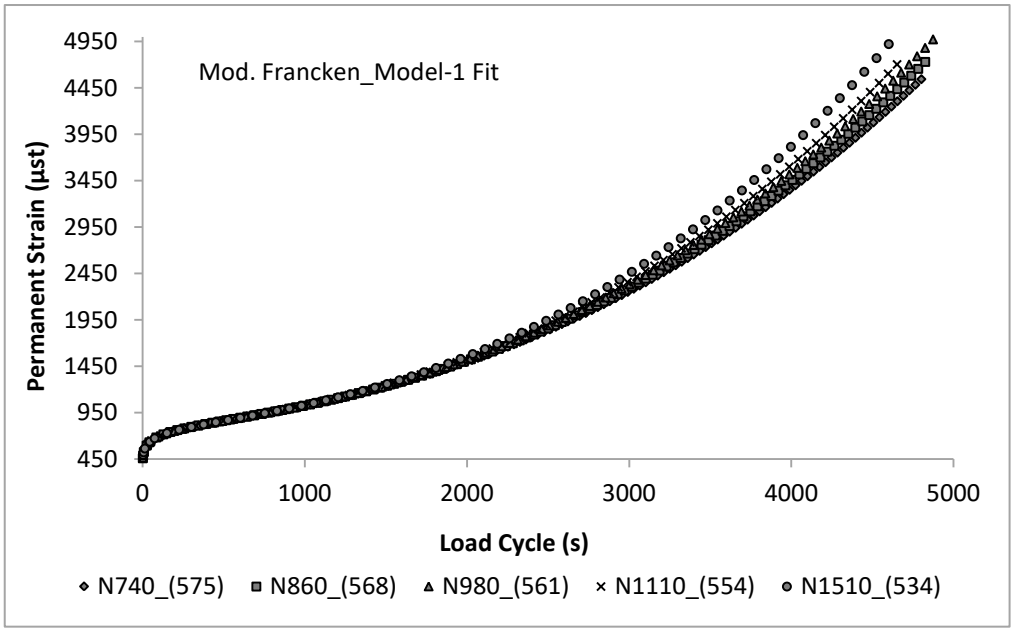

Figure A.4: Permanent Strain Data Fitted in to MFM-1 at Increasing level of the Tertiary Flow.

A.4 Correlation between FM and MFMs

Figure A.5 shows the correlation between FNs obtained using FM (FM_FN) and those estimated by MFM-1 PDC data fitting (MFM-1_FN). There seemed to be a moderate correlation between the different FNs. But as observed previously, the models behave in opposites manner due to their different mathematical nature. However, there will be a giving time range during the test when their various FNs come close to each other, and even intersect as will be shown later in Figure A.12. These will explain the out of point data and the fair correlation.

However, an excellent correlation between the FM_FN and the FNs estimated from MFM-2 fitted curves was observed as shown in Figure A.6. It can also be seen that the FM_FNs are generally slightly higher than the MFM-2_FNs as previously illustrated from results in Figure A.2 and Figure A.3.

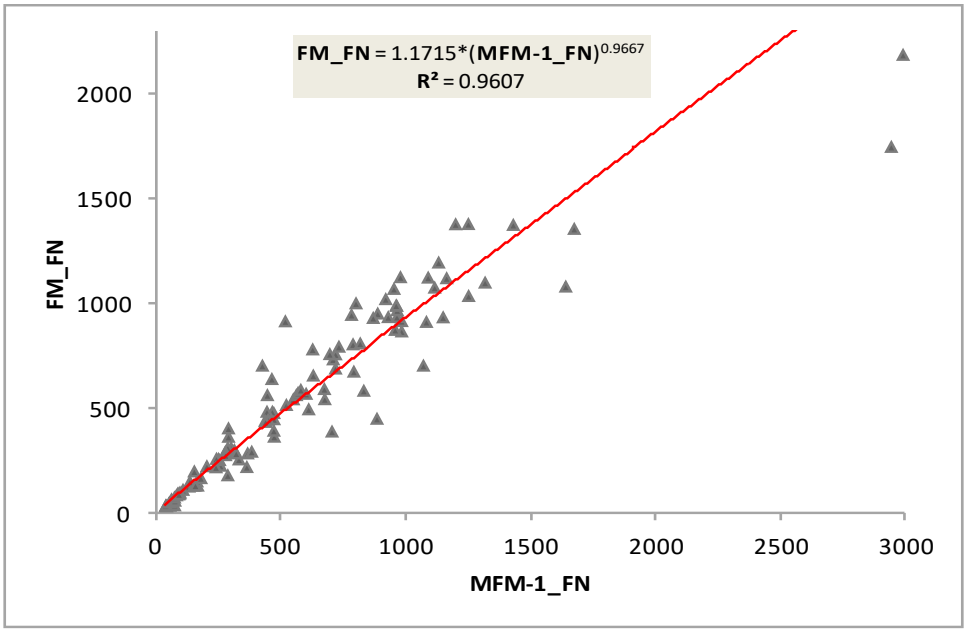

Figure A.5: FM_FN and MFM-1_FN Correlation.

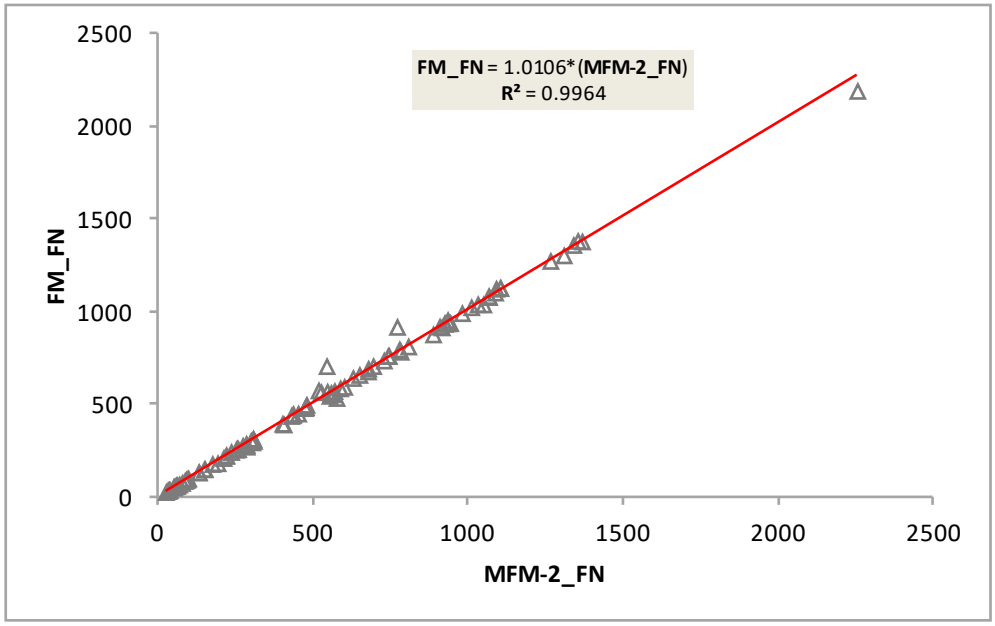

Figure A.6: FM_FN and MFM-2_FN Correlation.

A.5 STANDARD FN LIMITS AND HMA FN VARIATION WITH TEST TERMINATION TIME

To further demonstrate the implication of the test termination time effect on the estimated FN values. A plots of the FN variation for numerous analyzed PDC data with test duration was shown in Figure A.7 and Figure A.8. For the sake of plot clarity and objectivity, only one set is plotted in cases where the data sets completely overlapped.

Figure A**.7** show the FM and MFM-2 FN test time variation combined, as they follow the same trend. The general trend is obvious, higher FN values for prolong tertiary deformation. Another issue of great implication is the crossing of the FN limits for a given recommended traffic category by a single HMA mix. This causes a lot of doubt as to the validity of the FN specification limits and standard. It is obvious that the standard and its related methods has more to tackle.

Similar but fewer FN limits crossing can be observed in the case of MFM-1 as shown in Figure A.8. Plus lesser FN variation, especially within the high traffic category bounds. But still, the length of tertiary deformation affect the FN values. And any of the mix that happen to be close to the boundary can easily cross. Making a mix suitable for completely different traffic level. Hence nullifying the essence and soundness of the standard.

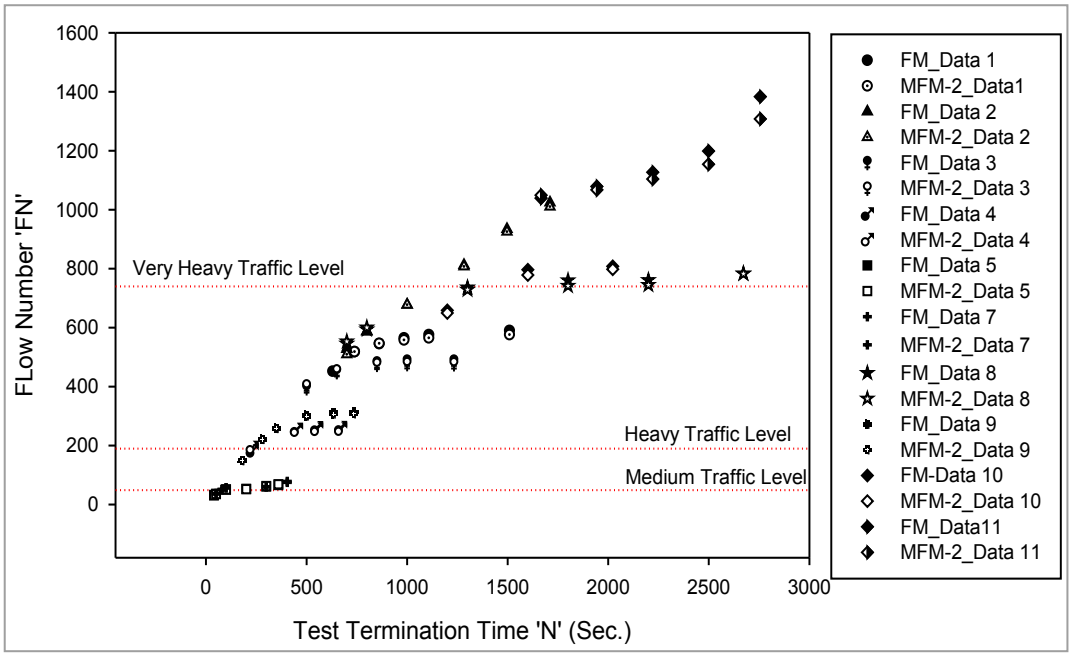

Figure A.7: FN Variation vs. Standard FN Limits Recommended for Different Traffic Categories.

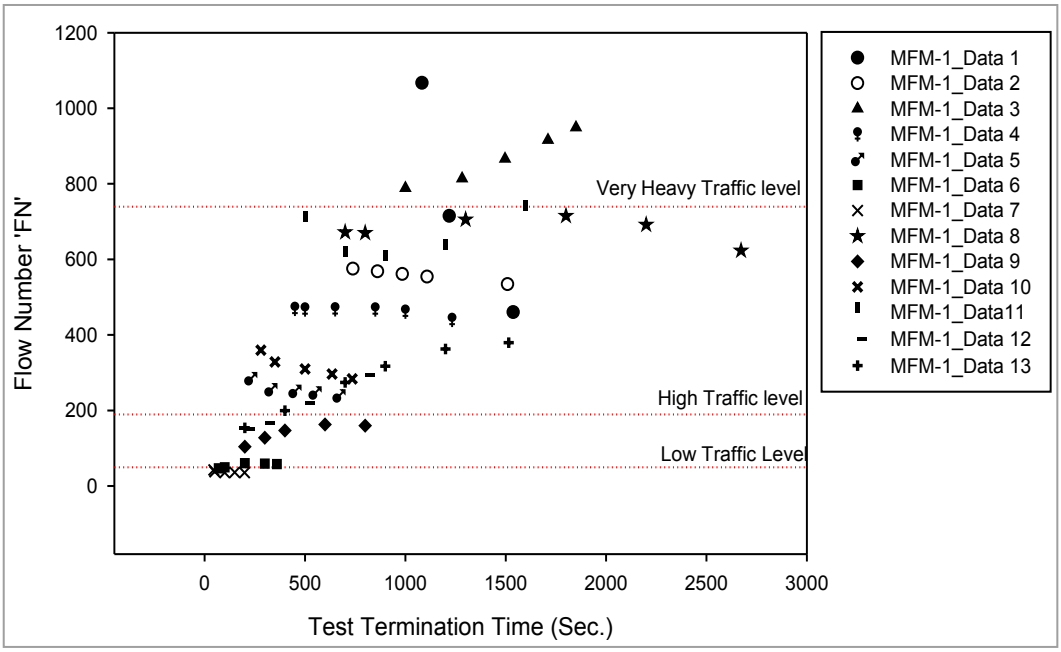

Figure A.8: MFM-1_FN Variation vs. Recommended Standard FN Limits.

A. 6 FLOW NUMBER TO TEST DURATION RATIO (FN:N)

After the previous attempts to solve the stated problem of FN variation but further discovered more. The simple and probably the best alternative is to standardize the FN to test duration (N) ratio (FN:N) for FN estimation. However, an in depth analysis of FN:N is needed for this to be actualized.

To fully understand FN:N of a given tested asphalt mix, one needs to also have a general knowledge of reciprocal functions. Generally, the reciprocal functions are represented by the equation (4.14). The function y is asymptotic to x & y axis, meaning it never crosses both axis.

$$y(x) = \frac{k}{x+m} + h \qquad (4.14)$$

where k, m and h are all constant.

FN:N is a special form of reciprocal function with $k = FN, x = N, m = 0 \; and \; h = 0$. Ideally, the FN of any single tested asphalt mix sample should be constant and unique to that mix type, for that given test conditions and material properties. Hence the only variable is the repeated loading, which keeps increasing. Figure A.9 further illustrates the behavior of $\frac{k}{N}$ plots, the exact form of FN:N. As the constant k increases the function $\frac{k}{N}$ shift further up.

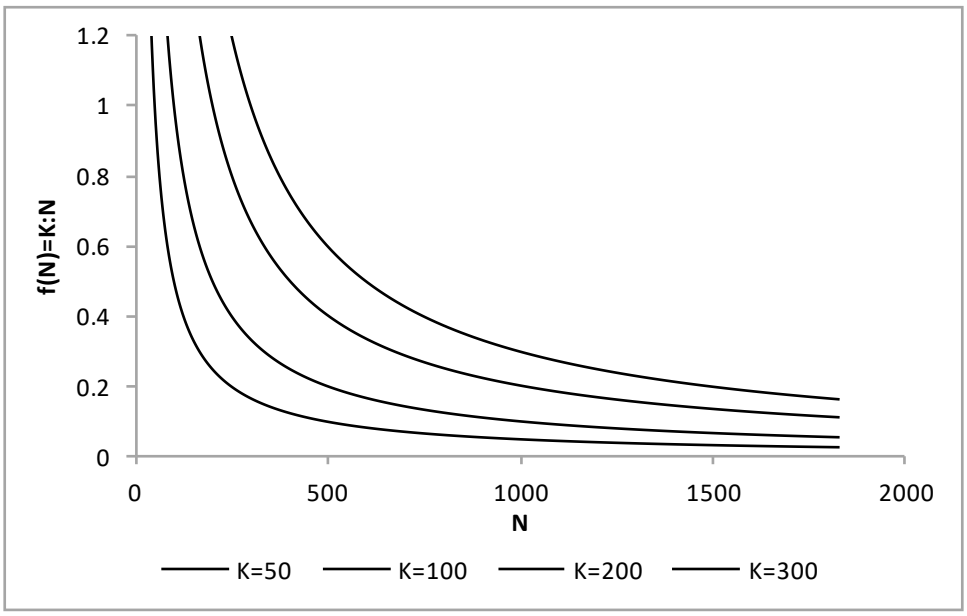

Figure A.9: General Reciprocal Function vs. FN:N.

Figure A.10 shows a typical FN:N plots of a given PDC for the various models (FM, MFM-1 and MFM-2). It can be clearly observed that the MFM-1 FN:N plot follows the actual and expected trend of the real function. But both FM and MFM-2 begin to stagnates at FN:N beyond 70%. This explains the progressive increment in FN values as the tertiary deformation progresses. But to further explain the FN increment even after the FM and MFM-2 FN:N settles to the expected function trend, the MFM-1 FN:N was fitted to a power model trend. Surprisingly, the power (exponent) on the independent variable

(N) is not unity, but very close. This is due to the fact that the FN values utilized to established the plots are not the same. This also applies to the MFM-2 and FM cases after settling in to the normal trend. The level of the FN:N curve contamination will be reflected by the amount it deviates from the real plot. This has brought us back to square one, but with potential possible solutions.

In order to generally assess the FN:N behavior of the different models, a correlation between the FM_FN:Ns and the MFM_FN:Ns is presented in Figure A.11. As expected, the FN:N behavior of the FM and MFM-2 are similar and almost the same. However, the relationship and trend depicted by Figure A.10 appears to be more than just an isolated case but a general one. The mathematical correlation between the FM_FN:N and the MFM-1_FN:N shows that the two models have the same FN:N at 35%. This could be a useful finding. Another important observation is that the MFM-1_FN:N of 100% corresponds to FM_FN:N of 75%.

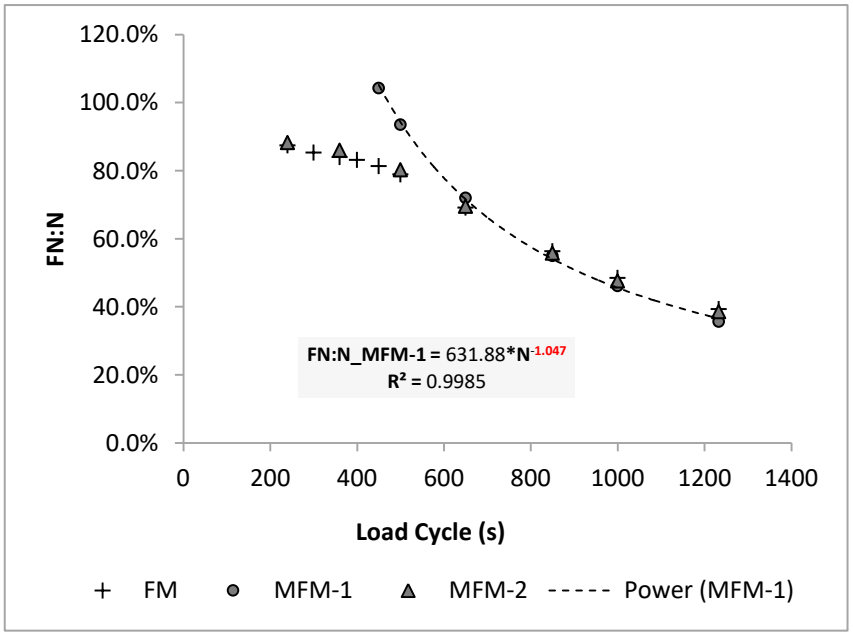

Figure A.10: Typical FN:N Plot for Test Data Fitted in to FM, MFM-1 and MFM-2.

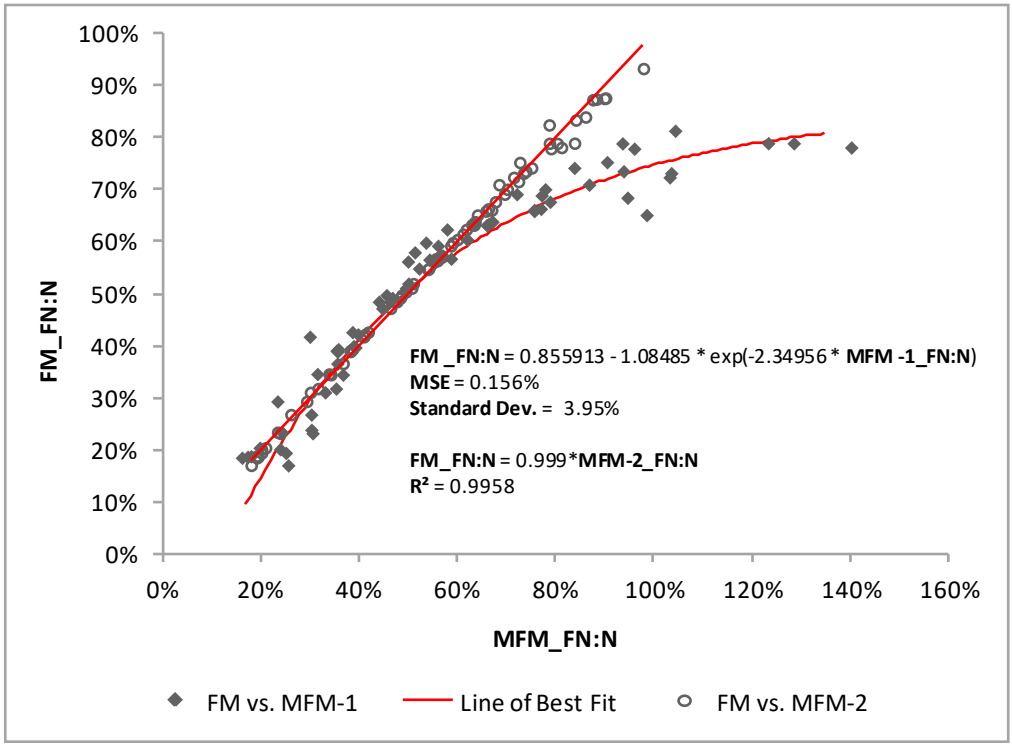

Figure A.11: FM_FN:N Correlation with MFM-1_FN:N and MFM-2_FN:N.

A.7 REFINING FN USING FN:N PLOT

The final and most important task is to utilize the FN:N and its ideal properties to estimate the actual or the approximate FN of the asphalt mix. Three possible options were identified that could all be applicable depending on the constraints that could be identified currently or later in the future.

A.7.1 Early Tertiary Flow Stage FN

Logically, the FN should be Identified as soon as the tertiary deformation begins. This is important since at this stage, the parent curve has had little or no effect on the FN value. The applicable FN referred to in this case is the FN value obtained at FN:N of 100% (FN_100). It is the PDC data length that just fits into a parent curve at exactly it's

natural point of inflexion. To explain the justification behind the choice of FN_100 further, a simple but bizarre analogy will be given. Consider the mathematical model like the human shoe model. Give her/him an under size or oversize shoe to advertise, and he/she cannot walk/stand naturally not to mention attractively. Hence the effect results in the value of the shoe to be lost to the consumers. Now, regard the PDC data length as the shoe and the shoe value to be the FN. The advantage of this option is a further reduced testing time. And the possibility of reusing the test sample for another different test such as dynamic modulus test, due to little damage sustained. But, MFM-1 is the only suitable model here, as it can easily detect the FN_100 with ease due it relative low curvature.

A.7.2 Intermediate Tertiary Flow State FN

The second option is to determine the FN at an intermediate point within the tertiary flow. The FN_100 cannot be said to be 100% free from the parent curve influence. But a twin curve analysis, utilizing model with opposite effect on the FN (e.g. FM and MFM-1) could be employed to determine a point of intersection, as seen in Figure A.12. This will be FN with the least possible error within the whole range. If FM or MFM-2 with MFM-1 are considered, FN obtained at 35% FN:N (FN_35) will be the recommended choice, according to the current findings.

A.7.3 Refining the FN:N function

Finally, this option is the most reliable, but a little tricky and technical. Due to the fact that the FN value available for FN:N to be plotted are most likely different as shown in Figure A.12 (increasing or decreasing). The FN:N plot fits in to a power function with

the form of Equation (4.15). Ideally, $\alpha = 0$ because $k = constant$. In order to sanitize the FN:N plot, the FN:N is fitted into a model that allow for k variation, as in Equation (4.16). When $f(N)$ is simplified further, the results is two component, Equation (4.17). The first component is the corrected FN:N plot (Equation 4.17) and the second component is FN error component, or the noise. This option disadvantage is it requires more time and some mathematical skills for accurate FN:N refinement.

$$f(N) = \frac{k}{N^{(1+\alpha)}} \tag{4.15}$$

$$k = FN + \beta * N^{\gamma}. \tag{4.16}$$

$\beta\ and\ \gamma$ are constants determined by the FN increasing or decreasing trend.

$$f(N) = \frac{FN}{N} + \beta * N^{\gamma - 1} \tag{4.17}$$

Fitting the obtained FN:N curve into equation (4.17) will separate the actual FN:N function from the noise.

$$f^{corr}(N) = \frac{FN}{N} \tag{4.18}$$

Figure A.13 showed an illustration of FN:N plot refinement for the two possible cases of FN variation. The second plot from the top represent an FN:N curve with a decreasing FN trend, and the second plot from the bottom is for FN:N curve with an increasing FN trend. These curves were then broken down in to two components in the form of Equation (4.17). The corrected FN:N plot were obtained and plotted separately as shown. The corrected FNs (FN_Corr) for the two curves are 382 and 117 respectively.

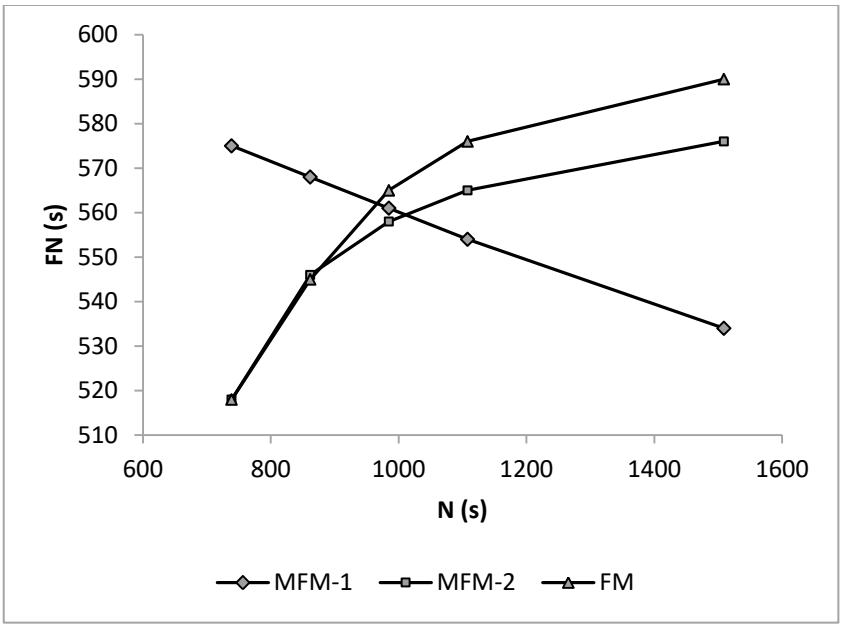

Figure A.12: Typical FN-N relationship and Trend.

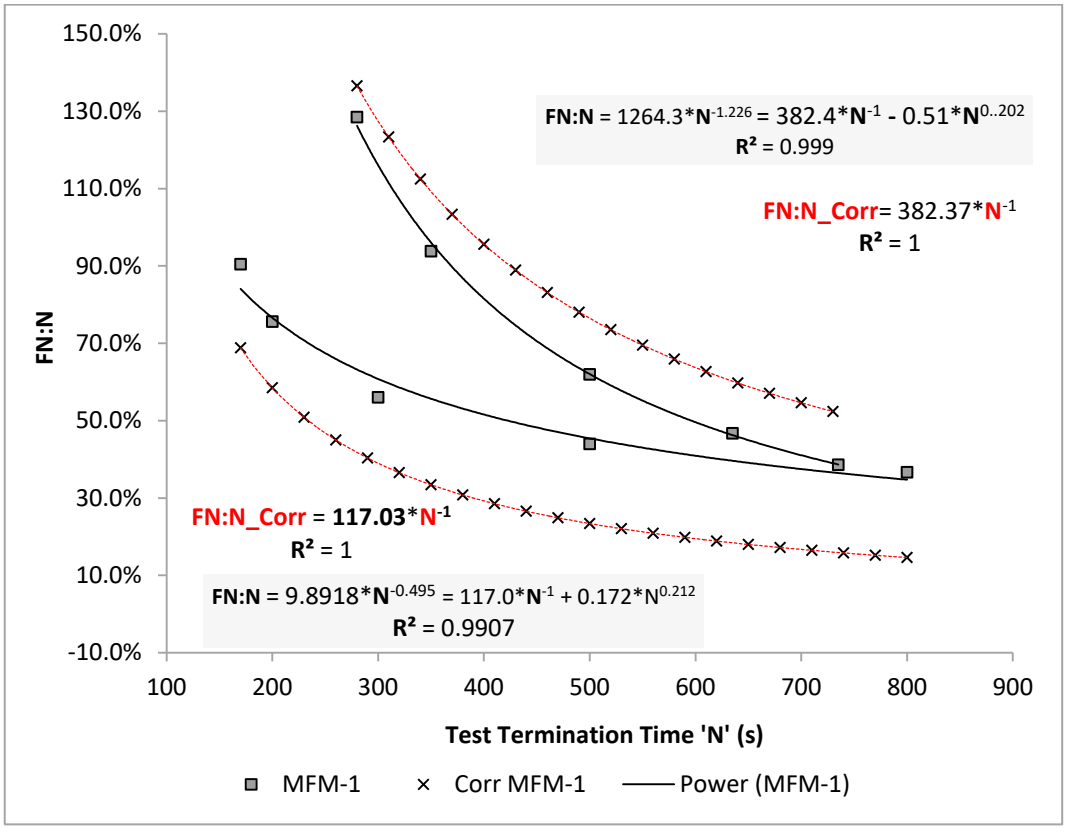

Figure A.13: Illustration of FN:N Plot Refinement.

A.7.4 Correlation between FN_Corr and FN_100

The correlation between the corrected FN using refinement (FN_Corr) and FN_100 is presented in Figure A.14. The results suggested that FN_100 is a little higher than the FN_Corr, confirming our initial suspicion. This correlation can be used to simplify the whole task of refinement, once FN_100 is obtained.

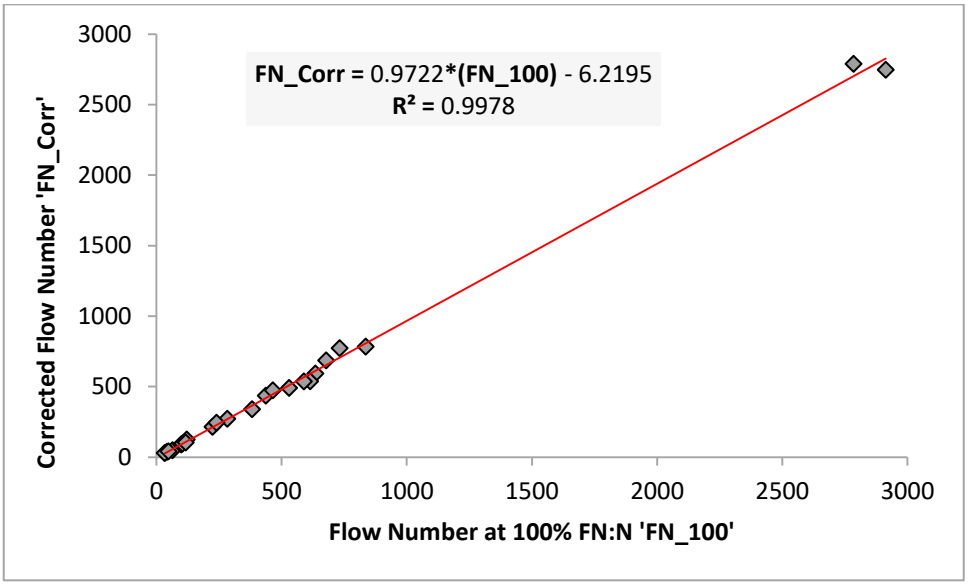

Figure A.14: FN_Corr vs. FN_100.

A.8 How Tertiary Flow Length Affects the AC FN and Solution

Two new PDC models (MFM-1, MFM-2) were obtained by modifying the Francken model (FM), and employed along with FM to investigate the effect of tertiary flow length on HMA FN. Gauss-Newton algorithm was used to generated more than 360 FN data point from the three different PDC models (FM, MFM-1, MFM-2). The mathematical structure of the PDC model used in analyzing the permanent strain data has a huge influence on the resulting FN, and the FN variation trend as the tertiary deformation stage progresses. Models with high curvature parent curves like FM and MFM-2 mostly result in increasing FN values as the tertiary flow evolves. But low curvature model like MFM-1 mainly results in lower FN as the HMA shear deformation advanced. However, this models can behave whichever way, depending on the PDC data rate of curvature change, which varies from mix type to test conditions. Mathematization of the PDC data, which happens to be a necessity, was the result of the FN variation. The estimated FN were found to represent the inflexion points of the fitted parent curve not the initiation permanent strain data. The FN variation has resulted in a situation where a single tested sample could be identified suitable for two different standard FN range recommended traffic levels by AASHTO TP 79-15.

Flow number to test duration ratio (FN:N) has been identified as the simple and ultimate solution for further standardization and refinement of FN test and FN value respectively. Three possible options of utilizing FN:N for the aforementioned purpose were recommended and highlighted. Methods of estimating the FN at early and Intermediate tertiary flow stage and a complete refinement of the adulterated FN:N were

discussed and illustrated. Important correlations and between the refinement options were also presented. The MFM-1 appears to be more robust than the FM and MFM-1 in the utilization of FN:N curve.

APPENDIX B

Table B 1: RLDPE-PB Asphalt Binders AASHTO MP 19-10 and AASHTO TP 70 Results Summary.

LDPE		**2.0%**	**2.0%**	**2.0%**	**2.0%**	**4.0%**	**4.0%**	**4.0%**	**4.0%**	**6.0%**	**6.0%**	**6.0%**	**6.0%**	**8.0%**	**8.0%**	**8.0%**	**8.0%**
HDPE		0.0%	0.0%	0.0%	0.0%	0.0%	0.0%	0.0%	0.0%	0.0%	0.0%	0.0%	0.0%	0.0%	0.0%	0.0%	0.0%
PP		0.0%	0.0%	0.0%	0.0%	0.0%	0.0%	0.0%	0.0%	0.0%	0.0%	0.0%	0.0%	0.0%	0.0%	0.0%	0.0%
SBS		0.0%	0.0%	0.0%	0.0%	0.0%	0.0%	0.0%	0.0%	0.0%	0.0%	0.0%	0.0%	0.0%	0.0%	0.0%	0.0%
Polybilt101 (PB)		**0.0%**	**1.0%**	**1.5%**	**2.0%**	**0.0%**	**1.0%**	**1.5%**	**2.0%**	**0.0%**	**1.0%**	**1.5%**	**2.0%**	**0.0%**	**1.0%**	**1.5%**	**2.0%**
Original Binder	T (°C)																
G*/sin(δ) (kPa)	64	4.132				6.899				10.77				18.02			
G*/sin(δ) (kPa)	70	1.847	2.089	2.645	2.472	2.989	2.545	2.683	2.793	4.528	3.481	3.997	7.705	7.112	3.972		5.753
G*/sin(δ) kPa)	76	0.893	1.017	1.35	1.223	1.427	1.25	1.234	1.354	2.122	1.695	1.988	3.609	2.897	1.944		2.519
G*/sin(δ) (kPa)	82	0.432	0.495	0.689	0.605	0.681	0.614	0.568	0.656	0.994	0.825	0.989	1.69	1.18	0.951		1.103
Pass/Fail Temp.		**75.1**	**76.1**	**78.7**	**77.7**	**78.9**	**77.9**	**77.6**	**78.5**	**82.0**	**80.4**	**81.9**	**86.2**	**83.1**	**81.6**		**82.7**
RTFO Residue	T (°C)																
G*/sin(δ) (kPa)	64	7.908				11.8				19.91				25.46			
G*/sin(δ) (kPa)	70	3.435	3.861	5.362	4.618	5.071	5.462	6.455	6.755	8.67	9.597	9.843	9.518	11.31	9.543		12.71
G*/sin(δ) (kPa)	76	1.621	1.799	2.311	2.155	2.403	2.511	2.932	3.068	4.165	4.218	4.313	3.636	5.628	4.212		5.633
G*/sin(δ) (kPa)	82	0.765	0.838	0.996	1.006	1.207	1.154	1.332	1.393	2.132	1.854	1.89	1.389	2.987	1.859		2.497
Pass/Fail Temp.		**73.6**	**74.4**	**76.4**	**75.8**	**76.7**	**77.0**	**78.2**	**78.5**	**81.2**	**80.8**	**80.9**	**79.1**	**84.1**	**80.8**		**82.9**
PG		**70**	**70**	**76**	**76**	**76**	**76**	**76**	**76**	**76**	**76**	**76**	**76**	**82**	**76**		**82**
MSCR at 76ºC																	
%R at 0.1 kPa			9.9	11.51	14.7	2.1	10.46	14.95	16.65	5.2	9.23	20.95	15.64	4.8	10.48		21.53
%R at 3.2 kPa			-2.5	-1.16	-1.9	-2.3	-1.99	-2.16	-1.65	-0.7	-1.10	5.01	-0.67	-1.1	-0.55		0.22
Jnr at 0.1 kPa			4.229	3.00	3.079	3.359	2.88	2.69	2.07	1.574	1.80	2.25	1.56	1.755	1.45		1.03
Jnr at 3.2 kPa			5.8	3.80	4.6	4.0	4.00	3.43	3.20	1.96	2.49	2.92	2.36	2.2	1.95		2.03
Jnrdiff (%)			38.0	26.73	50.3	20.2	39.05	27.55	54.48	24.9	38.64	20.95	51.26	25.1	34.36		97.62
Traffic			**N/A**	76S	**N/A**	76S	76S	76S	76S	76H	76S	76S	76S	76S	76H		76S
MSCR at 70ºC																	
%R at 0.1 kPa		1.2	16.20	17.25	17.04	4.3	11.63	24.43	17.25		17.81	20.95	28.85	1.4	17.51		46.18
%R at 3.2 kPa		-1.6	-0.49	0.50	0.44	-0.5	0.11	0.75	0.96		3.08	3.51	3.31	-1.5	4.97		25.60
Jnr at 0.1 kPa		2.274	1.55	1.63	1.27	1.422	1.22	1.19	0.86		0.68	0.66	0.54	2.244	0.49		0.10
Jnr at 3.2 kPa		2.6	2.26	1.91	1.86	1.7	1.64	1.52	1.30		0.90	0.92	0.93	2.7	0.62		0.16
Jnrdiff (%)		15.8	45.94	17.52	46.24	16.9	34.78	27.34	51.78		33.01	39.80	71.59	18.2	24.63		63.07
Traffic		70S	70S	70H	70H	70H	70H	70H	70H		70H	70V	70V	70S	70V		70V
AASHTO MP 19-10		**70(S)**	**70(S)**	**76(S)**	**70(H)**	**76(S)**	**76(S)**	**76(S)**	**76(S)**	**76(H)**	**76(S)**	**76(S)**	**76(S)**	**76(S)**	**76(H)**		**76(S)**
AASHTO TP 70		Failed	Failed	Failed	Failed	Fail	Failed	Failed	Failed	Failed	Failed	Failed	Failed	Failed	Failed		Failed

Table B 2: RLDPE-SBS Asphalt Binders AASHTO MP 19-10 and AASHTO TP 70 Results Summary.

LDPE		**2.0%**	**2.0%**	**2.0%**	**2.0%**	**4.0%**	**4.0%**	**4.0%**	**4.0%**	**6.0%**	**6.0%**	**6.0%**	**6.0%**	**8.0%**	**8.0%**	**8.0%**	**8.0%**
HDPE		0.0%	0.0%	0.0%	0.0%	0.0%	0.0%	0.0%	0.0%	0.0%	0.0%	0.0%	0.0%	0.0%	0.0%	0.0%	0.0%
PP		0.0%	0.0%	0.0%	0.0%	0.0%	0.0%	0.0%	0.0%	0.0%	0.0%	0.0%	0.0%	0.0%	0.0%	0.0%	0.0%
SBS		**0.0%**	**1.0%**	**1.5%**	**2.0%**	**0.0%**	**1.0%**	**1.5%**	**2.0%**	**0.0%**	**1.0%**	**1.5%**	**2.0%**	**0.0%**	**1.0%**	**1.5%**	**2.0%**
Polybilt101 (PB)		0.0%	0.0%	0.0%	0.0%	0.0%	0.0%	0.0%	0.0%	0.0%	0.0%	0.0%	0.0%	0.0%	0.0%	0.0%	0.0%
Original Binder	T (°C)																
G*/sin(δ) (kPa)	64	4.132				6.899				10.77				18.02			
G*/sin(δ) (kPa)	70	1.847		4.577	6.579	2.989	4.077	5.802	12.14	4.528	6.812	9.123	13.32	7.112	9.477		18.05
G*/sin(δ) kPa)	76	0.893	2.454	1.987	3.051	1.427	1.876	2.86	5.908	2.122	2.965	4.453	5.987	2.897	4.075		8.59
G*/sin(δ) (kPa)	82	0.432	1.204	0.863	1.415	0.681	0.863	1.41	2.875	0.994	1.291	2.174	2.691	1.18	1.752		4.088
Pass/Fail Temp.		**75.1**	**83.6**	**80.9**	**84.7**	**78.9**	**80.9**	**84.9**	**90.8**	**82.0**	**83.8**	**88.5**	**89.4**	**83.1**	**86.0**		**93.4**
RTFO Residue	T (°C)																
G*/sin(δ) (kPa)	64	7.908				11.8				19.91				25.46			
G*/sin(δ) (kPa)	70	3.435	7.514	9.358	10.91	5.071	7.502	9.92	18.87	8.67	9.958	12.74	20.4	11.31	17.26		25.29
G*/sin(δ) (kPa)	76	1.621	3.415	4.139	5.059	2.403	3.419	4.913	9.198	4.165	4.539	6.206	9.772	5.628	6.2		12.15
G*/sin(δ) (kPa)	82	0.765	1.552	1.831	2.346	1.207	1.558	2.433	4.483	2.132	2.069	3.023	4.681	2.987	2.227		5.837
Pass/Fail Temp.		**73.6**	**79.4**	**80.7**	**82.5**	**76.7**	**79.4**	**82.9**	**87.9**	**81.2**	**81.53**	**84.7**	**88.2**	**84.1**	**82.1**		**90.0**
PG		**70**	**76**	**76**	**82**	**76**	**76**	**82**	**82**	**76**	**76**	**82**	**88**	**82**	**82**		**
MSCR at 76ºC																	
%R at 0.1 kPa			10.90	22.69	13.05	2.1	8.30	10.78	19.12	5.2	7.85	15.70	16.36	4.8	6.88		29.98
%R at 3.2 kPa			3.90	14.29	3.63	-2.3	3.34	1.14	8.57	-0.7	2.47	2.19	5.02	-1.1	1.78		10.13
Jnr at 0.1 kPa			2.38	1.30	1.20	3.359	1.64	1.43	0.57	1.574	0.48	1.00	0.63	1.755	0.39		0.33
Jnr at 3.2 kPa			2.79	1.54	1.54	4.0	1.98	1.85	0.74	1.96	1.63	1.42	0.83	2.2	0.54		0.50
Jnrdiff (%)			17.07	18.08	28.88	20.2	20.55	29.38	28.57	24.9	31.39	42.79	32.42	25.1	37.00		50.56
Traffic			76S	76H	76H	76S	76H	76H	76V	76H	76H	76H	76V	76S	76H		76E
MSCR at 70ºC																	
%R at 0.1 kPa		1.2	13.90	34.35	19.39	4.3	16.30	21.96	30.40		17.85	23.28	28.77	1.4	16.88		46.18
%R at 3.2 kPa		-1.6	7.198	9.030	11.90	-0.5	4.336	8.028	21.57		6.47	10.37	15.51	-1.5	6.78		25.60
Jnr at 0.1 kPa		2.274	0.679	0.660	0.473	1.422	0.548	0.543	0.211		0.48	0.39	0.22	2.244	0.34		0.10
Jnr at 3.2 kPa		2.6	0.790	0.750	0.562	1.7	0.976	0.725	0.255		0.63	0.52	0.30	2.7	0.44		0.16
Jnrdiff (%)		15.8	16.42	13.68	18.87	16.9	78.25	33.35	20.85		32.39	33.94	35.17	18.2	27.00		63.07
Traffic		70S	70H	70H	70V	70H	N/A	70V	70E		70V	70V	70E	70S	70E		70E
AASHTO MP 19-10		**70(S)**	**76(S)**	**76(H)**	**76(H)**	**76(S)**	**76(H)**	**76(H)**	**76(V)**	**76(H)**	**76(H)**	**76(H)**	**76(V)**	**76(S)**	**76(H)**		**76(E)**
AASHTO TP 70		Failed	Failed	Failed	Failed	Failed	Failed	Failed	Failed	Failed	Failed	Failed	Failed	Failed	Failed		Failed

Table B 3: RHDPE-PB Asphalt Binders AASHTO MP 19-10 and AASHTO TP 70 Results Summary.

LDPE		0.0%	0.0%	0.0%	0.0%	0.0%	0.0%	0.0%	0.0%	0.0%	0.0%	0.0%	0.0%	0.0%	0.0%	0.0%	0.0%
HDPE		**2.0%**	**2.0%**	**2.0%**	**2.0%**	**4.0%**	**4.0%**	**4.0%**	**4.0%**	**6.0%**	**6.0%**	**6.0%**	**6.0%**	**8.0%**	**8.0%**	**8.0%**	**8.0%**
PP		0.0%	0.0%	0.0%	0.0%	0.0%	0.0%	0.0%	0.0%	0.0%	0.0%	0.0%	0.0%	0.0%	0.0%	0.0%	0.0%
SBS		0.0%	0.0%	0.0%	0.0%	0.0%	0.0%	0.0%	0.0%	0.0%	0.0%	0.0%	0.0%	0.0%	0.0%	0.0%	0.0%
Polybilt101 (PB)		**0.0%**	**1.0%**	**1.5%**	**2.0%**	**0.0%**	**1.0%**	**1.5%**	**2.0%**	**0.0%**	**1.0%**	**1.5%**	**2.0%**	**0.0%**	**1.0%**	**1.5%**	**2.0%**
Original Binder	T (°C)																
G*/sin(δ) (kPa)	64	9.651				18.28				66.04				134.5			
G*/sin(δ) (kPa)	70	4.203	3.149	3.362	2.136	7.87	5.267	5.543	5.023	28.22	14.63	27.06	30.76	57.67	34.14		144.7
G*/sin(δ) kPa)	76	1.949	1.598	1.786	1.03	3.652	2.543	2.423	2.144	13.06	7.318	11.85	12.72	24.54	15.48		80.2
G*/sin(δ) (kPa)	82	0.904	0.811	0.949	0.497	1.695	1.228	1.059	0.915	6.044	3.661	5.189	5.26	10.442	7.019		44.45
Pass/Fail Temp.		**81.2**	**80.1**	**81.5**	**76.2**	**86.1**	**83.7**	**82.4**	**81.4**	**96.0**	**93.2**	**94.0**	**93.3**	**98.5**	**96.8**		**120.6**
RTFO Residue	T (°C)																
G*/sin(δ) (kPa)	64	17.05				33.12				80.07				100.4			
G*/sin(δ) (kPa)	70	7.414	6.316	6.417	4.126	14.27	9.962	9.798	9.833	32.84	23.02	29.00	30.78	40.4	33.64		32.61
G*/sin(δ) (kPa)	76	3.351	2.608	2.709	1.832	6.481	3.893	4.379	4.182	14.42	9.918	11.76	12.4	17.03	13.38		14.59
G*/sin(δ) (kPa)	82	1.515	1.077	1.144	0.813	2.943	1.521	1.957	1.779	6.332	4.273	4.769	4.995	7.179	5.322		6.528
Pass/Fail Temp.		**79.2**	**77.2**	**77.5**	**74.7**	**84.2**	**79.6**	**81.1**	**80.5**	**89.7**	**86.7**	**87.1**	**87.4**	**90.2**	**87.8**		**90.1**
PG		**76**	**76**	**76**	**70**	**82**	**76**	**76**	**76**	**88**	**82**	**82**	**76**	**88**	**88**		**88**
MSCR at 76ºC																	
%R at 0.1 kPa		2.7	10.95	25.27	14.7	5.2	10.12	13.91	14.03	5.8	10.87	38.32	60.33	6.3	9.47		112.3
%R at 3.2 kPa		-1.6	-1.74	4.63	-1.9	0.3	2.42	2.66	-0.71	0.6	2.80	18.62	20.92	0.9	-0.51		50.88
Jnr at 0.1 kPa		2.603	2.60	1.14	3.079	1.206	1.51	0.63	1.76	1.004	0.62	0.22	0.20	0.788	1.48		-0.01
Jnr at 3.2 kPa		3.1	3.58	1.42	4.6	1.4	1.90	0.80	2.40	1.2	0.74	0.30	0.47	0.9	1.87		0.16
Jnrdiff (%)		17.7	37.91	23.82	50.3	20.1	25.82	27.20	36.08	18.2	19.45	37.55	128.5	12.1	26.09		-1202
Traffic		76 S	76S	76H	N/A	76 H	76H	76V	76S	82 H*	76V	76E	N/A	82 V*	76H		N/A
MSCR at 70ºC																	
%R at 0.1 kPa		5.3	12.09	34.80	22.28		11.33	20.71	21.49		19.26	44.40	64.07		12.44		108.1
%R at 3.2 kPa		0.8	1.27	0.93	-0.36		3.28	10.97	4.35		11.46	10.43	32.10		3.64		61.52
Jnr at 0.1 kPa		1.174	1.05	0.57	1.41		0.61	0.31	0.59		0.23	0.08	0.07		0.61		-0.01
Jnr at 3.2 kPa		1.3	1.35	0.64	2.32		0.74	0.37	0.82		0.26	0.11	0.16		0.74		0.06
Jnrdiff (%)		11.3	29.42	11.83	64.31		20.95	19.60	39.59		14.25	33.05	122.6		21.43		-1200
Traffic		70 H	70H	70V	70S		70V	70E	70V		70V	70E	N/A		70V		N/A
AASHTO MP 19-10		**76(S)**	**76(S)**	**76(H)**	**70(S)**	**76(H**	**76(H)**	**76(V)**	**76(S)**	**82(H)**	**76(V)**	**76(E)**	**N/A**	**82(V)**	**76(H)**		**N/A**
AASHTO TP 70		Failed	Failed	Failed	Failed	Fail	Fail	Failed	Failed	Failed	Failed	Failed	Failed	Failed	Failed		**N/A**

Table B 4: RHDPE-SBS Asphalt Binders AASHTO MP 19-10 and AASHTO TP 70 Results Summary.

HDPE		**2.0%**	**2.0%**	**2.0%**	**2.0%**	**4.0%**	**4.0%**	**4.0%**	**4.0%**	**6.0%**	**6.0%**	**6.0%**	**6.0%**	**8.0%**	**8.0%**	**8.0%**	**8.0%**
PP		0.0%	0.0%	0.0%	0.0%	0.0%	0.0%	0.0%	0.0%	0.0%	0.0%	0.0%	0.0%	0.0%	0.0%	0.0%	0.0%
SBS		**0.0%**	**1.0%**	**1.5%**	**2.0%**	**0.0%**	**1.0%**	**1.5%**	**2.0%**	**0.0%**	**1.0%**	**1.5%**	**2.0%**	**0.0%**	**1.0%**	**1.5%**	**2.0%**
Polybilt101 (PB)		0.0%	0.0%	0.0%	0.0%	0.0%	0.0%	0.0%	0.0%	0.0%	0.0%	0.0%	0.0%	0.0%	0.0%	0.0%	0.0%
Original Binder	T (°C)																
G*/sin(δ) (kPa)	64	9.651				18.28				66.04				134.5			
G*/sin(δ) (kPa)	70	4.203	5.28	4.271		7.87	7.713	4.923	15.18	28.22	18.68	16.74	26.7	57.67			
G*/sin(δ) kPa)	76	1.949	2.435	2.009	3.125	3.652	3.559	2.449	7.031	13.06	9.155	9.943	13.47	24.54			
G*/sin(δ) (kPa)	82	0.904	1.123	0.945	1.533	1.695	1.642	1.218	3.257	6.044	4.487	5.906	6.796	10.442			
Pass/Fail Temp.		**81.2**	**82.9**	**81.5**	**85.6**	**86.1**	**85.8**	**83.7**	**91.2**	**96.0**	**94.6**	**102.5**	**98.8**	**98.5**			
RTFO Residue	T (°C)																
G*/sin(δ) (kPa)	64	17.05				33.12				80.07				100.4			
G*/sin(δ) (kPa)	70	7.414	9.47	7.283	12.75	14.27	11.18	7.695	35.06	32.84	18.03	8.611	24.6	40.4			
G*/sin(δ) (kPa)	76	3.351	4.207	3.52	6.047	6.481	4.697	3.607	16.9	14.42	8.106	4.09	11.43	17.03			
G*/sin(δ) (kPa)	82	1.515	1.869	1.701	2.868	2.943	1.973	1.691	8.146	6.332	3.644	1.943	5.311	7.179			
Pass/Fail Temp.		**79.2**	**80.8**	**79.9**	**84.1**	**84.2**	**81.3**	**79.9**	**92.8**	**89.7**	**85.8**	**81.0**	**88.9**	**90.2**			
PG		**76**	**76**	**76**	**82**	**82**	**76**	**76**		**82**	**82**	**76**		**88**			
MSCR at 76ºC																	
%R at 0.1 kPa		2.7		7.79	19.59	5.2	3.97	33.9	18.96	5.8	18.97	25.02	25.24	6.3			
%R at 3.2 kPa		-1.6		0.20	10.02	0.3	-0.18	18.6	9.85	0.6	6.18	7.33	14.67	0.9			
Jnr at 0.1 kPa		2.603		2.62	0.91	1.206	1.58	0.609	0.88	1.004	0.66	1.01	0.39	0.788			
Jnr at 3.2 kPa		3.1		3.27	1.16	1.4	1.82	0.0	1.11	1.2	0.84	1.38	0.48	0.9			
Jnrdiff (%)		17.7		24.96	27.50	20.1	15.22	-91.8	25.92	18.2	26.77	36.89	24.90	12.1			
Traffic		76 S		76S	76H	76 H	76H	N/A	76H	82 H*	76V	76H	76E	82 V*			
MSCR at 70ºC																	
%R at 0.1 kPa		5.3	12.58	17.15	27.84		9.49	33.87	28.48		24.90	31.16	36.56				
%R at 3.2 kPa		0.8	6.65	5.43	20.76		4.06	13.86	20.76		14.32	15.58	27.14				
Jnr at 0.1 kPa		1.174	0.70	1.09	0.37		0.66	0.61	0.34		0.26	0.43	0.15				
Jnr at 3.2 kPa		1.3	0.81	1.44	0.43		0.74	0.87	0.41		0.32	0.53	0.18				
Jnrdiff (%)		11.3	14.99	32.35	16.94		12.53	43.10	19.32		23.09	22.65	23.38				
Traffic		70 H	70V	70H	70E		70H	70H	70E		70E	70V	70E				
AASHTO MP 19-10		**76(S)**	**70(V)**	**76(S)**	**76(H)**	**76(H**	**76(H)**	**70(H)**	**76(H)**	**82(H)**	**76(V)**	**76(H)**	**76(E)**	**82(V)**			
AASHTO TP 70		Failed	Failed	Failed	Failed	Fail	Failed	Failed	Failed	Failed	Failed	Failed	Failed	Failed			

Table B 5: RPP-PB Asphalt Binders AASHTO MP 19-10 and AASHTO TP 70 Results Summary.

LDPE		0.0%	0.0%	0.0%	0.0%	0.0%	0.0%	0.0%	0.0%	0.0%	0.0%	0.0%	0.0%	0.0%	0.0%	0.0%	0.0%
HDPE		0.0%	0.0%	0.0%	0.0%	0.0%	0.0%	0.0%	0.0%	0.0%	0.0%	0.0%	0.0%	0.0%	0.0%	0.0%	0.0%
PP		**2.0%**	**2.0%**	**2.0%**	**2.0%**	**4.0%**	**4.0%**	**4.0%**	**4.0%**	**6.0%**	**6.0%**	**6.0%**	**6.0%**	**8.0%**	**8.0%**	**8.0%**	**8.0%**
SBS		0.0%	0.0%	0.0%	0.0%	0.0%	0.0%	0.0%	0.0%	0.0%	0.0%	0.0%	0.0%	0.0%	0.0%	0.0%	0.0%
Polybilt101 (PB)		**0.0%**	**1.0%**	**1.5%**	**2.0%**	**0.0%**	**1.0%**	**1.5%**	**2.0%**	**0.0%**	**1.0%**	**1.5%**	**2.0%**	**0.0%**	**1.0%**	**1.5%**	**2.0%**
Original Binder	T (°C)																
G*/sin(δ) (kPa)	70	4.784	2.655	3.635	5.503	6.453	5.003	9.03	4.923	5.4	9.991	13.63	11.58	19.62			
G*/sin(δ) kPa)	76	2.14	1.258	2.158	2.467	2.865	2.378	5.261	2.257	2.377	5.846	6.318	5.473	8.698			
G*/sin(δ) (kPa)	82	0.957	0.596	1.281	1.106	1.272	1.13	3.065	1.035	1.046	3.421	2.929	2.587	3.856			
Pass/Fail Temp.		**81.7**	**77.8**	**84.8**	**82.8**	**83.8**	**83.0**	**94.4**	**82.3**	**82.3**	**95.8**	**90.4**	**89.6**	**92.0**			
RTFO Residue	T (°C)																
G*/sin(δ) (kPa)	70	8.887	6.59	6.969	8.15	12.53	6.096	19.92	9.488	16.3	20.94	21.62	25.15	40.96			
G*/sin(δ) (kPa)	76	4.075	4.117	3.773	3.758	5.611	2.783	8.01	4.366	7.554	9.939	10.02	8.742	19.12			
G*/sin(δ) (kPa)	82	1.869	2.572	2.043	1.733	2.513	1.271	3.22	2.009	3.501	4.717	4.644	3.039	8.925			
Pass/Fail Temp.		**80.7**	**84.0**	**81.3**	**80.2**	**83.0**	**77.8**	**84.5**	**81.3**	**85.6**	**88.1**	**87.8**	**83.8**	**99.2**			
PG																	
MSCR at 76ºC																	
%R at 0.1 kPa		1.9		20.93		80.3		31.11	17.64	1.2	18.02			13.1			
%R at 3.2 kPa		-1.3		9.83		-0.1		9.13	0.31	-1.4	1.44			3.5			
Jnr at 0.1 kPa		2.334		0.58		0.278		0.37	1.37	1.933	0.85			0.759			
Jnr at 3.2 kPa		2.7		0.71		1.8		0.55	2.20	2.2	1.23			0.9			
Jnrdiff (%)		14.6		22.90		542.0		50.59	60.58	12.2	44.99			19.0			
Traffic		76S		76V		N/A		76V	76S	76S	76H			76V			
MSCR at 70ºC																	
%R at 0.1 kPa		72.5		28.54		62.5	15.29	30.68			25.51	51.4	65.96				
%R at 3.2 kPa		2.2		22.20		5.5	8.85	20.85			7.90	23.77	4.03				
Jnr at 0.1 kPa		0.132		0.23		0.241	0.19	0.16			0.34	0.05	0.26				
Jnr at 3.2 kPa		0.6		0.26		0.7	0.20	0.20			0.46	0.07	0.42				
Jnrdiff (%)		355.1		11.55		185.5	8.13	22.27			35.32	22.69	60.27				
Traffic		N/A		70E		N/A	70E	70E			70E	70E	70E				
AASHTO MP 19-10		**76(S)**		**76(V)**		**N/A**	**70(E)**	**76(V)**	**76(S)**	**76(S)**	**76(H)**	**70(E)**	**70(E)**	**76(V)**			
AASHTO TP 70		Failed		Failed		Failed	Failed	Failed	Failed	Failed	Failed	Failed	Failed	Failed			

Table B 6: RPP-SBS Asphalt Binders AASHTO MP 19-10 and AASHTO TP 70 Results Summary.

LDPE		0.0%	0.0%	0.0%	0.0%	0.0%	0.0%	0.0%	0.0%	0.0%	0.0%	0.0%	0.0%	0.0%	0.0%	0.0%	0.0%
HDPE		0.0%	0.0%	0.0%	0.0%	0.0%	0.0%	0.0%	0.0%	0.0%	0.0%	0.0%	0.0%	0.0%	0.0%	0.0%	0.0%
PP		**2.0%**	**2.0%**	**2.0%**	**2.0%**	**4.0%**	**4.0%**	**4.0%**	**4.0%**	**6.0%**	**6.0%**	**6.0%**	**6.0%**	**8.0%**	**8.0%**	**8.0%**	**8.0%**
SBS		**0.0%**	**1.0%**	**1.5%**	**2.0%**	**0.0%**	**1.0%**	**1.5%**	**2.0%**	**0.0%**	**1.0%**	**1.5%**	**2.0%**	**0.0%**	**1.0%**	**1.5%**	**2.0%**
Polybilt101 (PB)		0.0%	0.0%	0.0%	0.0%	0.0%	0.0%	0.0%	0.0%	0.0%	0.0%	0.0%	0.0%	0.0%	0.0%	0.0%	0.0%
Original Binder	T (°C)																
G*/sin(δ) (kPa)	70	4.784	5.942	4.907	3.337	6.453	4.708	5.029	6.828	5.4	5.685	6.924	3.392	19.62	105.8		
G*/sin(δ) kPa)	76	2.14	2.767	2.373	1.586	2.865	2.172	2.37	3.255	2.377	2.541	3.291	1.604	8.698	36.58		
G*/sin(δ) (kPa)	82	0.957	1.289	1.148	0.754	1.272	1.002	1.117	1.552	1.046	1.136	1.564	0.758	3.856	12.65		
Pass/Fail Temp.		**81.7**	**84.0**	**83.1**	**79.7**	**83.8**	**82.0**	**82.9**	**85.6**	**82.3**	**82.9**	**85.6**	**79.8**	**92.0**	**96.3**		
RTFO Residue	T (°C)																
G*/sin(δ) (kPa)	70	8.887	9.019	7.432	6.242	12.53	7.652	8.6	10.36	16.3	10.87	16.85	14.24	40.96	165		
G*/sin(δ) (kPa)	76	4.075	3.509	3.521	2.915	5.611	3.53	4.078	4.787	7.554	4.956	7.943	6.993	19.12	71.42		
G*/sin(δ) (kPa)	82	1.869	1.365	1.668	1.361	2.513	1.628	1.934	2.212	3.501	2.26	3.744	3.435	8.925	30.91		
Pass/Fail Temp.		**80.7**	**79.0**	**79.8**	**78.2**	**83.0**	**79.7**	**81.0**	**82.0**	**85.6**	**82.2**	**86.2**	**85.8**	**99.2**	**100.9**		
PG																	
MSCR at 76ºC																	
%R at 0.1 kPa		1.9	12.30	19.83	14.11	80.3	14.52	29.48		1.2	13.69	31.89	17.51	13.1			
%R at 3.2 kPa		-1.3	4.95	11.91	6.17	-0.1	3.98	1.88		-1.4	1.93	3.73	2.14	3.5			
Jnr at 0.1 kPa		2.334	1.14	0.54	0.81	0.278	0.50	1.07		1.933	0.31	0.57	1.24	0.759			
Jnr at 3.2 kPa		2.7	1.36	0.62	1.29	1.8	0.83	1.83		2.2	0.53	0.97	1.80	0.9			
Jnrdiff (%)		14.6	19.85	16.40	58.40	542.0	66.80	71.34		12.2	70.20	68.99	45.29	19.0			
Traffic		76S	76H	76V	76H	N/A	76V	76H		76S	76V	76V	76H	76V			
MSCR at 70ºC																	
%R at 0.1 kPa		72.5	19.58	30.66	9.44	62.5		45.07			152.9	20.76	21.58				
%R at 3.2 kPa		2.2	13.86	24.77	2.96	5.5		8.74			32.09	11.71	6.68				
Jnr at 0.1 kPa		0.132	0.44	0.21	1.23	0.241		0.47			0.07	0.34	0.53				
Jnr at 3.2 kPa		0.6	0.50	0.23	1.45	0.7		0.68			0.10	0.39	0.70				
Jnrdiff (%)		355.1	12.43	13.15	18.28	185.5		44.11			43.68	15.89	30.74				
Traffic		N/A	70E	70E	70V	N/A		70V			70E	70E	70V				
AASHTO MP 19-10		**76(S)**	**76(H)**	**76(V)**	**76(H)**	**N/A**	**76(V)**	**76(H)**		**76(S)**	**76(V)**	**76(V)**	**76(H)**	**76(V)**			
AASHTO TP 70		Failed	Failed	Failed	Failed	Failed	Failed	Failed		Failed	Failed	Failed	Failed	Failed			

Table B 7: SBS and PB Asphalt Binder AASHTO MP 19-10 and AASHTO TP 70 Results Summary.

SBS		**1.00%**	**1.50%**	**2.00%**	0.00%	0.00%	0.00%
Polybilt101		0.00%	0.00%	0.00%	**1.00%**	**1.50%**	**2.00%**
Original Binder	**T (°C)**						
G*/sin(δ) (kPa)	64	6.597					
G*/sin(δ) (kPa)	70	3.057	3.753	4.144	1.009	1.257	1.49
G*/sin(δ) kPa)	76	1.456	1.759	2.02	0.5041	0.621	0.736
G*/sin(δ) (kPa)	82	0.693	0.824	0.985	0.252	0.307	0.364
Pass/Fail Temp.		79.0	80.5	81.9	70.1	71.9	73.4
RTFO RESIDUE	**T (°C)**						
G*/sin(δ) (kPa)	64						
G*/sin(δ) (kPa)	70	6.027	6.684	7.863	2.058	2.366	2.736
G*/sin(δ) (kPa)	76	2.845	3.214	3.774	1.018	1.219	1.297
G*/sin(δ) (kPa)	82	1.343	1.545	1.811	0.504	0.628	0.615
Pass/Fail Temp.		78.1	79.1	80.4	69.4	70.7	71.8
PG		**78.1**	**79.1**	**80.4**	**69.4**	**70.7**	**71.8**
MSCR at 76°C.							
%R at 0.1 kPa		3.9		9.4			56.6
%R at 3.2 kPa		0.2		3.1			-2.8
J_{nr} at 0.1 kPa		29.425		19.212			2.500
J_{nr} at 3.2 kPa		3.4		2.2			9.3
J_{nr}diff (%)		-88.6		-88.3			272.1
Traffic		76(S)		76(S)			NA
MSCR at 70°C.							
%R at 0.1 kPa		11.3		19.5	4.3		42.6
%R at 3.2 kPa		5.1		11.9	-1.2		-1.1
J_{nr} at 0.1 kPa		11.781		7.523	29.555		1.566
J_{nr} at 3.2 kPa		1.4		0.9	3.6		4.0
J_{nr}diff (%)		-88.4		-88.4	-87.9		154.9
Traffic							
AASHTO MP 19-10		70(H)		70(V)	70(S)		NA
AASHTO TP 70							

APPENDIX C

Table C 1: Laboratory Asphalt Storage Stability Results of RPW Modified Binder.

Blend	PG+	0 hours, 75°C						48 hours, 75°C						Degradation Ratio (DR)		SEPARATION STATUS	DEGRADATION STATUS
		G* (Pa)		δ (°C)		Separation Ratio (SR)		G* (Pa)		δ (°C)		Separation Ratio (SR)					
		Top	Bottom	Top	Bottom	SR(G*)	SR(δ)	Top	Bottom	Top	Bottom	SR(G*)	SR(δ)	DR(G*)	DR(δ)		
L4	70(H)	6593	6762	78.91	78.52	0.97	1.00	6951	7449	73.89	72.74	0.93	1.02	1.08	0.93	STABLE	STABLE
L2S2	70(H)	1151	1140	68.9	68.71	1.01	1.00	998	911	63.74	53.52	1.10	1.19	0.83	0.85	STABLE	STABLE
H2	70(H)	3151	2905	64.91	65.73	1.08	0.99	2913	2904	58.78	59.41	1.00	0.99	0.96	0.90	STABLE	STABLE
H2PB1	76(S)	1540	1527	70.22	70.02	1.01	1.00	1491	1528	65.63	65.26	0.98	1.01	0.98	0.93	STABLE	STABLE
H2S1	70(H)	6171	6494	76.38	76.4	0.95	1.00	6920	6967	73.94	74.27	0.99	1.00	1.10	0.97	STABLE	STABLE
P2	70(H)	10166	6899	64.97	78.33	**1.47**	0.83	7551	7650	72.8	72.65	0.99	1.00	0.89	1.02	STABLE	STABLE
P2PB1	70(H)	2582	2530	80.59	80.51	1.02	1.00	3846	3800	76.67	76.51	1.01	1.00	**1.50**	0.95	STABLE	Degrading
P2S1	70(H)	3851	3742	79.17	79.52	1.03	1.00	5312	5429	72.32	72.43	0.98	1.00	**1.41**	0.91	STABLE	Degrading
L6	76(H)	6548	7437	77.21	78.93	0.88	0.98	7066	7084	74.89	79.72	1.00	0.94	1.01	0.99	STABLE	STABLE
L4S1.5	76(H)	1319	1242	69.78	67.09	1.06	1.04	1503	1404	68.38	68.43	1.07	1.00	1.14	1.00	STABLE	STABLE
L6B1	76(H)	3471	3299	79.66	79.14	1.05	1.01	3730	3855	78.25	78.79	0.97	0.99	1.12	0.99	STABLE	STABLE
H4	76(H)	4553	4246	78.13	78.91	1.07	0.99	5301	4806	76.90	79.38	1.10	0.97	1.15	1.00	STABLE	STABLE
H2B1.5	76(H)	2745	2856	80.18	79.86	0.96	1.00	3224	3180	78.76	78.13	1.01	1.01	1.14	0.98	STABLE	STABLE
H4S1	76(H)	4458	4236	77.93	78.84	1.05	0.99	4877	4462	76.55	77.13	1.09	0.99	1.07	0.98	STABLE	STABLE
P4	76(H)	9082	3480	67.02	78.01	**2.61**	0.86	12242	13173	61.66	61.81	0.93	1.00	**2.02**	0.85	UNSTABLE	Degrading
P4B2	76(H)	3177	2960	77.3	79.03	1.07	0.98	4523	4992	76.22	75.96	0.91	1.00	**1.55**	0.97	STABLE	Degrading

Table C 2: Results of RPW Composition Statistics.

Label	1	2	3	4	5	6	Sub-Total
Name	**PET**	**HDPE**	**PVC**	**LDPE**	**PP**	**PS**	
Sample 1	34.5	44.5	0.0	14.5	7.5	2.5	103.5
Sample 2	43.0	22.0	0.0	10.5	5.0	0.0	80.5
Sample 3	23.5	0.0	0.0	12.5	16.5	12.5	65.0
**	**	**	**	**	**	**	**
**	**	**	**	**	**	**	**
Sample 14	8.5	0.0	0.0	10.0	28.0	15.0	61.5
Sample 15	44.0	0.0	20	13.0	14.0	2.0	93.0
Sample 16	0.0	14.0	0.0	8.0	0.0	11.5	33.5
Sample 17	28.0	14.0	0.0	12.0	0.0	22.0	76.0
Sample 18	17.0	24.0	12	24.0	0.0	3.5	80.5
Sample 19	18.0	0.0	0.0	12.0	18.0	14.0	62.0
Sample 20	38.0	28.0	0.0	8.0	20.0	9.0	103.0
Sample 21	0.0	0.0	15	16.0	0.0	0.0	31.0
Sample 22	2.5	18.0	8	18.0	15.0	9.0	70.5
Sample 23	42.0	26.0	0.0	8.0	0.0	0.0	76.0
Sample 24	28.0	54.0	0.0	8.0	0.0	5.0	95.0
Sample 25	40.0	32.0	0.0	8.0	8.0	0.0	88.0
Sample 26	69.0	22.0	10	14.0	16.0	18.0	149.0
Sample 27	30.0	0.0	0.0	13.0	18.0	0.0	61.0
Sample 28	57.5	37.0	0.0	14.0	22.5	4.0	135.0
Sample 29	0.0	0.0	0.0	10.0	0.0	0.0	10.0
Sample 30	28.0	30.0	0.0	20.0	2.5	0.0	80.5
Sample 31	0.0	28.5	0.0	15.0	12.5	15.0	71.0
Sample 32	50.0	0.0	0.0	8.0	26.0	0.0	84.0
Sample 33	0.0	55.0	0.0	10.0	5.0	0.0	70.0
Sample 34	34.0	0.0	0.0	8.0	22.0	1.0	65.0
Sample 35	50.0	0.0	0.0	18.0	5.5	0.0	73.5
Sample 36	46.0	10.0	15	20.0	12.0	0.0	103.0
Sample 37	40.0	0.0	0.0	8.0	0.0	0.0	48.0
Sample 38	40.0	20.0	10	12.0	0.0	20.0	102.0
Sample 39	16.0	28.0	0.0	8.0	14.0	9.0	75.0
Sample 40	28.0	38.0	0.0	12.0	0.0	12.0	90.0
Sample 41	34.0	26.0	20	8.0	0.0	4.0	92.0
Sample 42	10.0	0.0	0.0	10.0	0.0	7.0	27.0
Sample 43	0.0	16.5	13	24.0	0.0	9.0	62.5
Sample 44	0.0	19.0	0.0	13.0	5.0	2.0	39.0
Sample 45	10.0	26.0	0.0	18.0	22.0	15.0	91.0
Sample 46	52.0	0.0	0.0	16.5	15.5	10.0	94.0
Sample 47	18.0	10.5	0.0	15.0	0.0	0.0	43.5
Sample 48	0.0	52.5	0.0	15.0	0.0	9.0	76.5
Sample 49	28.0	39.5	0.0	13.0	0.0	18.0	98.5
Sample 50	22.0	0.0	0.0	15.0	12.5	2.0	51.5
Sample 51	38.0	0.0	0.0	12.5	28.0	0.0	78.5
Sample 52	0.0	34.5	0.0	12.5	0.0	8.0	55.0
Sample 53	8.0	0.0	0.0	15.0	0.0	15.0	38.0
Sub-Total	1384.0	1028.0	155.0	702.0	477.5	360.0	4106.5
% Proportion	33.7	25.0	3.8	17.1	11.6	8.8	100.0
UCI	46.4	36.7	8.9	27.2	20.3	16.4	
LCI	21.0	13.4	0.0	7.0	3.0	1.2	
Required Sample size (5% SL)	390	288	59	216	150	112	
Required Sample size (10% SL)	275	203	42	152	106	79	

Table C 3: Fresh AC Superpave Mix Design Results Summary.

Sample Results	Fresh (%Asphalt Content)				Optimum
	4.0	4.5	5.0	5.5	4.81
%Gmm(N-Initial)	84.7	84.3	89.8	90.3	87.70
%Gmm(N-Design)	92.2	92.2	98.3	98.5	96.00
%Gmm(N-Maximum)	93.6	94.5	100.6	100.9	98.31
%Air Voids(N-Design)	7.8	7.8	1.7	1.5	4.00
%VMA(N-Design)	19.00	19.08	15.81	16.66	17.06
%VFA(N-Design)	58.81	59.29	89.36	90.95	75.20

Table C 4: H4_76(H) AC Superpave Mix Design Results Summary.

Sample Results	H4 (%Asphalt Content)				Optimum
	4.5	5.0	5.5	6.0	5.71
%Gmm(N-Initial)	87.7	86.9	85.2		88.53
%Gmm(N-Design)	94.5	92.8	91.7		96.00
%Gmm(N-Maximum)	94.3	94.3	97.7		94.30
%Air Voids(N-Design)	5.5	7.2	8.3		4.00
%VMA(N-Design)	18.81	19.08	20.08		18.55
%VFA(N-Design)	70.70	62.47	58.71		75.53

Table C 5: L4S1.5_76(H) AC Superpave Mix Design Results Summary.

Sample Results	L4S1.5 (%Asphalt Content)				Optimum
	4.2	4.7	5.2	5.7	5.28
%Gmm(N-Initial)	84.4	84.5	87.3	90.6	87.86
%Gmm(N-Design)	91.0	90.5	95.3	99.7	96.00
%Gmm(N-Maximum)	92.9	92.4	97.0	101.0	97.61
%Air Voids(N-Design)	9.0	9.5	4.7	0.3	4.00
%VMA(N-Design)	20.27	20.35	17.19	15.96	16.99
%VFA(N-Design)	55.58	53.43	72.69	97.84	76.70

Table C 6: L6_76(H) AC Superpave Mix Design Results Summary.

Sample Results	L6 (%Asphalt Content)				Optimum
	4.2	4.7	5.2	5.7	5.16
%Gmm(N-Initial)	85.2	85.1	88.1		87.80
%Gmm(N-Design)	93.0	94.1	96.2		96.00
%Gmm(N-Maximum)	93.6	96.3	98.3	0.0	98.14
%Air Voids(N-Design)	7.0	5.9	3.8		4.00
%VMA(N-Design)	19.39	18.94	17.47	16.66	17.60
%VFA(N-Design)	63.68	68.81	78.14		75.33

Table C 7: RPW-AC Resilient Modulus Results (RPW Size Optimization).

	Resilient Modulus (MPa)								
	G2 S1-10 (254)		G2 S1-5 (127)		G2 S2-20 (484)		G2 S2-10 (254)		NEAT AC.
Temp. ^{o}C	20	40	20	40	20	40	20	40	20
Sample 1	4527	1631	5539	2510	4094	2580	4034	1321	8844
Sample 2	4503	1580	5802	2447	4077	2711	3936	1391	8777
Sample 3	4412	1635	4721	2464	3808	2691	3669	1336	8365
Sample 4	4507	1552	4669	2528	3077	2692	3711	1302	8241
Aver.	4487	1600	5183	2487	3764	2669	3838	1338	8557

Table C 8: RPW-AC Resilient Modulus Results.

	Resilient Modulus (MPa)													
	L6_76(H)		L4S1.5_76(H)		L6B1_76(H)		H4_76(H)		H2B1.5_76(H)		H4S1_76(H)		P2S1_(76)	
Temp. (^{o}C)	20	44	20	44	20	44	20	44	20	44	20	44	20	44
Sample1	15288	8605	12789	8552	14239	8492	9053	3133	12698	7298	9401	4201	12860	7667
Sample2	15263	8526	12788	8459	13945	9023	8961	3077	12806	7366	9082	3953	12806	7438
Sample3	15036	8573	13469	8551	--	--	8331	3248	11296	7188	--	--	14452	7327
Sample4	15224	8645	13309	8560	--	--	8329	3333	11323	7056	--	--	14154	7224
Aver.	15203	8587	13089	8531	14092	8758	8669	3198	12031	7227	9242	4077	13568	7414

Table C 9: Preliminary RPW size and Content Selection for AC Modification.

	G2 S1-10 (254)	G2 S1-5 (127)	G2 S2-20 (484)	G2 S2-10 (254)	Fresh
height (")	2.7	2.6	2.5	2.6	3.0
RM at 20 deg	4487	5183	3764	3838	8557
RM at 44 deg	1600	2487	2669	1338	**
ITS load (dry)	2352	2204	3073	1485	2881
ITS load (Wet)	1639	2058	2820	1262	2336
ITS -dry (psi)	140	135	194	91	151
RSI (%)	70	93	92	85	81

Table C 10: RPW-AC Indirect Tensile Strength and Resilient Modulus Results.

	L6_76(H)	L4S1.5_76(H)	L6B1_76(H)	H4_76(H)	H2B1.5_76(H)	H4S1_76(H)	P2S1_(76)
height (")	2.8	3.0	3	2.9	3.0	3	3.0
RM at 20 deg	15203	13089	14092	8669	12031	9242	13568
RM at 44 deg	8587	8531	8758	3198	7227	4077	7414
ITS load (dry)	5169	4676	4789	3207	4382	3824	5122
ITS load (Wet)	5160	3870	4329	3036	4284	3543	4308
ITS -dry (psi)	294	246	254	175	230	203	273
RSI (%)	99.83	83	90	95	98	93	84

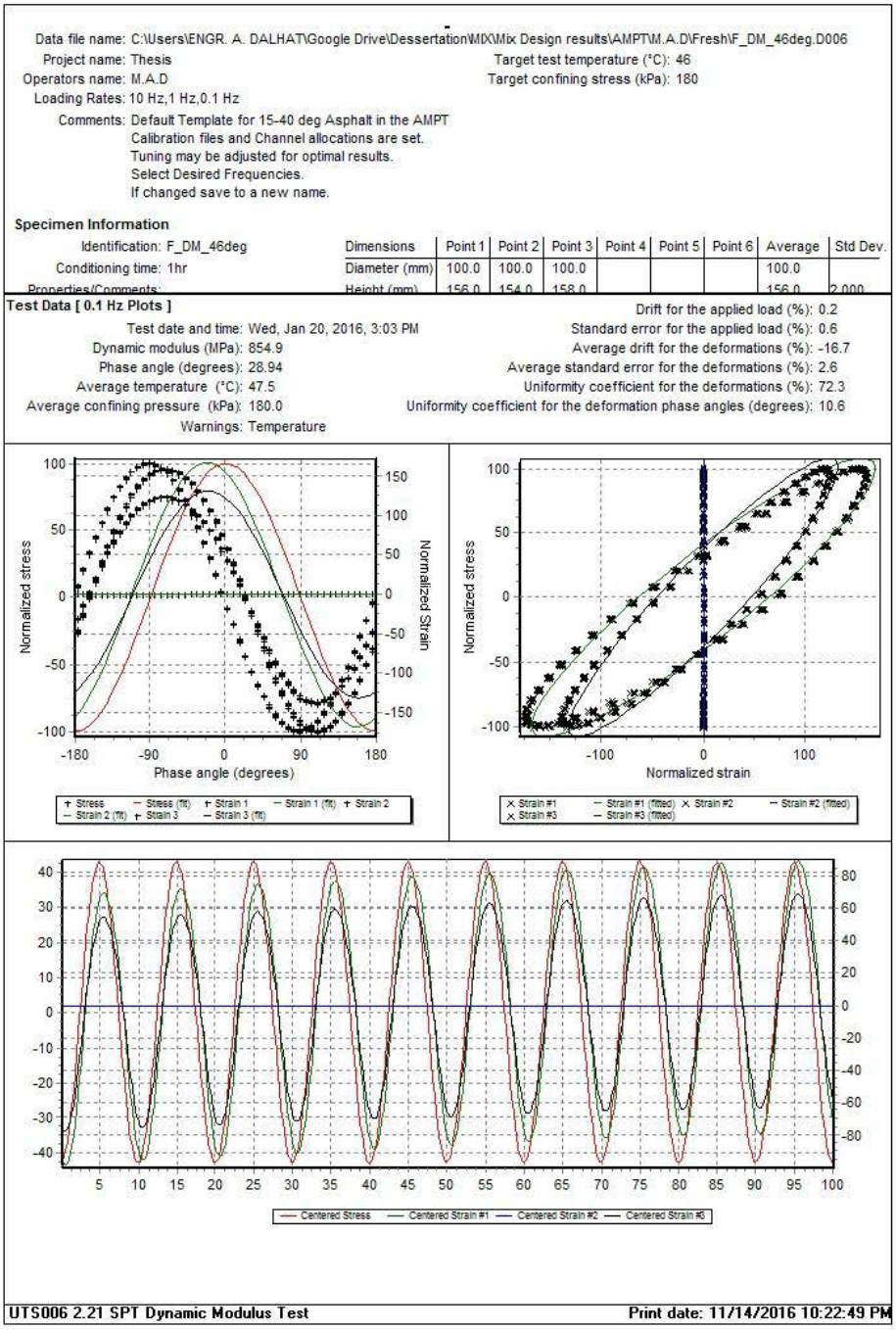

Figure C 1: Dynamic Modulus Test Out Put Summary Fresh AC at 46^{o}C, 0.1 Hz (1 of 2).

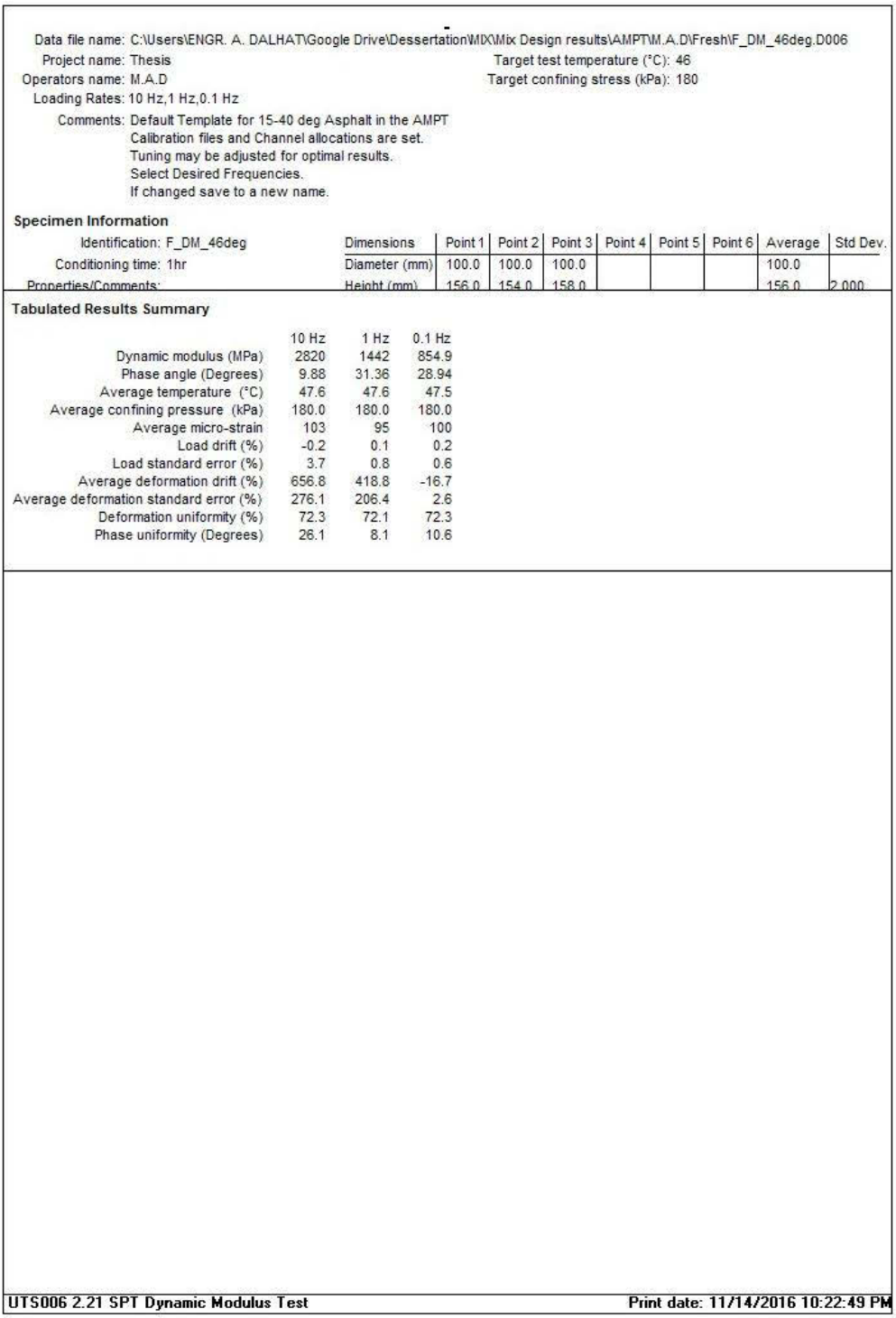

Data file name: C:\Users\ENGR. A. DALHAT\Google Drive\Dessertation\MIX\Mix Design results\AMPT\M.A.D\Fresh\F_DM_46deg.D006
Project name: Thesis
Target test temperature (°C): 46
Operators name: M.A.D
Target confining stress (kPa): 180
Loading Rates: 10 Hz,1 Hz,0.1 Hz
Comments: Default Template for 15-40 deg Asphalt in the AMPT
Calibration files and Channel allocations are set.
Tuning may be adjusted for optimal results.
Select Desired Frequencies.
If changed save to a new name.

Specimen Information

Identification: F_DM_46deg	Dimensions	Point 1	Point 2	Point 3	Point 4	Point 5	Point 6	Average	Std Dev.
Conditioning time: 1hr	Diameter (mm)	100.0	100.0	100.0				100.0	
Properties/Comments:	Height (mm)	156.0	154.0	158.0				156.0	2.000

Tabulated Results Summary

	10 Hz	1 Hz	0.1 Hz
Dynamic modulus (MPa)	2820	1442	854.9
Phase angle (Degrees)	9.88	31.36	28.94
Average temperature (°C)	47.6	47.6	47.5
Average confining pressure (kPa)	180.0	180.0	180.0
Average micro-strain	103	95	100
Load drift (%)	-0.2	0.1	0.2
Load standard error (%)	3.7	0.8	0.6
Average deformation drift (%)	656.8	418.8	-16.7
Average deformation standard error (%)	276.1	206.4	2.6
Deformation uniformity (%)	72.3	72.1	72.3
Phase uniformity (Degrees)	26.1	8.1	10.6

UTS006 2.21 SPT Dynamic Modulus Test
Print date: 11/14/2016 10:22:49 PM

Figure C 2: Dynamic Modulus Test Out Put Summary Fresh AC at 46^{o}C, 0.1 Hz (2 of 2).

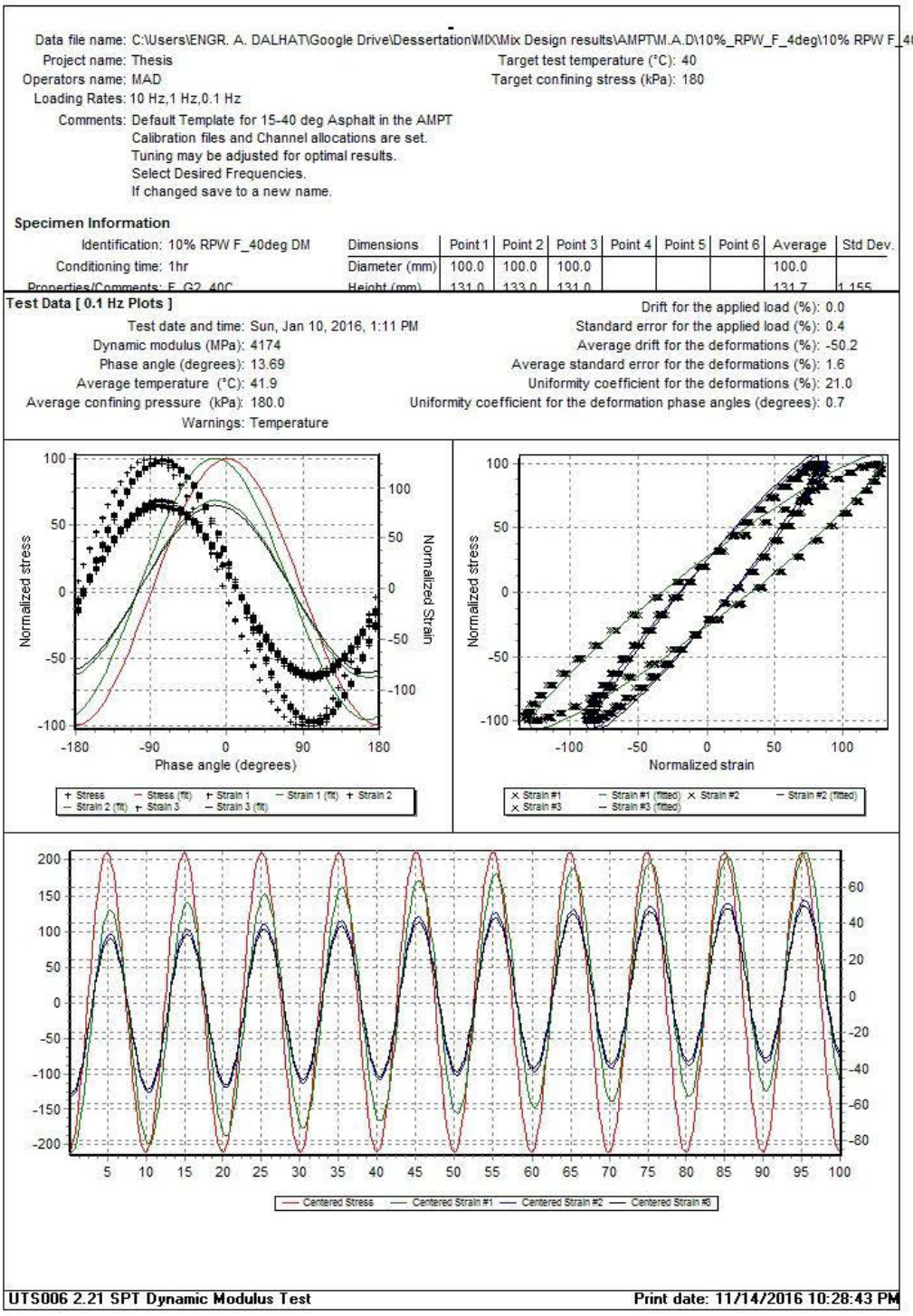

Figure C 3: Dynamic Modulus Test Out Put Summary 10% RPW AC at 40°C, 0.1 Hz (1 of 2).

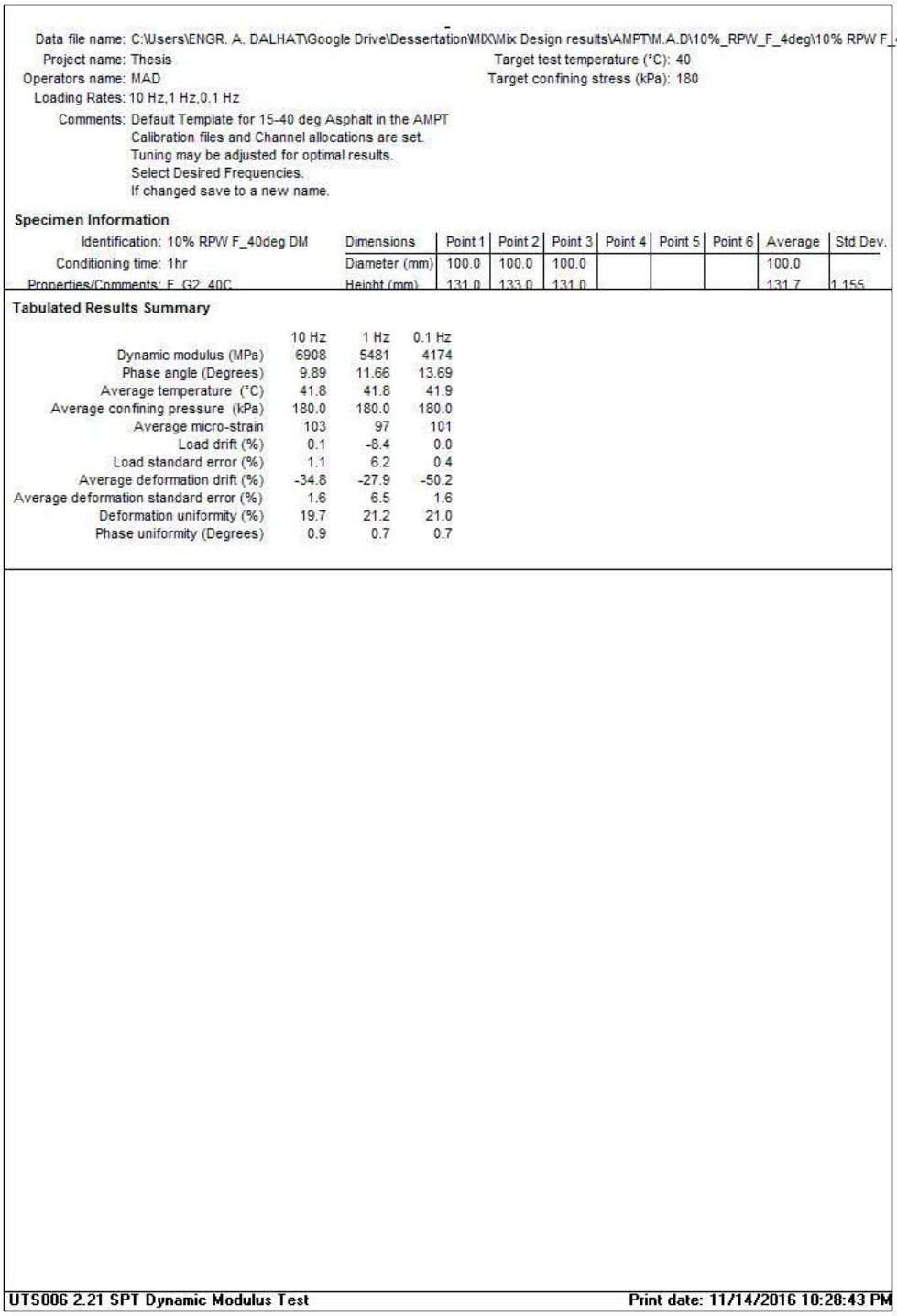

Data file name: C:\Users\ENGR. A. DALHAT\Google Drive\Dessertation\MIX\Mix Design results\AMPT\M.A.D\10%_RPW_F_4deg\10% RPW F_40deg DM
Project name: Thesis
Target test temperature (°C): 40
Operators name: MAD
Target confining stress (kPa): 180
Loading Rates: 10 Hz,1 Hz,0.1 Hz
Comments: Default Template for 15-40 deg Asphalt in the AMPT
Calibration files and Channel allocations are set.
Tuning may be adjusted for optimal results.
Select Desired Frequencies.
If changed save to a new name.

Specimen Information

Identification: 10% RPW F_40deg DM	Dimensions	Point 1	Point 2	Point 3	Point 4	Point 5	Point 6	Average	Std Dev.
Conditioning time: 1hr	Diameter (mm)	100.0	100.0	100.0				100.0	
Properties/Comments: F_G2_40C	Height (mm)	131.0	133.0	131.0				131.7	1.155

Tabulated Results Summary

	10 Hz	1 Hz	0.1 Hz
Dynamic modulus (MPa)	6908	5481	4174
Phase angle (Degrees)	9.89	11.66	13.69
Average temperature (°C)	41.8	41.8	41.9
Average confining pressure (kPa)	180.0	180.0	180.0
Average micro-strain	103	97	101
Load drift (%)	0.1	-8.4	0.0
Load standard error (%)	1.1	6.2	0.4
Average deformation drift (%)	-34.8	-27.9	-50.2
Average deformation standard error (%)	1.6	6.5	1.6
Deformation uniformity (%)	19.7	21.2	21.0
Phase uniformity (Degrees)	0.9	0.7	0.7

UTS006 2.21 SPT Dynamic Modulus Test
Print date: 11/14/2016 10:28:43 PM

Figure C 4: : Dynamic Modulus Test Out Put Summary 10% RPW AC at 40oC, 0.1 Hz (2 of 2).

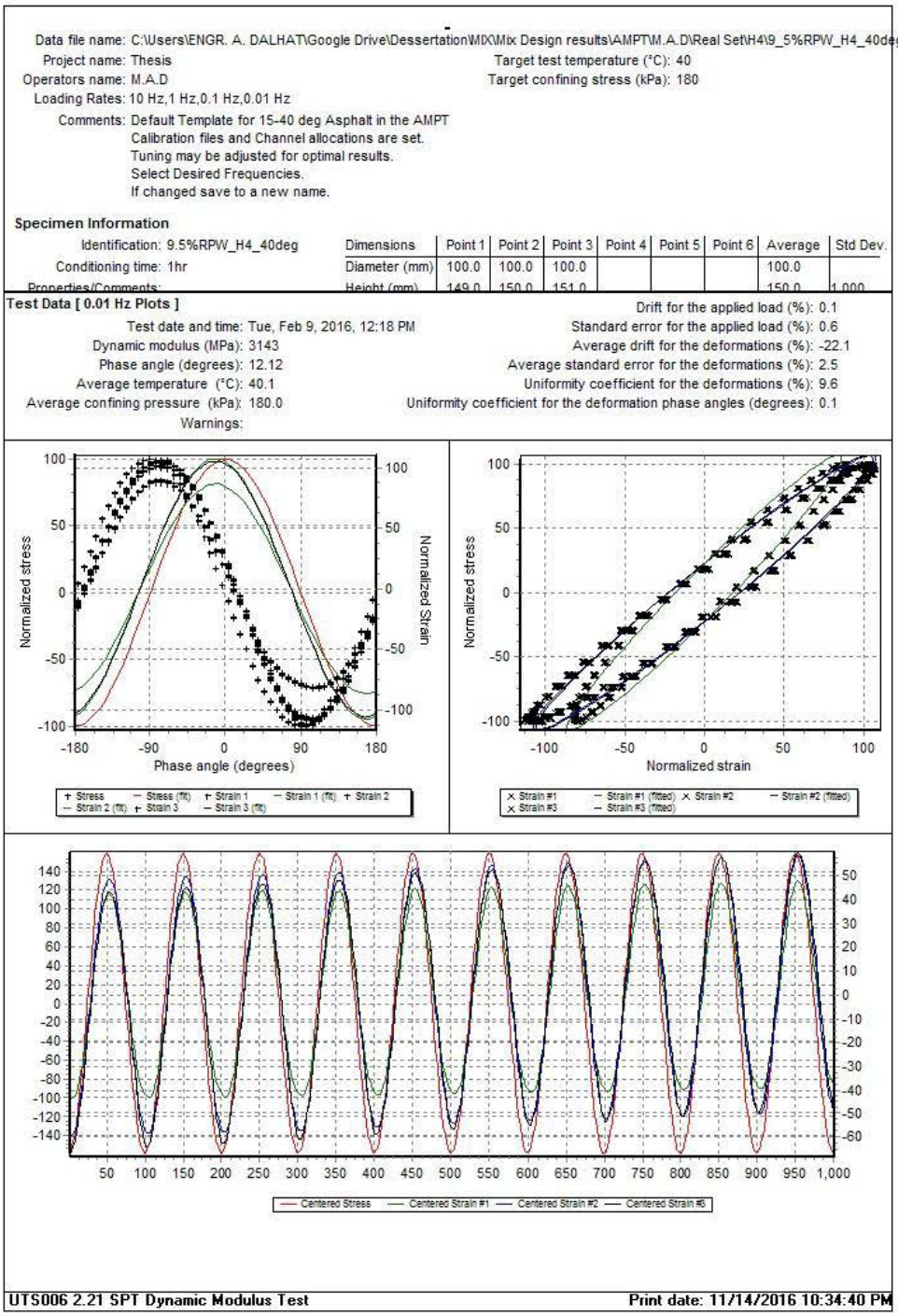

Figure C 5: Dynamic Modulus Test Out Put Summary H4_76(H)+RPW AC at 40oC, 0.1 Hz (1 of 2).

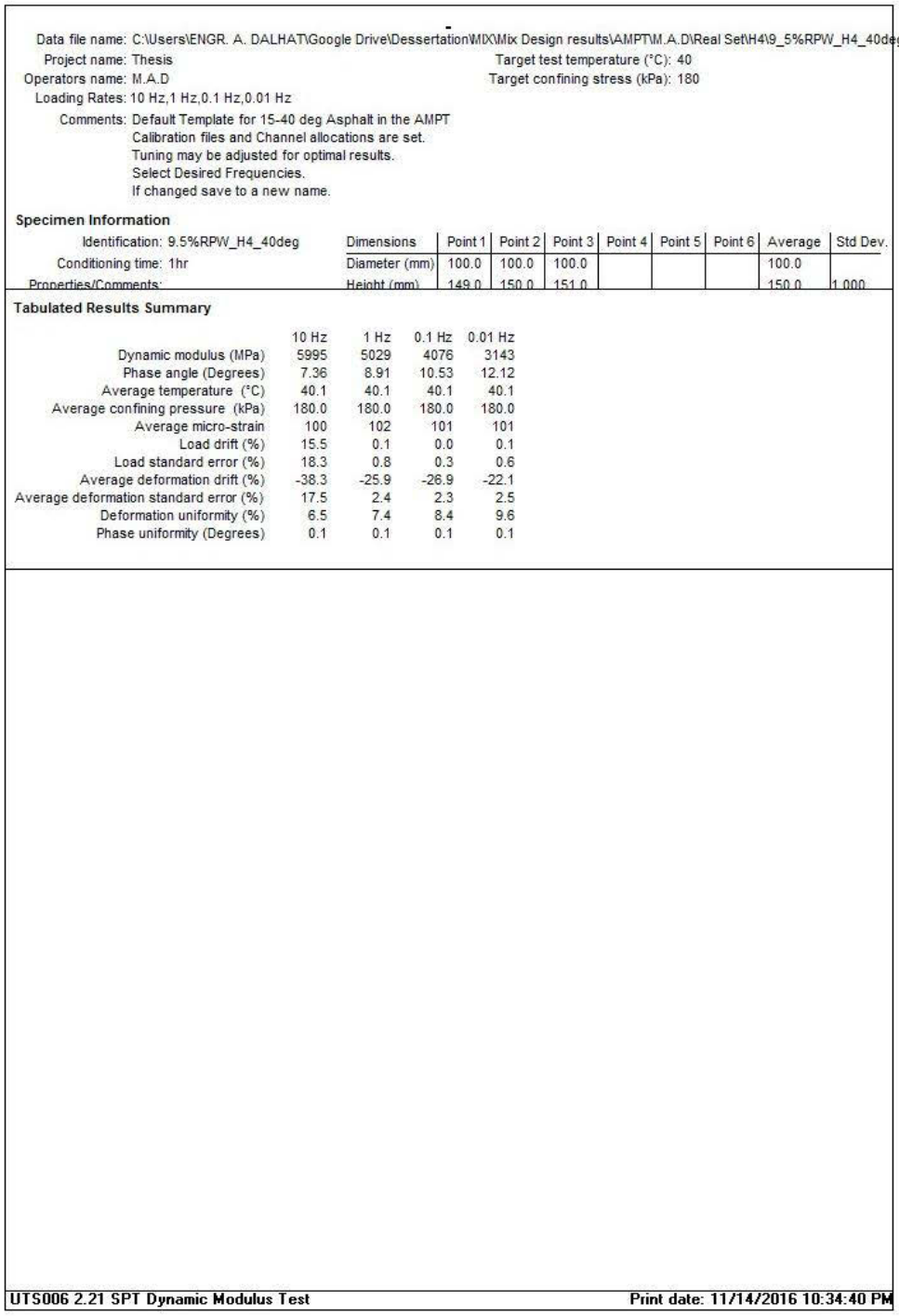

Data file name: C:\Users\ENGR. A. DALHAT\Google Drive\Dessertation\MIX\Mix Design results\AMPT\M.A.D\Real Set\H4\9_5%RPW_H4_40deg.D006
Project name: Thesis
Target test temperature (°C): 40
Operators name: M.A.D
Target confining stress (kPa): 180
Loading Rates: 10 Hz,1 Hz,0.1 Hz,0.01 Hz
Comments: Default Template for 15-40 deg Asphalt in the AMPT
Calibration files and Channel allocations are set.
Tuning may be adjusted for optimal results.
Select Desired Frequencies.
If changed save to a new name.

Specimen Information

Identification: 9.5%RPW_H4_40deg	Dimensions	Point 1	Point 2	Point 3	Point 4	Point 5	Point 6	Average	Std Dev.
Conditioning time: 1hr	Diameter (mm)	100.0	100.0	100.0				100.0	
Properties/Comments:	Height (mm)	149.0	150.0	151.0				150.0	1.000

Tabulated Results Summary

	10 Hz	1 Hz	0.1 Hz	0.01 Hz
Dynamic modulus (MPa)	5995	5029	4076	3143
Phase angle (Degrees)	7.36	8.91	10.53	12.12
Average temperature (°C)	40.1	40.1	40.1	40.1
Average confining pressure (kPa)	180.0	180.0	180.0	180.0
Average micro-strain	100	102	101	101
Load drift (%)	15.5	0.1	0.0	0.1
Load standard error (%)	18.3	0.8	0.3	0.6
Average deformation drift (%)	-38.3	-25.9	-26.9	-22.1
Average deformation standard error (%)	17.5	2.4	2.3	2.5
Deformation uniformity (%)	6.5	7.4	8.4	9.6
Phase uniformity (Degrees)	0.1	0.1	0.1	0.1

UTS006 2.21 SPT Dynamic Modulus Test
Print date: 11/14/2016 10:34:40 PM

Figure C 6: Dynamic Modulus Test Out Put Summary H4_76(H)+RPW AC at 40^{o}C, 0.1 Hz (2 of 2).

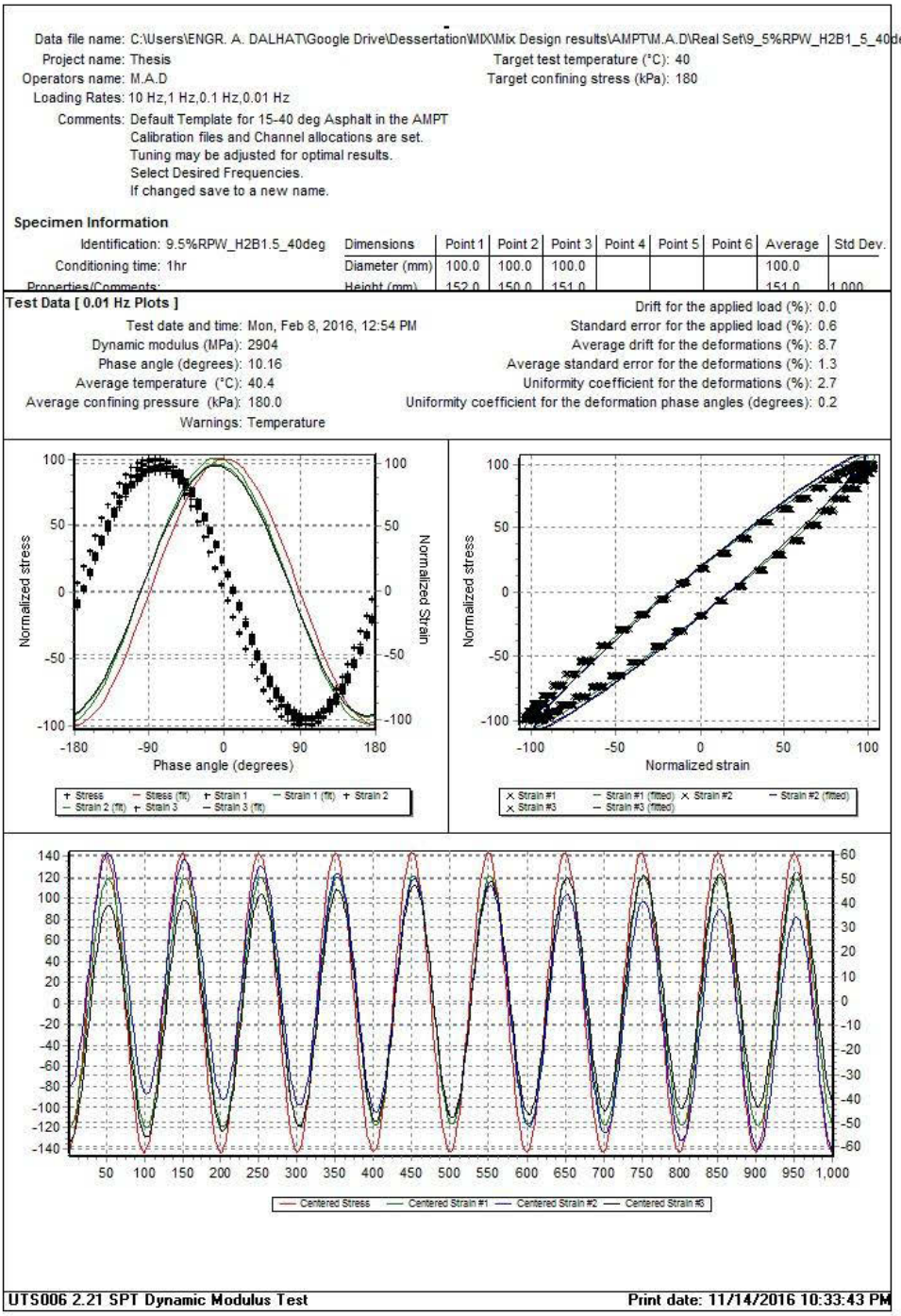

Figure C 7: Dynamic Modulus Test Out Put Summary H2B1.5_76(H)+RPW AC at 40°C, 0.1 Hz (1 of 2).

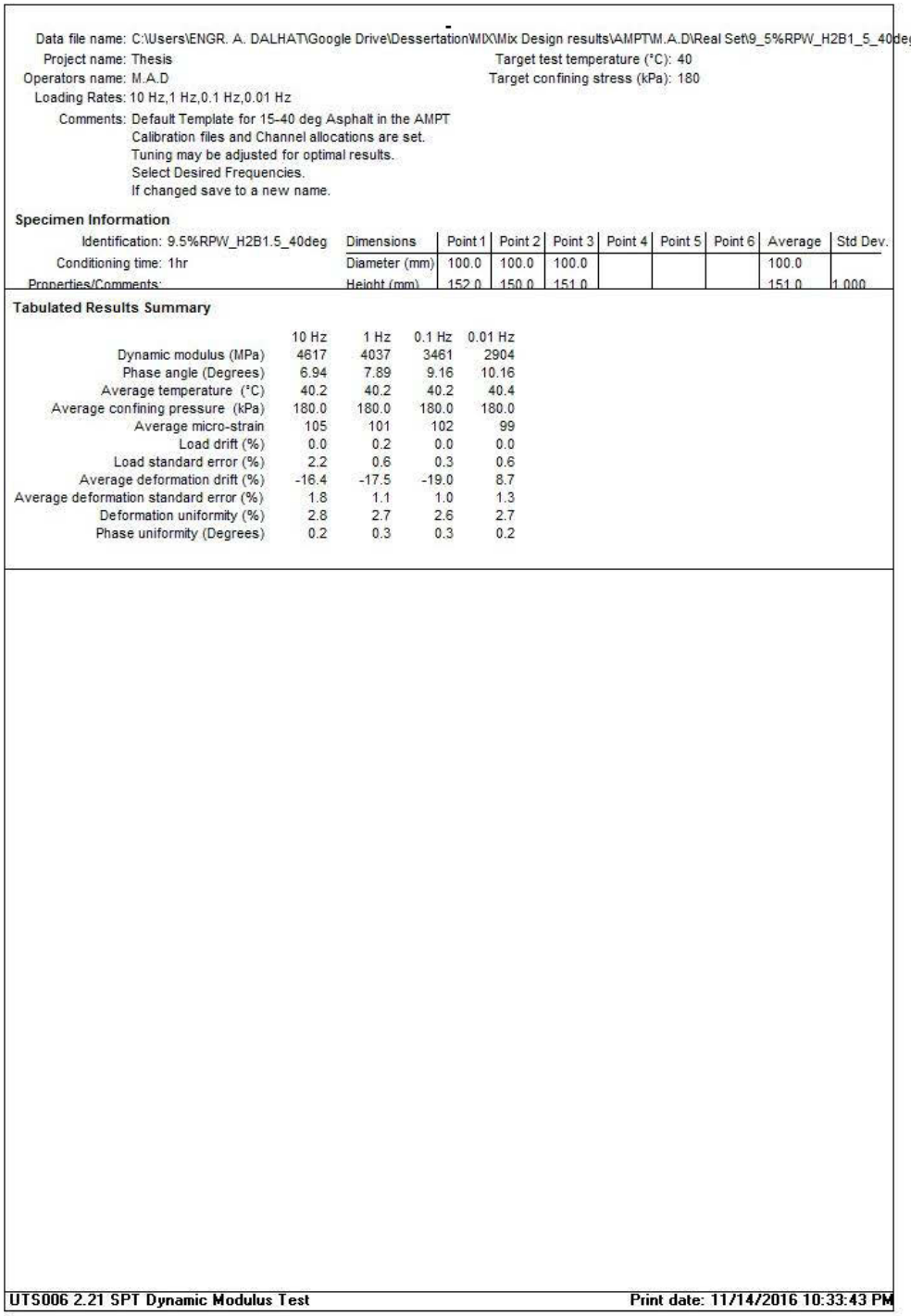

Data file name: C:\Users\ENGR. A. DALHAT\Google Drive\Dessertation\MIX\Mix Design results\AMPT\M.A.D\Real Set\9_5%RPW_H2B1_5_40deg\9_5%
Project name: Thesis
Target test temperature (°C): 40
Operators name: M.A.D
Target confining stress (kPa): 180
Loading Rates: 10 Hz,1 Hz,0.1 Hz,0.01 Hz
Comments: Default Template for 15-40 deg Asphalt in the AMPT
Calibration files and Channel allocations are set.
Tuning may be adjusted for optimal results.
Select Desired Frequencies.
If changed save to a new name.

Specimen Information

Identification: 9.5%RPW_H2B1.5_40deg	Dimensions	Point 1	Point 2	Point 3	Point 4	Point 5	Point 6	Average	Std Dev.
Conditioning time: 1hr	Diameter (mm)	100.0	100.0	100.0				100.0	
Properties/Comments:	Height (mm)	152.0	150.0	151.0				151.0	1.000

Tabulated Results Summary

	10 Hz	1 Hz	0.1 Hz	0.01 Hz
Dynamic modulus (MPa)	4617	4037	3461	2904
Phase angle (Degrees)	6.94	7.89	9.16	10.16
Average temperature (°C)	40.2	40.2	40.2	40.4
Average confining pressure (kPa)	180.0	180.0	180.0	180.0
Average micro-strain	105	101	102	99
Load drift (%)	0.0	0.2	0.0	0.0
Load standard error (%)	2.2	0.6	0.3	0.6
Average deformation drift (%)	-16.4	-17.5	-19.0	8.7
Average deformation standard error (%)	1.8	1.1	1.0	1.3
Deformation uniformity (%)	2.8	2.7	2.6	2.7
Phase uniformity (Degrees)	0.2	0.3	0.3	0.2

UTS006 2.21 SPT Dynamic Modulus Test
Print date: 11/14/2016 10:33:43 PM

Figure C 8: Dynamic Modulus Test Out Put Summary H2B1.5_76(H)+RPW AC at 40^{o}C, 0.1 Hz (2 of 2).

APPENDIX D

MiniTab Fatigue Life, Dynamic Modulus and Phase Angle Correlations Out-Put

Regression Analysis: Fatigue Life Strain Controlled, Hybrid RPW ACs

```
The regression equation is
Log (FL) = 8.99 - 2.00 Log (Strain) + 0.594 Log (DM) + 0.918 Log(Phase Angle)


Predictor           Coef  SE Coef       T      P
Constant           8.988    1.235    7.28  0.000
Log (Strain)     -1.9961   0.1137  -17.56  0.000
Log (DM)          0.5939   0.2785    2.13  0.043
Log(Phase Angle   0.9179   0.1670    5.50  0.000


S = 0.100024   R-Sq = 93.6%   R-Sq(adj) = 92.9%


Analysis of Variance

Source          DF      SS      MS       F      P
Regression       3  3.6726  1.2242  122.36  0.000
Residual Error  25  0.2501  0.0100
Total           28  3.9227


Source           DF  Seq SS
Log (Strain)      1  3.3669
Log (DM)          1  0.0035
Log(Phase Angle   1  0.3022
```

MiniTab Fatigue Life, Dynamic Modulus and Phase Angle Correlations Out-Put

Regression Analysis: Fatigue Life Stress Controlled, Hybrid RPW ACs

```
The regression equation is
Log (FL) = - 355 - 4.24 Log (Stress) + 191 Log (DM) + 1.38 Log(Phase Angle)
           - 24.4 Log(DM) Sq.


Predictor            Coef  SE Coef      T      P
Constant           -355.0    129.6  -2.74  0.011
Log (Stress)      -4.2369   0.6850  -6.19  0.000
Log (DM)           190.70    66.97   2.85  0.009
Log(Phase Angle)   1.3799   0.4220   3.27  0.003
Log(DM) Sq.       -24.381    8.602  -2.83  0.009


S = 0.240771   R-Sq = 69.1%   R-Sq(adj) = 64.0%


Analysis of Variance

Source          DF       SS       MS      F      P
Regression       4  3.11476  0.77869  13.43  0.000
Residual Error  24  1.39130  0.05797
Total           28  4.50606


Source            DF   Seq SS
Log (Stress)       1  2.24893
Log (DM)           1  0.01755
Log(Phase Angle)   1  0.38264
Log(DM) Sq.        1  0.46564
```

MiniTab Fatigue Life, Dynamic Modulus and Phase Angle Correlations Out-Put

Regression Analysis: Fatigue Life Strain Controlled, CRB_76 and Fresh ACs

```
* Log(Phase Angle is highly correlated with other X variables
* Log(Phase Angle has been removed from the equation.


The regression equation is
Log (FL) = 7.54 - 5.08 Log (Strain) + 2.62 Log (DM)


Predictor        Coef  SE Coef      T      P
Constant        7.536    2.707   2.78  0.032
Log (Strain)  -5.0814   0.6593  -7.71  0.000
Log (DM)       2.6177   0.7395   3.54  0.012


S = 0.289469   R-Sq = 90.8%   R-Sq(adj) = 87.8%


Analysis of Variance

Source          DF      SS      MS      F      P
Regression       2  4.9888  2.4944  29.77  0.001
Residual Error   6  0.5028  0.0838
Total            8  5.4916


Source        DF  Seq SS
Log (Strain)   1  3.9388
Log (DM)       1  1.0500
```

MiniTab Fatigue Life, Dynamic Modulus and Phase Angle Correlations Out-Put

Regression Analysis: Fatigue Life Stress Controlled, CRB_76 and Fresh ACs

The regression equation is
Log (FL) = 12.1 - 3.42 Log (Stress) + 0.897 Log (DM) + 1.04 Log(Phase Angle)

Predictor	Coef	SE Coef	T	P
Constant	12.116	4.227	2.87	0.008
Log (Stress)	-3.4211	0.7036	-4.86	0.000
Log (DM)	0.8974	0.7714	1.16	0.256
Log(Phase Angle)	1.0394	0.4579	2.27	0.032

S = 0.272539 R-Sq = 58.8% R-Sq(adj) = 53.8%

Analysis of Variance

Source	DF	SS	MS	F	P
Regression	3	2.64912	0.88304	11.89	0.000
Residual Error	25	1.85694	0.07428		
Total	28	4.50606			

Source	DF	Seq SS
Log (Stress)	1	2.24893
Log (DM)	1	0.01755
Log(Phase Angle)	1	0.38264

Unusual Observations

Obs	Log (Stress)	Log (FL)	Fit	SE Fit	Residual	St Resid
21	2.93	6.9955	6.3924	0.0683	0.6031	2.29R

R denotes an observation with a large standardized residual.

MiniTab Fatigue Life, Dynamic Modulus and Phase Angle Correlations Out-Put

Regression Analysis: Dynamic Modulus, RPW-Aggregate ACs

```
The regression equation is
Log(DM) = 3.97 - 0.421 Log(Temp.) - 26.4 %RPW Sq. + 0.130 Log (Freq.)
          + 6.78 %RPW


Predictor        Coef  SE Coef      T      P
Constant      3.97387  0.07420  53.56  0.000
Log(Temp.)   -0.42082  0.04400  -9.56  0.000
%RPW Sq.      -26.353    5.566  -4.73  0.000
Log (Freq.)   0.12966  0.01069  12.13  0.000
%RPW            6.784    1.479   4.59  0.000


S = 0.0717295   R-Sq = 89.3%   R-Sq(adj) = 87.9%


Analysis of Variance

Source          DF       SS       MS      F      P
Regression       4  1.33464  0.33366  64.85  0.000
Residual Error  31  0.15950  0.00515
Total           35  1.49414


Source       DF   Seq SS
Log(Temp.)    1  0.46014
%RPW Sq.      1  0.00973
Log (Freq.)   1  0.75655
%RPW          1  0.10822


Unusual Observations

Obs  Log(Temp.)  Log(DM)     Fit  SE Fit  Residual  St Resid
  4        0.60   3.9941  4.1235  0.0364   -0.1294     -2.09R
 25        1.32   3.6210  3.4609  0.0277    0.1601      2.42R

R denotes an observation with a large standardized residual.
```

MiniTab Fatigue Life, Dynamic Modulus and Phase Angle Correlations Out-Put

Regression Analysis: Dynamic Modulus, RPET-aggregate ACs

The regression equation is
Log(DM) = 4.36 - 0.931 Log(Temp.) - 5.87 %RPET + 0.266 Log (Freq.)

Predictor	Coef	SE Coef	T	P
Constant	4.3612	0.4306	10.13	0.000
Log(Temp.)	-0.9315	0.2652	-3.51	0.002
%RPET	-5.873	1.455	-4.04	0.001
Log (Freq.)	0.26583	0.03227	8.24	0.000

S = 0.176743 R-Sq = 82.3% R-Sq(adj) = 79.7%

Analysis of Variance

Source	DF	SS	MS	F	P
Regression	3	2.91287	0.97096	31.08	0.000
Residual Error	20	0.62476	0.03124		
Total	23	3.53763			

Source	DF	Seq SS
Log(Temp.)	1	0.28416
%RPET	1	0.50881
Log (Freq.)	1	2.11990

Unusual Observations

Obs	Log(Temp.)	Log(DM)	Fit	SE Fit	Residual	St Resid
13	1.32	1.4771	2.0106	0.0837	-0.5334	-3.43R

R denotes an observation with a large standardized residual.

MiniTab Fatigue Life, Dynamic Modulus and Phase Angle Correlations Out-Put

Regression Analysis: Phase Angle, RPW-Aggregate ACs

```
The regression equation is
Log(Phase Angle) = 1.77 - 0.0680 Log (Freq.) - 1.19 Log(Temp.)
                   + 0.687 Log(Temp.) Sq. - 9.35 %RPW + 32.4 %RPW Sq.


Predictor            Coef   SE Coef      T      P
Constant           1.7713    0.1132  15.65  0.000
Log (Freq.)     -0.067955  0.008061  -8.43  0.000
Log(Temp.)        -1.1933    0.2039  -5.85  0.000
Log(Temp.) Sq.    0.68706   0.08705   7.89  0.000
%RPW               -9.349     1.117  -8.37  0.000
%RPW Sq.           32.438     4.200   7.72  0.000


S = 0.0540757   R-Sq = 90.7%   R-Sq(adj) = 89.2%


Analysis of Variance

Source          DF       SS       MS      F      P
Regression       5  0.85940  0.17188  58.78  0.000
Residual Error  30  0.08773  0.00292
Total           35  0.94713


Source          DF   Seq SS
Log (Freq.)      1  0.20780
Log(Temp.)       1  0.18886
Log(Temp.) Sq.   1  0.21059
%RPW             1  0.07776
%RPW Sq.         1  0.17439


Unusual Observations

         Log  Log(Phase
Obs  (Freq.)     Angle)      Fit   SE Fit  Residual  St Resid
 13    -2.00    0.80494  0.92002  0.02393  -0.11508     -2.37R

R denotes an observation with a large standardized residual.
```

MiniTab Fatigue Life, Dynamic Modulus and Phase Angle Correlations Out-Put

Regression Analysis: Phase Angle, RPET-Aggregate ACs

The regression equation is
Log(Phase Angle) = 0.422 + 0.350 Log(Temp.) + 6.29 %RPET - 0.0752 Log (Freq.)

Predictor	Coef	SE Coef	T	P
Constant	0.4220	0.1056	4.00	0.001
Log(Temp.)	0.35036	0.06505	5.39	0.000
%RPET	6.2903	0.3570	17.62	0.000
Log (Freq.)	-0.075210	0.007915	-9.50	0.000

S = 0.0433541 R-Sq = 95.4% R-Sq(adj) = 94.7%

Analysis of Variance

Source	DF	SS	MS	F	P
Regression	3	0.77174	0.25725	136.86	0.000
Residual Error	20	0.03759	0.00188		
Total	23	0.80933			

Source	DF	Seq SS
Log(Temp.)	1	0.01846
%RPET	1	0.58359
Log (Freq.)	1	0.16970

Unusual Observations

Obs	Log(Temp.)	Log(Phase Angle)	Fit	SE Fit	Residual	St Resid
4	1.32	1.02407	1.12458	0.02188	-0.10051	-2.69R

R denotes an observation with a large standardized residual.

VITAE

NAME: Muhammad Abubakar Dalhat

NATIONALITY: Nigerian

HOME ADDRESS: No. 10, Sambo road, Tudun Jukun Zaria, Kaduna State, Nigeria.

POSTAL ADDRESS: P. o Box 1548, No. 10, Sambo road, Tudun Jukun Zaria, Kaduna State, Nigeria.

EMAIL: muhammadabubakardalhat@yahoo.com

EDUCATIONAL QUALIFICATIONS

Doctor of Philosophy in Civil Engineering (Pavement Material).

Feb. 2013 - Mar. 2017

King Fahd University of Petroleum and Minerals,

Dhahran, Saudi Arabia.

Master of Science in Civil Engineering (Transportation)

Feb. 2011 - Nov. 2012

King Fahd University of Petroleum and Minerals,

Dhahran, Saudi Arabia.

Bachelor of Engineering (Civil)

Jan. 2005 - Mar. 2010

Ahmadu Bello University,

Zaria, Nigeria.

Related Publications:

1. Al-Abdul Wahhab H.I. and **Dalhat M.A.**, 2016. *Storage Stability and High Temperature Performance of Recycled Plastic Modified Asphalt Binder*. Road Material and Pavement Design. DIO: 10.1080/14680629.2016.1207554.

2. **Dalhat M.A.** and Al-Abdul Wahhab H.I., 2016. *Cement-less and asphalt-less concrete bounded by recycled plastic*. Construction and Building Materials. 119, 206–214

3. **Dalhat M.A.** and Al-Abdul Wahhab H.I., 2015. *Performance of recycled plastic waste modified asphalt binder in Saudi Arabia.* International Journal of Pavement Engineering, DOI: 10.1080/10298436.2015.1088150.

Relevant link: https://www.researchgate.net/profile/Muhammad_A_Dalhat/contributions